Title
Synthesis, Reactivity, and Catalysis of Group 3 and Lanthanide Alkyl Complexes

Author
Levine, Daniel Steven

Publication Date
2016

Peer reviewed|Thesis/dissertation

Synthesis, Reactivity, and Catalysis of Group 3 and Lanthanide Alkyl Complexes

By

Daniel Steven Levine

A dissertation submitted in partial satisfaction of the

requirements for the degree of

Doctor of Philosophy

in

Chemistry

in the

Graduate Division

of the

University of California, Berkeley

Committee in charge:

Professor T. Don Tilley, Co-Chair
Professor Richard A. Andersen, Co-Chair
Professor Alexis T. Bell

Summer 2016

Abstract

Synthesis, Reactivity, and Catalysis of Group 3 and Lanthanide Alkyl Complexes

by

Daniel Steven Levine

Doctor of Philosophy in Chemistry

University of California, Berkeley

Professor T. Don Tilley, Co-Chair
Professor Richard A. Andersen, Co-Chair

Chapter 1. A series of scandium dialkyl complexes, (PNP)ScR_2 (R = neopentyl, trimethylsilylmethyl), supported by the monoanionic, chelating PNP ligand (2,5-bis(dialkylphosphinomethyl)pyrrolide; alkyl = cyclohexyl, *tert*-butyl) was synthesized and the reactivities of these complexes toward simple hydrocarbons was investigated. The scandium–carbon bonds undergo σ-bond metathesis reactions with hydrogen and these complexes are catalysts for the hydrogenation of alkenes. Reactions with primary amines led to formation of amido complexes that undergo cyclometalation *via* σ-bond metathesis, without involvement of an imido complex intermediate. A variety of carbon-hydrogen bonds are also activated, including *sp*-, sp^2-, and sp^3-C–H bonds (intramolecularly in the latter case). Levine, D. S.; Tilley, T. D.; Andersen, R. A. *Organometallics* **2015**, *34* (19), 4647.

Chapter 2. Terminal group 3 methylidene complexes are generated by thermolysis of monoanionic PNP-supported scandium and yttrium dialkyl complexes. The reaction mechanism has been probed by deuterium-labeling experiments and DFT calculations. Abstraction of a γ-hydrogen from one alkyl group by the other affords a metallacyclobutane that undergoes [2+2] cycloreversion, analogous to a key step in the olefin metathesis reaction, to generate a methylidene complex and isobutene. The resulting methylidene complex dimerizes in the case of scandium and decomposes to a mixture of products in the case of yttrium. Levine, D. S.; Tilley, T. D.; Andersen, R. A. *Organometallics,* Articles ASAP, 10.1021/acs.organomet.6b00394.

Chapter 3. Scandium and yttrium congeneric complexes, supported by a monoanionic PNP ligand, were studied as catalysts for alkene hydrogenation and hydrosilation, and alkyne semihydrogenation and semihydrosilation. The yttrium congener was found to be much more active in all cases, but this greater activity led to more rapid catalyst decompostion, and therefore higher total yields for some of the reactions when employing scandium. Calculations indicate that the reaction proceeds via σ-bond metathesis of the alkyl complex to form a metal hydride complex into which alkenes/alkynes insert.

Chapter 4. PNP-supported rare earth complexes (M = Sc, Y, Ho, Lu) were found to be highly selective and efficient amine-silane dehydrocoupling catalysts with hindered and unhindered primary and secondary amines and primary, secondary, and tertiary silanes. A comparison of the

activity of the different metal complexes reveal that Y ~ Ho > Lu > Sc in terms of reactivity. Computational investigation indicates that the reaction proceeds in a stepwise manner with initial formation of a 5-coordinate aminosilicate intermediate, followed by β-H elimination assisted by a Si–H agostic interaction in the aminosilicate intermediate. Energy decomposition analysis indicates that the reaction rate is principally determined by steric interaction, and secondarily by metal complex polarizability.

Chapter 5. Theoretical calculations of polarizability and reaction barrier heights have been calculated and found to be correlated. Energy decomposition analysis (EDA) of the ground state and transition state of the σ-bond metathesis reaction indicate that polarizability is an important feature of σ-bond metathesis because there is increased covalency in the transition-state and therefore increased polarizability preferentially stabilizes the transition state over the ground state.

Chapter 6. We have designed an energy decomposition analysis (EDA) to gain deeper understanding of single chemical bonds, that is, those in which the interacting fragments are doublet open-shell systems but the supersystem is closed-shell. The method is a spin-pure extension of the absolutely localized molecular orbital (ALMO) EDA to the one-pair perfect pairing energy (equivalently to an active space of two electrons in two orbitals). The total interaction energy is broken up into four terms: frozen interactions, spin-coupling, polarization, and charge-transfer. A variety of single bonds are analyzed and in addition we use this method to show how solvation changes the nature of bonds, producing different results in the gas-phase and with explicit solvent molecules.

Chapter 7. Efforts to prepare 1,3-dilithiopropanes are described. Direct metalation and Li/element exchanges lead to cyclized products. Borylation followed by Hg/B exchange appears most likely to work although there are safety and environmental reasons for not pursuing this pathway.

Synthesis, Reactivity, and Catalysis of Group 3 and Lanthanide Alkyl Complexes

Table of Contents

Introduction

Chemistry is fundamentally about making and breaking chemical bonds. Generally, with the early main group compounds that form the stuff of organic chemistry: polymers, fuels, medicines, and the plethora of other products people think of as "chemicals", this is difficult to do. Fundamentally, this is due to fact that the early main group elements do not readily support electronic or coordinative unsaturation; reducing, oxidizing, or H-abstraction from, for example, methane is hard. One cannot simply rip the molecules apart and reassemble them in the desired fashion. Organometallic compounds do not suffer from the requirement of full saturation and their unique ability to act as surrogates for the electronic and coordinative needs of the early main group allow them to catalyze a huge variety of molecular transformations.

While most of the transition metals can begin to carry out these transformations by first oxidatively adding a main group compound to produce a new metal complex with main group ligands, which can then be functionalized or rearranged to the desired product, this requires the presence of *d*-electrons to serve as reducing equivalents. The early transition metals and lanthanides, which are present principally as d^0 complexes, therefore do not have this reaction pathway available. Instead, their reducing equivalents are stored in their metal–ligand σ bonds, and the addition of new main group compounds to the metal center, proceeds by σ-bond metathesis in which those reducing equivalents are smoothly transferred to a new set stored in a new metal–ligand σ bond.

This reaction pathway can perform some of the most difficult molecular transformation, including the breaking of the C–H bond of methane. Yet relatively little is known about this mechanism, how exactly it operates, and what factors promote or prevent high activity. In this work, we put forward a hypothesis based on the use of highly polarizable, PNP-pincer ligands. Chapter 1 discusses the synthesis and preliminary reactivity of such complexes and establishes that they can adequately carry out the σ-bond metathesis reaction. Chapter 2 investigates unique reactivity obtainable with these complexes owing to the fact that there are two sites capable of storing two reducing equivalents in total: they can rearrange to a metal-alkylidene complex, another two reducing equivalent ligand. Chapter 3 establishes that the fundamental σ-bond metathesis reactivity of these molecules can be harnessed into a catalytic cycle for the functionalization of organic substrates, the ultimate goal of studying these sorts of reactions. Chapter 4 addresses a hypothesis advanced in Chapter 3 to explain rapid catalyst decomposition and shows that extremely high catalytic activity can be obtained with these complexes by selecting substrates that very rapidly trap the least stable catalytic intermediates. In light of the experimental successes exemplified in the first four chapters, in Chapter 5, we carry out theoretical calculations to obtain further support for the hypothesis of the experimental work, that polarizability is the most relevant factor in determining σ-bond metathesis activity. Insight is sought through the use of an energy decomposition analysis to quantify what effects lead to lower reaction barriers. Chapter 6 elaborates on these preliminary analyses, which required presumptions about the nature of the metal-ligand interactions, by describing a more general energy decomposition analysis method to analyze reaction barriers like that in σ-bond metathesis. Chapter 7 describes attempts to prepare reagents for the readier preparation of the metal-alkylidene complexes described in Chapter 2, which could open up whole, new reaction mechanisms to these early metal complexes.

In general, this dissertation describes a journey to understand the σ-bond metathesis reaction, one of the fundamental reactions in organometallic chemistry.

Acknowledgements

My journey through graduate school has had many twists and turns along the way and a number of people have helped shape it into a productive and ultimately rewarding period of my life. I'd like to take a moment to thank the people who made this possible.

First, I want to thank my first advisors, Don Tilley and Dick Andersen. They allowed me to pursue research directions that interested me and gave me the freedom to pivot when I felt that a particular project wasn't going in a direction I wanted to go. I greatly appreciate the guidance they offered me for both my scientific present and future. Mostly, I am thankful that they allowed me to grow into my own, independent scientist.

I want to thank Rosemary Tilley, Don's administrative assistant, for keeping the lab stocked with chemicals, having non-chemistry-related conversations, and buying me a new pie plate after I smashed one on the front step of her and Don's house.

Drs. Kathy Durkin and Antonio DiPasquale, as heads of Berkeley's computational and X-ray diffraction facilities both played key roles in my ability to carry out the work in this thesis and also for guiding me from knowing literally nothing to being a competent researcher.

There have been a number of important lab members in my development as well. Mark Lipke, Allegra Liberman-Martin, and Mike Lipschutz were senior graduate students when I joined the group and provided advice, training, sounding boards for ideas, laughs in good times and encouragement in bad. Mark was the first person to get me into theoretical chemistry and as my longtime fellow late-night/early-morning worker, he was probably the person I saw most my first year. Mike and Allegra were my go-to people for chemistry advice and sanity checks. Mike taught me one of the most important features of the department, that the Parking and Transportation department never enforces the parking limits behind the chemistry buildings, which facilitated many a late-night lab session. Allegra was a true friend and fantastic chemist, offering equal parts optimism and advice, and getting in on my dancing in lab.

I also want to thank lab contemporaries Micah Ziegler, for his infinite capacity to drop whatever he was doing and help me with crystallography or whatever I needed (like editing fellowship applications), and Patrick Smith, for his comradery and help reshaping some of the lab's practices from voodoo to science.

I also want to thank my roommate since my second year of graduate school, Tobias Sjölander, who listened to hours and hours and hours of talk about synthetic inorganic chemistry that no physical chemist could possibly actually want to listen to. He *was* listening though and without his insightful encouragement (which I ignored for years) and persistence (which was good because it took years), I would not be writing this thesis today.

Finally, I want to thank my soon-to-be post-doctoral advisor, Martin Head-Gordon. He was willing to take on a poor synthetic chemist who knew next to nothing about theory and give me a place to start the next chapter in my personal and professional development. I am extremely grateful for his faith in me and I hope I don't let him down.

Chapter 1. C–H Bond Activations by Monoanionic, PNP-Supported Scandium Dialkyl Complexes

INTRODUCTION

For the past 30 years, there has been a concerted effort by synthetic chemists to cleave the C–H bonds of unactivated hydrocarbons in a selective, catalytic manner.[1,-4] The direct functionalization of C–H bonds could lead to new ways to produce organic substances, such as polymers, pharmaceuticals, and fuels.[5-7] One mechanism for C–H activation, mainly associated with d^0 metals, is a σ-bond metathesis process.[8-10] Notable advances in this area, by the groups of Watson[11,12] and Bercaw,[13] demonstrated aliphatic C–H bond activation (including methane) by permethylscandocene and permethyllanthanocene (Ln=Y, Lu) alkyl complexes. While a number of related systems have been discovered, few have been incorporated into a catalytic cycle. Previous work in this laboratory demonstrated the catalytic hydromethylation of alkenes,[14b] dehydrocoupling of silanes,[14c] and dehydrogenative silation of methane[14d] with $Cp^*_2ScCH_3$ or $[CpCp^*HfMe]^+$ as the catalyst. However, these catalytic reactions suffer from long reaction times and low turnover numbers.[14]

The rapid and efficient functionalization of unactivated substrates such as methane remains one of the great challenges in chemistry, and the transformations described above indicate that d^0 complexes offer a potentially viable pathway to achieve this goal. Notably, productive methane conversion by σ-bond metathesis is exclusively associated with the ancillary Cp* (Cp*= η^5–C_5Me_5) ligand set, or modifications thereof. Additionally, considerable work has focused on various strategies for development of "non-Cp-based" ligand sets that might promote comparable or greater σ-bond-metathesis activity.[15] Properties of the Cp* ligand thought to be relevant to σ-bond metathesis reactivity at a d^0 metal center are its steric bulk, polarizability, and strongly donating character. Thus, for this work, a PNP ligand set was designed to possess these same properties, which are readily tuned by straightforward synthetic modifications. Contemporaneous with this study, these same ligands were synthesized and explored with late transition metal systems.[16]

Polarizable ligands may be key to producing active complexes for σ-bond metathesis with d^0 metal centers. Computational studies indicate that the σ-bond metathesis transition state may be described as a proton transfer between carbanion- or hydride-like groups that are stabilized by the electropositive metal center (see Scheme 1).[17]

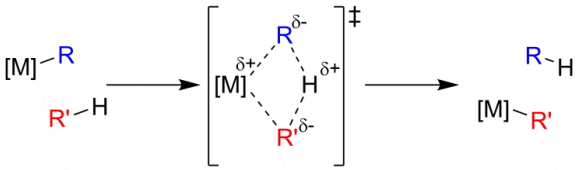

Scheme 1. The σ-bond metathesis reaction.

Ligands with polarizable donor groups increase the polarizability of the metal center, and this may stabilize the charge buildup in the transition state, and lower the activation energy for the proton transfer reaction. Experimental support for the proposition that increasing metal polarizability promotes σ-bond metathesis may be found by noting the increase in the rate of reactions of Cp^*_2MMe (M = Sc, Y, Lu) with methane,[18] in the order Y > Lu > Sc, which parallels the polarizability of the free metal atoms.[18,19] However, a broader experimental study and theoretical underpinnings for the role of polarizability in σ-bond metathesis reactivity is currently lacking. Further studies of monomeric complexes supported by polarizable ligands are therefore needed.

Due to their electropositive nature and high Lewis acidity, the early transition and f-block metals are mainly associated with ligands possessing non-polarizable donor atoms (e.g. N, O). Relatively few complexes of these metals feature softer donor atoms such as phosphorus, but notable exceptions involve PNP and P2N2 donor sets developed by Fryzuk,[20] and the PNP ligand employed by Mindiola[3,21a,b] and Hou[21d] (Figure 1). The σ-bond metathesis chemistry of these complexes has not been extensively explored. In this context, the results reported here target investigations of scandium alkyl complexes supported by ligands possessing polarizable donors (phosphines) and an anionic, anchoring pyrrolide group.

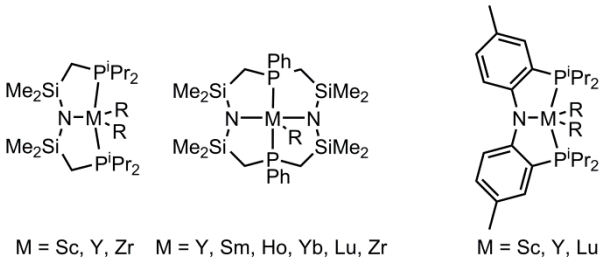

Figure 1. Examples of PNP-supported early transition metal or lanthanide complexes.

RESULTS AND DISCUSSION

Synthesis of monanionic, phosphine-based ligands. The ligands 2,5-bis(dicyclohexylphosphinomethyl) pyrrole (PNP-CyH) and 2,5-bis(di-*tert*-butylphosphinomethyl)pyrrole (PNP-^{t}BuH) were prepared by an adaptation of the method described by Kumar and coworkers.[22] Two equivs of $HPCy_2$ or HP^tBu_2 were added to 2,5-bis(dimethylamino)pyrrole, and the reaction mixture was heated to 140° C. The compound PNP-CyH was readily crystallized in 76% yield from pentane over 3 days. Subsequent deprotonation with $LiN(SiMe_3)_2$ afforded (PNP-Cy)Li (78% isolated yield). All attempts to isolate pure PNP-^{t}BuH by crystallization or sublimation were unsuccessful. However, after deprotonation with $LiN(SiMe_3)_2$, pure (PNP-^{t}Bu)Li was readily isolated by washing the resulting solid with pentane in 48% yield over two steps. This material was protonated with dimethylamine hydrochloride in THF to afford (PNP-*t*Bu)H after trituration with pentane to remove LiCl. The protonated ligand is a waxy solid in pure form, possibly accounting for the difficulty in crystallization.

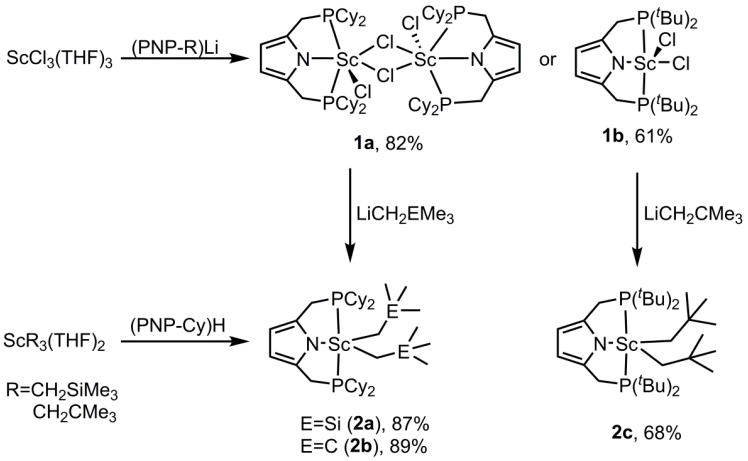

Scheme 2. Synthesis of PNP-supported scandium complexes **1a,b** and **2a-c**.

Synthesis of scandium alkyl complexes. Salt metathesis reactions of $ScCl_3(THF)_3$ with the (PNP-R)Li reagents yielded $[(PNP\text{-}Cy)ScCl_2]_2$ (**1a**) and (PNP-^{t}Bu)$ScCl_2$ (**1b**) in 82% and 45% isolated yields, respectively. These complexes were structurally characterized by X-ray crystallography (see Figure 3). Complex **1a** crystallizes as the chloride-bridged dimer while **1b** forms a monomeric, distorted square pyramid with one chloride occupying the apical position. Both structures feature Sc–P bond lengths of ~2.76 Å (see Table 1). This bond length is within the range of those reported for Sc–P bonds.[20,21] Complexes **1a,b** react readily with alkyllithium reagents to afford monomeric dialkyl complexes (PNP-Cy)$Sc(CH_2SiMe_3)_2$ (**2a**), (PNP-Cy)$ScNp_2$, (**2b**, Figure 2; Np = -CH_2CMe_3), and (PNP-^{t}Bu)$ScNp_2$ (**2c**, Figure 4). Complex **2b** was also prepared more directly by addition of the protonated ligand (PNP-Cy)H to $ScNp_3(THF)_2$.[23] The cyclohexyl derivatives **2a** and **2b** crystallize in the same space group with very similar metrical parameters. Notably, two crystallographically independent molecules are present in the unit cell, one of which adopts a distorted trigonal bipyramidal structure with the phosphine groups occupying the axial positions, while the other exhibits a square pyramidal coordination geometry with one alkyl group in the apical position (Figure 2). The *tert*-butyl complex **2c** crystallizes with the metal center in a distorted trigonal bipyramidal environment (Figure 3). Comparison of the Sc–P bond lengths (see Table 1) in **2b** and **2c** appears to reflect a higher steric demand for PNP-^{t}Bu as compared to PNP-Cy.

Reactions of scandium alkyl complexes with hydrogen. Initial reactivity studies with the dineopentyl complexes involved examination of their interactions with hydrogen. Addition of hydrogen (1 atm) to a benzene-d_6 solution of **2b** or **2c** led to the release of 2 equiv of neopentane, as observed by ^{1}H NMR spectroscopy, and apparent decomposition of the resulting scandium complex to a mixture of unidentified species after 1 h. In both cases, the expected initial product of this reaction is the scandium dihydride complex $[(PNP\text{-}R)ScH_2]_x$**,** but this species is too reactive to isolate or directly observe. Consistent with this postulate, addition of D_2 to **2b** or **2c** afforded 2 equiv of neopentane-d_1 after 1 h and decomposition of the scandium-containing product as determined by ^{1}H NMR spectroscopy. The ^{2}H NMR spectrum did not reveal incorporation of deuterium into any well-defined product other than neopentane-d_1. However, in the presence of 10 equivs of 1-hexene, treatment of **2b** with H_2 resulted in formation of the new dialkyl complex (PNP-Cy)Sc(*n*-hexyl)$_2$ (**2d,** Scheme 3), presumably by insertion of the alkene into the Sc—H bonds of putative $[(PNP\text{-}Cy)ScH_2]_x$. This suggests that the unobserved dihydride complex is stable enough to engage in reactions with suitable trapping reagents, such as unsaturated hydrocarbons.

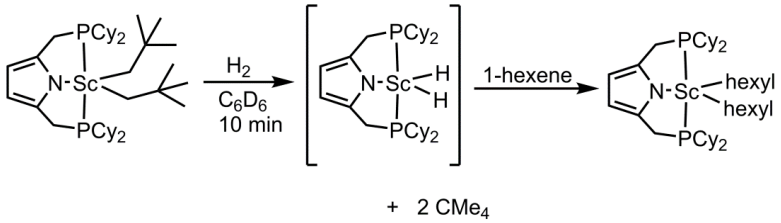

Scheme 3. Addition of hydrogen and 1-hexene to **2b**.

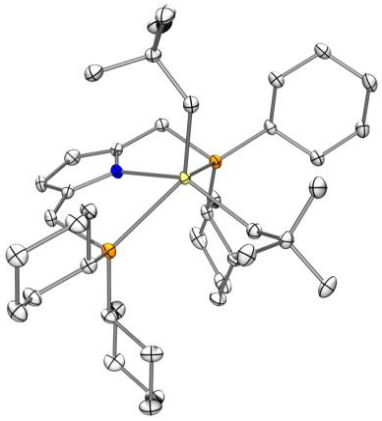

Figure 2. Crystal structure of (PNP-Cy)$ScNp_2$ (**2b**), with a square pyramidal geometry. Hydrogen atoms have been omitted for clarity. Thermal ellipsoids are set at the 50% probability level. Carbon atoms are shown in gray, phosphorus in orange, nitrogen in blue, and scandium in yellow.

a) b)

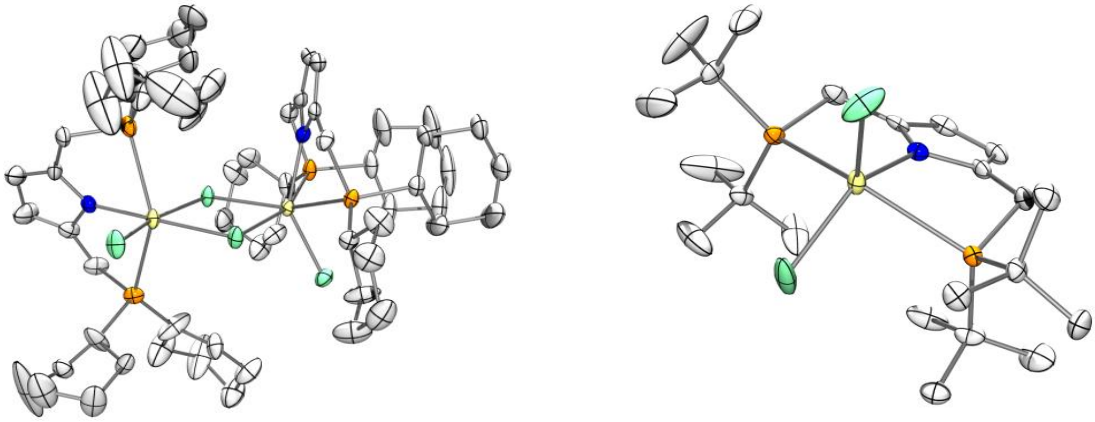

Figure 3. Crystal structure of a) **1a** and b) **1b**. Hydrogen atoms have been omitted for clarity. Thermal ellipsoids are set at the 50% probability level. Chlorine shown in green.

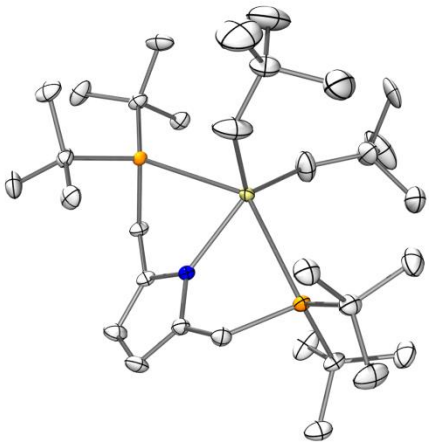

Figure 4. Crystal structure of (PNP-^{t}Bu)$ScNp_2$ (**2c**). Hydrogen atoms have been omitted for clarity. Thermal ellipsoids are set at the 50% probability level.

Table 1. Selected bond lengths (Å) for (PNP-R')ScX compounds (TBP = trigonal bipyramidal, SP = square pyramidal, t = terminal, μ = bridging, ax = axial, eq = equatorial).

Compound	Sc-N	Sc-P	Sc-X (X = Cl, R)
$[(PNP\text{-}Cy)ScCl_2]_2$ **(1a)**	Sc(1): 2.150(3) Sc(2): 2.133(3)	Sc(1): 2.753(12) 2.7540(12) Sc(2): 2.7228(13) 2.7288(13)	Sc(1): 2.3661(11) (t) 2.5222(11) (μ) 2.5695(11) (μ) Sc(2): 2.3632(12) (t) 2.5606(11) (μ) 2.5851(11) (μ)
$(PNP\text{-}^tBu)ScCl_2$ (**1b**)	Sc(1): 2.145(2) Sc(2) 2.135(2)	Sc(1): 2.7198(9) 2.7557(9) Sc(2): 2.7948(9) 2.7400(9)	Sc(1): 2.3717(10) 2.3287(11) Sc(2): 2.3658(9) 2.3373(10)
$(PNP\text{-}Cy)Sc(CH_2SiMe_3)_2$ (**2a**)	TBP: 2.141(3) SP: 2.1780(18)	TBP: 2.7927(7) SP: 2.7876(7) 2.7587(7)	TBP: 2.216(3) SP: 2.202(2) (ax) 2.242(2) (eq)
$(PNP\text{-}Cy)ScNp_2$, (**2b**)	TBP: 2.174(3) SP: 2.188(2)	TBP: 2.8291(7) SP: 2.7955(8) 2.7773(8)	TBP: 2.223(3) SP: 2.202(3) (ax) 2.256(3) (eq)
$(PNP\text{-}^tBu)ScNp_2$ (**2c**)	2.1783(19)	2.8667(7) 2.8887(7)	2.187(3) (ax) 2.240(3) (eq)

These results led us to suspect that complexes **2a-c** might be effective hydrogenation catalysts. Indeed, treatment of a sample of 1-octene and 5 mol % of **2b** or **2c** with hydrogen in C_6D_6 led to the formation of octane (>99% yield by ^{1}H NMR spectroscopy and GC/MS) over the course of 12 hours. The di(octyl) complexes analogous to **2b** were observed during catalysis by ^{1}H NMR spectroscopy, suggesting that these species are resting states in the catalysis. These data suggest that olefin hydrogenation in these complexes proceeds by a mechanism analogous to that found by Marks and coworkers with lanthanocene catalysts.[24]

Reactions of scandium alkyl complexes with amines. Complex **2c** reacted cleanly with 1 equiv of 2,6-diphenyl-*p*-toluidine in benzene-d_6 to afford the complex $(PNP\text{-}^tBu)Sc(NHAr)Np$ (**3**) (Ar = 4-methyl-2,6-diphenylbenzene) with loss of neopentane as determined by ^{1}H NMR spectroscopy. On heating to 60° C, **3** underwent cyclometalation of one of the phenyl groups of the amido ligand to form **4** (Scheme 4). The cyclometalated product **4** was isolated in 83% yield

and characterized by X-ray crystallography (see Appendix). To determine whether this cyclometalation proceeded *via* σ-bond metathesis, or by formation of a transient scandium imido complex (Scheme 4), 2,6-diphenyl-*p*-toluidene-d_2 was added to **2c** to afford (PNP-^{t}Bu)Sc(NDAr)Np with loss of neopentane-d_1 by ^{1}H and ^{2}H NMR spectroscopy.

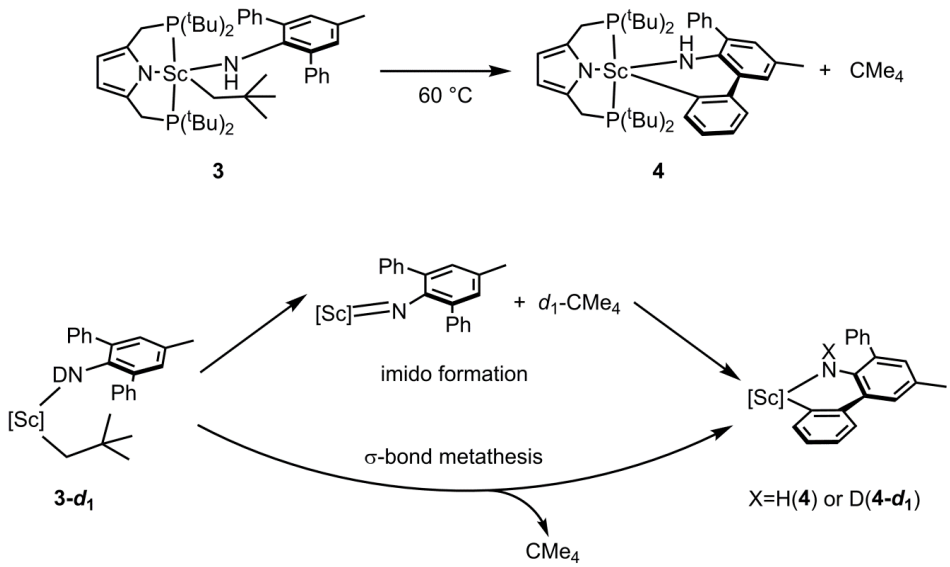

Scheme 4. Possible mechanisms for formation of **3**.

This complex (**3-*d*$_1$**) was heated to 60°C, at which point clean cyclometalation occurred with loss of neopentane-d_0; less than 1% neopentane-d_1 was observed. Since only unlabeled neopentane was evolved in the latter reaction, α-abstraction of the N–D bond by the neopentyl group does not occur, and cyclometalation likely proceeds *via* an intramolecular σ-bond metathesis pathway. Addition of deuterium (1 atm) to the cyclometalated complex in benzene-d_6 resulted in deuterium incorporation into all of the *ortho* positions of the amido ligand phenyl substituents after 5 h at 60 °C, indicating that this C–H activation is reversible. Cyclometalation of **3** could also be induced at 22 °C by addition of two equivs of DMAP to form complex **5** (eq 1).

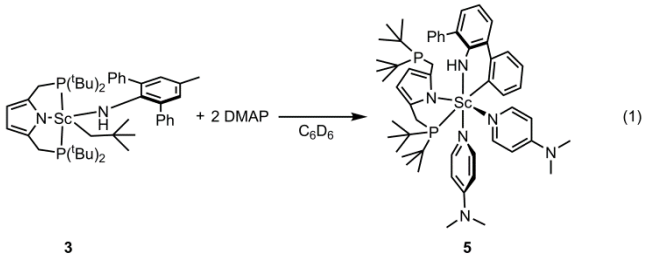

Crystallographic analysis of **5** reveals two coordinated DMAP molecules, while one of the phosphine group arms is completely dissociated from the metal center (Figure 5). The ^{1}H NMR spectrum at room temperature indicates the presence of two inequivalent phosphine groups. However, on heating to 45 °C, the molecule is dynamic on the NMR time-scale as both phosphine arms are equivalent. Treatment of **3c-*d*$_1$** with DMAP afforded **5** with loss of neopentane-d_0 (<1% neopentane-d_1 was observed), indicating that the DMAP-induced pathway also proceeds by direct activation of the phenyl groups with no intermediacy of a scandium imido complex.

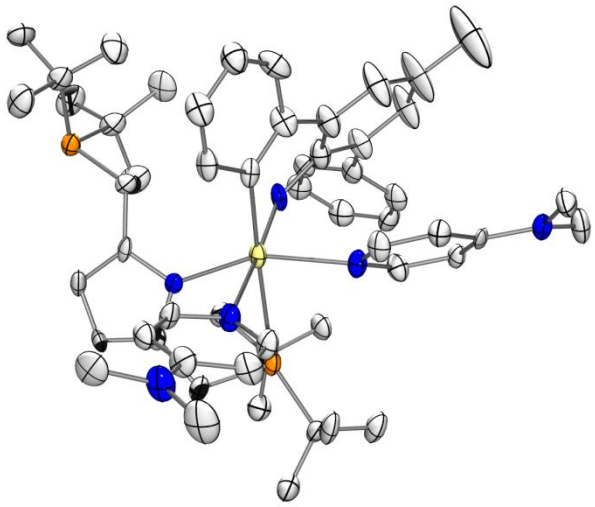

Figure 5. Crystal structure of **5**. Hydrogen atoms have been omitted for clarity. Thermal ellipsoids are set at the 50% probability level.

Reactions of scandium alkyl complexes with alkynes. Complexes **2b,c** were found to cleanly engage in certain intermolecular C—H activation reactions. Thus, treatment of **2c** with *iso*-propylacetylene (10 equiv) in benzene-d_6 cleanly afforded two equivs of neopentane and the bis(acetylide) complex (PNP-^{t}Bu)Sc(C≡CCHMe$_2$)$_2$ (**6b**) after 1.5 h, as determined by ^{1}H NMR spectroscopy. No evidence for polymerization of the alkyne was observed by ^{1}H NMR spectroscopy, although some insoluble material is observed when very large (>20 equiv) amounts of *iso*-propylacetylene are used. The insolubility of this material and its low yield (<10%) has prevented its characterization. The reaction of *iso*-propylacetylene (3 equiv, Scheme 5) in benzene-d_6 with **2b** was much faster (<10 minutes), affording the bis(acetylide) complex (PNP-Cy)Sc(C≡CCHMe$_2$)$_2$ (**6a**), which was isolated in 67% yield as a slightly yellow solid by recrystallization from pentane as a bridging acetylene complex (Figure 6).

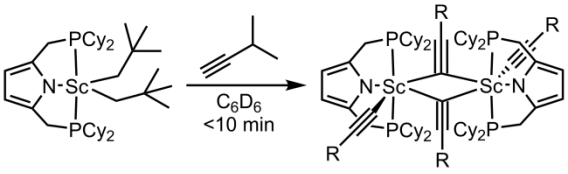

Scheme 5. Addition of *iso*-propylacetylene to **2b**.

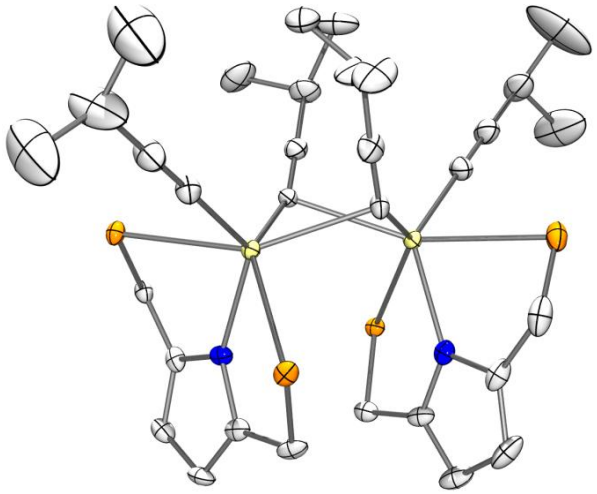

Figure 6. Crystal structure of (PNP-Cy)Sc(C≡CCHMe$_2$)$_2$ (**6a**). Hydrogen atoms and cyclohexyl groups have been omitted for clarity. Thermal ellipsoids are set at the 50% probability level.

Reactions of scandium alkyl complexes with benzene. The mild conditions for formation of the bis(acetylide) complex suggested that **2b,c** might engage in more challenging C—H activations (i.e. involving less acidic aryl or alkyl C—H bonds) at higher temperatures. Heating **2b** to 100 °C in benzene affords (PNP-Cy)ScPh$_2$ (**7**) and neopentane after 12 h in approximately 10% yield, as determined by ^{1}H NMR spectroscopy. The identity of **7** was confirmed by an independent synthesis from **1a** and phenyllithium. Additionally, heating **2c** to 100 °C in benzene-d_6 for 36 h led to formation of (PNP-Cy)ScPh$_2$-d_{10} in approximately 10 % yield, as determined by ^{1}H NMR spectroscopy. Notably, this appears to be the first example of a non-cyclopentadienyl-supported scandium complex that undergoes an intermolecular σ-bond metathesis reaction with an sp^2 hybridized C–H bond. Complex **2b** reacts less readily with toluene-d_8, and requires heating to 120 °C for elimination of neopentane-d_1 to be observed by ^{1}H NMR spectroscopy, at which point many scandium containing products were observed. No reaction was observed between **2b** and tetramethylsilane or methane in toluene-d_8 at 100 °C.

Reaction of scandium alkyl complexes with intramolecular sp^3 bonds. Intramolecular activation of the sp^3 carbon-hydrogen bonds of the PNP ligands was observed for both **2b** and **2c**. After heating **2b** to 100 °C in toluene-d_8 for 5 days, trace amounts (~0.1 equivalents) of cyclohexene were liberated. Similarly, heating **2c** to 60 °C in benzene-d_6 liberated ~2 equivs of neopentane and ~1 equiv of isobutylene over 24 h and led to decomposition of the complex. The isobutylene is likely formed by C–H activation and elimination from the *tert*-butyl groups of the phosphine ligand in a manner analogous to an E2 reaction. To obtain more evidence for this mechanistic proposal, labelled complex (PNP-^{t}Bu)Sc(CD$_2$CMe$_3$)$_2$ (**2c-*d*$_4$**) was prepared and heated to 60 °C for 24 h. The isobutylene produced in this reaction (~1 equiv) was observed to contain no deuterium (as probed by ^{1}H and ^{2}H NMR spectroscopy), consistent with activation of the *tert*-butyl groups and inconsistent with, for example, β-methyl elimination of the neopentyl groups, which would result in deuterium incorporation into the vinyl position of the isobutylene (Scheme 6). In the case of both complexes, this activation-elimination of the phosphine substituent is concurrent with decomposition of the metal complex into a complex mixture and

illustrates a major weak point for these ligands. No reaction was observed between **2b** and tetramethylsilane or methane in toluene-d_8 at 100 °C.

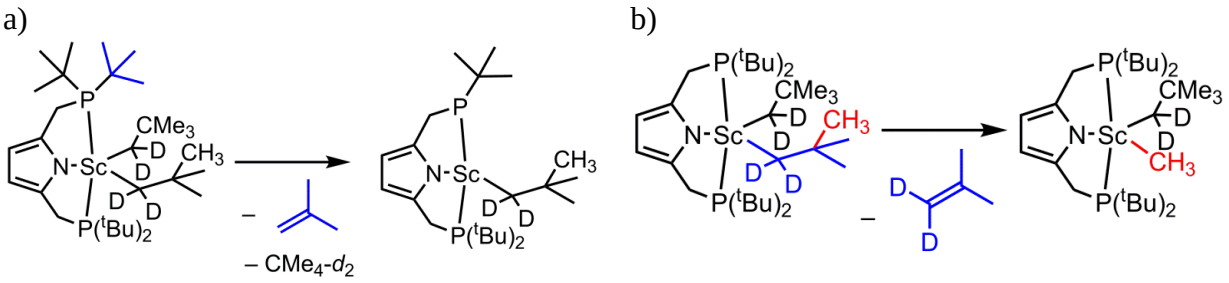

Scheme 6. Possible mechanisms for isobutylene formation from **2c-*d*$_4$**. Pathway (a) is an E2-like mechanism, while pathway (b) is a β-methyl elimination. Each proposal gives a different pattern for deuterium incorporation.

SUMMARY AND CONCLUSIONS

A series of novel monoanionic PNP-supported scandium complexes has been prepared and characterized and their reactivity with C–H bonds has been examined. In addition to well-known hydrogen, amine, and *sp* C–H bond activation, reactivity with intermolecular sp^2 bonds was also observed. To the best of our knowledge, this type of C–H bond activation has not previously been observed for non-Cp-supported complexes of scandium or the lanthanides. These results suggest that the key to generation of reactive centers for σ-bond metathesis may be to employ strongly donating, highly polarizable ligands. This strategy is being investigated.

EXPERIMENTAL SECTION

General Considerations. Unless otherwise noted, all experiments were conducted with dry, oxygen-free solvents using standard Schlenk techniques or in a N_2 atmosphere glovebox. Deuterated solvents, deuterium, and methane-d_4 were purchased from Cambridge Isotope Laboratories, Inc. Benzene-d_6 was dried by vacuum distillation from Na/K alloy. Toluene-d_8 was dried by refluxing over molten sodium metal followed by vacuum distillation. Unless otherwise noted, reagents were obtained from commercial suppliers and used as received. Pyrrole was obtained from Aldrich, dried over CaH_2, and distilled. 2,5-bis(dimethylaminomethyl)pyrrole, $ScCl_3(THF)_3$, and $LiCD_2CMe_3$ were prepared according to literature procedures.[25,26,27]

Analytical Methods. Solution NMR spectroscopy was performed using Bruker AV-300, AVB-400, AVQ-400, AV-500, or AV-600 MHz spectrometers at room temperature. ^1H, $^{13}C\{^1H\}$, and $^{31}P\{^1H\}$ NMR spectra were calibrated internally to either the resonance for the solvent or residual proteo solvent relative to tetramethylsilane. Elemental analyses were carried out by the College of Chemistry Microanalytical Laboratory at the University of California, Berkeley. Melting points were determined on a Mel-Temp II melting point apparatus.

X-ray Crystallography Details. X-ray diffraction data for crystals of $ScNp_3(THF)_2$, (PNP-*t*Bu)$ScCl_2$, (PNP-*t*Bu)$ScNp_2$, (PNP-Cy)$ScCl_2$, (PNP-Cy)$Sc(CH_2SiMe_3)_2$, (PNP-Cy)$ScNp_2$, (PNP-*t*Bu)ScNHAr, (PNP-*t*Bu)ScNHAr(DMAP)$_2$, and (PNP-Cy)$Sc(C{\equiv}CCHMe_2)_2$ were collected using a Bruker AXS modified four-circle diffractometer coupled CCD detector with Mo Kα (λ = 0.71073 Å) radiation monochromated by a system of QUAZAR multilayer mirrors.

Crystals were kept at 100(2) K throughout collection. Data collection, refinement, and reduction were performed with Bruker APEX2 software (v. 2013.4). Structures were solved by direct methods using SHELXS-97. All structures were refined with SHELXL-97 with refinement of F^2 against all reflections by full-matrix least squares. In all models, non-hydrogen atoms were refined anisotropically, and hydrogen atoms were included at their geometrically-calculated positions and refined using a riding model. The 3D molecular structure figures were visualized with ORTEP 3.2, rendered with POV-Ray 3.6. Crystal data and complete details are available in the Appendix.

Synthesis of 2,5-bis(dicyclohexylphosphinomethyl)pyrrole, (PNP-CyH). A Schlenk flask was charged with 2,5-bis(dimethylaminomethyl)pyrrole (1.80 g, 9.93 mmol). Dicyclohexylphosphine (1.23 mL, 6.62 mmol) was added and the reaction mixture was stirred for 22 h at 150 °C. The reaction mixture was allowed to cool to 22 °C and toluene (3 mL) was added to dissolve the resulting amorphous solid. The volatile components were removed *in vacuo* and the resulting foam was dissolved in pentane (10 mL) and stored at -35°C for 3 d to afford a colorless solid (3.0 g, 62% yield) that was isolated by filtration. ^{1}H NMR (400.13 MHz, C_6D_6) δ 8.22 (br s, 1H, N*H*), 6.09 (d, *J* = 2.7 Hz, 2H, pyr-C*H*), 2.67 (s, 4H, -C*H*$_2$PCy$_2$), 1.91-1.46 (m, 28H, -*Cy*), 1.35-1.17 (m, 16H, -*Cy*). ^{13}C{^{1}H} NMR (150.90 MHz, C_6D_6) δ 134.48 (d, *J* = 12.1 Hz), 107.05 (d, *J* = 4.8 Hz), 33.94 (d, *J* = 15.1 Hz), 30.33 (d, *J* = 13.5 Hz), 29.39 (d, *J* = 8.8 Hz), 27.77 (d, *J* = 10.6 Hz), 27.67 (d, *J* = 7.8 Hz), 26.93, 21.38 (d, *J* = 19.6 Hz). ^{31}P{^{1}H} NMR (161.98 MHz, C_6D_6) δ -8.06. Anal. Calcd. for $C_{30}H_{51}NP_2$: C, 73.88; H, 10.54; N, 2.87. Found: C, 74.02; H, 10.57; N, 2.83.

Synthesis of lithium 2,5-bis(dicyclohexylphosphinomethyl) pyrrolide, (PNP-Cy)Li. A solution of lithium bis(trimethylsilylamide) (380 mg, 2.25 mmol) in THF (5 mL) was added to a solution of 2,5-bis(dicyclohexylphosphinomethyl)pyrrole (1.00 g, 2.05 mmol) in THF (5 mL). The solution was stirred for 4.5 h and remained homogeneous throughout the course of the reaction. THF was removed *in vacuo* and the resulting white powder was washed with pentane (3 x 2 mL) to afford analytically pure product (792 mg, 78% yield). The product is insoluble in pentane but is slightly soluble in aromatic solvents. ^{1}H NMR (400.13 MHz, C_6D_6) δ 6.39 (s, 2H, pyr-C*H*), 3.43 (s, 4H, -C*H*$_2$PCy$_2$), 2.07-1.51 (m, 32H, -*Cy*), 1.60-1.21 (m, 12H, -*Cy*). ^{13}C{^{1}H} NMR (150.90 MHz, C_6D_6) δ 136.03, 108.52, 33.08 (br), 30.25 (br), 29.80 (br), 27.74 (br), 26.85, 25.33 (br). ^{31}P{^{1}H} NMR (161.98 MHz, C_6D_6) δ -10.18 (hept, $^{1}J_{LiP}$=24.0 Hz). Anal. Calcd. for $C_{30}H_{50}NP_2Li$: C, 73.00; H, 10.21; N, 2.84. Found: C, 72.65; H, 10.09; N, 2.72.

Synthesis of lithium 2,5-bis(di-*tert*-phosphinomethyl) pyrrolide, (PNP-*t*Bu)Li. A Schlenk flask was charged with 2,5-bis(dimethylaminomethyl)pyrrole (1.20 g, 6.62 mmol). Di-*tert*-butylphosphine (2.50 mL, 13.2 mmol) was added and the reaction mixture was stirred for 22 h at 150 °C. The reaction mixture was cooled to 22 °C to afford a dark brown viscous oil consisting principally of 2,5-bis(di-*tert*--butyl)phosphinomethyl)pyrrole. ^{1}H NMR (400.13 MHz, C_6D_6) δ 8.55 (br s, 1H, N*H*), 6.01 (d, *J* = 2.7 Hz, 2H, pyr-C*H*), 2.71 (s, 4H, -C*H*$_2$P(C(CH$_3$)$_3$)$_2$), 1.03 (d, *J*=10.8 Hz, 36H, -P(C(CH$_3$)$_3$)$_2$). ^{13}C{^{1}H} NMR (100.61 MHz, C_6D_6) δ 128.86 (d, *J* = 12.2 Hz), 106.93 (d, *J* = 5.6 Hz), 31.40 (d, *J* = 22.8 Hz), 29.78 (d, *J* = 13.1 Hz), 20.73 (d, *J* = 23.6 Hz). ^{31}P{^{1}H} NMR (161.98 MHz, C_6D_6) δ 22.28. The oil was dissolved in THF (4 mL). To this solution was added lithium bis(trimethylsilylamide) (1.17 g, 7.00 mmol) in THF (5 mL). The reaction mixture was stirred for 12 h, at which point the THF was removed *in vacuo*. The

resulting peach-colored solid was collected on a fritted funnel and washed with pentane (5 x 2.5 mL) to afford a white powder (883 mg, 34.3% yield over two steps). Caution: the material was highly pyrophoric. ^{1}H NMR (400.13 MHz, DMSO-d_6) δ 5.38 (s, 2H, pyr-C*H*), 2.72 (s, 4H, -C*H*$_2$P(C(CH$_3$)$_3$)$_2$), 1.03 (d, *J* = 9.9 Hz, 36H, -P(C(C*H*$_3$)$_3$)$_2$). ^{13}C{^{1}H} NMR (100.61 MHz, DMSO-d_6) δ 133.71, 102.83 (d, *J* = 6.7 Hz), 30.83 (d, *J* = 23.6 Hz), 29.87 (d, *J* = 12.6 Hz), 24.05 (d, *J* = 19.2 Hz). ^{31}P{^{1}H} NMR (161.98 MHz, DMSO-d_6) δ 22.80. Anal. Calcd. for $C_{22}H_{42}LiNP_2$: C, 67.85; H, 10.87; N, 3.60. Found: C, 67.56; H, 11.01; N, 3.74.

Synthesis of (2,5-bis(dicyclohexylphosphinomethyl) pyrrolyl)scandium dichloride (1a), (PNP-Cy)ScCl$_2$. ScCl$_3$(THF)$_3$ (309 mg, 0.841 mmol) and (PNP-Cy)Li (415 mg, 0.841 mmol) were combined as solids and suspended in toluene (15 mL). The reaction mixture became yellow and homogenous in about 30 s, and the reaction mixture was stirred for 5 h, at which point the reaction mixture was turbid. All solvent was removed under vacuum, and toluene (2 mL) was added. The mixture was filtered to remove lithium chloride. Solvent was removed *in vacuo* to afford a yellow powder (413 mg, 82% yield). ^{1}H NMR (600.13 MHz, C_6D_6) δ 6.03 (s, 2H, pyr-C*H*), 3.17 (d, *J* = 4.6 Hz, 4H, -C*H*$_2$PCy$_2$), 2.04 (d, *J* = 12.8 Hz, 4H, -*Cy*), 1.90 (d, *J* = 10.9 Hz, 8H, -*Cy*), 1.69 (br s, 8H, -*Cy*), 1.56 (d, *J* = 10.4 Hz, 4H, -*Cy*), 1.48 (t, *J* = 11.8 Hz, 8H, -*Cy*), 1.25-1.02 (m, 12H, -*Cy*). ^{13}C{^{1}H} NMR (150.90 MHz, C_6D_6) δ 135.48, 106.07, 33.75, 29.39, 27.86, 27.56, 26.42. ^{31}P{^{1}H} NMR (161.98 MHz, C_6D_6) δ 9.63. Anal. Calcd. for $C_{30}H_{50}Cl_2NP_2Sc$: C, 59.80; H, 8.36; N, 2.32. Found: C, 60.08; H, 8.53; N, 2.09.

Synthesis of (2,5-bis(di-*tert*-butylphosphinomethyl) pyrrolyl)scandium dichloride (1b), (PNP-*t*Bu)ScCl$_2$. ScCl$_3$(THF)$_3$ (539 mg, 1.47 mmol) and (PNP-*t*Bu)Li (571 mg, 1.47 mmol) were combined as solids and suspended in toluene (15 mL). The reaction mixture became pink and homogenous in about 30 s and was stirred for 12 h, at which point the reaction mixture had become turbid. All solvent was removed by vacuum and fresh toluene (2 mL) was added. The mixture was filtered to remove lithium chloride. Pentane (4 mL) was added to the toluene solution and the mixture was stored at -35 °C for 48 h to afford slightly orange blocks which were collected and dried under vacuum (330 mg, 45% yield). ^{1}H NMR (500.23 MHz, C_6D_6) δ 6.12 (s, 2H, pyr-C*H*), 2.99 (d, *J* = 6.2 Hz, 4H, -C*H*$_2$P(C(CH$_3$)$_3$)$_2$), 1.13 (d, *J* = 12.7 Hz, 36H, -P(C(CH$_3$)$_3$)$_2$). ^{13}C{^{1}H} NMR (100.61 MHz, C_6D_6) δ 136.83, 107.01 (t, *J* = 4.2Hz), 33.09 (t, *J* = 2.4 Hz), 29.38 (t, *J* = 2.8 Hz), 21.04 (t, *J* = 4.3 Hz). ^{31}P{^{1}H} NMR (161.98 MHz, C_6D_6) δ 33.94 (br). Anal. Calcd. for $C_{22}H_{42}Cl_2NP_2Sc$: C, 53.02; H, 8.49; N, 2.81. Found: C, 53.31; H, 8.69; N, 2.70. Mp: 175-179 °C.

Synthesis of ScNp$_3$(THF)$_2$. Neopentyllithium (318.6 mg, 4.08 mmol) was dissolved in pentane (8 mL) and added dropwise to a stirred suspension of ScCl$_3$(THF)$_2$ (500 mg, 4.08 mmol) in pentane (8 mL). The reaction mixture became cloudy and produced a fine white precipitate. After stirring for 4 h, the reaction mixture was filtered through a fritted funnel and the filtrate was concentrated to 10 mL. The concentrated filtrate was cooled at -35 °C for 10 h to afford the product as large, colorless, single-crystal needles (270 mg, 49 % yield). A second crop was obtained by concentrating the mother liquor (131 mg, 24 % yield, total combined: 401 mg, 73 % yield). ^{1}H NMR (500 MHz, C_6D_6) δ 3.80 – 3.75 (m, 8H, O(C*H*$_2$CH$_2$)$_2$), 1.33 (s, 27H, J_{CH} = 121.6 Hz, -CH$_2$C(C*H*$_3$)$_3$), 1.25 – 1.22 (m, 8H, O(CH$_2$C*H*$_2$)$_2$), 0.62 (s, 6H, $^{1}J_{CH}$ = 99.6 Hz, -C*H*$_2$C(CH$_3$)$_3$). ^{13}C NMR (151 MHz, C_6D_6) δ 71.44 (-*C*H$_2$C(CH$_3$)$_3$), 70.55 (O(*C*H$_2$CH$_2$)$_2$), 36.07

(-$CH_2C(CH_3)_3$), 34.89 (-$CH_2C(CH_3)_3$), 25.25 ($O(CH_2CH_2)_2$). The assignments and coupling constants were determined by ^{1}H-^{13}C HSQC and ^{1}H-^{13}C HMBC experiments (see Appendix).

Synthesis of (2,5-bis(dicyclohexylphosphinomethyl) pyrrolyl) bis((trimethylsilyl)methyl)scandium (2a), (PNP-Cy)Sc($CH_2SiMe_3)_2$.

Method 1: Trimethylsilylmethyllithium (15.6 mg, 0.166 mmol) in pentane (3 mL) was added dropwise over 20 min to a stirred solution of (PNP-Cy)$ScCl_2$ (50.0 mg, 0.083 mmol) in pentane (2 mL). The reaction mixture was stirred for 14 hours and then filtered to remove lithium chloride. The filtrate was then stored at -35 °C for nine days to afford colorless crystals (11.0 mg, 20% yield).

Method 2: A solution of (PNP-Cy)H (100 mg, 0.205 mmol) in pentane (3 mL) was added to a solution of $Sc(CH_2SiMe_3)_3(THF)_2$ (92.4 mg, 0.205 mmol) in pentane (5 mL) and the reaction mixture was then stirred for 1 h. The volatile materials were removed to afford the desired product in high purity (129.5 mg, 89% yield).

^{1}H NMR (600.13 MHz, C_6D_6) δ 6.20 (s, 2H, pyr-C*H*, $^1J_{CH}$ = 163.3 Hz), 3.04 (d, $^2J_{HP}$ = 3.8 Hz, 4H, -C$H_2$$PCy_2$, $^1J_{CH}$ = 131.4 Hz), 1.92-1.85 (m, 4H, -Cy), 1.82-1.71 (m, 8H, -Cy), 1.70-1.58 (m, 8H, -Cy), 1.57-1.49 (m, 4H, -Cy), 1.38-1.27 (m, 8H, -Cy), 1.16-1.01 (m, 12H, -Cy), 0.62 (s, 4H, -C$H_2$$SiMe_3$, $^1J_{CH}$ = 100.3 Hz), 0.41 (s, 18H, -$CH_2SiC(CH_3)_3$, $^1J_{CH}$ = 117.1 Hz). ^{13}C{^{1}H} NMR (150.90 MHz, C_6D_6) δ 134.30 (t, $^2J_{CP}$ = 4.5 Hz, pyr-*C*), 106.46 (pyr-*C*H), 55.45 (br, -*C*$H_2$$SiMe_3$), 33.54, 30.04, 28.98, 27.52 (q, *J* = 4.4 Hz), 26.38, 24.50, 21.75 (d, $^1J_{CP}$ = 5.6 Hz, -*C*$H_2$$PCy_2$), 4.41 (-$CH_2Si(CH_3)_3$). ^{31}P{^{1}H} NMR (161.98 MHz, C_6D_6) δ 0.84. Anal. Calcd. for $C_{38}H_{72}NP_2ScSi_2$: C, 64.64; H, 10.28; N, 1.98. Found: C, 64.27; H, 10.02; N, 1.86. mp: 97-100 °C.

Synthesis of (2,5-bis(dicyclohexylphosphinomethyl) pyrrolyl)di(neopentyl) scandium (2b), (PNP-Cy)$ScNp_2$.

Method 1: Neopentyllithium (3.0 mg, 0.04 mmol) in toluene (3 mL) was added dropwise over 20 min to a stirred solution of (PNP-Cy)$ScCl_2$ (12.2 mg, 0.020 mmol) in toluene (2 mL). The reaction mixture was stirred for 1 h and filtered to remove lithium chloride. The toluene was removed under vacuum and pentane (2 mL) was then added to dissolve the resulting foam. This solution was then stored at -35 °C for 9 d to afford colorless crystals (6.0 mg, 45% yield).

Method 2: A solution of (PNP-Cy)H (171.0 mg, 0.351 mmol) in pentane (3 mL) was added to a solution of $ScNp_3(THF)_2$ (141.2 mg, 0.351 mmol) in pentane (5 mL) and the resulting reaction mixture was stirred for 1 h. The volatile materials were removed to afford analytically pure product (222 mg, 94% yield).

^{1}H NMR (500.23 MHz, C_6D_6) δ 6.19 (s, 2H, pyr-C*H*, $^1J_{CH}$ = 164.1 Hz), 3.05 (d, $^2J_{HP}$ = 3.7 Hz, 4H, -C$H_2$$PCy_2$, $^1J_{CH}$ = 130.5 Hz), 2.00-1.87 (m, 4H, -Cy), 1.87-1.70 (m, 9H, -Cy), 1.70-1.58 (m, 9H, -Cy), 1.58-1.50 (m, 4H, -Cy), 1.44 (s, 18H, -$CH_2CC(CH_3)_3$, $^1J_{CH}$ = 122.7 Hz), 1.43-1.31 (m, 6H, -Cy), 1.14 (s, 4H, -C$H_2$$CMe_3$, $^1J_{CH}$ = 98.9 Hz), 1.15-1.01 (m, 12H, -Cy). ^{13}C{^{1}H} NMR (150.90 MHz, C_6D_6) δ 134.38 (t, *J* = 4.3 Hz, pyr *C*), 106.33 (pyr *C*H), 84.54 (br, -*C*$H_2C(CH_3)_3$), 36.54, 36.31 (-$CH_2C(CH_3)_3$), 33.92, 31.62, 29.97, 29.08, 27.63 (t, J_{CP} = 5.0 Hz), 26.44, 22.23 (d, $^1J_{CP}$ = 6.2 Hz, -*C*H_2PCy_2). Note the resonance for the carbon directly attached to the scandium is difficult to observe, but was confirmed by a ^{1}H-^{13}C HSQC experiment (see Appendix). ^{31}P{^{1}H} NMR (161.98 MHz, C_6D_6) δ -1.28. Anal. Calcd. for $C_{40}H_{72}NP_2Sc$: C, 71.29; H, 10.77; N, 2.08. Found: C, 70.92; H, 10.95; N, 2.42.

Synthesis of (2,5-bis(di-*tert*-butylphosphinomethyl) pyrrolyl)di(neopentyl)scandium (2c), (PNP-*t*Bu)ScNp$_2$.
Method 1: Neopentyllithium (47.0 mg, 0.602 mmol) in benzene (13 mL) was added dropwise over 45 min to a stirred solution of (PNP-*t*Bu)ScCl$_2$ (150.0 mg, 0.301 mmol) in benzene (2 mL). The reaction solution changed from peach-colored to yellow over the course of the addition. The reaction mixture was allowed to stir for 8 h and filtered to remove lithium chloride. The solvent was removed under vacuum to afford a brown powder. The powder was dissolved in pentane (1.5 mL) and stored at -35 °C for 24 h to afford colorless crystals (66.0 mg, 39% yield).
Method 2: A solution of (PNP-*t*Bu)H (95.5 mg, 0.248 mmol) in pentane (3 mL) was added to a solution of ScNp$_3$(THF)$_2$ (100.4 mg, 0.248 mmol) in pentane (5 mL) and the resulting reaction mixture was stirred for 1 h. The volatile materials were removed under vacuum. Pentane (1 mL) was added to the resulting oily material and subsequently removed to afford pure product (96.4 mg, 68% yield).
^{1}H NMR (400.13 MHz, C_6D_6) δ 6.13 (s, 2H, pyr-C*H*), 3.10 (d, *J* = 3.2 Hz, 4H, -C*H*$_2$P(C(CH$_3$)$_3$)$_2$), 1.45 (s, 18H, -CH$_2$C(C*H*$_3$)$_3$), 1.26 (s, 4H, -C*H*$_2$CMe$_3$), 1.14 (d, *J* = 11.5 Hz, 36H, -CH$_2$P(C(C*H*$_3$)$_3$)$_2$). ^{13}C{^{1}H} NMR (100.61 MHz, C_6D_6) δ 134.75 (t, *J* = 4.3 Hz, pyr-*C*), 106.53 (pyr-*C*H), 87.95 (br, -*C*H$_2$C(CH$_3$)$_3$), 36.82 (-CH$_2$C(*C*H$_3$)$_3$), 36.35, 33.18, 30.14 (t, *J* = 3.0 Hz, -CH$_2$P(C(*C*H$_3$)$_3$)$_2$), 22.18 (-*C*H$_2$P(C(*C*H$_3$)$_3$)$_2$). ^{31}P{^{1}H} NMR (161.98 MHz, C_6D_6) δ 25.29. Anal. Calcd. for $C_{32}H_{64}NP_2Sc$: C, 67.46; H, 11.32; N, 2.46. Found: C, 67.63; H, 11.57; N, 2.33.

Reaction of scandium alkyl complexes with hydrogen or deuterium. A sample of **2a**, **2b**, or **2c** (14.1 mg or 13.5 mg or 11.4 mg, 0.020 mmol) was dissolved in benzene-d_6 (0.6 mL) in a 5 mm NMR tube with a Teflon screw cap. The tube was degassed to remove nitrogen, cooled to 77 K, and placed under vacuum. The tube was opened to hydrogen or deuterium at 1 atm for 2 min and then sealed. The sealed tube was allowed to warm to room temperature to attain a hydrogen (or deuterium) pressure of approximately 3.9 atm due to gas expansion. With **2a**, tetramethylsilane or tetramethylsilane-d_1 (0.040 mmol, >99% yield as determined by ^{1}H NMR spectroscopy) was produced after 12 h with hydrogen or deuterium, respectively. With **2b** or **2c**, neopentane or neopentane-d_1 (0.040 mmol, >99% yield as determined by ^{1}H NMR spectroscopy) was produced after 1 h with hydrogen or deuterium, respectively. In all cases, the scandium-containing product appeared to decompose to an intractable mixture.

Hydrogenation of 1-octene by scandium alkyl complexes. A sample of **2b**, or **2c** (13.5 mg or 11.4 mg, 0.020 mmol) and 1-octene (11.2 mg, 0.10 mmol) was dissolved in benzene-d_6 (0.6 mL) in a 5 mm NMR tube with a Teflon screw cap. The tube was degassed to remove nitrogen, cooled to 77 K, and placed under vacuum. The tube was opened to hydrogen or deuterium at 1 atm for 2 min and then sealed. The sealed tube was allowed to warm to room temperature to attain a hydrogen (or deuterium) pressure of approximately 3.9 atm due to gas expansion. After 12 hours, analysis by ^{1}H NMR spectroscopy and GC/MS showed complete conversion of 1-octene and >99% yield of *n*-octane.

Synthesis of cyclometalated scandium complex (4). A sample of 2, 6-diphenyltoluidine (43.9 mg, 0.169 mmol) in pentane (2 mL) was added to **2c** (96.4 mg, 0.169 mmol) in pentane (8 mL) and this solution was stirred for 1 h. The concentration must be at least this low to prevent formation of the bis(anilide) complex. The volatile materials were removed under vacuum to afford the anilido alkyl complex **3**. ^{1}H NMR (400.13 MHz, C_6D_6) δ 7.50 – 7.44 (m, 4H), 7.24 –

7.18 (m, 4H), 7.14 – 7.08 (m, 2H), 6.95 (s, 2H), 5.96 (s, 2H), 2.84 (dd, *J* = 15.5, 9.5 Hz, 2H, -C*H*$_2$P(C(CH$_3$)$_3$)$_2$), 2.54 (d, *J* = 15.5 Hz, 2H, -C*H*$_2$P(C(CH$_3$)$_3$)$_2$), 2.17 (s, 3H, ArC*H*$_3$), 2.11 (s, 1H, -N*H*Ar), 1.15 (d, *J* = 12.1 Hz, 18H, -CH$_2$P(C(C*H*$_3$)$_3$)$_2$), 1.09 (d, *J* = 11.3 Hz, 18H, -CH$_2$P(C(C*H*$_3$)$_3$)$_2$), 1.00 (s, 9H, -CH$_2$C(C*H*$_3$)$_3$), 0.82 (d, *J* = 2.2 Hz, 2H, -C*H*$_2$CMe$_3$). ^{31}P{^{1}H} NMR (161.98 MHz, C_6D_6) δ 25.26. This material began to very slowly cyclometalate in the 2-position of an arm of the terphenyl at room temperature. Heating the material to 60 °C for 1 h resulted in the clean formation of **4** with production of neopentane. This material was isolated by removal of all volatile materials under vacuum (96.0 mg, 83% yield). ^{1}H NMR (500 MHz, C_6D_6) δ 7.86 (dd, *J* = 6.8, 1.6 Hz, 1H), 7.83 (d, *J* = 8.0 Hz, 1H, *o*-Ar*H* of metalated phenyl group), 7.69 (d, *J* = 2.2 Hz, 1H), 7.59 (dd, *J* = 7.9, 1.2 Hz, 2H, *o*-Ar*H* of non-metalated phenyl group), 7.37 – 7.24 (m, 4H), 7.21 (s br, 1H), 7.10 (d, *J* = 2.2 Hz, 1H), 6.22 (s, 2H, pyr-C*H*), 3.13 (dd, *J* = 16.3, 3.8 Hz, 2H, -C*H*$_2$PC(CH$_3$)$_2$), 2.90 (dd, *J* = 16.2, 7.5 Hz, 2H, -C*H*$_2$PC(CH$_3$)$_2$), 2.35 (s, 3H, ArC*H*$_3$), 2.23 (s, 1H, -N*H*Ar), 0.92 (d, *J* = 12.4 Hz, 18H, -CH$_2$PC(C*H*$_3$)$_2$), 0.84 (d, *J* = 12.2 Hz, 18H, -CH$_2$PC(C*H*$_3$)$_2$). ^{13}C NMR (151 MHz, C_6D_6) δ 148.14, 147.86, 143.50, 136.33 (t, *J* = 5.3 Hz), 133.10, 131.90, 131.46, 130.55, 130.17, 129.81, 129.26, 128.97, 128.73, 128.55, 126.67, 124.95, 123.94, 107.05 (t, *J* = 4.2 Hz), 35.70, 32.70, 31.63, 29.44 (dt, *J* = 26.4, 3.3 Hz), 21.81 (d, *J* = 3.9 Hz), 21.02. ^{31}P NMR (202 MHz, C_6D_6) δ 29.00 (s br). Anal. Calcd. for $C_{41}H_{57}N_2P_2Sc$: C, 71.91; H, 8.39; N, 4.09. Found: C, 72.27; H, 8.07; N, 3.76.

Synthesis of 2,6-diphenyltoluidine-*N*-*d*$_2$. 2,6-diphenyltoluidine (125 mg, 0.482 mmol) was dissolved in MeCN (2 mL), and D_2O (0.6 mL) was added to this solution. The solvent was removed under vacuum to afford the product as a slightly yellow oil (125 mg, 99 % yield). The NMR spectra of the product are identical to those of 2,6-diphenyltoluidine except that the -NH$_2$ resonance is absent from the ^{1}H NMR spectrum and present in the ^{2}H NMR spectrum: ^{2}H NMR (92 MHz, C_6D_6) δ 3.39 (s br).

Deuterium-labeling study of cyclometalation of 2,6-diphenyltoluidine. 2,6-diphenyltoluidine-*N*-*d*$_2$ (3.3 mg, 0.0126 mmol) was dissolved in benzene-*d*$_6$ (0.3 mL) and added to a solution of **2c** (7.2 mg, 0.0126 mmol) in benzene-*d*$_6$ (0.5 mL) in a 5 mm NMR tube with a Teflon screw cap. Formation of **3-*d*$_2$** was apparent by ^{1}H NMR spectroscopy, resulting in the same spectrum as **3** except the absence of the resonance at δ 2.11, which is assignable as the -NH resonance. Neopentane-*d*$_1$ was observed in the ^{1}H NMR spectrum as 1:1:1 triplet at δ 0.89 and in the ^{2}H{^{1}H} NMR spectrum as a singlet at δ 0.87. The volatile materials were removed from the NMR tube by vacuum transfer and fresh benzene-*d*$_6$ was added. The sample was heated to 60 °C for 1 h, resulting in the formation of **4-*d*$_1$** and neopentane quantitatively by ^{1}H and ^{2}H NMR spectroscopy.

Reaction of 4 with deuterium. A sample of **4** (7.0 mg, 0.01 mmol) was dissolved in benzene-*d*$_6$ (0.8 mL) in a 5mm NMR tube with a Teflon screw cap. The tube was degassed to remove nitrogen, cooled to 77 K, and placed under vacuum. Deuterium at 1 atm was admitted into the tube for 2 min and the tube was then sealed. The sealed tube was allowed to warm to room temperature to attain a deuterium pressure of approximately 3.9 atm due to gas expansion. The sample was heated to 60 °C at which point deuterium was observed to scramble into all *ortho*-positions on the terphenyl arms (the phenyl groups), by selective loss of the resonance corresponding to these *ortho* hydrogens in the ^{1}H NMR spectrum over the course of 5 h.

Synthesis of cyclometalated scandium bis(DMAP) complex (5). A solution of 4-dimethylaminopyridine (25.8 mg, 0.211 mmol) in pentane (5 mL) was added to **3** (80 mg, 0.108 mmol) in pentane (5 mL). This led to the rapid formation (~10 min) of the cyclometalated complex. Concentration of the reaction mixture to 1 mL and cooling to -35 °C resulted in 80 mg of yellow crystalline product. Single crystals suitable for X-ray diffraction could be obtained by recrystallization from pentane. ^{1}H NMR (600 MHz, C_6D_6, 45 °C) δ 8.25 (s br, 4H), 7.89 (d, *J* = 7.9 Hz, 1H), 7.71 (d, *J* = 7.6 Hz, 2H), 7.66 (s br, 1H), 7.49 (s br, 1H), 7.36 (t, *J* = 7.6 Hz, 2H), 7.31 (t, *J* = 7.6 Hz, 1H), 7.14 – 7.10 (m, 2H), 7.07 – 6.91 (m, 3H), 6.86 (s, 1H), 6.65 (s br, 2H), 5.85 (d, *J* = 6.1 Hz, 2H), 3.18 (s br, 4H, -C*H*$_2$PC(CH$_3$)$_2$), 2.27 (s, 3H, ArC*H*$_3$), 2.15 (s, 12H, pyr-N(C*H*$_3$)$_2$), 1.06 (d, *J* = 10.8 Hz, 36H, -CH$_2$PC(C*H*$_3$)$_2$). (600 MHz, C_6D_6, 20 °C) δ 7.71 (s br, 2H), 7.53 (s br, 2H), 7.40 (s br, 3H), 7.26 (s br, 2H), 7.12 (s, 1H), 7.10 – 7.04 (m, 2H), 7.03 – 6.93 (m, 4H), 6.89 (br s, 1H), 5.95 (s, 2H), 2.83 (dd, *J* = 15.5, 9.3 Hz, 2H, -C*H*$_2$PC(CH$_3$)$_2$), 2.54 (d, *J* = 15.4 Hz, 2H, -C*H*$_2$PC(CH$_3$)$_2$), 2.17 (s, 3H, ArC*H*$_3$), 1.15 (d, *J* = 11.9 Hz, 18H, -CH$_2$PC(C*H*$_3$)$_2$), 1.09 (d, *J* = 11.0 Hz, 18H, -CH$_2$PC(C*H*$_3$)$_2$). ^{13}C NMR (151 MHz, C_6D_6, 45 °C) δ 154.59, 151.12, 145.15, 137.91, 136.19 (t, *J* = 5.1 Hz), 134.08, 133.19, 131.84, 131.08, 130.67, 130.50, 129.33, 129.04, 129.00, 128.55, 126.20, 126.14, 125.69, 123.29, 106.28, 38.23, 32.32 (d, *J* = 15.3 Hz), 30.39 (d, *J* = 10.5 Hz), 21.40, 21.09. ^{31}P NMR (202 MHz, C_6D_6) δ 24.00 (s br). Anal. Calcd. for $C_{55}H_{77}N_6P_2Sc$: C, 71.10; H, 8.35; N, 9.04. Found: C, 70.87; H, 8.30; N, 9.07.

Synthesis of (2,5-bis(dicyclohexylphosphinomethyl) pyrrolyl)bis(*iso*-propylacetylide) scandium (6a), (PNP-Cy)Sc(C≡CCHMe$_2$)$_2$. A sample of **2b** (75.0 mg, 0.111 mmol) was dissolved in benzene-d_6 (0.6 mL) in a 5mm NMR tube with a Teflon screw cap and *iso*-propylacetylene (22 mg, 0.222 mmol) was added. After 10 min, the reaction mixture had converted to (PNP-Cy)Sc(C≡CCHMe$_2$)$_2$ and neopentane (>99% yield as determined by ^{1}H NMR spectroscopy). The volatile materials were removed by vacuum transfer and the resulting solid was recrystallized from pentane at -35 °C over 1 d (50.4 mg, 67% yield). ^{1}H NMR (600 MHz, C_6D_6) δ 6.01 (s, 2H, pyr-C*H*), 3.01 (d, *J* = 5.0 Hz, 4H, -C*H*$_2$PCy$_2$), 2.62 (hept, *J* = 6.8 Hz, 2H, -CCC*H*Me$_2$), 2.50 – 2.34 (m, 4H, -Cy), 2.18 – 2.03 (m, 8H, -Cy), 1.89 – 1.76 (m, 13H, -Cy), 1.75 – 1.66 (m, 7H, -Cy), 1.64 – 1.49 (m, 12H, -Cy), 1.25 (d, *J* = 6.8 Hz, 12H, -CCCH(C*H*$_3$)$_2$). ^{13}C NMR (150.90 MHz, C_6D_6) δ 135.64 (t, *J* = 3.5 Hz), 105.61 (d, *J* = 6.0 Hz), 33.13 (t, *J* = 4.4 Hz), 29.85, 29.22, 28.23 (dd, *J* = 22.2, 9.0 Hz), 27.73 – 27.24 (m), 26.92, 26.43, 24.27, 23.15 (d, *J* = 8.0 Hz) Note that the resonance for the carbon directly attached to the scandium was not observed. This effect is a common feature of scandium alkyl compounds, owing to the large quadrupole moment of ^{45}Sc (100% abundance, I=7/2, -0.22 barns)[28,29]. ^{31}P NMR (202 MHz, C_6D_6) δ 3.34. Anal. Calcd. for $C_{40}H_{64}NP_2Sc$: C, 72.15; H, 9.69; N, 2.10. Found: C, 71.92; H, 9.57; N, 2.03.

Synthesis of (2,5-bis(di-*tert*-butylphosphinomethyl) pyrrolyl)bis(*iso*-propylacetylide) scandium (6b), (PNP-*t*Bu)Sc(C≡CCHMe$_2$)$_2$. A sample of **2c** (11.4 mg, 0.020 mmol) was dissolved in benzene-d_6 (0.6 mL) in a 5mm NMR tube with a Teflon screw cap and *iso*-propylacetylene (20 mL, 0.2 mmol) was added. After 44 h, the reaction mixture had converted to (PNP-tBu)Sc(C≡CCHMe$_2$)$_2$ and neopentane (>99% yield as determined by ^{1}H NMR spectroscopy). ^{1}H NMR (400.13 MHz, C_6D_6) δ 6.17 (s, 2H, pyr-C*H*), 3.09 (d, *J* = 6.0 Hz, 4H, -C*H*$_2$P(C(CH$_3$)$_3$)$_2$), 2.53 (hept, *J* = 6.8 Hz, 2H, -CCC*H*Me$_2$), 1.31 (d, *J* = 12.3 Hz, 36H, -CH2P(C(C*H*$_3$)$_3$)$_2$), 1.17 (d, *J* = 6.8 Hz, 12H, -CCCH(C*H*$_2$)$_2$). ^{13}C{^{1}H} NMR (100.61 MHz, C_6D_6)

δ 136.38, 106.50, 100.27, 33.15, 29.74, 23.84, 21.45, 21.22. The carbon of the acetylide attached to the scandium was not observed. $^{31}P\{^{1}H\}$ NMR (161.98 MHz, C_6D_6) δ 28.51.

Thermolysis of 2b. A sample of **2b** (12.2 mg) was dissolved in toluene-d_8 (0.8 mL) in a 5 mm NMR tube with a Teflon screw cap. This sample was heated to 100 °C for 5 days. Approximately 0.1 equivalents of cyclohexene were observed to be formed by ^{1}H NMR spectroscopy.

Thermolysis of 2c. A sample of **2c** (10.8 mg) was dissolved in benzene-d_6 (0.8 mL) in a 5 mm NMR tube with a Teflon screw cap. This sample was heated to 60 °C for 24 h. Approximately 1 equiv of isobutylene and 2 equiv of neopentane were observed to be formed by ^{1}H NMR spectroscopy.

Synthesis of $ScNp_3(THF)_2$-d_6. Neopentyllithium-d_2 (at α position) (16.3 mg, 0.20 mmol) was dissolved in pentane (3 mL) and added dropwise to a stirred suspension of $ScCl_3(THF)_2$ (25.0mg, 0.068 mmol) in pentane (5 mL). The reaction mixture became cloudy and produced a white precipitate. After stirring for 4 h, the reaction mixture was filtered to remove LiCl. The volatile materials were removed from the filtrate by vacuum (22.4 mg, 81 % yield). The material showed the same NMR spectra as $ScNp_3(THF)_2$, except for the absence of the resonance at 0.62 ppm from the ^{1}H NMR spectrum and the appearance of a resonance in the ^{2}H NMR spectrum at δ 0.62 (s).

Synthesis of (2,5-bis(di-*tert*-butylphosphinomethyl) pyrrolyl)di(neopentyl)scandium-d_4 (2c-d_4), (PNP-*t*Bu)$ScNp_2$-d_4. A solution of (PNP-*t*Bu)H (8.4 mg, 0.024 mmol) in pentane (3 mL) was added to a solution of $ScNp_3(THF)_2$-d_6 (9.5 mg, 0.024 mmol) in pentane (5 mL) and the resulting reaction mixture was stirred for 1 h. The volatile materials were removed under vacuum. The material showed the same NMR spectra as **2c**, except for the absence of the resonance at 1.26 ppm from the ^{1}H NMR spectrum and the appearance of a resonance in the ^{2}H NMR spectrum at δ 1.26 (s).

Thermolysis of 2c-d_4. A sample of **2c-d_4** (13.4 mg, 0.023 mmol) was dissolved in benzene-d_6 (0.8 mL) in a 5 mm NMR tube with a Teflon screw cap. This sample was heated to 60 °C for 24 h. Approximately 1 equiv of isobutylene and 2 equiv of neopentane-d_2 were observed to be formed by ^{1}H NMR spectroscopy.

Synthesis of (2,5-bis(dicyclohexylphosphinomethyl) pyrrolyl)di(phenyl) scandium (7), (PNP-Cy)$ScPh_2$. Phenyllithium (16.7 mg, 0.199 mmol) was dissolved in benzene (8 mL) and diethyl ether (2 mL) and added dropwise (1 drop/6 second, the slow rate was necessary to obtain high yield) to a sample of **1a** (60.0 mg, 0.0996 mmol) in benzene (2 mL). The reaction mixture was stirred for 2 h and then filtered through a fritted funnel. The volatiles were removed and pentane (1 mL) was added to dissolve the product. Removal of solvent afforded the desired product as a white foam (49.1 mg, 72% yield). ^{1}H NMR (500 MHz, C_6D_6) δ 8.30 (d, J = 6.8 Hz, 4H), 7.42 (t, J = 7.2 Hz, 4H), 7.32 (t, J = 7.3 Hz, 2H), 6.35 (s, 2H, pyr-C*H*), 3.15 (d, J = 4.7 Hz, 4H, - CH_2PCy_2), 1.71 – 1.26 (m, 24H, -Cy), 1.14 – 0.73 (m, 20H, -Cy). ^{13}C NMR (126 MHz, C_6D_6) δ 135.44 (br), 133.90, 128.59, 127.97, 127.14, 106.76, 33.44 (m), 29.27, 28.63, 27.42 (m), 27.26 (m), 26.12, 22.41 (m). $^{31}P\{^{1}H\}$ NMR (202 MHz, C_6D_6) δ 1.71.

REFERENCES

(1) Arndtsen, B. A.; Bergman, R. G.; Mobley, T. A.; Peterson, T. H. *Acc. Chem. Res.* **1995**, *28*, 154-162.
(2) Bergman, R. G. *Nature* **2007**, *446*, 391-393.
(3) Scott, J.; Basuli, F.; Fout, A. R.; Huffman, J. C.; Mindiola, D. J. *Angew. Chem. Int. Ed.* **2008**, *47*, 8502-8505.
(4) (a) Flores, J. A, Cavaliere, V. N.; Buck, D.; Pinter, B.; Chen, G.; Crestani, M. G.; Bail, M.; Mindiola, D. J. *Chem. Sci.* **2011**, *2*, 1457-1462. (b) Konnick, M. M.; Hashiguchi, B. G.; Devaraja, D.; Boaz, N. C.; Gunnoe, T. B.; Groves, J. T.; Gunsalus, N.; Ess, D. H.; Periana, R. A. *Angew. Chem. Int. Ed.* **2014**, *53*, 10490-10494.
(5) Labinger, J. A.; Bercaw, J. E. *Nature* **2002**, *417*, 507-514.
(6) Crabtree, R. H. *J. Chem. Soc., Dalton Trans.* **2001**, 2437-2450.
(7) Balcells, D.; Clot, E.; Eisenstein, O. *Chem. Rev.* **2010**, *110*, 749–823.
(8) Ziegler, T.; Folga, E.; Berces, A. *J. Am. Chem. Soc.* **1993**, *115*, 636-646.
(9) Balcells, D.; Clot, E.; Eisenstein, O. *Chem. Rev.* **2010**, *110*, 749-823.
(10) (a) Tsurugi, H.; Yamamoto, K.; Nagae, H.; Kaneko, H. & Mashima, K. *Dalton Trans.* **2013**, *43*, 2331-2343. (b) Waterman, R. *Organometallics*, **2013**, *32*, 7249-7263.
(11) Watson, P. L. *J. Am. Chem. Soc.* **1983**, *105*, 6491-6493.
(12) Watson, P. L. *J. Chem. Soc., Chem. Commun.* **1983**, 276-277.
(13) Thompson, M. E.; Baxter, S. M.; Bulls, A. R.; Burger, B. J.; Nolan, M. C.; Santarsiero, B. D.; Schaefer, W. P.; Bercaw, J. E. *J. Am. Chem. Soc.* **1987**, *109*, 203-219.
(14) (a) Castillo, I.; Tilley, T. D. *Organometallics* **2001**, *20*, 5598-5605. (b) Sadow, A. D.; Tilley, T. D. *J. Am. Chem. Soc.* **2003**, *125*, 7971-7977. (c) Sadow, A. D.; Tilley, T. D. *Organometallics* **2003**, *22*, 3577-3585. (d) Sadow, A. D.; Tilley, T. D. *Angew. Chem. Int. Ed.* **2003**, *42*, 803-805. (e) Sadow, A. D.; Tilley, T. D. *J. Am. Chem. Soc.* **2005**, *127*, 643-656.
(15) Piers, W. E.; Emslie, D. *J. Coord. Chem. Rev.* **2002**, *233-234*, 131-155.
(16) (a) Venkanna, G. T.; Tammineni, S.; Arman, H. D.; Tonzetich, Z. J. *Organometallics* **2013**, *32*, 4656-4663. (b) Venkanna, G. T.; Arman, H. D.; Tonzetich, Z. J. *ACS Catalysis*, **2014**, *4*, 2941-2950. (c) Kreye, M.; Freytag, M.; Jones, P. G.; Williard, P. G.; Bernskoetter, W. H.; Walter, M. D. *Chem. Comm.* **2015**, *51*, 2946-2949.
(17) Barros, N.; Eisenstein, O.; Maron, L.; Tilley, T. D. *Organometallics* **2006**, *25*, 5699-5708.
(18) Watson, P. L.; Parshall, G. W. *Acc. Chem. Res.* **1985**, *18*, 51-56.
(19) Miller, T. M. Atomic and Molecular Polarizabilities. In *CRC Handbook of Chemistry and Physics*, 89th ed.; Lide, D. R., Ed.; CRC Press: Boca Raton, FL, 2008-2009; p 10-193-10-194.
(20) (a) Fryzuk, M. D.; Haddad, T. S.; Rettig, S. J. *Organometallics* **1991**, *10*, 2026-2036. (b) Fryzuk, M. D.; Giesbrecht, G.; Rettig, S. J. *Organometallics* **1996**, *15*, 3329-3336. (c) Fryzuk, M. D.; Love, J. B.; Rettig, S. J.; Young, V. G. *Science* **1997**, *275*, 1445-1447. (d) Cohen, J. D.; Fryzuk, M. D.; Loehr, T. M.; Mylvaganam, M.; Rettig, S. J. *Inorg. Chem.* **1998**, *37*, 112-119. (e) Fryzuk, M. D.; Love, J. B.; Rettig, S. J. *Organometallics* **1998**, *17*, 846-853. (f) Fryzuk, M. D.; Jafarpour, L.; Kerton, F. M.; Love, J. B.; Patrick, B. O.; Rettig, S. J. *Organometallics* **2001**, *20*, 1387-1396.
(21) (a) Scott, J.; Fan, H.; Wicker, B. F.; Fout, A. R.; Baik, M.-H.; Mindiola, D. J. *J. Am. Chem. Soc.* **2008**, *130*, 14438-14439. (b) Wicker, B. F.; Fan, H.; Hickey, A. K.; Crestani, M. G.; Scott, J.; Pink, M.; Mindiola, D. J. *J. Am. Chem. Soc.* **2012**, *134*, 20081-20096. (c) Cheng, J.; Shima, T.; Hou, Z. *Angew. Chem. Int. Ed.* **2011**, *50*, 1857-1860.

(22) Kumar, S.; Mani, G.; Mondal, S.; Chattaraj, P. K. *Inorg. Chem.* **2012**, *51*, 12527-12539.
(23) Lappert, M. F.; Pearce, R. *J. Chem. Soc., Chem. Commun.* **1973**, *4*, 126.
(24) Jeske, G.; Lauke, H.; Mauermann, H.; Schumann, H.; Marks, T. J. *J. Am. Chem. Soc.* **1985,** *107*, 8111-8118
(25) Bachman, G. B.; Heisey, L. V. *J. Am. Chem. Soc.* **1946**, *68*, 2496-2499.
(26) Manzer, L. E.; Deaton, J.; Sharp, P.; Schrock, R. R. In *Inorganic Syntheses*; Jr, J. P. F., Ed.; John Wiley & Sons, Inc., 1982; p 135-140.
(27) Fellman, J. D, Schrock, R. R. *J. Am. Chem. Soc.* **1978**, *100*, 3359-3370.
(28) Thompson, M. E.; Baxter, S. M.; Bulls, A. R.; Burger, B. J.; Nolan, M. C.; Santarsiero, B. D.; Schaefer, W. P.; Bercaw, J. E. *J. Am. Chem. Soc.* **1987**, *109*, 203-219.
(29) St. Clair, M.; Schaefer, W. P.; Bercaw, J. E. *Organometallics* **1991**, *10*, 525-527.

Chapter 1 Appendix

Spectroscopic Characterization

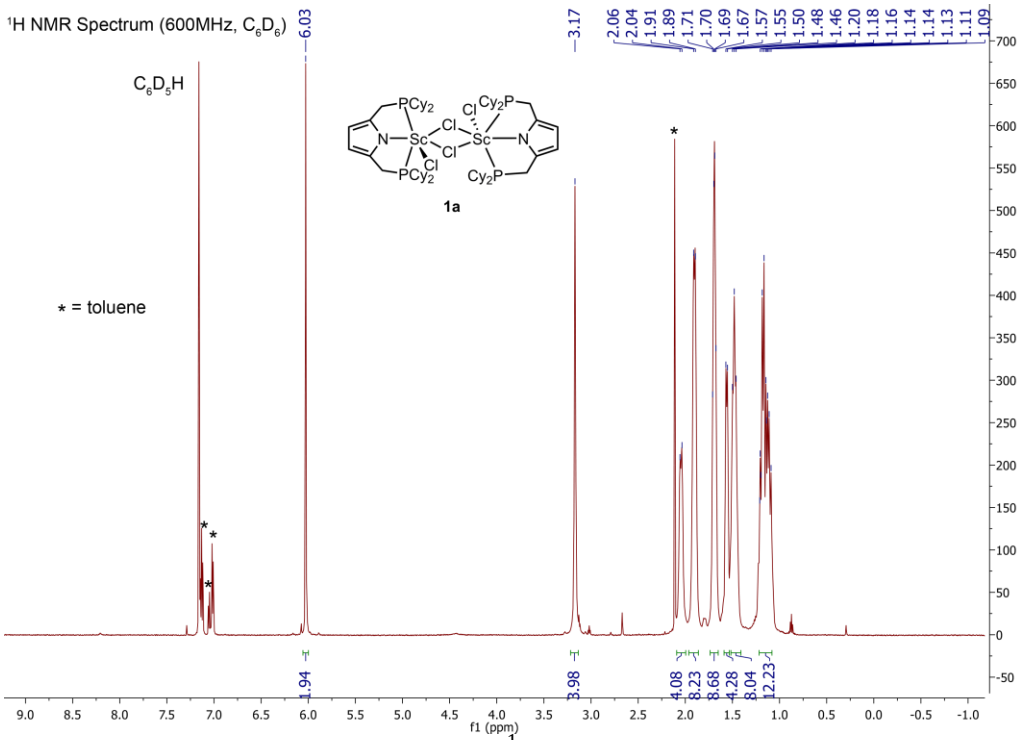

$[(PNP\text{-}Cy)ScCl_2]_2$ ^1H NMR Spectrum.

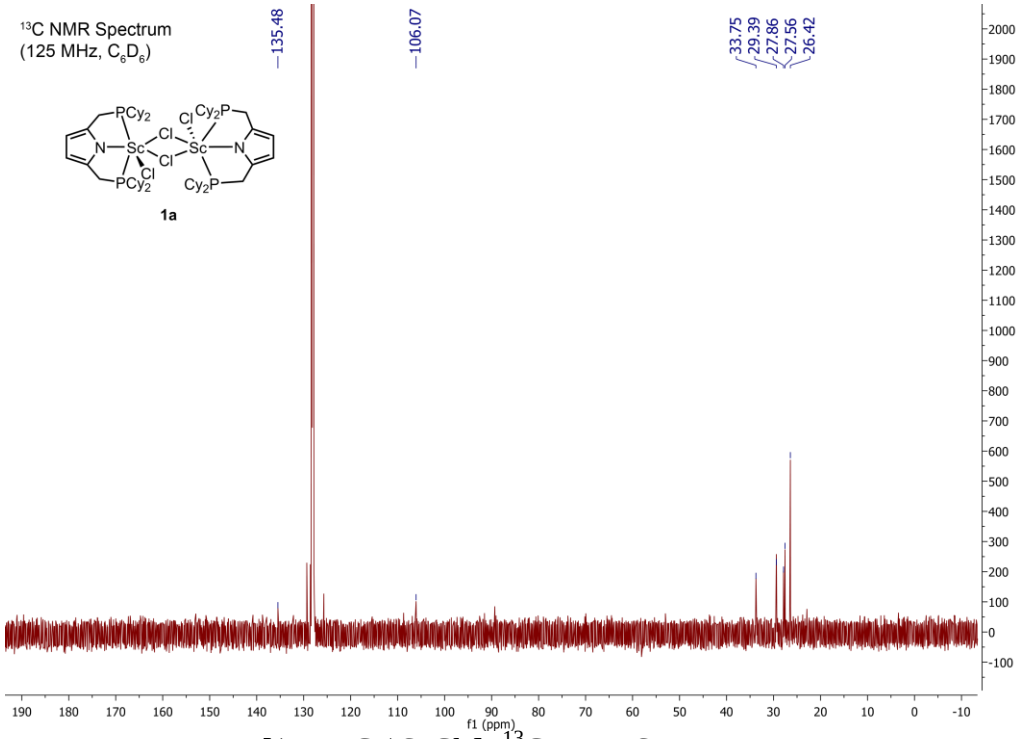

$[(PNP\text{-}Cy)ScCl_2]_2$ ^{13}C NMR Spectrum.

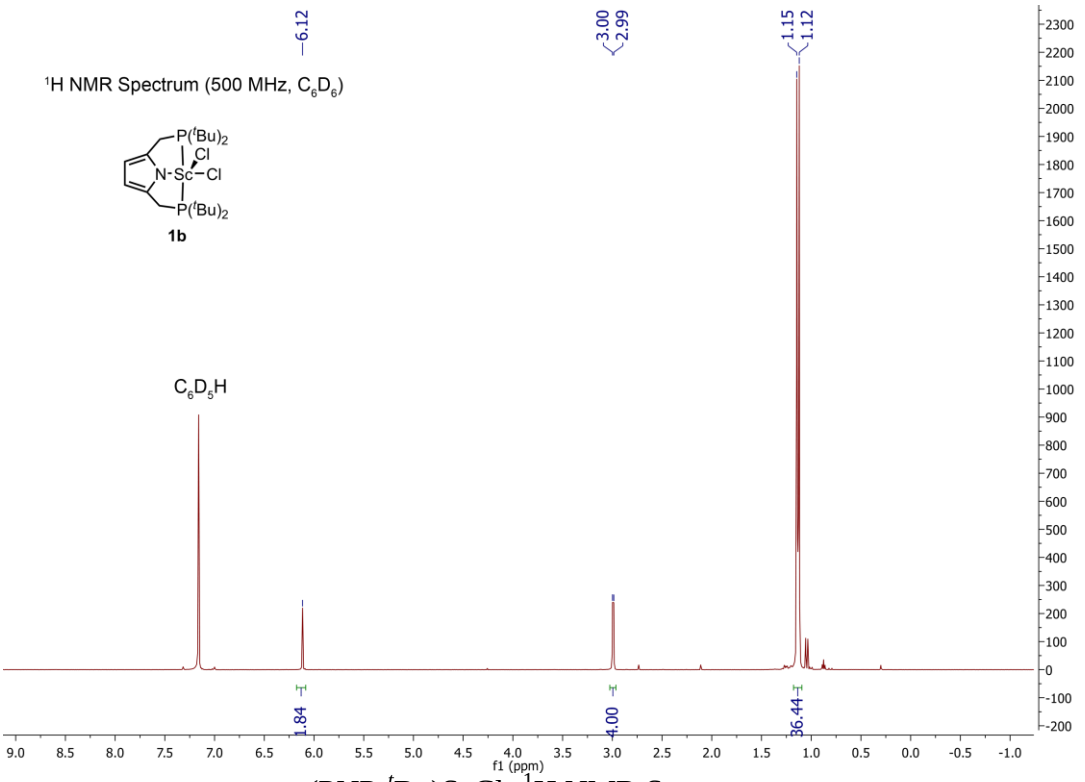

(PNP-^{t}Bu)ScCl$_2$ ^{1}H NMR Spectrum.

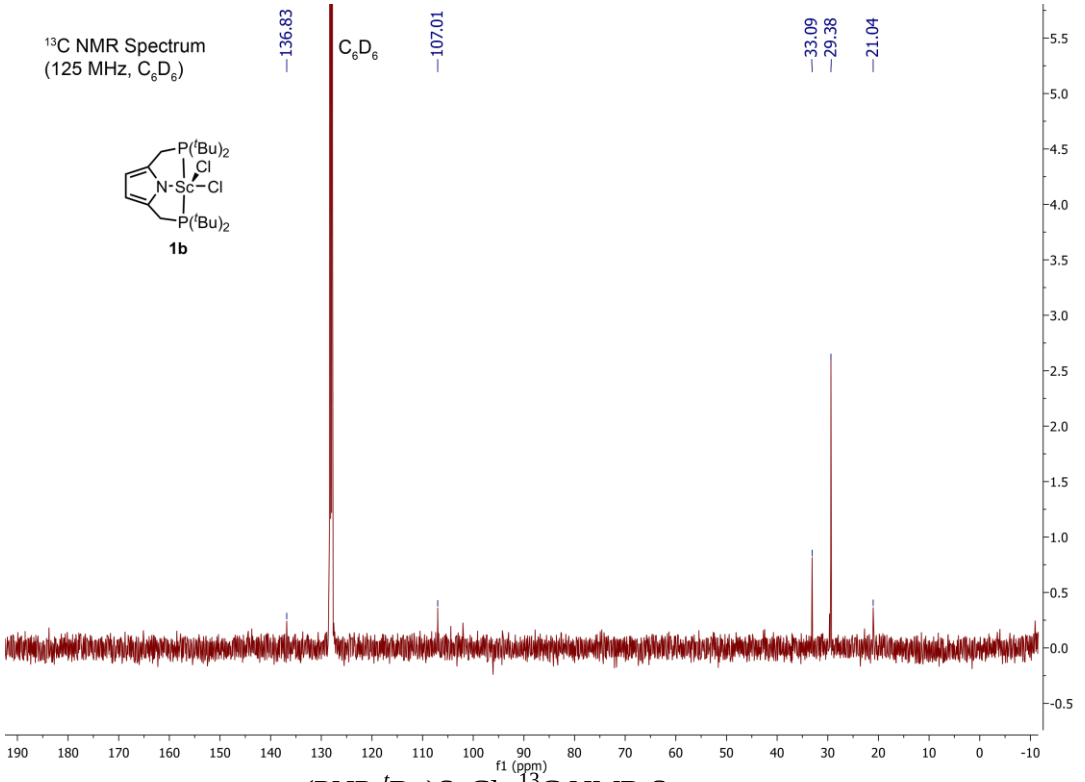

(PNP-^{t}Bu)ScCl$_2$ ^{13}C NMR Spectrum.

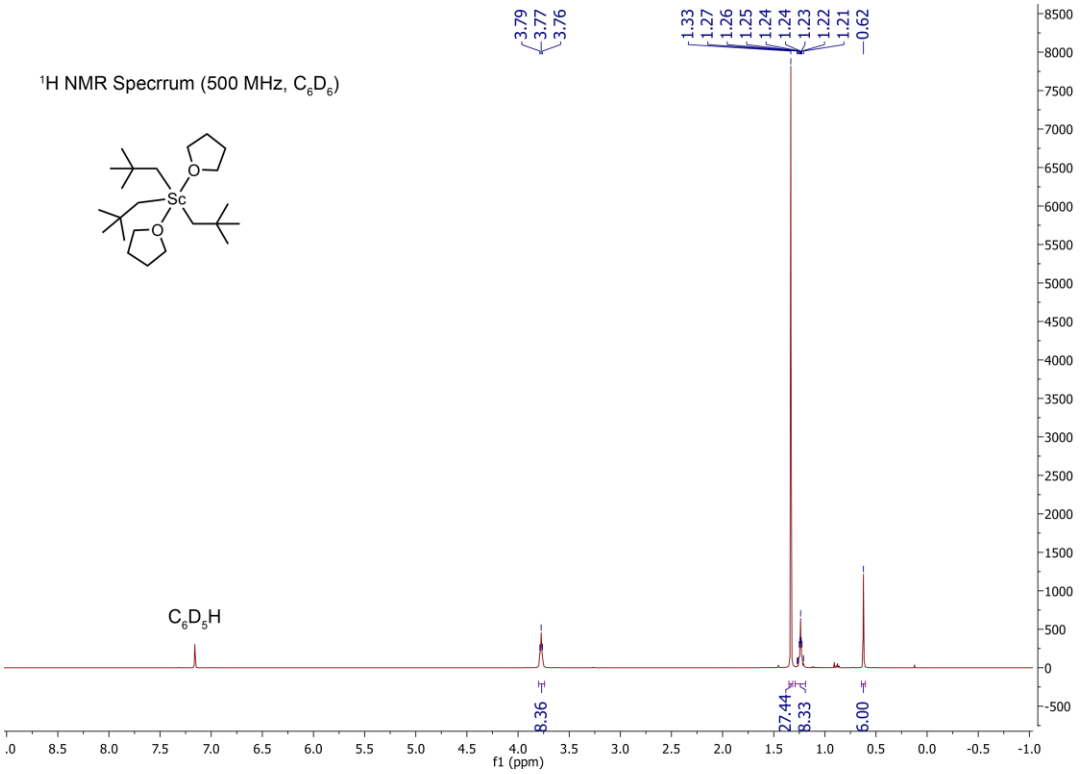

$ScNp_3(THF)_3$ ^{1}H NMR Spectrum.

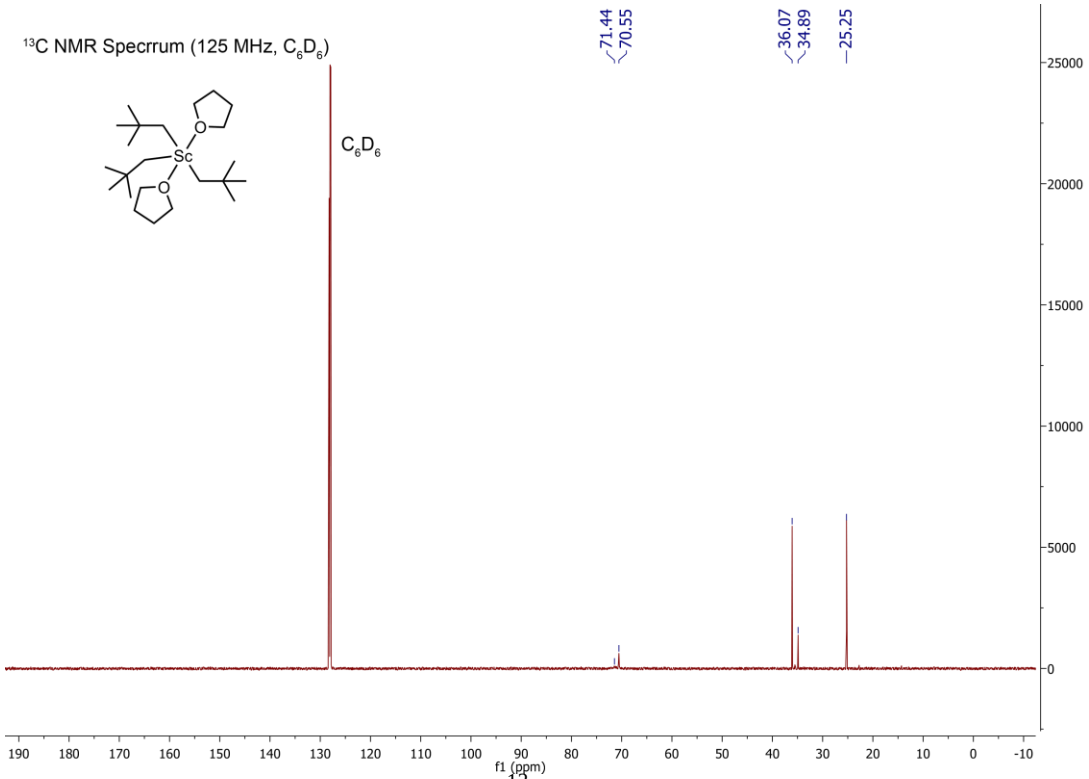

$ScNp_3(THF)_3$ ^{13}C NMR Spectrum.

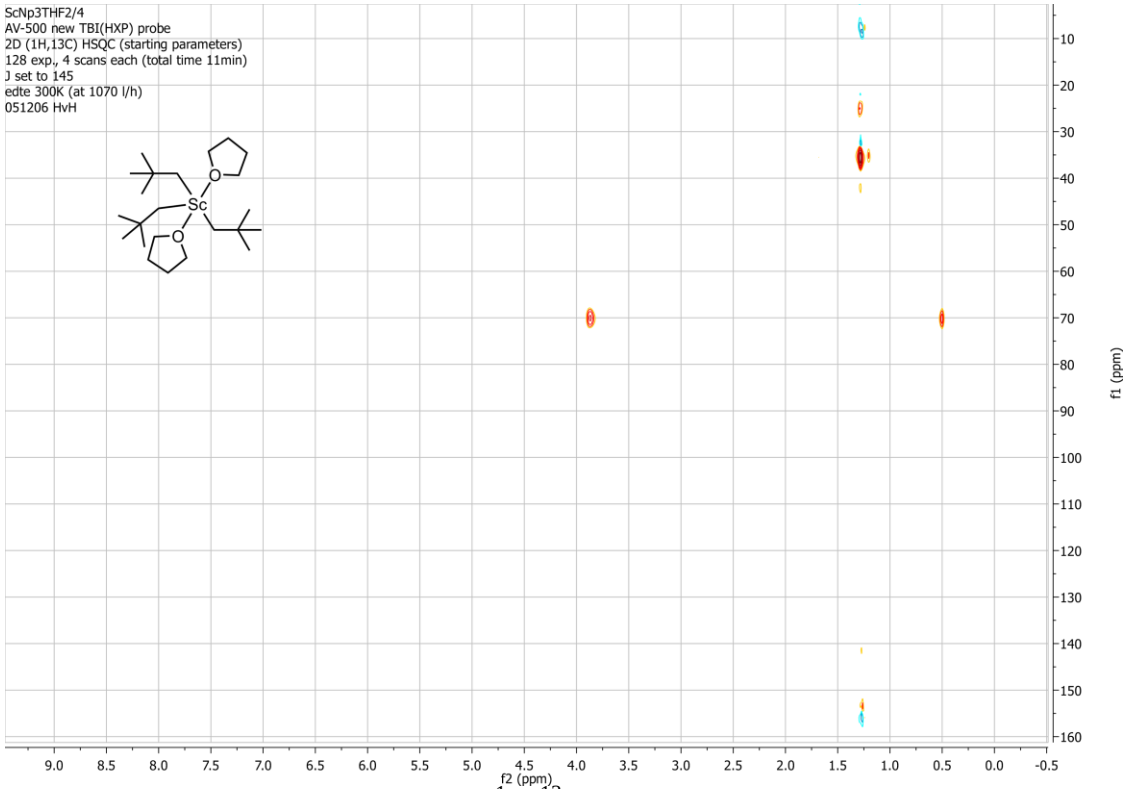

$ScNp_3(THF)_3$ ^{1}H-^{13}C HSQC Spectrum.

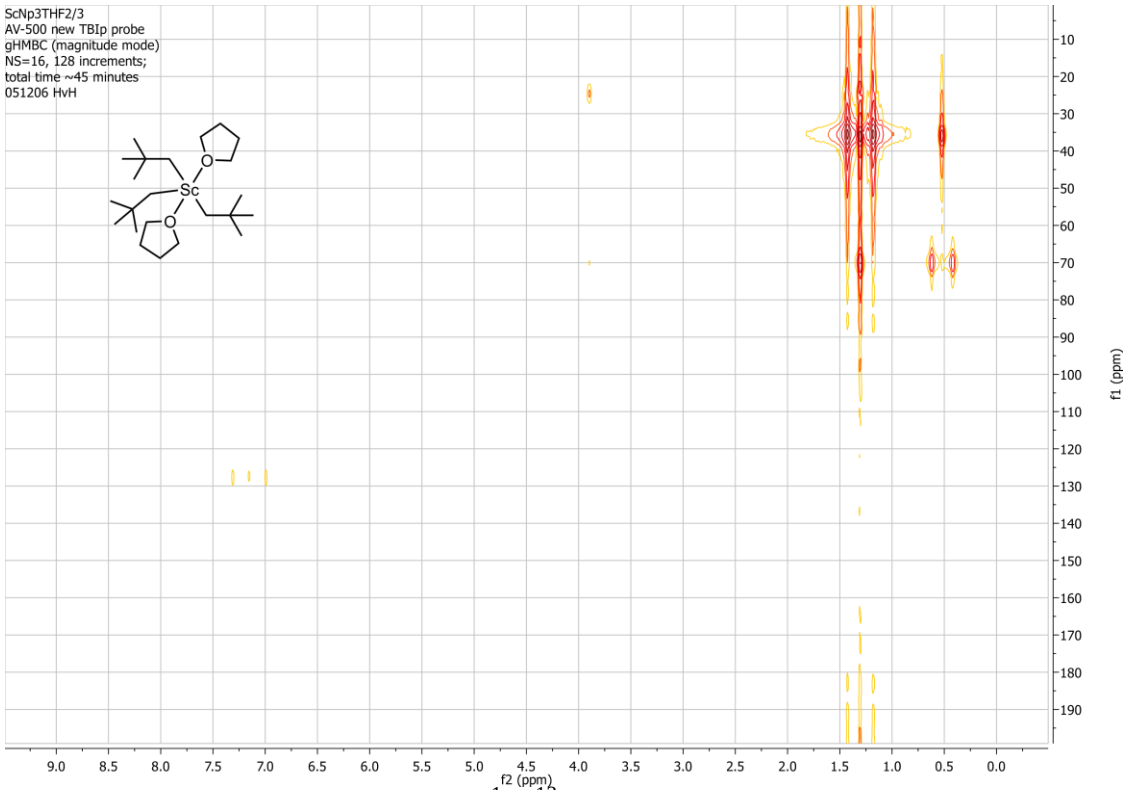

$ScNp_3(THF)_3$ ^{1}H-^{13}C HMBC Spectrum.

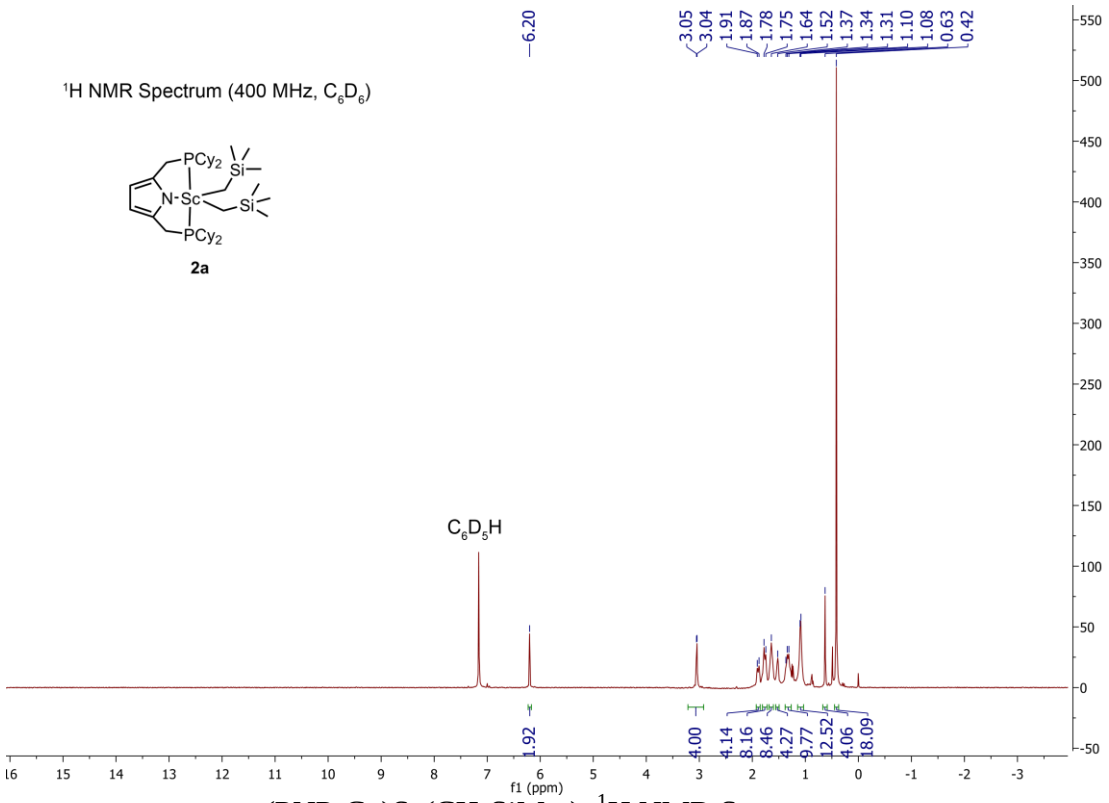

$(PNP\text{-}Cy)Sc(CH_2SiMe_3)_2$ ^{1}H NMR Spectrum.

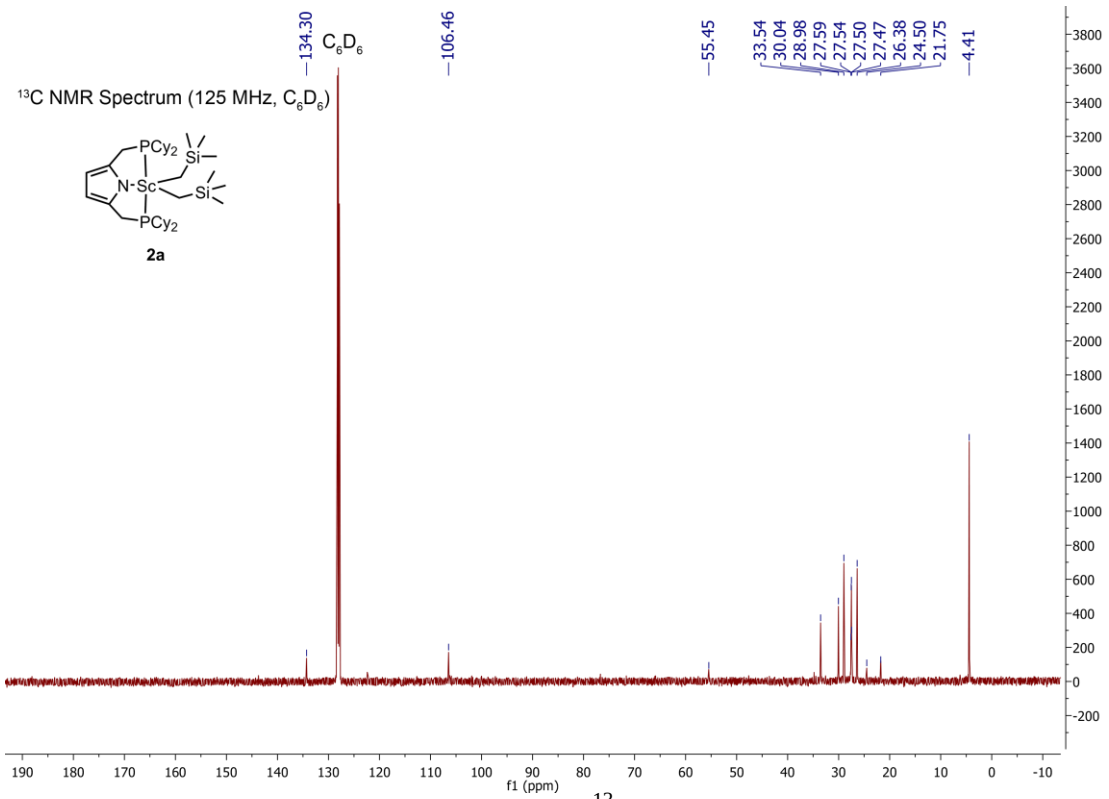

$(PNP\text{-}Cy)Sc(CH_2SiMe_3)_2$ ^{13}C NMR Spectrum.

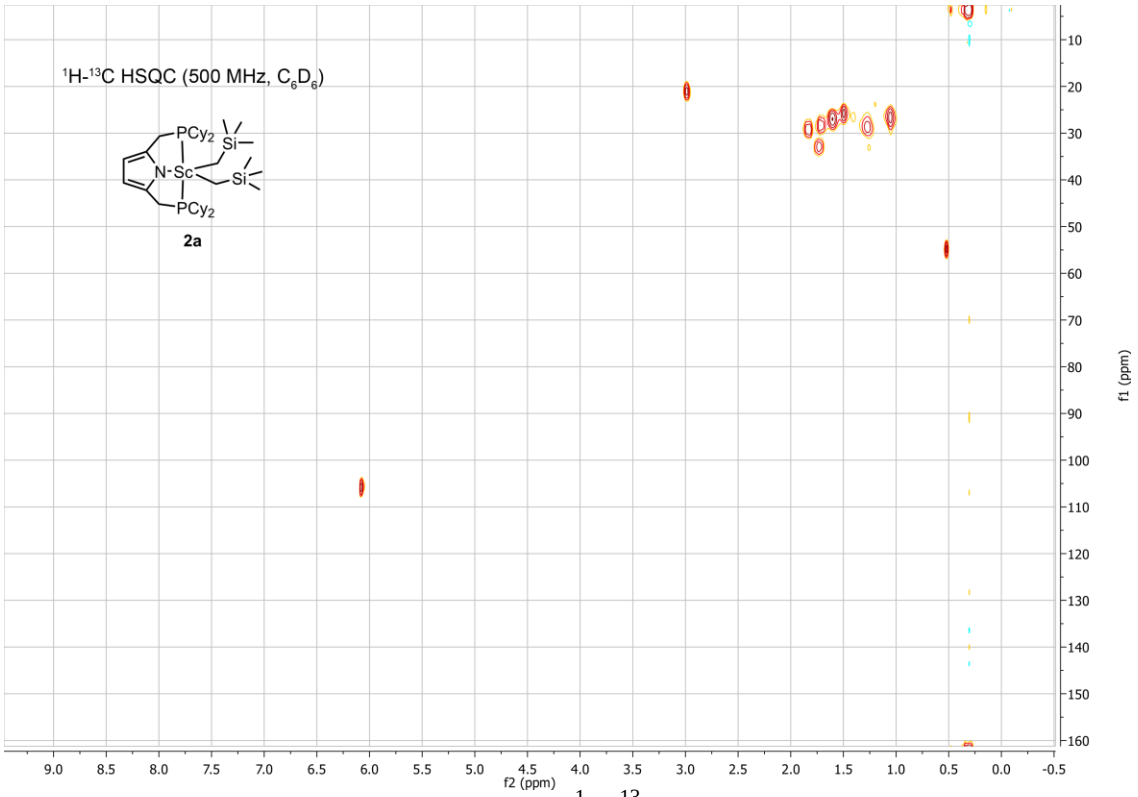

(PNP-Cy)Sc(CH_2SiMe_3)$_2$ ^{1}H-^{13}C HSQC Spectrum.

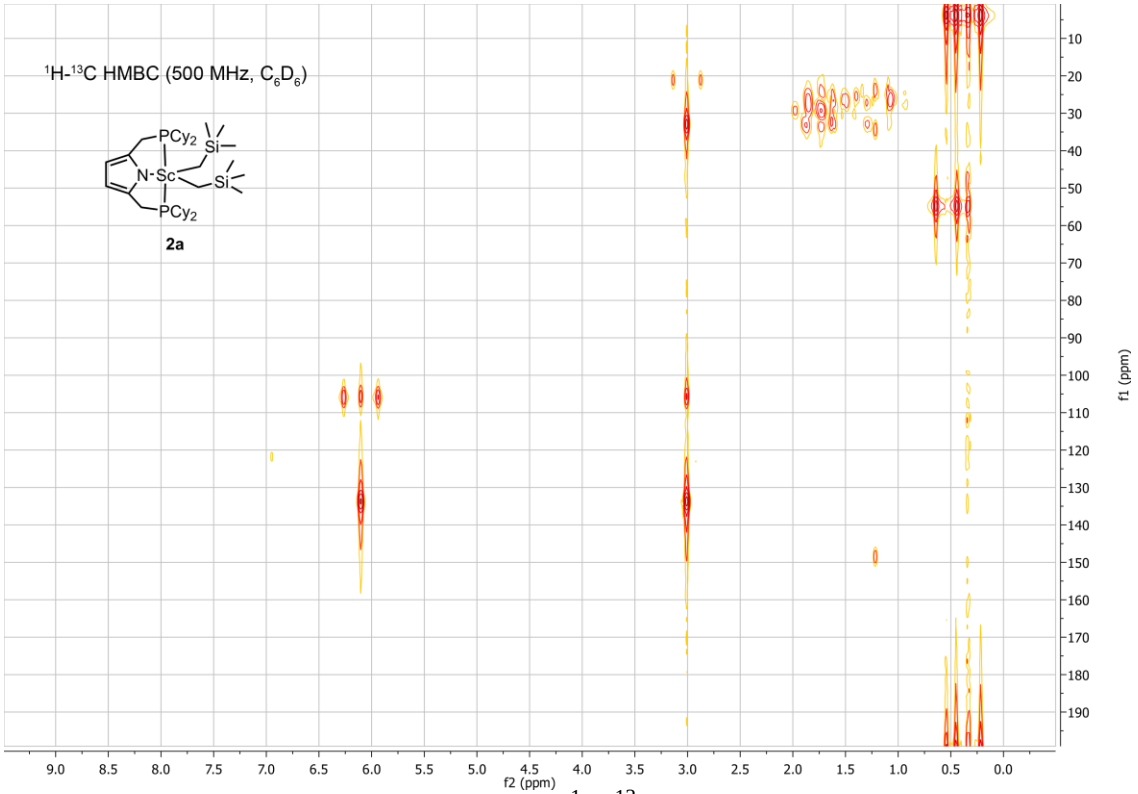

(PNP-Cy)Sc(CH_2SiMe_3)$_2$ ^{1}H-^{13}C HMBC Spectrum.

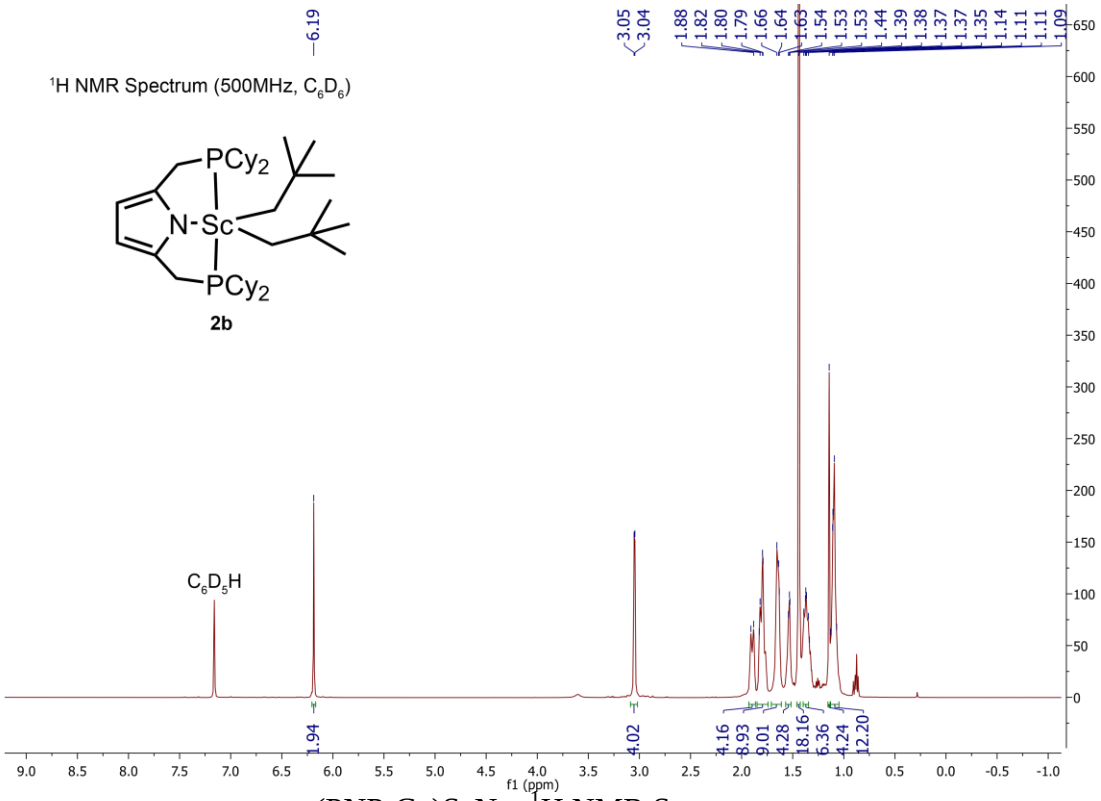

(PNP-Cy)ScNp$_2$ ^{1}H NMR Spectrum.

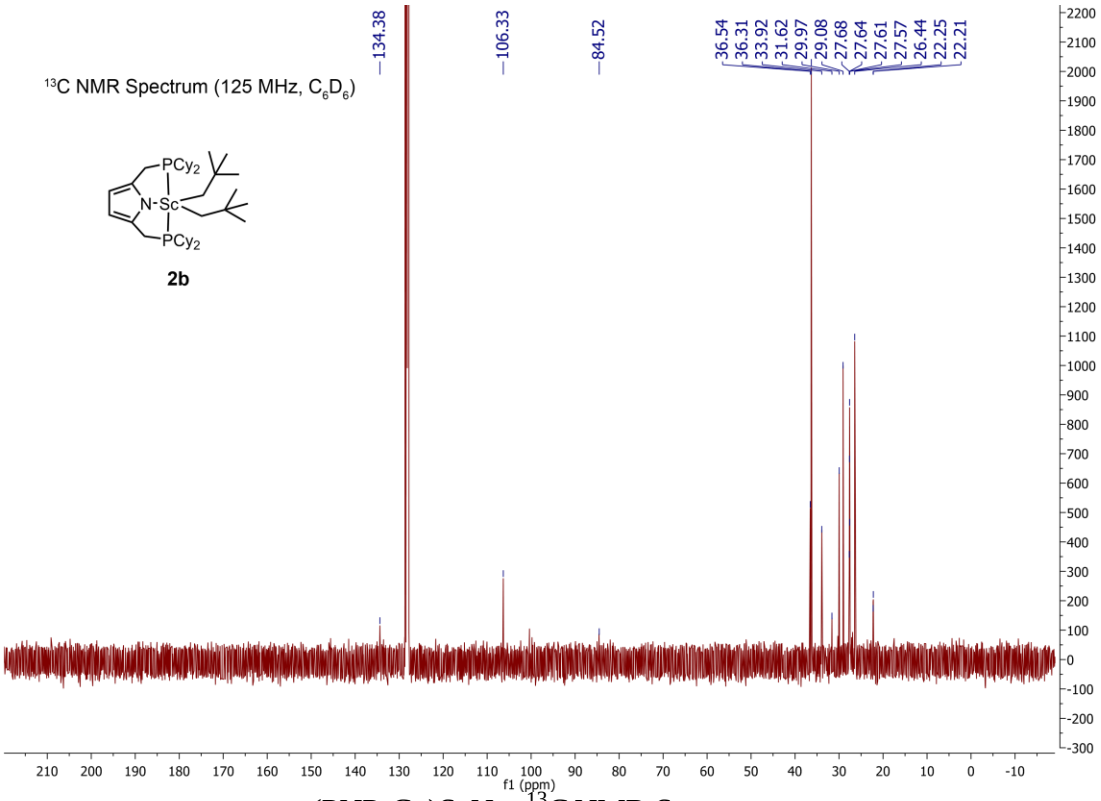

(PNP-Cy)ScNp$_2$ ^{13}C NMR Spectrum:

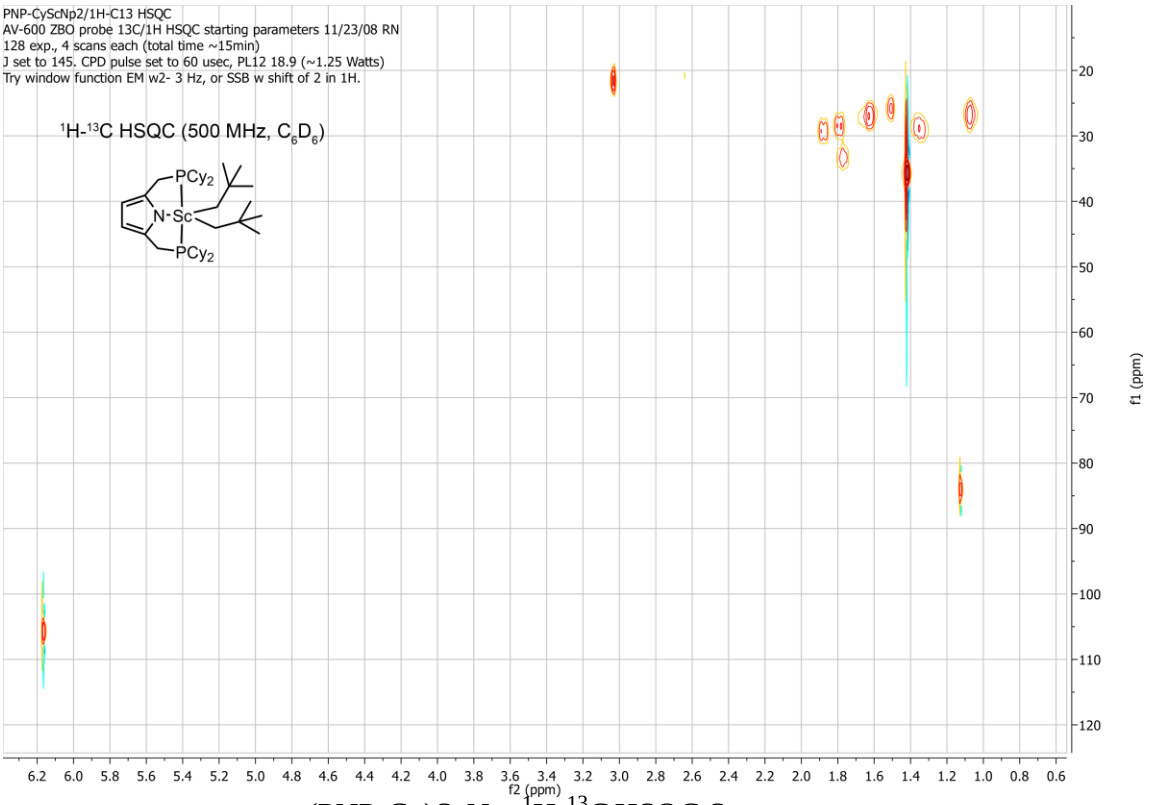

(PNP-Cy)ScNp$_2$ ^{1}H-^{13}C HSQC Spectrum.

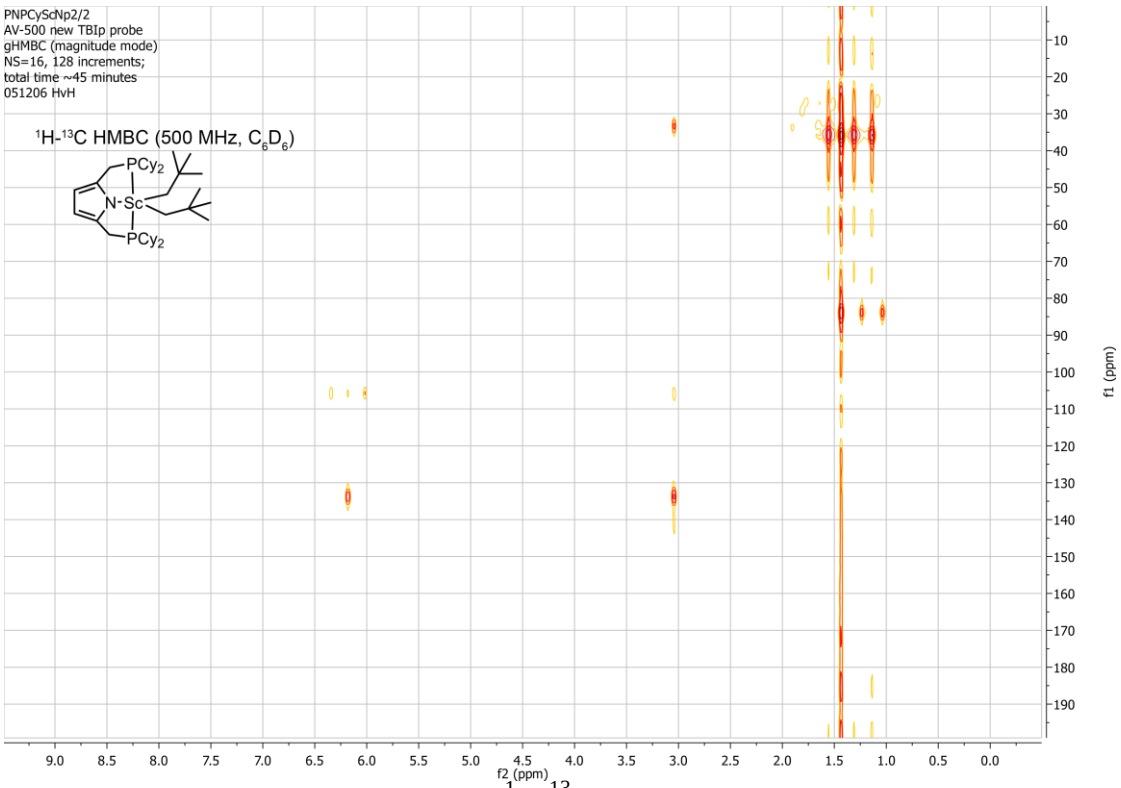

(PNP-Cy)ScNp$_2$ ^{1}H-^{13}C HMBC Spectrum.

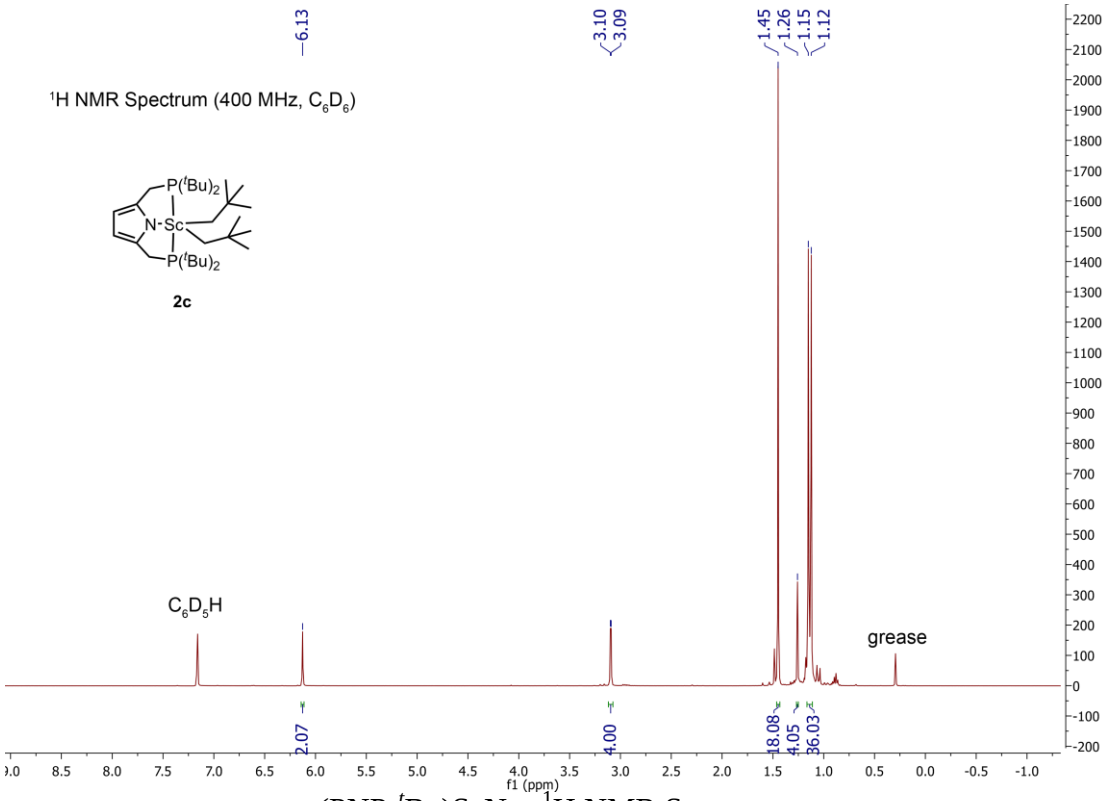

(PNP-^{t}Bu)ScNp$_2$ ^{1}H NMR Spectrum.

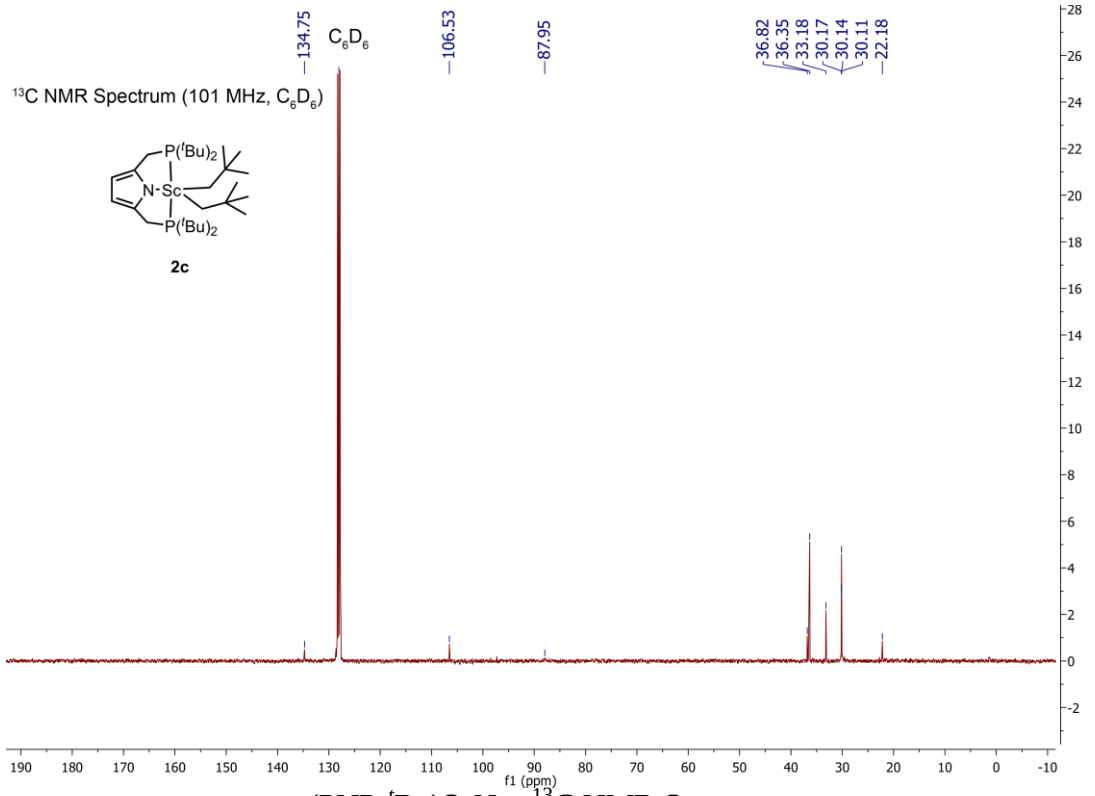

(PNP-^{t}Bu)ScNp$_2$ ^{13}C NMR Spectrum

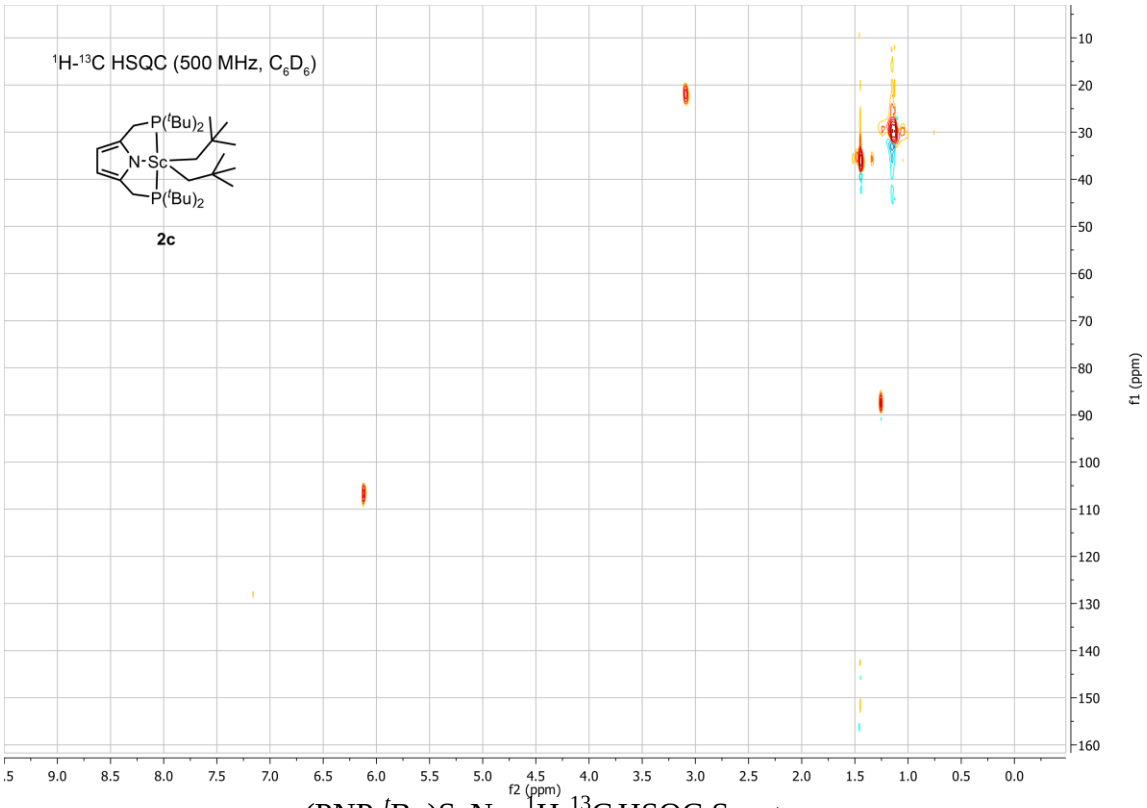

(PNP-^{t}Bu)ScNp$_2$ ^{1}H-^{13}C HSQC Spectrum.

X-Ray Crystallography

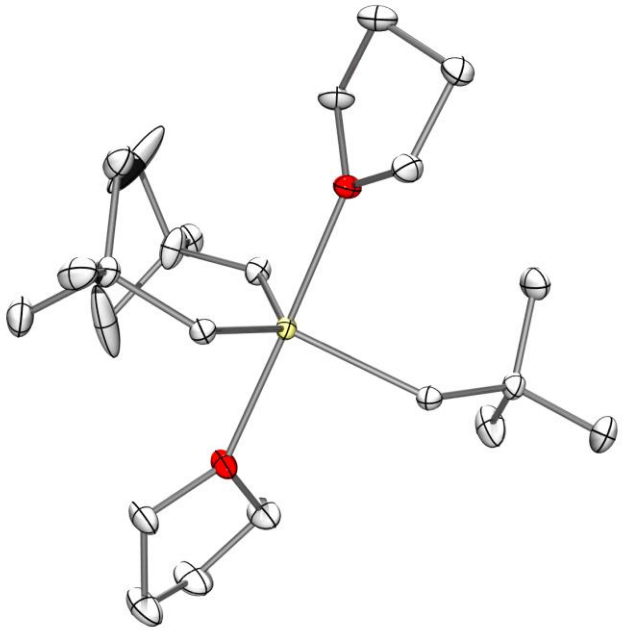

Crystal structure of ScNp$_3$(THF)$_2$.

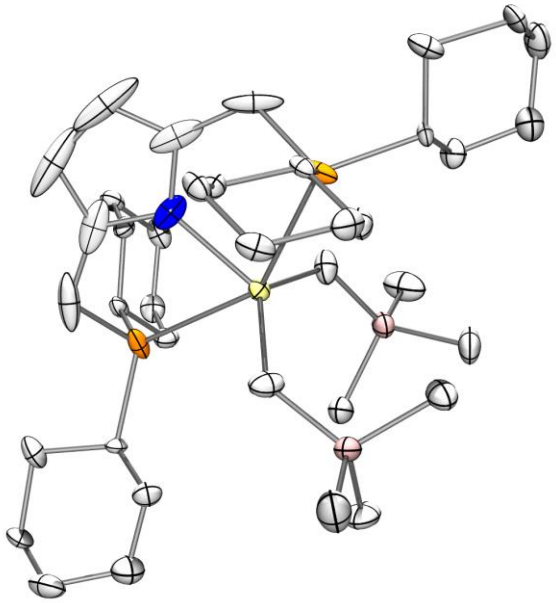

Crystal structure of (PNP-Cy)Sc(CH_2SiMe_3)$_2$ (**2a**) (Trigonal bipyramidal structure, phosphine occupy axial positions, and pyrrole and alkyl groups occupy equatorial positions).

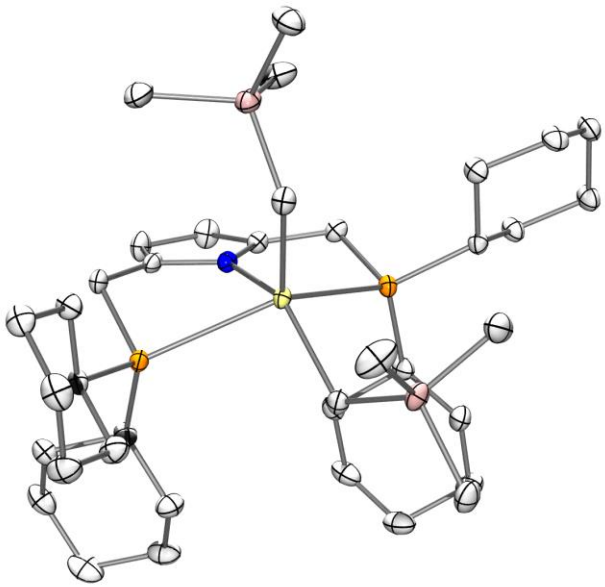

Crystal structure of (PNP-Cy)Sc(CH_2SiMe_3)$_2$ (**2a**) (Square pyramidal structure, phosphines, pyrrole, and one alkyl group from basal plane, remaining alkyl group is in the apical position).

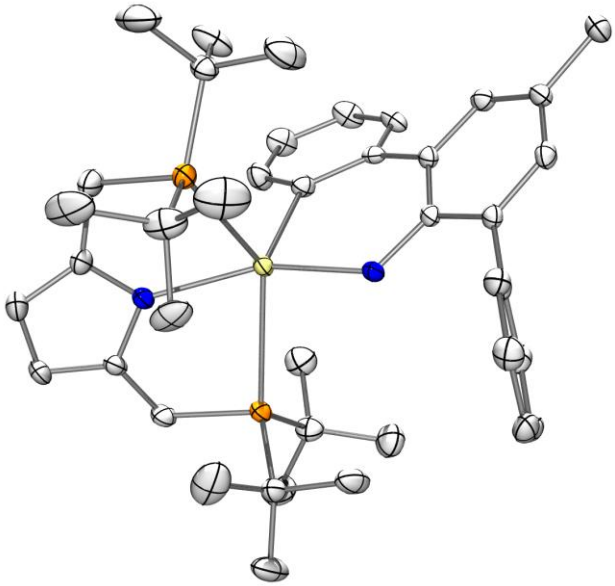

Crystal structure of (PNP-tBu)ScNHAr (**4**).

X-ray Data Tables

Crystal data and structure refinement for $ScNp_3(THF)_2$.

Empirical formula	C23 H49 O2 Sc	
Formula weight	402.58	
Temperature	100(2) K	
Wavelength	0.71073 Å	
Crystal system	Monoclinic	
Space group	$P2_1/n$	
Unit cell dimensions	a = 10.0932(5) Å	α= 90°.
	b = 17.2222(8) Å	β= 93.760(2)°.
	c = 14.5726(6) Å	γ = 90°.
Volume	2527.7(2) $Å^3$	
Z	4	
Density (calculated)	1.058 Mg/m^3	
Absorption coefficient	0.304 mm^{-1}	
F(000)	896	
Crystal size	0.10 x 0.10 x 0.05 mm^3	
Theta range for data collection	1.833 to 25.400°.	
Index ranges	-12<=h<=12, -20<=k<=20, -17<=l<=17	
Reflections collected	36715	
Independent reflections	4637 [R(int) = 0.0455]	
Completeness to theta = 25.000°	100.0 %	
Absorption correction	Semi-empirical from equivalents	
Max. and min. transmission	0.7452 and 0.6739	
Refinement method	Full-matrix least-squares on F^2	
Data / restraints / parameters	4637 / 0 / 244	
Goodness-of-fit on F^2	1.057	
Final R indices [I>2sigma(I)]	R1 = 0.0358, wR2 = 0.0838	
R indices (all data)	R1 = 0.0466, wR2 = 0.0899	
Extinction coefficient	n/a	
Largest diff. peak and hole	0.274 and -0.282 $e.Å^{-3}$	

Crystal data and structure refinement for (PNP-*t*Bu)$ScCl_2$.

Empirical formula	C22 H42 Cl2 N1 P2 Sc	
Formula weight	498.36	
Temperature	100(2) K	
Wavelength	0.71073 Å	
Crystal system	Orthorhombic	
Space group	Pca2(1)	
Unit cell dimensions	a = 12.1315(5) Å	α= 90°.
	b = 27.9260(12) Å	β= 90°.
	c = 15.9238(6) Å	γ = 90°.
Volume	5394.7(4) $Å^3$	
Z	8	
Density (calculated)	1.227 Mg/m^3	

Absorption coefficient	0.598 mm^{-1}
F(000)	2128
Crystal size	0.10 x 0.10 x 0.03 mm^3
Theta range for data collection	1.46 to 25.37°.
Index ranges	-14<=h<=14, -33<=k<=33, -19<=l<=19
Reflections collected	97035
Independent reflections	9837 [R(int) = 0.0510]
Completeness to theta = 25.00°	100.0 %
Absorption correction	Semi-empirical from equivalents
Max. and min. transmission	0.9823 and 0.9426
Refinement method	Full-matrix least-squares on F^2
Data / restraints / parameters	9837 / 1 / 539
Goodness-of-fit on F^2	1.045
Final R indices [I>2sigma(I)]	R1 = 0.0358, wR2 = 0.0720
R indices (all data)	R1 = 0.0427, wR2 = 0.0752
Absolute structure parameter	0.00(2)
Largest diff. peak and hole	0.739 and -0.761 e.$Å^{-3}$

Crystal data and structure refinement for (PNP-*t*Bu)$ScNp_2$.

Empirical formula	C32 H64 N P2 Sc	
Formula weight	569.74	
Temperature	100(2) K	
Wavelength	0.71073 Å	
Crystal system	Monoclinic	
Space group	P2(1)/c	
Unit cell dimensions	a = 15.2218(5) Å	α= 90°.
	b = 11.6604(4) Å	β= 108.445(2)°.
	c = 21.0181(8) Å	γ = 90°.
Volume	3538.9(2) $Å^3$	
Z	4	
Density (calculated)	1.069 Mg/m^3	
Absorption coefficient	0.317 mm^{-1}	
F(000)	1256	
Crystal size	0.10 x 0.09 x 0.08 mm^3	
Theta range for data collection	1.41 to 25.40°.	
Index ranges	-18<=h<=18, -13<=k<=14, -25<=l<=25	
Reflections collected	47510	
Independent reflections	6499 [R(int) = 0.0331]	
Completeness to theta = 25.00°	100.0 %	
Absorption correction	Semi-empirical from equivalents	
Max. and min. transmission	0.9751 and 0.9690	
Refinement method	Full-matrix least-squares on F^2	
Data / restraints / parameters	6499 / 0 / 368	
Goodness-of-fit on F^2	1.038	

Final R indices [I>2sigma(I)]	R1 = 0.0468, wR2 = 0.1191
R indices (all data)	R1 = 0.0548, wR2 = 0.1252
Largest diff. peak and hole	1.528 and -0.622 e.Å^{-3}

Crystal data and structure refinement for [(PNP-Cy)ScCl2]2.

Empirical formula	C60 H100 Cl4 N2 P4 Sc2	
Formula weight	1205.02	
Temperature	100(2) K	
Wavelength	0.71073 Å	
Crystal system	Monoclinic	
Space group	$P2_1/n$	
Unit cell dimensions	a = 15.4534(9) Å	α= 90°.
	b = 14.4104(8) Å	β= 104.156(2)°.
	c = 30.3498(18) Å	γ = 90°.
Volume	6553.4(7) Å^3	
Z	4	
Density (calculated)	1.221 Mg/m^3	
Absorption coefficient	0.504 mm^{-1}	
F(000)	2576	
Crystal size	0.100 x 0.070 x 0.050 mm^3	
Theta range for data collection	1.573 to 25.366°.	
Index ranges	-18<=h<=18, -17<=k<=17, -36<=l<=34	
Reflections collected	103924	
Independent reflections	11986 [R(int) = 0.0840]	
Completeness to theta = 25.000°	99.8 %	
Absorption correction	Semi-empirical from equivalents	
Max. and min. transmission	0.8620 and 0.8239	
Refinement method	Full-matrix least-squares on F^2	
Data / restraints / parameters	11986 / 0 / 688	
Goodness-of-fit on F^2	1.022	
Final R indices [I>2sigma(I)]	R1 = 0.0644, wR2 = 0.1539	
R indices (all data)	R1 = 0.0839, wR2 = 0.1642	
Extinction coefficient	n/a	
Largest diff. peak and hole	1.134 and -0.530 e.Å^{-3}	

Crystal data and structure refinement for (PNP-Cy)Sc(CH_2SiMe_3)$_2$.

Empirical formula	C28.50 H54 N0.75 P1.50 Sc0.75 Si1.50	
Formula weight	529.53	
Temperature	100(2) K	
Wavelength	0.71073 Å	
Crystal system	Monoclinic	
Space group	C 2/c	
Unit cell dimensions	a = 14.0824(7) Å	α= 90°.
	b = 16.2330(7) Å	β= 95.3980(10)°.
	c = 55.407(3) Å	γ = 90°.

Volume	12609.8(10) Å^3
Z	16
Density (calculated)	1.116 Mg/m^3
Absorption coefficient	0.333 mm^{-1}
F(000)	4632
Crystal size	0.080 x 0.080 x 0.050 mm^3
Theta range for data collection	1.477 to 25.350°.
Index ranges	-16<=h<=16, -19<=k<=19, -65<=l<=66
Reflections collected	109591
Independent reflections	11428 [R(int) = 0.0723]
Completeness to theta = 25.000°	99.7 %
Absorption correction	Semi-empirical from equivalents
Max. and min. transmission	0.9833 and 0.9735
Refinement method	Full-matrix least-squares on F^2
Data / restraints / parameters	11428 / 0 / 642
Goodness-of-fit on F^2	1.026
Final R indices [I>2sigma(I)]	R1 = 0.0426, wR2 = 0.0884
R indices (all data)	R1 = 0.0603, wR2 = 0.0958
Extinction coefficient	n/a
Largest diff. peak and hole	0.820 and -0.591 e.Å^{-3}

Crystal data and structure refinement for (PNP-Cy)ScNp$_2$.

Empirical formula	C40 H72 N1 P2 Sc1	
Formula weight	673.88	
Temperature	100(2) K	
Wavelength	0.71073 Å	
Crystal system	Monoclinic	
Space group	C2/c	
Unit cell dimensions	a = 13.9103(4) Å	α= 90°.
	b = 15.5320(4) Å	β= 95.279(2)°.
	c = 55.3947(14) Å	γ = 90°.
Volume	11917.5(5) Å^3	
Z	12	
Density (calculated)	1.127 Mg/m^3	
Absorption coefficient	0.292 mm^{-1}	
F(000)	4440	
Crystal size	0.08 x 0.06 x 0.05 mm^3	
Theta range for data collection	1.48 to 25.49°.	
Index ranges	-16<=h<=16, -18<=k<=16, -66<=l<=67	
Reflections collected	67786	
Independent reflections	10987 [R(int) = 0.0692]	
Completeness to theta = 25.00°	99.8 %	
Absorption correction	Semi-empirical from equivalents	
Max. and min. transmission	0.9855 and 0.9770	

Refinement method	Full-matrix least-squares on F^2
Data / restraints / parameters	10987 / 0 / 605
Goodness-of-fit on F^2	1.040
Final R indices [I>2sigma(I)]	R1 = 0.0495, wR2 = 0.0891
R indices (all data)	R1 = 0.0805, wR2 = 0.0994
Largest diff. peak and hole	0.353 and -0.512 e.Å^{-3}

Crystal data and structure refinement for (PNP-tBu)ScNHAr.

Empirical formula	C41 H57 N2 P2 Sc	
Formula weight	684.79	
Temperature	100(2) K	
Wavelength	0.71073 Å	
Crystal system	Monoclinic	
Space group	$P2_1/n$	
Unit cell dimensions	a = 14.3460(19) Å	α= 90°.
	b = 13.9805(19) Å	β= 104.687(7)°.
	c = 19.889(3) Å	γ = 90°.
Volume	3858.7(9) Å^3	
Z	4	
Density (calculated)	1.179 Mg/m^3	
Absorption coefficient	0.303 mm^{-1}	
F(000)	1472	
Crystal size	0.07 x 0.07 x 0.01 mm^3	
Theta range for data collection	1.80 to 25.43°.	
Index ranges	-16<=h<=17, -16<=k<=16, -24<=l<=23	
Reflections collected	55555	
Independent reflections	7073 [R(int) = 0.0999]	
Completeness to theta = 25.00°	99.9 %	
Absorption correction	Semi-empirical from equivalents	
Max. and min. transmission	0.9801 and 0.8970	
Refinement method	Full-matrix least-squares on F^2	
Data / restraints / parameters	7073 / 0 / 459	
Goodness-of-fit on F^2	1.013	
Final R indices [I>2sigma(I)]	R1 = 0.0462, wR2 = 0.0877	
R indices (all data)	R1 = 0.0891, wR2 = 0.1026	
Largest diff. peak and hole	0.409 and -0.284 e.Å^{-3}	

Crystal data and structure refinement for (PNP-tBu)ScNHAr$(DMAP)_2$.

Empirical formula	C55 H77 N6 P2 Sc
Formula weight	929.12
Temperature	100(2) K
Wavelength	0.71073 Å
Crystal system	Orthorhombic
Space group	$Pna2_1$

Unit cell dimensions	a = 23.1810(9) Å	α= 90°.
	b = 22.5100(8) Å	β= 90°.
	c = 25.2361(10) Å	γ = 90°.
Volume	13168.3(9) $Å^3$	
Z	8	
Density (calculated)	0.937 Mg/m^3	
Absorption coefficient	0.193 mm^{-1}	
F(000)	4000	
Crystal size	0.080 x 0.080 x 0.030 mm^3	
Theta range for data collection	1.497 to 25.405°.	
Index ranges	-27<=h<=27, -18<=k<=27, -30<=l<=30	
Reflections collected	92497	
Independent reflections	23416 [R(int) = 0.0507]	
Completeness to theta = 25.000°	99.9 %	
Absorption correction	Semi-empirical from equivalents	
Max. and min. transmission	0.7452 and 0.6462	
Refinement method	Full-matrix least-squares on F^2	
Data / restraints / parameters	23416 / 1 / 1188	
Goodness-of-fit on F^2	1.033	
Final R indices [I>2sigma(I)]	R1 = 0.0760, wR2 = 0.1899	
R indices (all data)	R1 = 0.0991, wR2 = 0.2067	
Absolute structure parameter	0.52(5)	
Extinction coefficient	n/a	
Largest diff. peak and hole	0.973 and -0.870 $e.Å^{-3}$	

Crystal data and structure refinement for (PNP-Cy)Sc(C#CCHMe2)2.

Empirical formula	C44.75 H69.25 N P2 Sc	
Formula weight	728.16	
Temperature	100(2) K	
Wavelength	0.71073 Å	
Crystal system	Triclinic	
Space group	P -1	
Unit cell dimensions	a = 14.0240(5) Å	α= 73.2353(15)°.
	b = 17.1492(5) Å	β= 84.4873(18)°.
	c = 20.2172(7) Å	γ = 67.1130(14)°.
Volume	4288.4(3) $Å^3$	
Z	4	
Density (calculated)	1.128 Mg/m^3	
Absorption coefficient	0.276 mm^{-1}	
F(000)	1583	
Crystal size	0.100 x 0.080 x 0.030 mm^3	
Theta range for data collection	1.052 to 25.399°.	
Index ranges	-16<=h<=16, -20<=k<=20, -24<=l<=24	
Reflections collected	112231	

Independent reflections	15695 [R(int) = 0.0610]
Completeness to theta = 25.000°	99.9 %
Absorption correction	Semi-empirical from equivalents
Max. and min. transmission	0.9280 and 0.8506
Refinement method	Full-matrix least-squares on F^2
Data / restraints / parameters	15695 / 0 / 904
Goodness-of-fit on F^2	1.048
Final R indices [I>2sigma(I)]	R1 = 0.0616, wR2 = 0.1495
R indices (all data)	R1 = 0.0902, wR2 = 0.1680
Extinction coefficient	n/a
Largest diff. peak and hole	1.557 and -0.678 e.$Å^{-3}$

Chapter 2. Evidence for the Existence of Group 3 Terminal Methylidene Complexes

INTRODUCTION

Transition metal-ligand multiple bonds have been studied for decades due to their unique reactivity, their important role in catalysis, and the fundamental insights they provide into the nature of the chemical bond.[1] Despite intense investigation, there is a paucity of examples with group 3 metals and the lanthanides (collectively, the rare earth elements).[2] Only in the last seven years have examples of group 3 imido complexes been reported,[3–8] and no examples of Schrock-type alkylidene complexes analogous to those of early metals in groups 4-6 have been reported.[9–14] There are numerous examples of bridging methylene complexes for the lanthanides,[15–18] and some examples of monomeric zwitterionic complexes (bearing C-bound carbodiphosphorane ligands) described as "carbene-like" (see Figure 1).[19–22]

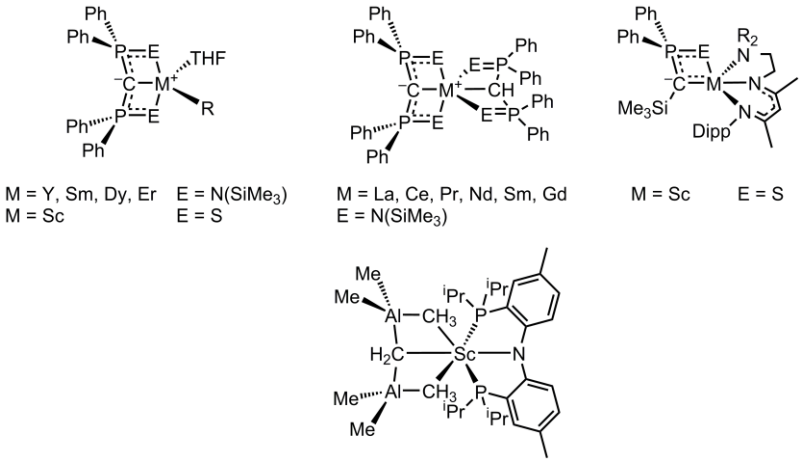

Figure 1. Zwitterionic "carbene-like" C-bound carbodiphosphorane complexes and related carbene complexes.[18–21]

Further discussion of these C-bound carbodiphosphorane complexes is warranted, since their reactivity is somewhat intermediate between that of traditional Fischer and Schrock carbene complexes. The first example of such a complex was published by Cavell *et al.* in 2000 with a bis(iminophosphorane) ligand that has since been employed with many group 3 and lanthanide metals.[19] Since then, several related examples have been developed by Liddle, Le Floch, and Mézailles, and this chemistry was recently reviewed.[20] Using a different methodology, Mindiola *et al.* prepared a conceptually distinct zwitterionic complex (Figure 1, bottom), though the electronic structure is very similar to those of the carbodiphosphorane-supported systems.[21] These complexes are sometimes (though not always[23]) drawn with a double bond between the metal and the carbon bearing the negative charge. However, this representation does not accurately describe the nature of the metal-carbon interaction, since classical metal carbene complexes are characterized by shorter metal-carbon bond distances and significant charge-transfer stabilization; that is, electron-sharing between the atoms' orbitals (as quantified by computational techniques such as NBO analysis to determine Wiberg bond orders). In these zwitterionic, carbodiphosphorane complexes, the metal–carbon bond lengths are in the range of *bona fide* metal–carbon single bonds for these metals, though typically on the shorter end of the range. DFT calculations of Wiberg bond orders typically show relatively low calculated bond orders (~0.6) consistent with metal–carbon single bonds for these metals.[22,24] Additionally, the

"excess" negative charge on carbon has been shown to be more strongly donated into the rest of the ligand, rather than onto the metal center.[22–25] More recently,[26] another multidentate phosphorus-stabilized carbene was reported (Figure 1, right) which was calculated to be more alkylidene-like, with a Wiberg bond order of 0.73.

In light of these considerations, it remains an open question whether the preparation of terminal alkylidene complexes of group 3 or rare earth elements is possible.[27] We herein report evidence for the formation of such species – in particular, evidence for intermediate, terminal methylidene complexes of scandium and yttrium.

RESULTS AND DISCUSSION

Characterization of (PNP-Cy)Sc(μ-CH_2)$_2$Sc(PNP-Cy) (1) from Thermolysis of (PNP-Cy)Sc(CH_2CMe_3)$_2$. We have previously reported dialkyl complexes of scandium featuring a monoanionic PNP ligand (2,5-bis(dicyclohexylphosphinomethyl)pyrrolide), and their C–H activation reactions.[28] Such complexes undergo intermolecular activations of sp and sp^2 C–H bonds, and intramolecularly activate sp^3 bonds at higher temperatures. The study described here concerns the thermolytic elimination of isobutylene from one of these complexes, the bis(neopentyl) derivative (PNP-Cy)ScNp_2 (Np = –CH_2CMe_3). Heating a sample of this complex in toluene-d_8 or benzene-d_6 for three days at 100 °C resulted in conversion of the dialkyl complex to isobutylene (~0.3 equiv by ^{1}H VT-NMR spectroscopy at -60 °C to promote dissolution of the alkene), neopentane (~1.1 equiv), scandium-containing product **1 (**~0.3 equiv), and methane (~0.03 equiv at -60 °C). Approximately, 0.3 equiv of starting material remained. Given these quantities, it is apparent that about one-third of the starting material decomposes to undefined material that is not observed in the ^{1}H NMR spectrum. However, the observed ratio of isobutylene to **1** is 1:1 at this point, and at earlier time points. Continued heating (6 days in total) resulted in decomposition of all remaining starting material and **1** to unobserved material and an increase in methane (~0.7 equiv by VT-NMR spectroscopy at -60 °C). Repeated attempts to obtain **1** as a pure solid by workup and crystallizations from the product mixture were not successful. However, as described below, multinuclear 1D and 2D NMR spectroscopy delineate the basic structural features of **1** in solution as a methylene-bridged dimer.

The scandium-containing product of the thermal elimination reaction (**1**) is identical (by ^{1}H NMR spectroscopy) for reactions carried out in benzene-d_6 or toluene-d_8, suggesting that solvent is not activated and/or incorporated into the product; in both cases, **1** is formed in 20% yield relative to the starting material. Reactions of **1** with D_2O, methanol-d_4, or 3,5-di-*tert*-butylphenol-d_1 afforded the free PNP ligand deuterated at the pyrrole nitrogen and methane-d_2; no deuterium was incorporated into any other positions of the ligand (by ^{2}H NMR spectroscopy). These data indicate that the ligand remains intact and that metalation of other ligand positions does not occur in the formation of **1**.

In contrast to previously reported scandium complexes supported by this PNP ligand,[28] which feature a singlet in the aromatic region of the ^{1}H NMR spectrum for the symmetry-related pyrrole backbone protons, the ^{1}H NMR spectrum of **1** contains four inequivalent resonances in this region (Figure 2a). Moreover, the ^{31}P NMR spectrum of **1** features four inequivalent phosphorus resonances. Diffusion ordered spectroscopy (DOSY) indicates that all four resonances in the pyrrole region are associated with a molecule of the same size (presumably, the same molecule). Furthermore, this molecule has a lower diffusion coefficient ($1.78 \cdot 10^{-9}$ m^2/s vs. $1.61 \cdot 10^{-9}$ m^2/s) than the starting material (PNP-Cy)ScNp_2, indicating a larger hydrodynamic

radius (11% larger), which is quantitatively consistent with the calculated hydrodynamic radius of a dimeric structure vs. the starting material (see Appendix). Evidence for the dimeric nature of **1** was also found by EI mass spectrometry, which revealed a mass peak at 1108.6 assigned to $[1 \cdot H_2O]^+$; this water adduct of **1** is likely produced in the mass spectrometer.

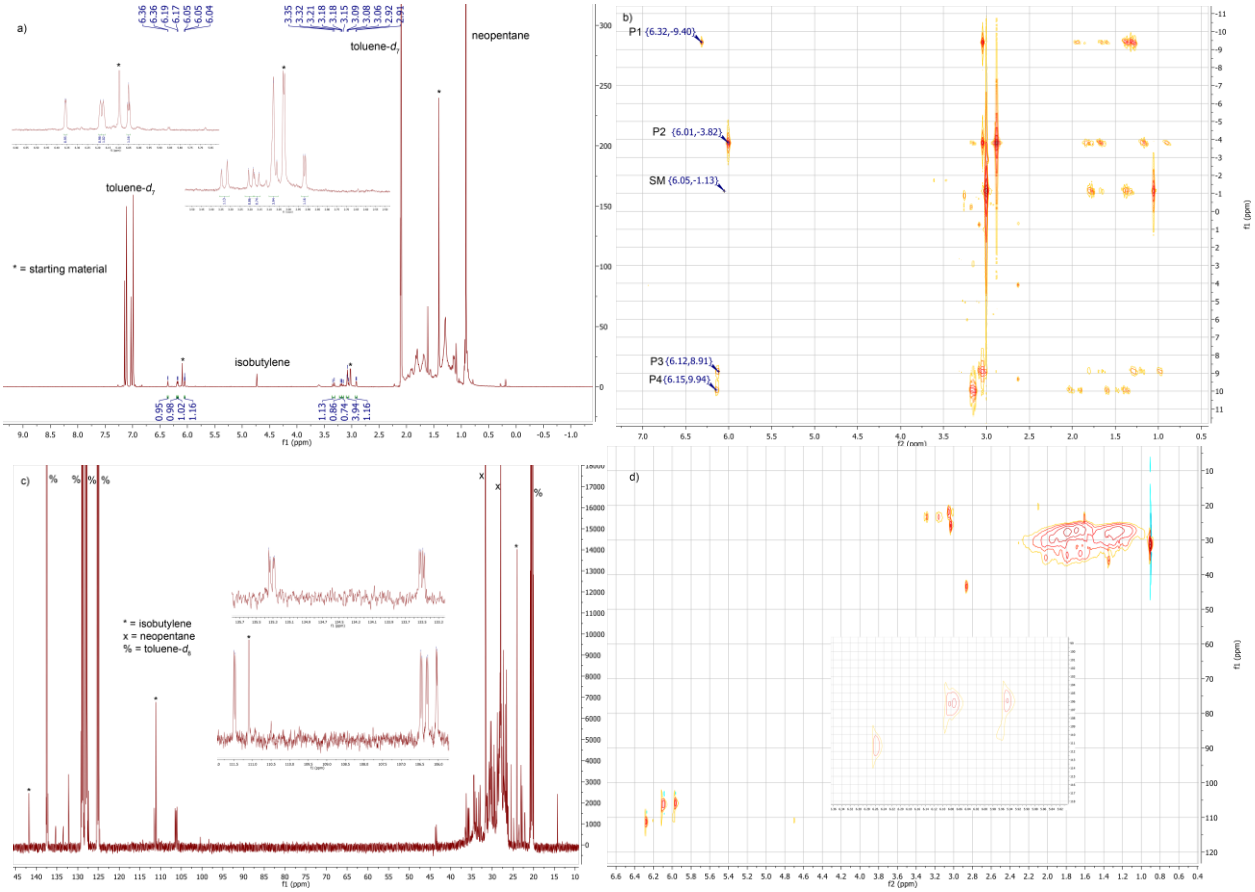

Figure 2. a) ^{1}H NMR spectrum of **1**. b) ^{1}H-^{31}P HMBC spectrum of **1**. Based on a separate ^{1}H COSY experiment, P1 and P2 are on one ligand, while P3 and P4 are on the other. Note the distinct set of ligand backbone resonances for each phosphorus resonance due to the C1 symmetry of complex **1**. c) ^{13}C{^{1}H} NMR spectrum of **1**. Note the eight pyrrole carbon resonances. d) ^{1}H-^{13}C HSQC spectrum of **1**. Note the four distinct carbon resonances assignable to the ligand methylene, again indicating a C1 symmetric dimer. Expanded versions of these spectra are available in the Supporting Information

Two-dimensional correlation studies (^{1}H-^{31}P HMBC) indicate that each ^{31}P NMR resonance is correlated with a unique ^{1}H NMR resonance for each of the inequivalent pyrrole hydrogens (Figure 2b). These data indicate that **1** is a dimer containing two inequivalent PNP-Cy ligands and two scandium centers in C_1 symmetry. By analogy to the crystallographically characterized $[(PNP\text{-}Cy)ScCl_2]_2$ dimer,[28] we propose the structure of **1** shown in Figure 3.

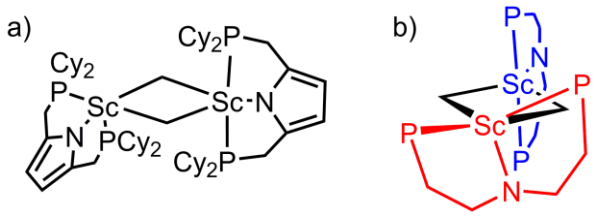

Figure 3. Proposed structure of **1**, a) side view, b) end-on view, with pyrrole ring and cyclohexyl groups omitted and subunits colored for clarity. In both ligand sets, one phosphorus lies above the Sc_2C_2 ring and one is below.

Due to steric constraints of the cyclohexyl groups, the two phosphorus atoms of both ligands lie on opposite faces of the Sc_2C_2 core (Figure 3b), one pyrrole group symmetrically lies perpendicular to the dimetallacycle core, and one pyrrole group lies entirely on one face of the core (Figure 3a), resulting in a molecule containing no symmetry elements. On the basis of 2D NMR correlation studies (see Table 1), all of the non-cyclohexyl group resonances are assigned to the ligands in **1**, although assignments to specific PNP-Cy ligands cannot be made (see Figure 4 and Table 1).

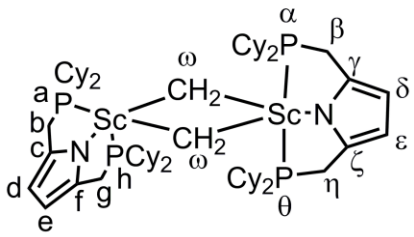

Figure 4. Assignments of resonances for **1**. ^{31}P NMR (δ) α: -9.46, θ: -3.86, a: 10.01, h: 8.97, ^{13}C NMR (δ) β: 25.49, γ: 133.52, δ: 111.48, ε: 106.05, ζ: 133.48, η: 43.47, b: 22.77, c: 135.29, d: 106.46, e: 106.30, f: 135.34, g: 23.03, ^{1}H NMR (δ) β: 3.06 (2H), δ:, 6.34, ε: 6.03, η: 2.90 (2H), b: 3.06, 3.05, d: 6.17, e: 6.15, g: 3.31, 3.17, ω: 1.51, 1.48, 1.13, 1.09

Table 1. 2D NMR correlations between protons and other nuclei.

^{1}H δ	^{31}P HMBC	^{13}C HSQC	^{13}C HMBC	^{1}H COSY
6.34	-9.46	111.48	133.52	6.03, 3.06
6.17	10.01	106.46	135.29	6.15, 3.05
6.15	8.97	106.30	135.34	6.17, 3.31, 3.17
6.03	-3.86	106.05	133.48	6.34, 2.90
3.31, 3.17	8.97	23.03	106.30, 135.34	6.15, 3.17, 3.31
3.06 (2H)	-9.46	25.49	111.48, 133.52	6.34
3.06,3.05	10.01	22.77	135.29	6.17
2.90 (2H)	-3.86	43.57	106.05, 133.48, 133.52	6.03

The $[(PNP\text{-}Cy)ScCl_2]_2$ dimer possesses an analogous C_1 structure in the solid state and at temperatures below 0 °C in toluene-d_8 solution as shown by variable temperature NMR spectroscopy. The ^{1}H resonances of the pyrrole ligands are averaged at 20 °C, but they decoalesce as the temperature is lowered. By -70°C, the pattern is consistent with the C_1

symmetry structure observed in the solid state and matches that observed for **1** at 20 °C. These spectra are available in the Supporting Information. The lower fluxional barriers in the chloride bridged dimer are consistent with the expectation that a μ_2-Cl group is a weaker bridging group than a μ_2-CH_2 group. At temperatures above 65 °C in toluene-d_8, **1** has C_s symmetry by NMR spectroscopy as the resonances on the either the ligand in red or blue in Figure 3b equilibrate on the NMR time scale. For comparison, the X-ray crystal structure of $[(PNP\text{-}Cy)ScCl_2]_2$ and the DFT optimized structure of **1** are shown in Figure 5.

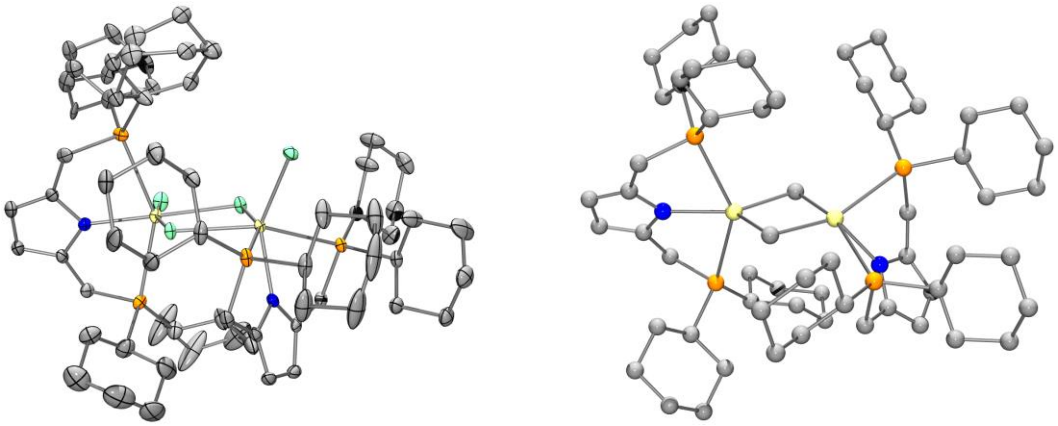

Figure 5. Comparison of X-ray structure of $[(PNP\text{-}Cy)ScCl_2]_2$ (left, ref 27) and calculated structure of $[(PNP\text{-}Cy)Sc(CH_2)]_2$ (right). Hydrogen atoms are omitted for clarity.

The formation of methane-d_2 on addition of acidic deuteron sources supports the presence of a methylene ligand in **1**. This assignment is also consistent with a deuterium-labeling experiment involving thermolysis of $(PNP\text{-}Cy)Sc(CD_2CMe_3)_2$ (*vide infra*), to form deuterated **1** (**1-*d*$_n$**). Analysis of **1-*d*$_n$** (n = 0, 2, 4) by EI mass spectrometry shows a shift of the center of the mass peak to 1110.6 as well as broadening of the peak, consistent with a mixture of **1-*d*$_0$**+H_2O, **1-*d*$_2$**+H_2O, and **1-*d*$_4$**+H_2O (see Appendix). Moreover, a small peak centered at 1092.6 with a profile similar to that of the mass peak for $[1\cdot H_2O]^+$ is attributed to a mixture of **1-*d*$_0$**, **1-*d*$_2$**, and **1-*d*$_4$**.

This partial deuteration of the $Sc_2(CH_2)_2$ core for **1-*d*$_n$** results in four inequivalent resonances in the ^{2}H NMR alkyl region at 1.51, 1.48, 1.13, and 1.09 ppm (for all four chemically inequivalent positions), the sum of which integrates to 1:1 with respect to the signal for the isobutylene-d_0 formed in this reaction (using $Ph_2Si(CH_3)(CD_3)$[29] as the internal standard to allow quantifications between ^{1}H and ^{2}H NMR spectra). Note that the corresponding proton resonances are obscured by the cyclohexyl resonances in the ^{1}H NMR spectrum of **1**. Thus, the formation of complex **1** is associated with the elimination of one equiv of isobutylene per Sc center.

Attempts to obtain X-ray quality crystals of **1**, or adducts of **1** with ligands such as DMAP or *p*-phenylpyridine, have been unsuccessful.

Mechanism of the formation of 1. The formation of isobutylene in this reaction is particularly interesting, since it is unlikely to arise from degradation of the cyclohexyl groups. Thus, it seems possible that the isobutylene is derived from the neopentyl group of $(PNP\text{-}Cy)ScNp_2$ *via* C–C bond cleavage. To establish the source of the isobutylene, a deuterium-labelling study was undertaken to distinguish between several potential mechanisms for its formation (Figure 6).[30]

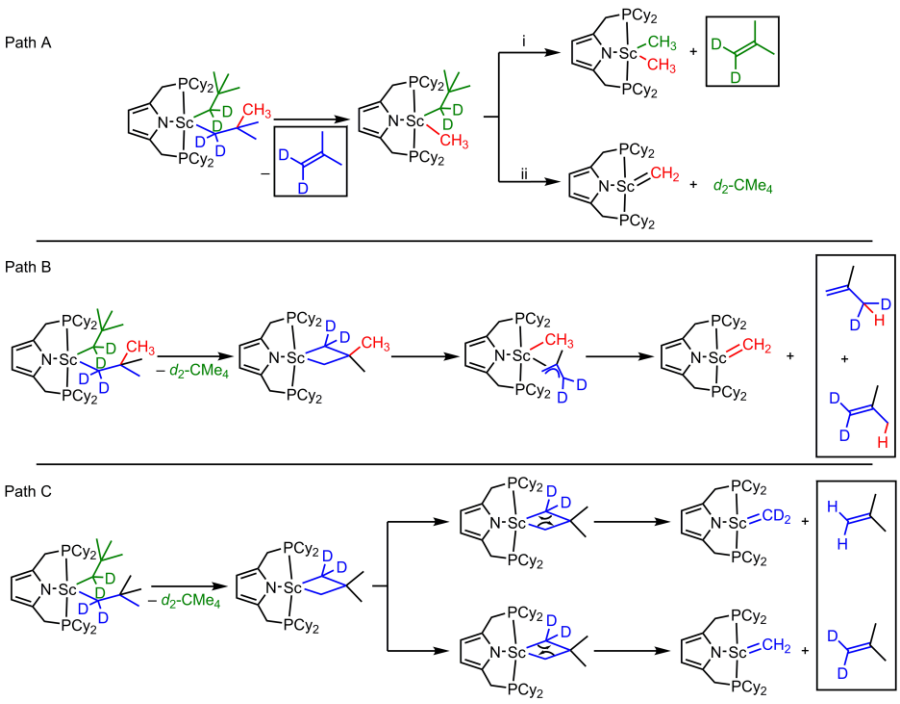

Figure 6. Possible mechanisms for the formation of isobutylene.

These mechanisms were differentiated by use of the α-tetradeuteroneopentyl isotopomer (PNP-Cy)Sc(CD_2CMe_3)$_2$ since each mechanistic hypothesis in Figure 6 predicts a different pattern of deuterium incorporation into the isobutylene product.

The most likely mechanism, given the known reactivity of scandium alkyl complexes, appeared to be β-methyl elimination to directly form isobutylene and a scandium methyl complex (Figure 6, Path A).[31] This mechanism predicts that all isobutylene formed in this reaction is deuterated at the vinylic position.

It is also conceivable that the scandium complex undergoes cyclometalation by γ-abstraction analogous to the dineopentyl thorium complex of Marks and coworkers.[32] The resulting scandacyclobutane could then undergo β-methyl elimination[32] (Figure 6, Path B) to form a scandium methyl allyl complex. Isobutylene would then be formed by α-abstraction of the methyl group to produce a terminal methylidene complex and isobutylene. In this case, the deuterium is predicted to occupy either the vinylic or methyl positions of the isobutylene.

The scandacyclobutane could also undergo retro-[2+2] cycloaddition as in the metathesis reaction[34] observed for titanacyclobutanes,[35] to form isobutylene and a terminal methylidene complex (Figure 6, Path C). This pathway has been observed for dineopentyl nickel phosphine complexes[36] and this mechanistic hypothesis predicts that the isobutylene will possess no deuterium, or deuterium only at the vinylic position. This appears to be the only mechanism that can directly account for formation of isobutylene-d_0. Path A. ii. could form isobutylene-d_0 if the resulting methylidene complex reacted with the eliminated isobutylene-d_2 to generate a metalacyclobutane, at which point Path C and this Path are indistinguishable.

Heating a sample of (PNP-Cy)Sc(CD_2CMe_3)$_2$ in toluene-d_8 or benzene-d_6 to 100 °C for three days afforded a mixture of isobutylene-d_2 (deuterated at the vinyl position) and isobutylene-d_0 in a ratio of 1:2.33 ± 0.04 (quantified using the internal standard

$Ph_2Si(CH_3)(CD_3)$). A relatively large amount of neopentane-d_2 (7:1 ratio with respect to isobutylene-d_0) was also observed, suggesting that after cyclometalation, only a fraction of the complex undergoes the retro-[2+2] reaction *via* Path C. These results also suggest that the pathway involving a neopentyl methyl intermediate that undergoes α-H abstraction to afford a methylidene (Path A ii.) is unlikely since this would yield an isobutylene to neopentane ratio of 1 : <1, rather than 1 : 7. Neopentane-d_3 was also observed when the solvent is benzene due to a competitive solvent activation reaction[28] which does not affect the intramolecular KIE determination. No neopentane-d_3 was observed when the reaction was carried out in toluene-d_8, indicating that α-abstraction to form a neopentylidene was not occurring.

The observed 1:2.3 ratio of eliminated isobutylene *vs.* isobutylene-d_2 reflects a kinetic isotope effect in breakup of the metallacycle in Path C. On the basis of calculations presented below, this effect is likely due to the presence of *α*-agostic interactions in the subsequent methylidene intermediates and transition states, which is not present in the starting material.

The mechanism of Path C predicts that a 1:2.3 stoichiometry for the isobutylene-d_0/isobutylene-d_2 elimination should result in a 2.3:1 ratio of CH_2/CD_2 ligands in **1-*d*$_n$** (see Figure 7). Indeed, treatment of a benzene-d_6 solution of **1-*d*$_n$** with hydrogen (1 atm) afforded a mixture of methane-d_0 and methane-d_2 in a 1:2.1 ratio by ^{1}H NMR spectroscopy (~0.2 equiv relative to **1-*d*$_n$**; presumably more methane is in the head space of the NMR tube); the scandium-containing product decomposed to an intractable mixture as has been previously reported.[28]

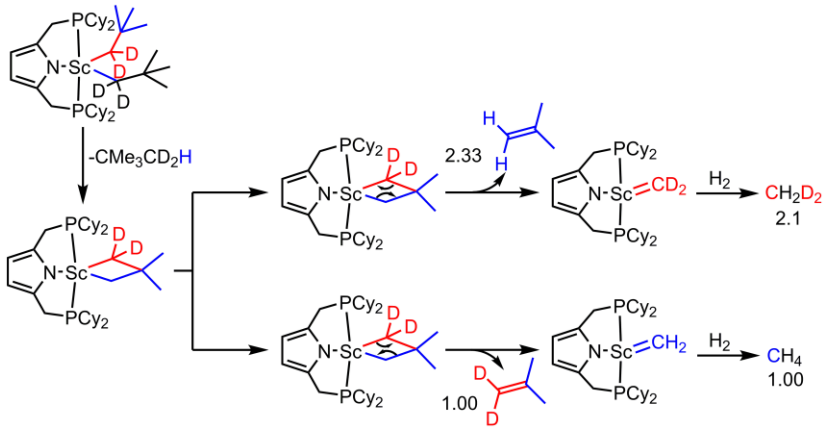

Figure 7. Location of deuterons after thermolysis and hydrogenolysis of (PNP-Cy)ScNp$_2$-d_4. Note the inverse proportions of deuterated isobutylene to proteo-isobutylene (1 : 2.3) and deuterated methane to proteo-methane (2.3 : 1). Numbers represent observed ratios of products.

It is worth noting that when the thermolysis is carried out using (PNP-^{t}Bu)Sc(CD_2CMe_3)$_2$,[28] only isobutylene-d_0 is observed, indicating that, in this case, the isobutylene is formed by activation of the *tert*-butyl groups of the ligand.

Computational studies.

Calculation of the reaction pathway. Path C was investigated by DFT to determine the feasibility of this proposed mechanism. Based on the fact that no complex identifiable as the scandacyclobutane is observed by ^{1}H NMR spectroscopy, we anticipate that the rate-limiting step

is cyclometalation to form this product. Moreover, since the reaction is slow, taking approximately 3.5 days to reach completion at 100 °C, an activation energy of approximately 31 kcal/mol ($t_{½} \approx 36$ h), based on Eyring theory, is expected. Figure 8 depicts the calculated reaction coordinate for Path C at 100 °C.

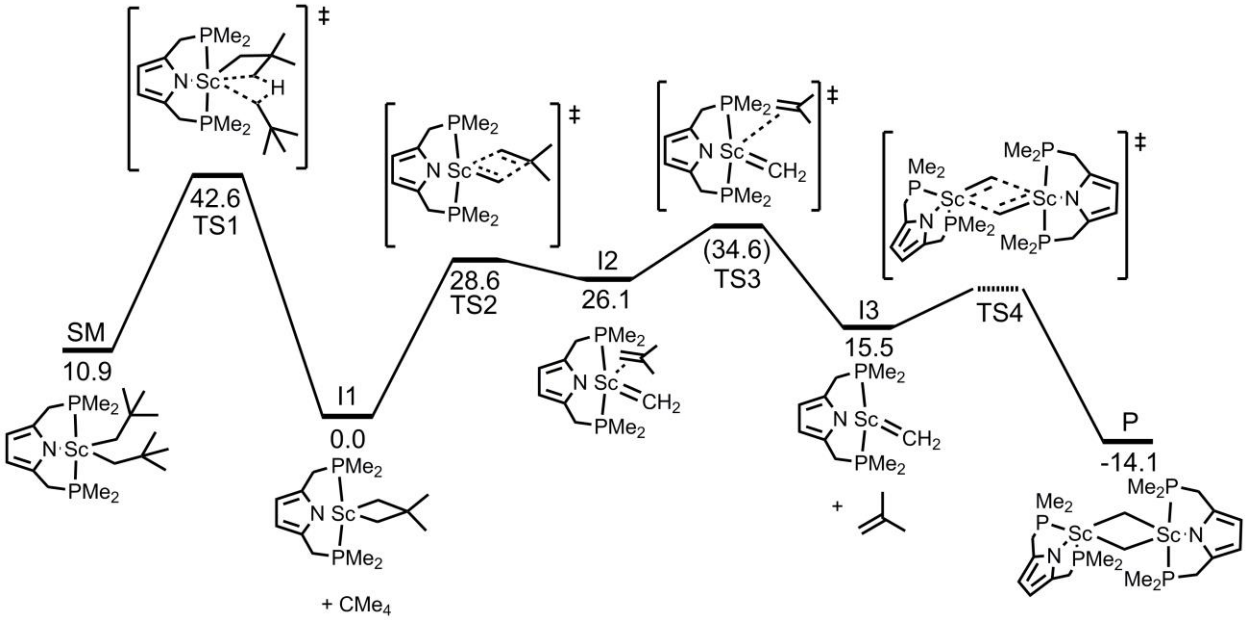

Figure 8. DFT calculated reaction pathway for thermolysis of (PNP-Cy)$ScNp_2$ at 100 °C, (Gibbs) energies are in kcal/mol; all species except the last are, in fact, two equivalents to balance the overall reaction. The transition state TS3 could not be fully converged due to the flat PES in this region. The $\Delta G^{‡}$ value in parenthesis is the closest solution obtained containing one negative eigenvalue and the correct intrinsic reaction coordinate. The last TS structure TS4 could not be located owing to the computational challenge of simulating such a large molecule. It is not clear if the pathway to **1** after formation of the methylene-isobutylene complex is exactly the pathway calculated here.

Consistent with expectations, the rate-determining step is calculated to be initial cyclometalation; the calculated Gibbs activation energy of 31.7 kcal/mol is consistent with the estimated experimental rate, based on the formation of isobutylene and **1**. The activation energy associated with the [2+2]-cycloreversion TS2 was found to be 28.6 kcal/mol, which is kinetically accessible under the reaction conditions.

The structure of the product scandium dimer **1** was optimized by DFT and the resulting geometry is consistent with the proposed geometry deduced from NMR spectra. It is worth noting that the dimer is considerably lower in energy than the free alkylidene complex, indicating that breakup of the dimer to reform the terminal methylidene complex is unlikely.

With respect to the possibility of Path A. ii., we find a calculated barrier of 40.2 kcal/mol for α-abstraction, suggesting that this mechanism is not operative. Path B was also calculated and the isobutylene-forming step is found to have an activation energy of 40.5 kcal/mol.

Electronic and Physical Structure of the methylidene complexes. Natural bond orbitals (NBOs) were calculated for comparison with other systems described as "carbenes" (Figure 1). In contrast to the low Wiberg bond orders (~0.6-0.7) determined for the zwitterionic complexes

described above (Figure 1), the calculated bond order for the Sc=C bond in the methylidene-isobutylene complex (I2 in Figure 8) is 1.6. Contributions of the scandium 3*d* orbitals are significant (20-30%) in the σ and π bonds of the interaction (see Appendix). The calculated Sc=C bond lengths in the isobutylene π-complex (I2) and free methylidene complex (I3) of 1.96 Å and 1.93 Å, respectively, are considerably shorter than any reported Sc–C bond distance and shorter than the average Sc–C bond length by 0.3 Å.[37] We therefore conclude that the putative methylidene complexes formed in this reaction are true Schrock-type alkylidenes similar to those well-known for other early transition metals.[38,39] The calculated structure of the methylidene features a significant α-CH agostic interaction (see Figure 9), similar to that observed in other early metal methylidene complexes.[12]

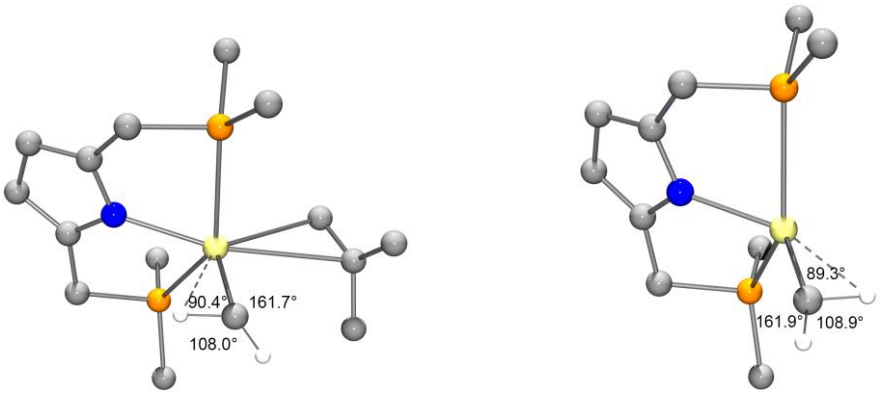

Figure 9. Calculated structures of proposed methylidene intermediates I2 (left) and I3 (right). Bond angles around the methylene carbon are shown to highlight α-CH agostic interactions.

Trapping studies.

As mentioned above, it is somewhat surprising that no evidence of 1,2-addition of benzene-d_6 or toluene-d_8 was observed in this reaction (by either NMR or mass spectroscopy), considering the reactivity of other first-row alkylidenes.[40,41] Further evidence for the formation of the methylidene complex was sought by attempting to generate the alkylidene in the presence of a trap. Such traps were ineffective. Addition of trimethylphosphine (10 equiv) to a sample of (PNP-Cy)ScNp_2 (30 mg) in toluene-d_8 (1.0 mL) had no effect on the course of the thermolysis reaction; only dimer-**1** and free trimethylphosphine were observed by ^{1}H and ^{31}P NMR spectroscopy after three days, and there was no apparent coordination of trimethylphosphine to either starting material or product. Presumably, the scandium methylidene complexes in solution dimerize too raidly to allow for a competing trapping reaction to occur.

A complication encountered with several traps was their inhibition of the alkylidene-forming reaction. Addition of DMAP (1, 2, or 4 equiv) to (PNP-Cy)ScNp_2 (30 mg) in toluene-d_8 (1.0 mL) rendered the resulting adduct stable at 100 °C for over a week with no evidence of alkylidene formation (as determined by an absence of isobutylene in the ^{1}H NMR spectrum) and little (< 10%) conversion of starting material. In an attempt to test for a methylidene complex *via* carbonyl olefination, benzophenone (2 equiv) was added to (PNP-Cy)ScNp_2 (30 mg) in toluene-d_8 (1.0 mL). The starting material immediately reacted with the ketone to form the bis(alkoxide) product (PNP-Cy)Sc$(OCPh_2Np)_2$, as determined by ^{1}H NMR spectroscopy and GC-MS of the acidified reaction mixture. Fluorinated borane Lewis acids have been used to stabilize transition metal-carbon multiple bonds.[42] Unfortunately, $B(C_6F_6)_3$ (2 equiv) abstracted an alkyl group from

(PNP-Cy)$ScNp_2$ (30 mg) in toluene-d_8 at room temperature to form a thermally unstable product (as observed by ^{1}H NMR spectroscopy). Triphenylboron (2 equiv) does not react with (PNP-Cy)$ScNp_2$ (30 mg) in toluene-d_8 (1.0 mL) at room temperature over 12 h, but does react at 100 °C in an unknown way, fully converting the starting material while inhibiting the formation of isobutylene and hence of methylidene complex as well. Addition of excess (>10 equiv) cyclopentene or 3-hexyne to (PNP-Cy)$ScNp_2$ (30 mg) in toluene-d_8 (1.0 mL) and heating to 100 °C for 3 d resulted in conversion of the starting material into a complex mixture of products which could not be identified, in addition to some isobutylene (~0.1 equiv). Full experimental details for these experiments are given in the Supporting Information.

Synthesis and thermolysis of yttrium complexes. We had previously found that complexes of the type (PNP-R)$Sc(CH_2CMe_3)_2$ are easily prepared by addition of the protonated ligand (PNP-R)H to $ScNp_3(THF)_2$. Using the yttrium complex $YNp_3(THF)_2$, which we found to be a stable crystalline solid (an ORTEP diagram is available in the Supporting Information), the yttrium congeners could also be synthesized. Addition of 1 equiv of (PNP-^{t}Bu)H (80.2 mg) to $YNp_3(THF)_2$ (1 equiv, 93.4 mg) in toluene (5 mL) afforded (PNP-^{t}Bu)YNp_2 (an ORTEP diagram is shown in Figure 10).

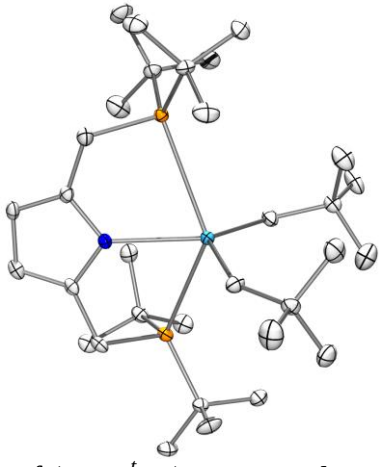

Figure 10. ORTEP diagram of (PNP-^{t}Bu)YNp_2. Hydrogen atoms omitted for clarity.

Generation of (PNP-^{t}Bu)$Y(CD_2CMe_3)_2$ (from 9.6 mg of (PNP-^{t}Bu)H and 11.3 mg of $Y(CD_2CMe_3)_3(THF)_2$) in benzene-d_6 and subsequent heating of the solution (80 °C, 2 h) resulted in complete conversion of the starting material and afforded only isobutylene-d_0, as was observed for (PNP-^{t}Bu)$Sc(CD_2CMe_3)_2$, indicating activation of the *t*-butyl groups of the ligand rather than those of the neopentyl ligand. Addition of 1 equiv of (PNP-Cy)H (10.9 mg) to $YNp_3(THF)_2$ (1 equiv, 10.0 mg) in C_6D_6 in a sealed NMR tube afforded a product with the expected ^{1}H NMR spectrum for (PNP-Cy)YNp_2 (see Appendix). After three days at room temperature, no starting material remained and isobutylene (0.1 equiv) was observed. The yttrium congener of **1** does not form selectively; the ^{1}H NMR spectrum contains only an unassignable mixture of resonances in regions where ligand resonances appear. Generation of (PNP-Cy)$Y(CD_2CMe_3)_2$ and storage at room temperature in a sealed NMR tube for three days produced a mixture of isobutylene-d_2 (deuterated at the vinyl position) and isobutylene-d_0 as was observed for the scandium congener, suggesting that a similar yttrium alkylidene species is

formed. However, the putative (PNP-Cy)YNp_2 thermally decomposes at room temperature and extremely rapidly under vacuum, preventing its isolation.

The kinetic selectivity for C–H activation of the P^tBu_2 groups in (PNP-^{t}Bu)MNp_2 (M = Sc, Y), in contrast to preferred activation of the neopentyl groups in (PNP-Cy)MNp_2, may be due a combination several factors. The increased steric hindrance around the cyclohexyl group β-hydrogens (on a 2° carbon) vs. around the *t*-butyl group β-hydrogens (on a 1° carbon) make the cyclohexyl group more difficult to activate.[43] At the same time, the bulky t-butyl groups push the β-hydrogens closer to the metal center, lowering the barrier to activation. Additionally, there are a statistically larger number of available hydrogens on the *t*-butyl group (9 vs. 2; only 2 of the 4 β-hydrogens on the cyclohexyl groups are accessible because one set of the diastereotopic β-hydrogens always points away from the metal when the cyclohexyl group is close to the metal) making cyclohexyl group activation comparatively less likely. In other words, both the enthalpy and entropy of activation disfavor cyclohexyl activation relative to *t*-butyl activation, and this difference can give rise to the observed selectivity.

Investigation of the yttrium pathway. DFT computation of the analogous Path C for yttrium confirms that the cyclometallation/cycloreversion mechanism is viable, and is predicted to proceed with a slightly lower activation energy (by 0.5 kcal/mol) than the corresponding scandium pathway (see Appendix). Hence, cyclometalation/cycloreversion may be a general route to rare earth alkylidenes, provided that all other competitive pathways are higher in energy. As with scandium, trapping studies with the yttrium congener were unsuccessful. Addition of a solution of DMAP (2 or 4 equivs) and (PNP-Cy)H (1 equiv) to $YNp_3(THF)_2$ (1 equiv) rapidly formed the observed, intractable product mixture and isobutylene (0.1 equiv). Addition of a solution of 2-butyne (10 equiv) and (PNP-Cy)H (1 equiv) to $YNp_3(THF)_2$ (1 equiv) gave the same products and time course as the reaction without 2-butyne present.

CONCLUSION

For the first time, evidence is presented for the intermediate formation of terminal group 3 alkylidene complexes. These complexes are proposed to form by γ-activation of C–H bonds of a neopentyl group to generate a metallacyclobutane, which then undergoes [2+2]-cycloreversion to produce the alkylidene complex with release of isobutylene. In the case of scandium, the methylidene complex dimerizes to form a doubly-bridging methylene complex, whose solution structure was determined by 1D and 2D NMR spectroscopy. The general application of this method may allow for the formation of additional, new types of rare earth terminal alkylidene complexes.

EXPERIMENTAL SECTION

General

Unless otherwise noted, all experiments were conducted in dry, oxygen-free solvents using standard Schlenk techniques or in a N_2 atmosphere glovebox. Deuterated solvents were purchased from Cambridge Isotope Laboratories, Inc. Benzene-d_6 was dried by vacuum distillation from Na/K alloy. Toluene-d_8 was dried by refluxing over molten sodium metal followed by vacuum distillation. Unless otherwise noted, reagents were obtained from commercial suppliers and used as received. 4-phenylpyridine was obtained from Aldrich and

sublimed. (PNP-Cy)H, (PNP-^{t}Bu)H, (PNP-Cy)$ScNp_2$ were prepared according to literature procedures.[28]

Analytical Methods

Solution NMR spectroscopy was performed using Bruker AV-300, AVB-400, AVQ-400, AV-500, or AV-600 MHz spectrometers at room temperature. ^{1}H, ^{13}C{^{1}H}, and ^{31}P{^{1}H} NMR spectra were calibrated internally to either the resonance for the solvent or residual proteo solvent relative to tetramethylsilane. Elemental analyses were carried out by the College of Chemistry Microanalytical Laboratory at the University of California, Berkeley. Mass spectrometry was carried out by the combined QB3/Chemistry Mass Spectrometry Facility at the University of California, Berkeley.

Computational Details

Calculations were carried out with the Gaussian09 rev D01 suite of programs, employing the B3PW91 hybrid functional and 6-31++G** basis set for non-metal atoms. Metal atoms were treated with the relativistic ECP and basis set of the Stuttgart group. Gibbs free energies were calculated at 298 K and 1 atm of pressure and adjusted to 373 K using Gaussian's freqchk utility. The ligand cyclohexyl groups were truncated to methyl groups to save computational time; selected calculations employing the untruncated ligand produced identical results within the error of the calculation.

X-ray Crystallography Details

X-ray diffraction data for crystals of $YNp_3(THF)_2$ and (PNP-^{t}Bu)YNp_2 were collected using a Bruker AXS modified four-circle diffractometer coupled CCD detector with Mo Kα (λ = 0.71073 Å) radiation monochromated by a system of QUAZAR multilayer mirrors. Crystals were kept at 100(2) K throughout collection. Data collection, refinement, and reduction were performed with Bruker APEX2 software (v. 2013.4). Structures were solved by direct methods using SHELXS-97. All structures were refined with SHELXL-97 with refinement of F^2 against all reflections by full-matrix least squares. In all models, non-hydrogen atoms were refined anisotropically, and hydrogen atoms were included at their geometrically-calculated positions and refined using a riding model. The 3D molecular structure figures were visualized with ORTEP 3.2, rendered with POV-Ray 3.6, and annotated with Adobe Photoshop CS6.

Thermolysis of (PNP-Cy)$ScNp_2$ to 1. A sample of (PNP-Cy)$ScNp_2$ (33.7 mg, 0.05 mmol) was dissolved in benzene-d_6 or toluene-d_8 (0.6 mL) in a 5 mm NMR tube with a Teflon screw cap. The sample was placed in a pre-heated 100 °C oil bath for 3.5 days. The resulting sample could be used for subsequent reactivity and spectroscopic studies but could not be isolated as a pure, crystalline solid. ^{1}H NMR (500 MHz, Toluene-d_8) δ 6.34 (d, J = 1.8 Hz, 1H), 6.17 (d, J = 0.9 Hz, 1H), 6.15 (s, J = 0.9 Hz, 1H), 6.03 (t, J = 2.6 Hz, 1H), 3.31 (d, J = 15.0 Hz, 1H), 3.17 (dd, J = 14.5 Hz, 11.5 Hz, 1H), 3.08 – 3.04 (m, 4H), 2.90 (d, J = 4.6 Hz, 2H), 2.01 – 1.61 (m, 42H),1.51 (1H), 1.48 (1H) 1.36 – 1.09 (m, 46H), 1.13 (1H), 1.09 (1H). ^{13}C{^{1}H} NMR (151 MHz, Toluene-d_8) δ 135.34 (d, J = 2.2 Hz), 135.29 (d, J = 1.8 Hz), 133.52 (d, J = 2.8 Hz), 133.48 (d, J = 2.8 Hz), 111.48 (d, J = 5.8 Hz), 106.46 (d, J = 6.5 Hz), 106.30 (d, J = 5.9 Hz), 106.05 (d, J = 4.1 Hz), 43.57 (d, J = 36.5 Hz), 36.53 , 36.25 , 35.82 (d, J = 23.8 Hz), 35.57 (dd, J = 7.1, 2.0 Hz), 34.43 (d, J = 17.5 Hz), 34.35 (d, J = 17.4 Hz), 34.08 (d, J = 12.0 Hz), 33.70 (d, J = 8.2 Hz), 33.24 (d, J = 4.2 Hz), 32.91 (d, J = 5.4 Hz), 31.67 , 31.52 , 31.48 , 30.78 (d, J = 11.9

Hz), 30.74 (d, J = 12.4 Hz), 30.53 , 30.47 (d, J = 3.6 Hz), 30.34 (d, J = 12.0 Hz), 30.25 , 30.23 , 30.00 (d, J = 5.3 Hz), 29.59 , 29.40 (d, J = 1.9 Hz), 28.74 , 28.58 (d, J = 11.3 Hz), 28.31 (d, J = 7.0 Hz), 28.23 (d, J = 7.9 Hz), 28.21 (d, J = 8.8 Hz), 28.11 (d, J = 8.2 Hz), 28.01 , 27.99 , 27.94 (d, J = 6.3 Hz), 27.88 , 27.82 , 27.80 , 27.76 (d, J = 3.2 Hz), 27.59 (d, J = 10.5 Hz), 27.31 , 27.29 , 26.87 , 26.51 , 26.49 , 26.37 , 26.20 (d, J = 17.1 Hz), 25.49 , 24.84 , 23.66 – 23.46 (m), 23.03 , 22.77 , 22.14 (d, J = 8.4 Hz), 14.26. $^{31}P\{^{1}H\}$ NMR (202 MHz, Toluene-d_8) δ 10.01, 8.97, -3.86, -9.46. All of these resonances are assigned using the 2D spectra as indicated in Table 1 and Figures 2 and 4 and 1D spectra in Supporting Information. Preparation of α-^{13}C-neopentyllithium was attempted in order to also carry out ^{13}C-labeling experiments. However, the difficulties in preparing small amounts (due to the cost of ^{13}C-labeled starting materials) of neopentyllithium by reduction with Li metal[44] precluded such experiments. Without ^{13}C labels, it is very difficult to observe ^{13}C resonances directly attached to scandium,[45] although they can sometimes be located by 2D experiments.[28] We were unable to locate the ^{13}C shifts of the bridging methylene groups.

Synthesis of (PNP-Cy)Sc(CD_2CMe_3)$_2$. A solution of (PNP-Cy)H (34 mg, 0.073 mmol) in pentane (3 mL) was added to a solution of $ScNp_3(THF)_2$-d_6[28] (30.0 mg, 0.073 mmol) in pentane (5 mL) and the resulting reaction mixture was stirred for 1 h. The volatile materials were removed under vacuum. The material showed the same NMR spectra as (PNP-Cy)$ScNp_2$, except for the absence of the resonance at 1.16 ppm from the ^{1}H NMR spectrum and the appearance of a resonance in the ^{2}H NMR spectrum at δ 1.16 (s).

Synthesis of $YNp_3(THF)_2$. Neopentyllithium (366 mg, 4.69 mmol) was dissolved in pentane (10 mL) and added dropwise to a stirred suspension of $YCl_3(THF)_{3.5}$ (700 mg, 1.56 mmol) in pentane (8 mL). The reaction mixture became cloudy and produced a fine white precipitate. After stirring for 4 h, the reaction mixture was filtered through a fritted funnel and the filtrate was concentrated to 10 mL. The concentrated filtrate was cooled at -35 °C for 3 d to afford the product as colorless, single-crystal needles (501 mg, 72 % yield). ^{1}H NMR (500 MHz, benzene-d_6) δ 4.08 – 3.99 (m, 8H), 1.33 (s, 27H, $^{1}J_{CH}$ = 122.8 Hz), 1.31 (m, 8H), 0.12 (d, 6H, $^{2}J_{YH}$ = 2.1 Hz, $^{1}J_{CH}$ = 99.5 Hz). ^{1}H NMR (500 MHz, THF-d_8) δ 3.66 – 3.61 (m, 8H), 1.82 – 1.76 (m, 8H), 0.99 (s, 27H), -0.10 (d, 6H, J_{YH} = 2.7 Hz). Note: $YNp_3(THF)_2$ does not exchange THF in THF-d_8. $^{13}C\{^{1}H\}$ NMR (151 MHz, benzene-d_6) δ 71.03 (THF, 2, 5 position), 65.61 (d, $^{1}J_{YC}$ = 43.7 Hz, -$CH_2C(CH_3)_3$), 36.86 (-$CH_2C(CH_3)_3$), 35.19 (-$CH_2C(CH_3)_3$) , 25.09 (THF, 3, 4 position). Note: assignments and coupling constants were determined by ^{1}H-^{13}C HSQC and ^{1}H-^{13}C HMBC experiments. NMR data is consistent with previous report of this compound.[46]

Synthesis of (PNP-^{t}Bu)YNp_2.(PNP-^{t}Bu)H (80.2 mg, 0.209 mmol) was dissolved in toluene (5 mL) and added dropwise to a stirred solution of $YNp_3(THF)_2$ (93.4 mg, 0.209 mmol) in toluene (5 mL). After stirring for 1 h, the reaction mixture was concentrated *in vacuo* and stored at -35 °C for 3 d to afford the product as colorless, crystalline material (89.0 mg, 69 % yield). ^{1}H NMR (400 MHz, benzene-d_6) δ 6.19 (s, 2H), 3.08 (d, $^{2}J_{PH}$ = 3.4 Hz, 4H), 1.50 (s, 18H), 1.09 (d, $^{3}J_{PH}$ = 12.0 Hz, 36H), 0.81 (d, $^{2}J_{YH}$ = 2.5 Hz, 4H). ^{13}C NMR (151 MHz, benzene-d_6) δ 134.70 (t, $^{2}J_{PC}$ = 3.8 Hz), 106.61 (t, $^{3}J_{PC}$ = 3.6 Hz), 83.42 (d, $^{1}J_{YC}$ = 45.1 Hz, -$CH_2C(CH_3)_3$), 36.38 (-$CH_2C(CH_3)_3$), 36.05, 32.49, 29.49 (t, J = 3.3 Hz, -$CH_2P((C(CH_3)_3)_2$), 22.00 (-$CH_2P(C(CH_3)_3)_2$). ^{31}P NMR (162 MHz, benzene-d_6) δ 26.48 (d, $^{1}J_{PY}$ = 67.0 Hz). An ORTEP

diagram and crystal data are available in the Supporting Information. Anal Calcd. for $C_{32}H_{64}NP_2Y$: C, 62.63; H, 10.51; N, 2.28. Found: C, 62.50; H, 10.32; N, 2.14.

Thermolysis of (PNP-Cy)YNp$_2$. A sample of (PNP-Cy)H (10.9 mg, 0.022 mmol) was dissolved in benzene-d_6 or toluene-d_8 (0.6 mL) and added to a solution in the same solvent of $YNp_3(THF)_2$ (10 mg, 0.022 mmol) in a 5 mm NMR tube with a Teflon screw cap. The sample appeared to consist principally (>90 % yield relative to starting material by ^{1}H NMR spectroscopy) of a material with the expected NMR characteristics of (PNP-Cy)YNp$_2$. ^{1}H NMR (400 MHz, Benzene-d_6) δ 6.25 (s, 2H), 3.06 (d, J = 3.6 Hz, 4H), 2.02- 1.04 (m, 44H), 1.50 (s, 18H), 0.76 (d, J_{YH} = 2.5 Hz, 4H). ^{31}P{^{1}H} NMR (162 MHz, Benzene-d_6) δ 0.63 (d, J_{YP} = 68.6 Hz). Storing this material in benzene-d_6 for 3 days at room temperature, in the absence of light, afforded isobutylene (0.1 equiv relative to (PNP-Cy)YNp$_2$) and an intractable mixture of products.

Trapping Studies: Trimethylphosphine. A sample of (PNP-Cy)ScNp$_2$ (7.0 mg, 0.01 mmol) was dissolved in benzene-d_6 (0.6 mL) in a 5 mm NMR tube with a Teflon screw cap and trimethylphosphine (3 mg, 0.05 mmol) was added. The sample was heated to 100 °C for 48 h. The trimethylphosphine had no effect on the thermolysis reaction (as determined by NMR spectroscopy).

Trapping Studies: Benzophenone. A sample of (PNP-Cy)ScNp$_2$ (7.0 mg, 0.01 mmol) was dissolved in benzene-d_6 (0.5 mL) in a 5 mm NMR tube with a Teflon screw cap and a solution of benzophenone (5.7 mg, 0.03 mmol) in benzene-d_6 (0.5 mL) was added. This immediately afforded material consistent with (PNP-Cy)Sc(OCPh$_2$Np)$_2$. ^{1}H NMR (600 MHz, Benzene-d_6) δ 7.79 (d, J = 7.8 Hz, 4H), 7.70 (d, J = 7.3 Hz, 4H), 7.25 (t, J = 7.7 Hz, 4H), 7.12 (t, J = 7.6 Hz, 4H), 7.03 (t, J = 8.0 Hz, 2H), 6.07 (s, 2H), 2.65 (s, 4H), 1.84 – 1.48 (m, 24H), 1.34 – 1.01 (m, 20 H), 1.03 (s, 4H), 0.93 (s, 18H). ^{31}P{^{1}H} NMR (203 MHz, Benzene-d_6) δ -0.26 (br s). Hydrolysis of the sample with 6.0 M HCl (1.0 mL) and subsequent GC-MS analysis revealed HOCPh$_2$Np.

Trapping Studies: B(C$_6$F$_5$)$_3$. A sample of (PNP-Cy)ScNp$_2$ (12.5 mg, 0.022 mmol) was dissolved in benzene-d_6 (0.5 mL) in a 5 mm NMR tube with a Teflon screw cap and a solution of B(C$_6$F$_5$)$_3$ (11.2 mg, 0.022 mmol) in benzene-d_6 (0.5 mL) was added. The product was immediately converted into a benzene-soluble intimate ion pair (analysis of the ^{19}F NMR spectrum of the product clearly indicates that the boron is 4-coordinate[48]). ^{1}H NMR (500 MHz, benzene-d_6) δ 6.57 (d, J = 1.6 Hz, 1H), 6.22 (s, 2H), 4.84 (d, J = 13.6 Hz, 1H), 3.29 (s, 1H), 3.01 (br s, 5H), 2.79 (d, J = 15.4 Hz, 1H), 2.52 (ddd, J = 15.5, 11.4, 4.7 Hz, 1H), 2.22 – 1.91 (m, 2H), 1.85 – 0.89 (m). ^{31}P NMR (162 MHz, benzene-d_6) δ 4.65, 1.40, -1.22 (br). ^{19}F NMR (376 MHz, benzene-d_6) δ -128.59 , -131.85 , -159.10 (t, J = 20.8 Hz), -163.84 (t, J = 17.9 Hz). ^{11}B NMR (128 MHz, benzene-d_6) δ -16.01 (d, J = 89.4 Hz). This product was found to be thermally sensitive, decomposing over 24 h at room temperature into an intractable mixture of products (as determined by NMR spectroscopy).

Trapping Studies: BPh$_3$. A sample of (PNP-Cy)ScNp$_2$ (7.0 mg, 0.01 mmol) was dissolved in benzene-d_6 (0.5 mL) in a 5 mm NMR tube with a Teflon screw cap and a solution of triphenylboron (5.7 mg, 0.025 mmol) in benzene-d_6 (0.5 mL) was added. The sample was heated

to 100 °C for 5 d. No isobutylene was observed and several unidentified resonances were observed by NMR spectroscopy.

Trapping Studies: DMAP. A sample of (PNP-Cy)$ScNp_2$ (30.0 mg, 0.045 mmol) was dissolved in benzene-d_6 (0.5 mL) in a 5 mm NMR tube with a Teflon screw cap and a solution of DMAP (5.5, 11, or 22 mg, 0.045, 0.090, or 0.180 mmol) in benzene-d_6 (0.5 mL) was added. The sample was heated to 100 °C for 7 d. No isobutylene was observed by NMR spectroscopy. Less than 10% of the starting material was converted.

Trapping Studies: Norbornene. A sample of (PNP-Cy)$ScNp_2$ (37.0 mg, 0.055 mmol) was dissolved in benzene-d_6 (0.5 mL) in a 5 mm NMR tube with a Teflon screw cap and a solution of norbornene (83 mg, 0.88 mmol) in benzene-d_6 (0.5 mL) was added. The sample was heated to 100 °C for 2 d. No isobutylene was observed by NMR spectroscopy. Moreover, the starting material was converted to an intractable mixture of products.

Trapping Studies: Cyclopentene. A sample of (PNP-Cy)$ScNp_2$ (36.0 mg, 0.053 mmol) was dissolved in benzene-d_6 (1.0 mL) in a 5 mm NMR tube with a Teflon screw cap and cyclopentene (73 mg, 1.07 mmol) was added. The sample was heated to 100 °C for 4 d. Some isobutylene (0.1 equiv) was observed by NMR spectroscopy. Moreover, the starting material was converted to a complex mixture of products.

Trapping Studies: 3-hexyne with Sc. A sample of (PNP-Cy)$ScNp_2$ (30.0 mg, 0.045 mol) and 3-hexyne (24 mg, 0.30 mmol) was dissolved in benzene-d_6 (1.0 mL) in a 5 mm NMR tube with a Teflon screw cap. The sample was heated to 100 °C for 3 d. Some isobutylene (0.1 equiv) was observed by NMR spectroscopy. Moreover, the starting material was converted to a complex mixture of products. New olefinic peaks were observed: ^{1}H NMR (500 MHz, benzene-d_6) δ 5.11 (dp, J = 9.4, 3.1 Hz), 5.06 (dp, J = 10.0, 3.4 Hz), 1.56 (d, J = 3.3 Hz), 1.54 (d, J = 3.2 Hz)., but this product could not be identified.

Trapping Studies: 2-butyne with Y. A sample of (PNP-Cy)H (10.9 mg, 0.022 mol), 2-butyne (5 mg, 0.1 mmol), and $YNp_3(THF)_2$ (10.0 mg, 0.022 mmol) was dissolved in benzene-d_6 (0.8 mL) in a 5 mm NMR tube with a Teflon screw cap. Over the course of 1 d, the thermolysis reaction proceeded as in the case without 2-butyne present.

REFERENCES

(1) Nugent, W. A.; Mayer, J. M. *Metal-Ligand Multiple Bonds: The Chemistry of Transition Metal Complexes Containing Oxo, Nitrido, Imido, Alkylidene, or Alkylidyne Ligands*, 1 edition.; Wiley-Interscience: New York, 1988.

(2) Giesbrecht, G. R.; Gordon, J. C. *Dalton Trans.* **2004**, 16, 2387–2393.

(3) Scott, J.; Basuli, F.; Fout, A. R.; Huffman, J. C.; Mindiola, D. J. *Angew. Chem. Int. Ed.* **2008**, *47*, 8502–8505.

(4) Lu, E.; Li, Y.; Chen, Y. *Chem. Commun.* **2010**, *46*, 4469–4471.

(5) Wicker, B. F.; Fan, H.; Hickey, A. K.; Crestani, M. G.; Scott, J.; Pink, M.; Mindiola, D. J. *J. Am. Chem. Soc.* **2012**, *134*, 20081–20096.

(6) Rong, W.; Cheng, J.; Mou, Z.; Xie, H.; Cui, D. *Organometallics* **2013,** *32*, 5523–5529.

(7) Chu, T.; Piers, W. E.; Dutton, J. L.; Parvez, M. *Organometallics* **2013**, *32*, 1159–1165.

(8) Chu, J.; Han, X.; Kefalidis, C. E.; Zhou, J.; Maron, L.; Leng, X.; Chen, Y. *J. Am. Chem. Soc.* **2014,** *136*, 10894–10897.

(9) Flores, J. A.; Cavaliere, V. N.; Buck, D.; Pintér, B.; Chen, G.; Crestani, M. G.; Baik, M.-H.; Mindiola, D. J. *Chem. Sci.* **2011**, *2*, 1457–1462.

(10) Kamitani, M.; Pinter, B.; Chen, C.-H.; Pink, M.; Mindiola, D. J. *Angew. Chem. Int. Ed.* **2014**, *53*, 10913–10951.

(11) Marinescu, S. C.; Levine, D. S.; Zhao, Y.; Schrock, R. R.; Hoveyda, A. H. *J. Am. Chem. Soc.* **2011**, *133*, 11512–11514.

(12) Liu, A. H.; Murray, R. C.; Dewan, J. C.; Santarsiero, B. D.; Schrock, R. R. *J. Am. Chem. Soc.* **1987**, *109*, 4282–4291.

(13) Schrock, R. R. *Acc. Chem. Res.* **1979**, *12*, 98–104.

(14) Mindiola, D. J.; Bailey, B. C.; Basuli, F. *Eur. J. Inorg. Chem.* **2006**, *2006*, 3135–3146.

(15) Kratsch, J.; Roesky, P. W. *Angew. Chem. Int. Ed.* **2014**, *53*, 376–383.

(16) Dietrich, H. M.; Törnroos, K. W.; Anwander, R. *J. Am. Chem. Soc.* **2006**, *128*, 9298–9299.

(17) Luo, G.; Luo, Y.; Qu, J.; Hou, Z. *Organometallics* **2015**, *34*, 366–372.

(18) Zhou, J.; Li, T.; Maron, L.; Leng, X.; Chen, Y. *Organometallics* **2015**, *34*, 470–476.

(19) Aparna, K.; Ferguson, M.; Cavell, R. G. *J. Am. Chem. Soc.* **2000**, *122*, 726-727.

(20) Liddle, S. T.; Mills, D. P.; Wooles, A. J. *Chem. Soc. Rev.* **2011**, *40*, 2164–2176.

(21) Scott, J.; Fan, H.; Wicker, B. F.; Fout, A. R.; Baik, M.-H.; Mindiola, D. J. *J. Am. Chem. Soc.* **2008**, *130*, 14438–14439.

(22) Liddle, S. T.; McMaster, J.; Green, J. C.; Arnold, P. L. *Chem. Commun.* **2008**, No. 15, 1747–1749.

(23) Cantat, T.; Mézailles, N.; Ricard, L.; Jean, Y.; Le Floch, P. *Angew. Chem. Int. Ed.* **2004**, *43*, 6382–6385.

(24) Fustier, M.; Le Goff, X. F.; Le Floch, P.; Mézailles, N. *J. Am. Chem. Soc.* **2010**, *132*, 13108–13110.

(25) Fustier, M.; Le Goff, X.-F.; Lutz, M.; Slootweg, J. C.; Mézailles, N. *Organometallics* **2015**, *34*, 63–72.

(26) Wang, C.; Zhou, J.; Zhao, X.; Maron, L.; Leng, X.; Chen, Y. *Chem. – Eur. J.* **2016**, *22*, 1258–1261.

(27) Mindiola, D. J.; Scott, J. *Nat. Chem.* **2011**, *3*, 15–17.

(28) Levine, D. S.; Tilley, T. D.; Andersen, R. A. *Organometallics* **2015**, *34*, 4647–4655.

(29) Lipke, M. C.; Neumeyer, F.; Tilley, T. D. *J. Am. Chem. Soc.* **2014**, *136*, 6092–6102.

(30) Other mechanisms involving di- or multinuclear intermediate species were considered, but are considered less likely due to the fact that the reaction rate does not depend on the initial concentration of starting material.
(31) Hajela, S.; Bercaw, J. E. *Organometallics* **1994**, *13*, 1147–1154.
(32) Fendrick, C. M.; Marks, T. J. *J. Am. Chem. Soc.* **1986**, *108*, 425–437.
(33) McNeill, K.; Andersen, R. A.; Bergman, R. G. *J. Am. Chem. Soc.* **1995**, *117*, 3625–3626.
(34) Schrock, R. R. *Chem. Rev.* **2009**, *109*, 3211–3226.
(35) Straus, D. A.; Grubbs, R. H. *Organometallics* **1982**, *1*, 1658–1661.
(36) Miyashita, A.; Ohyoshi, M.; Shitara, H.; Nohira, H. *J. Organomet. Chem.* **1980**, *338*, 103–111.
(37) Allen, F. H. *Acta Crystallogr. B* **2002**, *58*, 380–388.
(38) Tebbe, F. N.; Harlow, R. L. *J. Am. Chem. Soc.* **1980**, *102*, 6149–6151.
(39) Scott, J.; Mindiola, D. J. *Dalton Trans.* **2009**, No. 40, 8463–8472.
(40) Heijden, H. van der; Hessen, B. *J. Chem. Soc. Chem. Commun.* **1995**, No. 2, 145–146.
(41) Coles, M. P.; Gibson, V. C.; Clegg, W.; Elsegood, M. R. J.; Porrelli, P. A. *Chem. Commun.* **1996**, No. 16, 1963–1964.
(42) van der Eide, E. F.; Piers, W. E.; Romero, P. E.; Parvez, M.; McDonald, R. *Organometallics* **2004**, *23*, 314–316.
(43) Arndtsen, B. A.; Bergman, R. G.; Mobley, T. A.; Peterson, T. H. *Acc. Chem. Res.* **1995**, *28*, 154–162.
(44) Larabi, C.; Merle, N.; Norsic, S.; Taoufik, M.; Baudouin, A.; Lucas, C.; Thivolle-Cazat, J.; de Mallmann, A.; Basset, J.-M. *Organometallics* **2009**, *28*, 5647–5655.
(45) St. Clair, M.; Schaefer, W. P.; Bercaw, J. E. *Organometallics* **1991**, *10*, 525–527.
(46) Lappert, M. F.; Pearce, R. *J. Chem. Soc. Chem. Commun.* **1973**, No. 4, 126–126.

Chapter 2 Appendix

Spectroscopic Characterization

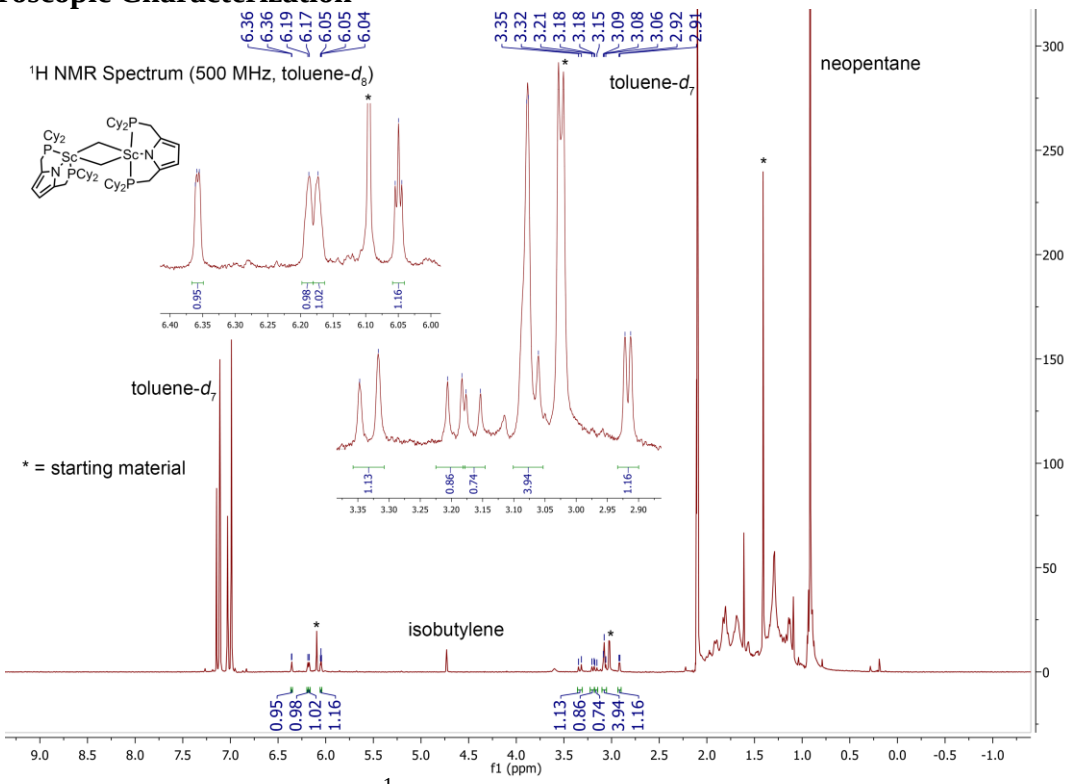

^{1}H NMR Spectrum of **1**.

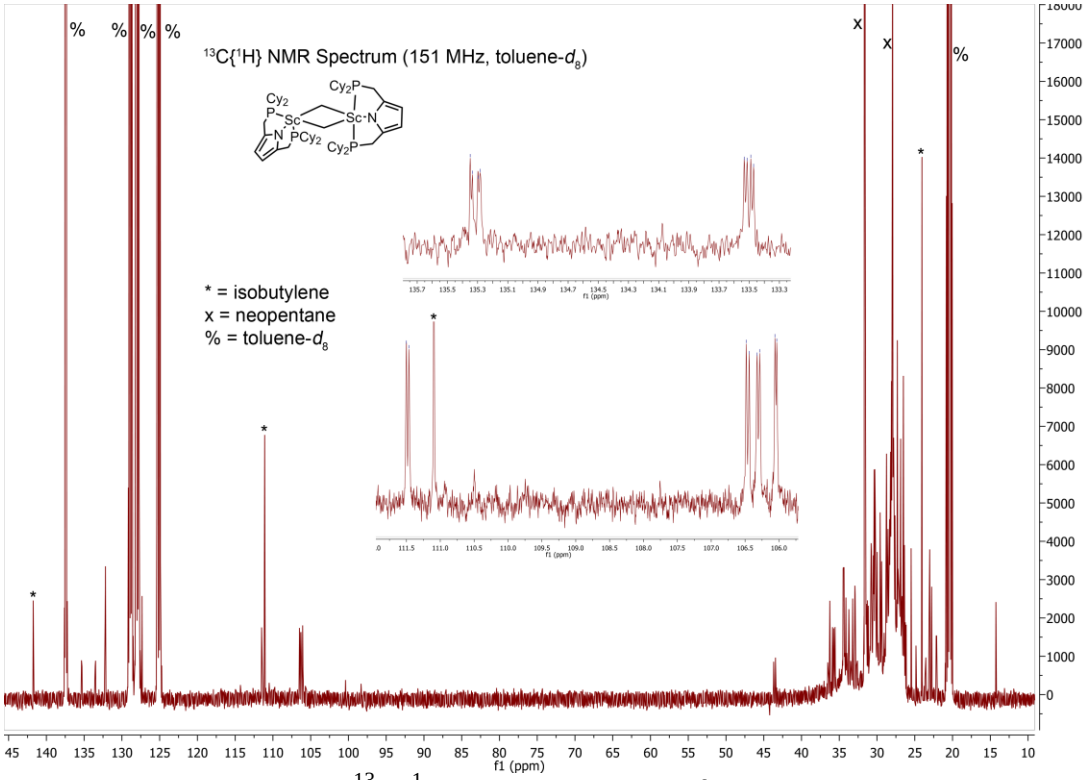

^{13}C{^{1}H} NMR Spectrum of **1**.

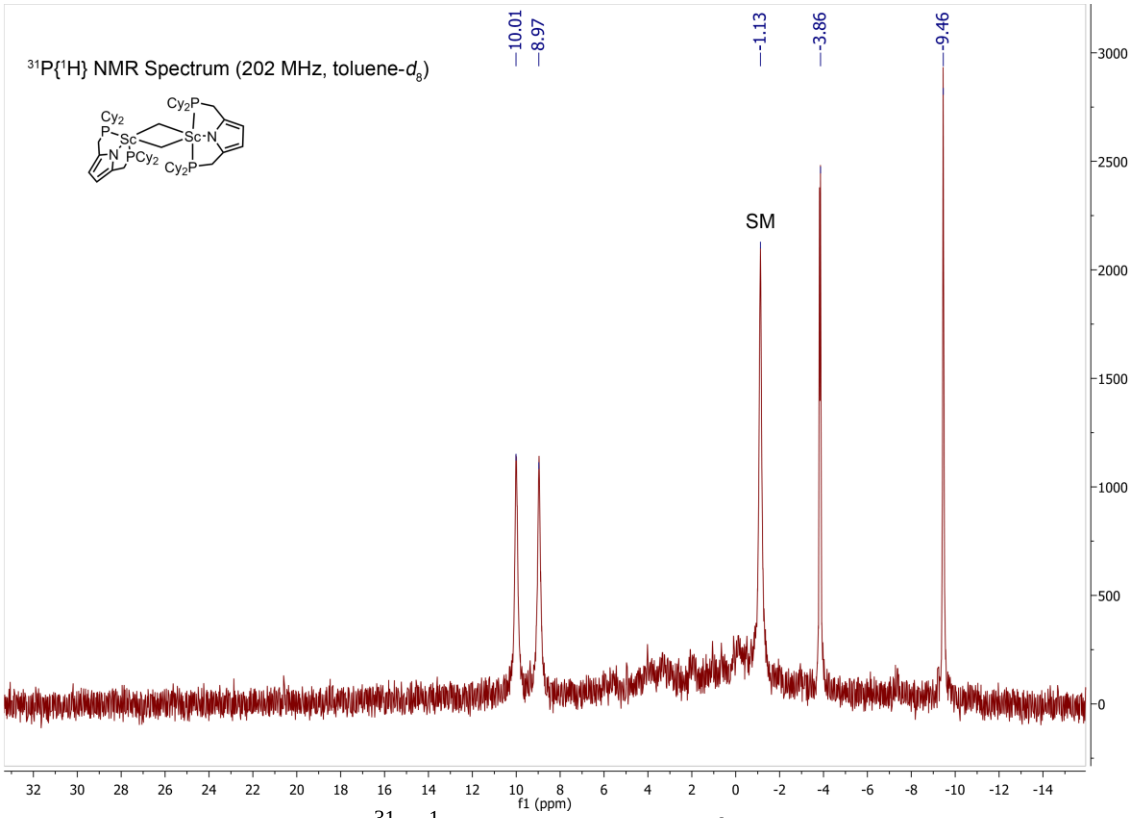

$^{31}P\{^{1}H\}$ NMR Spectrum of **1**.

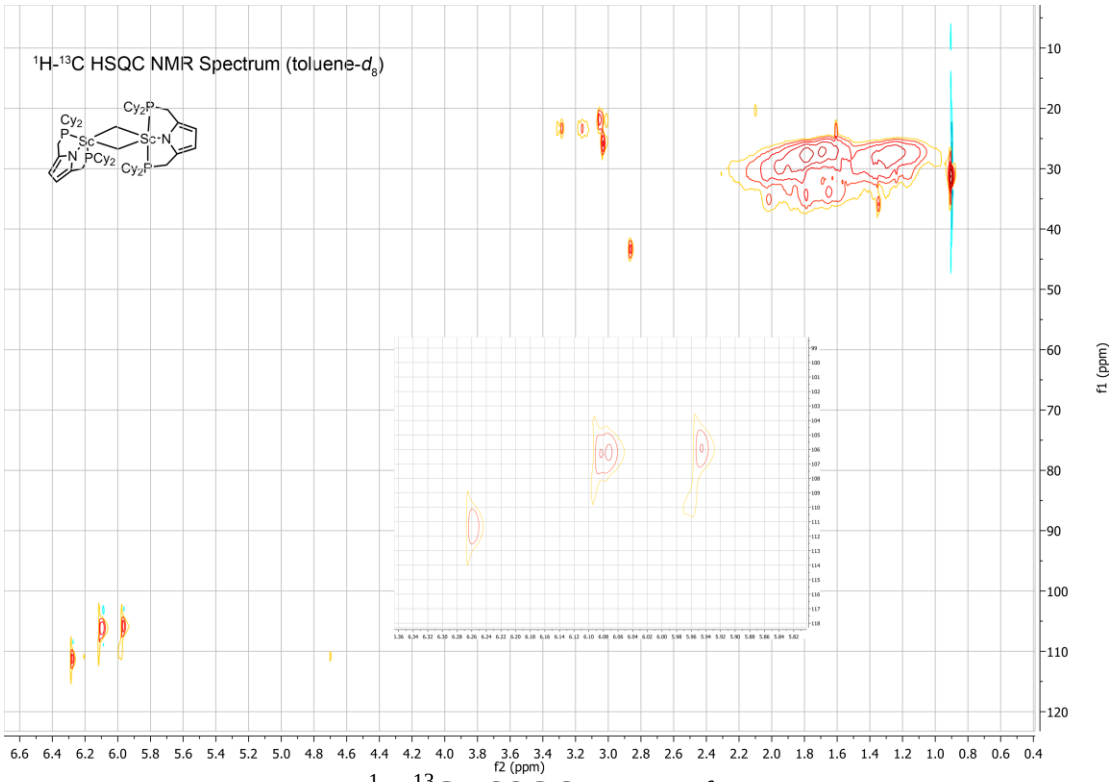

^{1}H-^{13}C HSQC Spectrum of **1**.

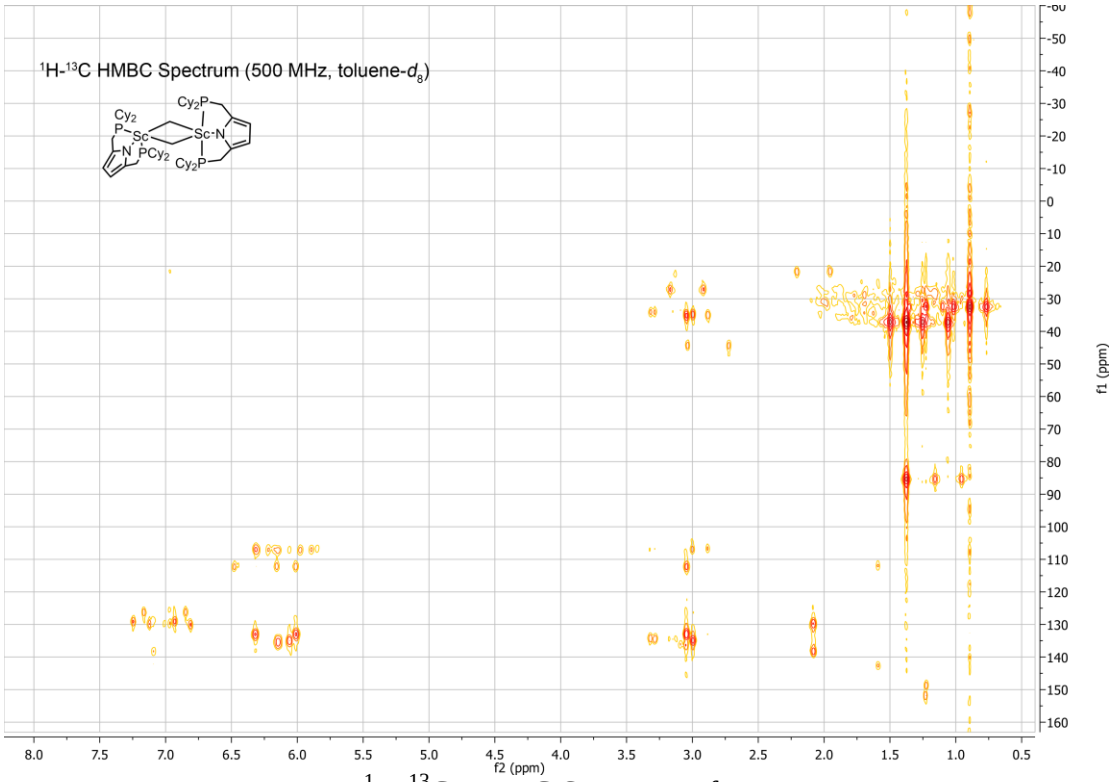

^{1}H-^{13}C HMBC Spectrum of **1**.

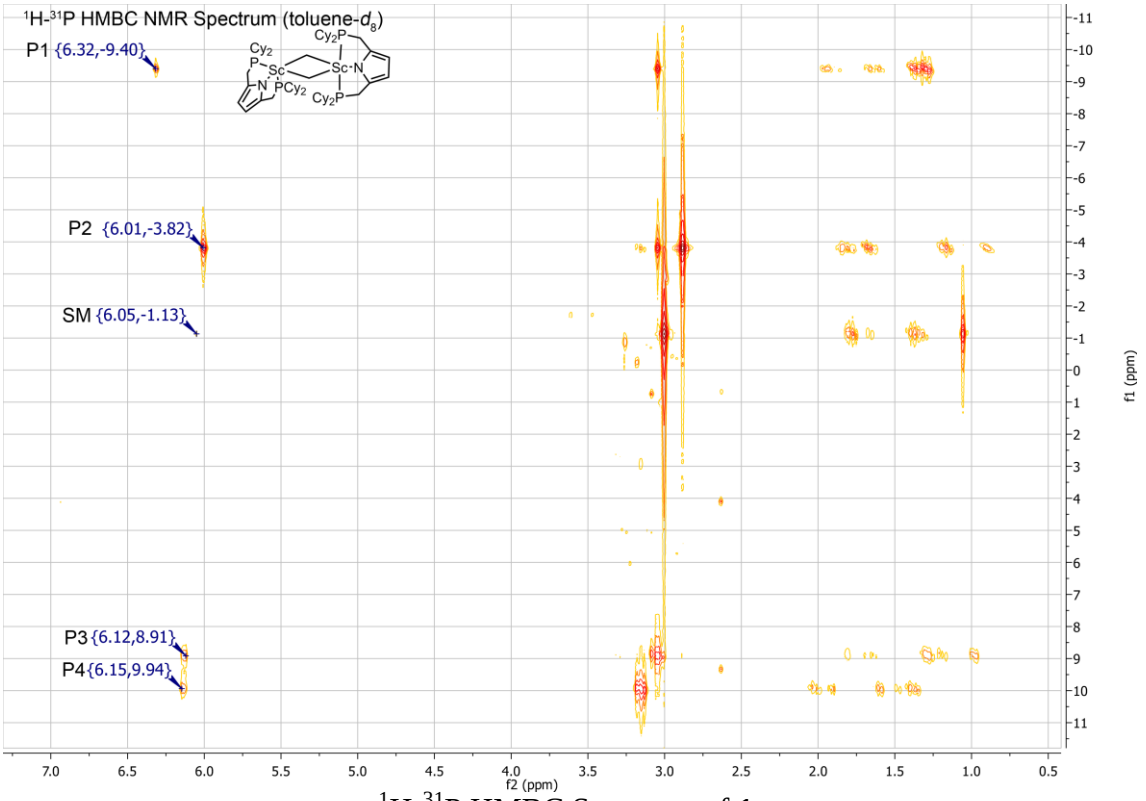

^{1}H-^{31}P HMBC Spectrum of **1**.

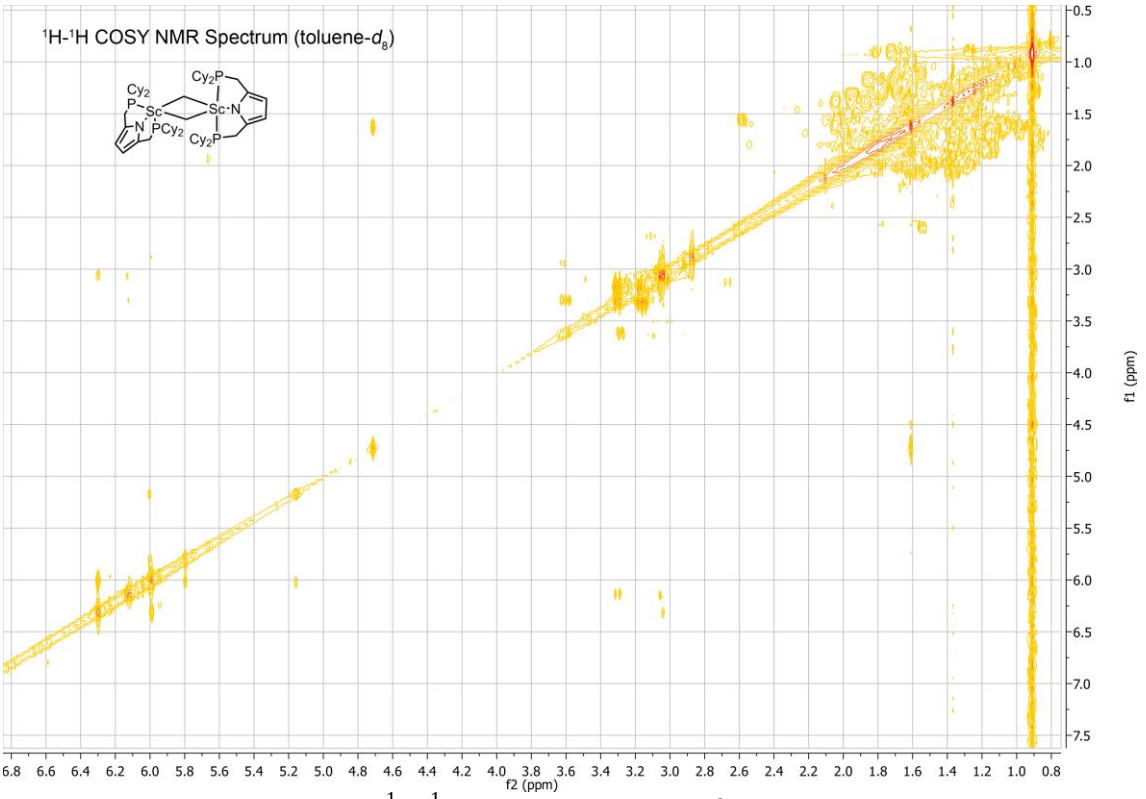

^{1}H-^{1}H COSY Spectrum of **1**.

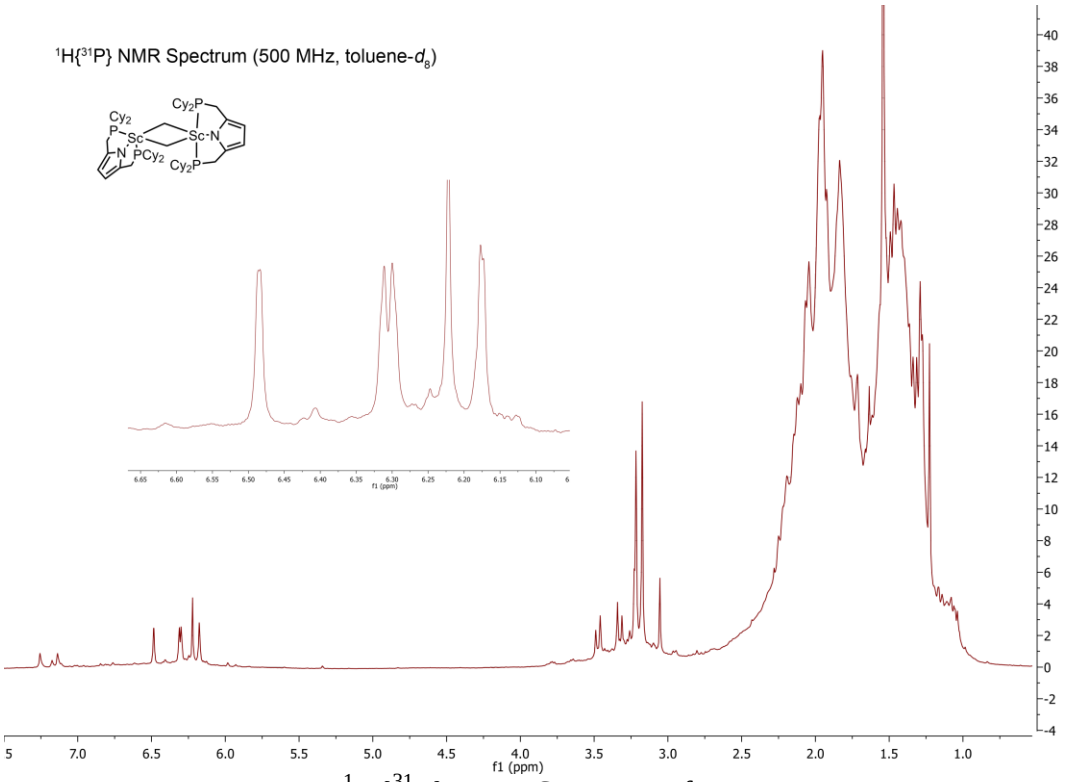

$^{1}H\{^{31}P\}$ NMR Spectrum of **1**.

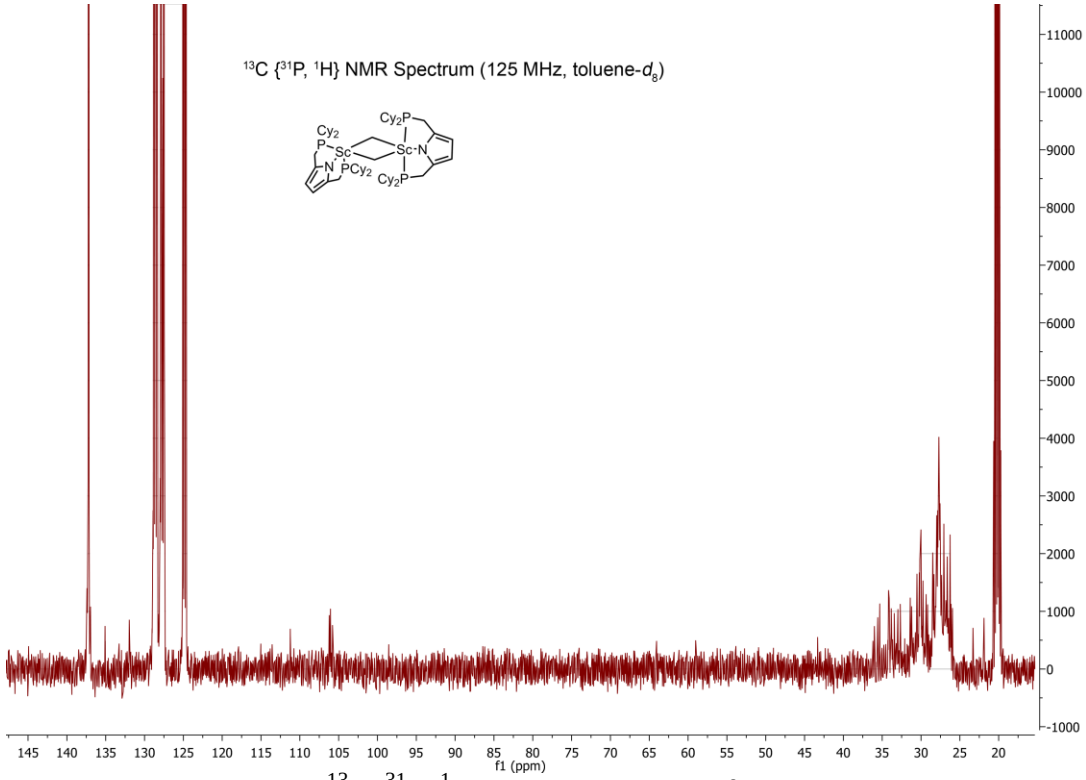

$^{13}C\{^{31}P,\ ^{1}H\}$ NMR Spectrum of **1**.

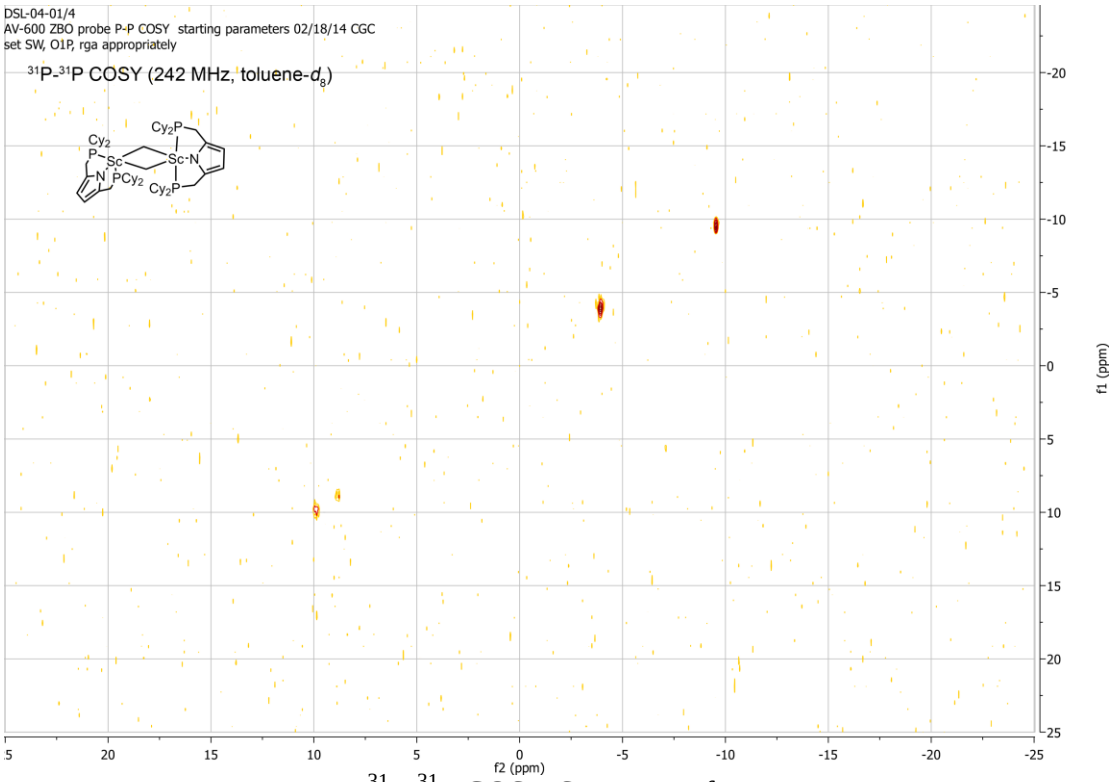

^{31}P-^{31}P COSY Spectrum of **1**.

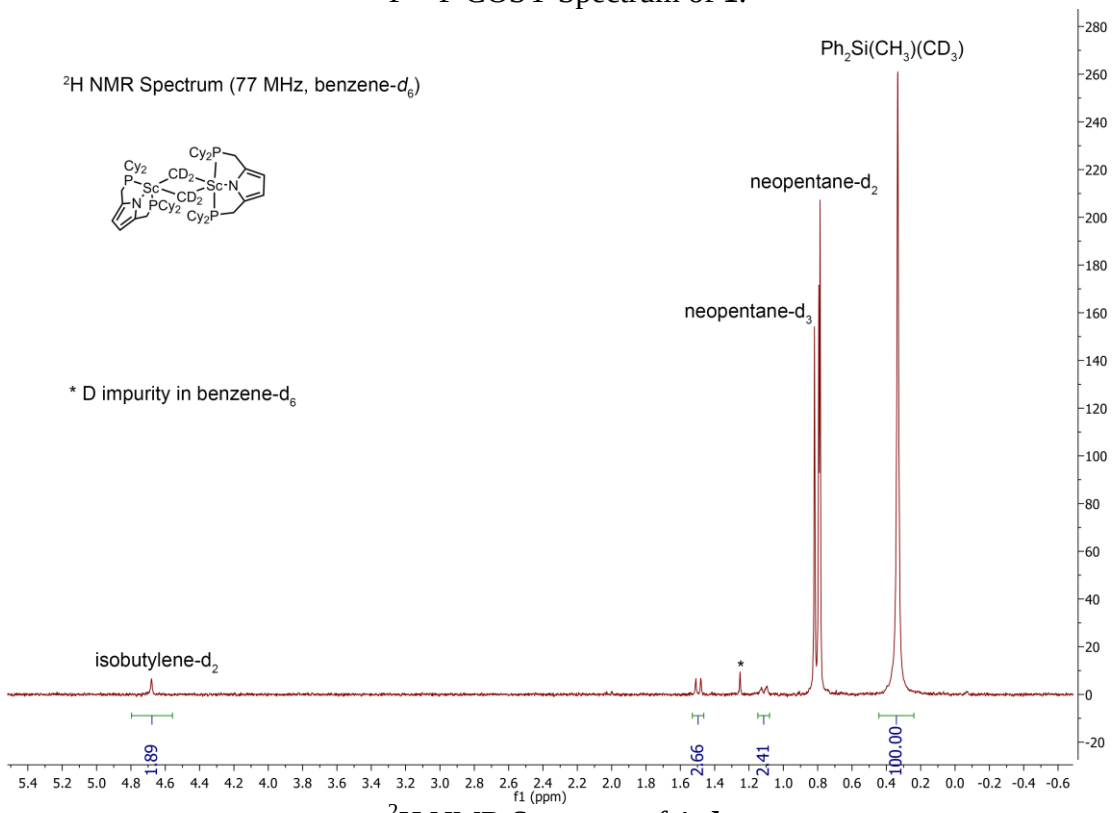

^{2}H NMR Spectrum of **1-*d***.

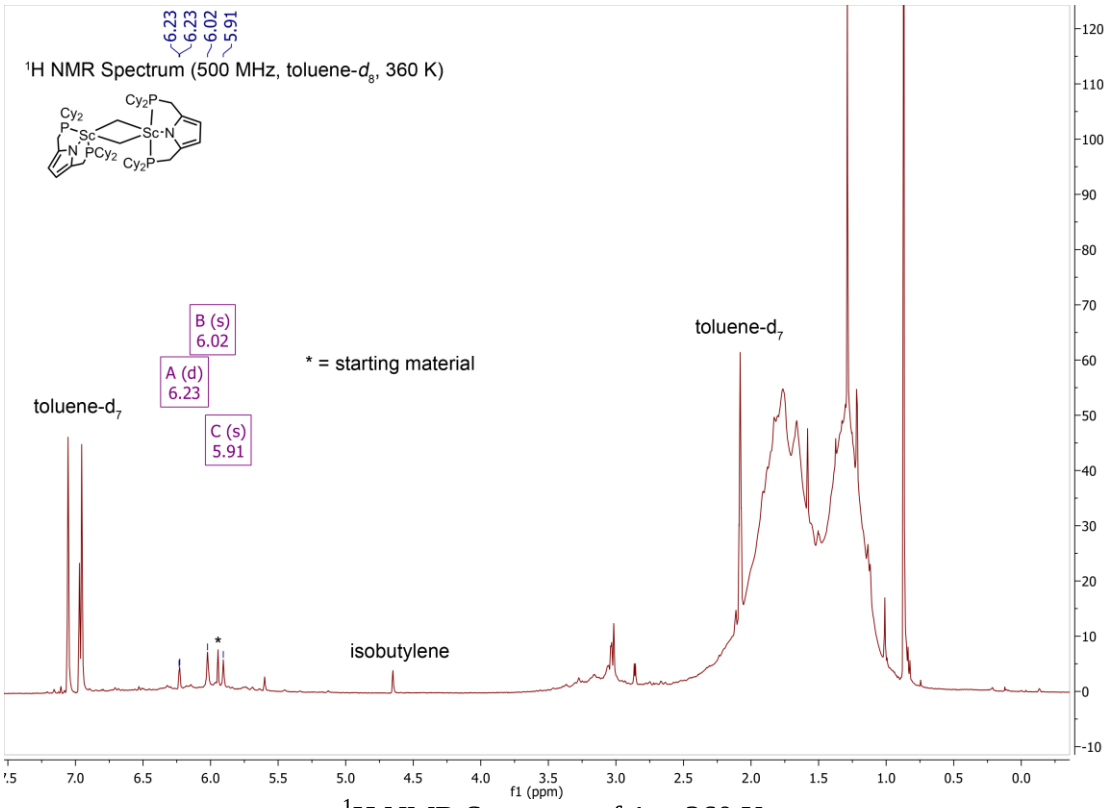

^{1}H NMR Spectrum of **1** at 360 K.

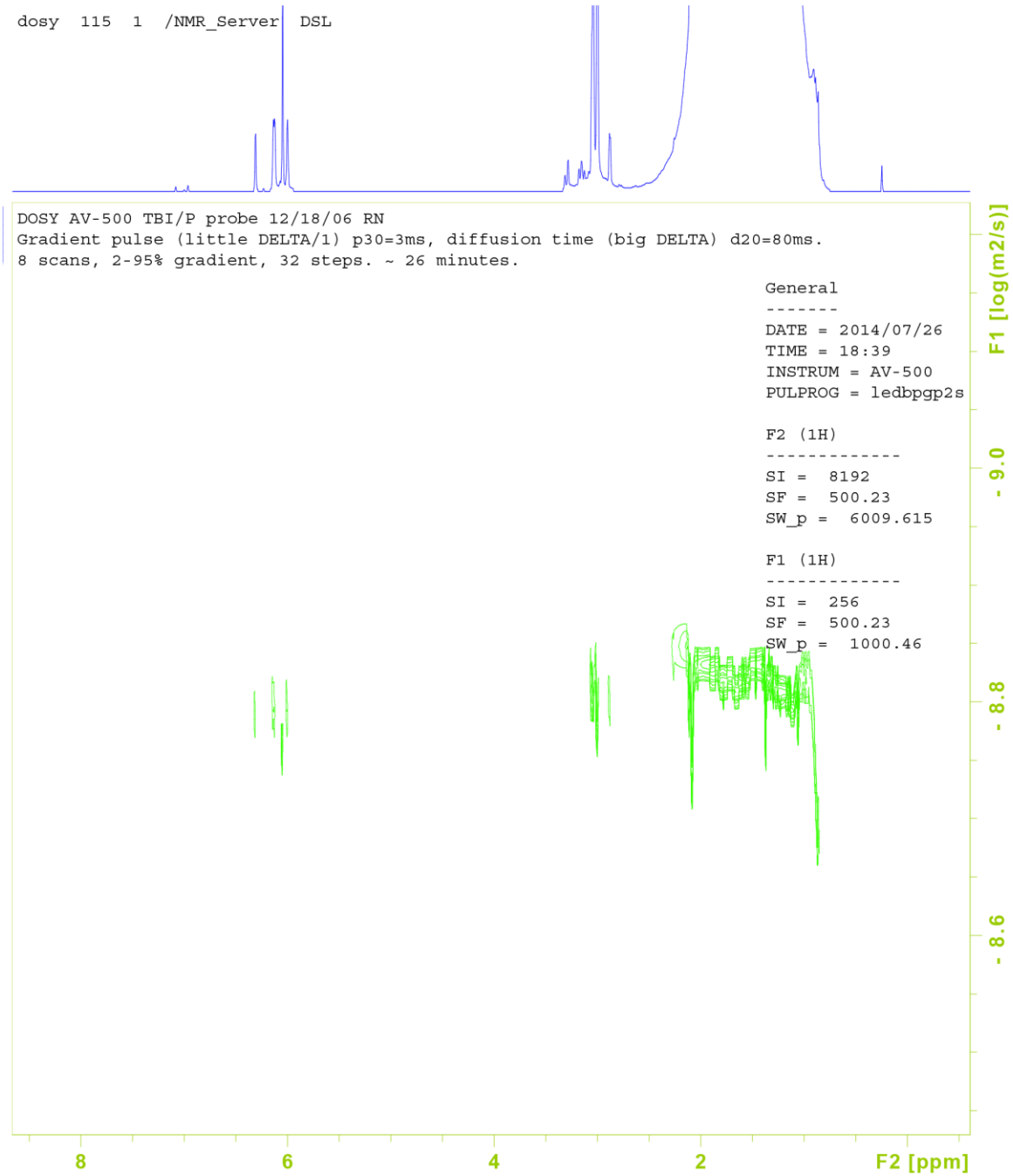

DOSY NMR Spectrum of **1**.

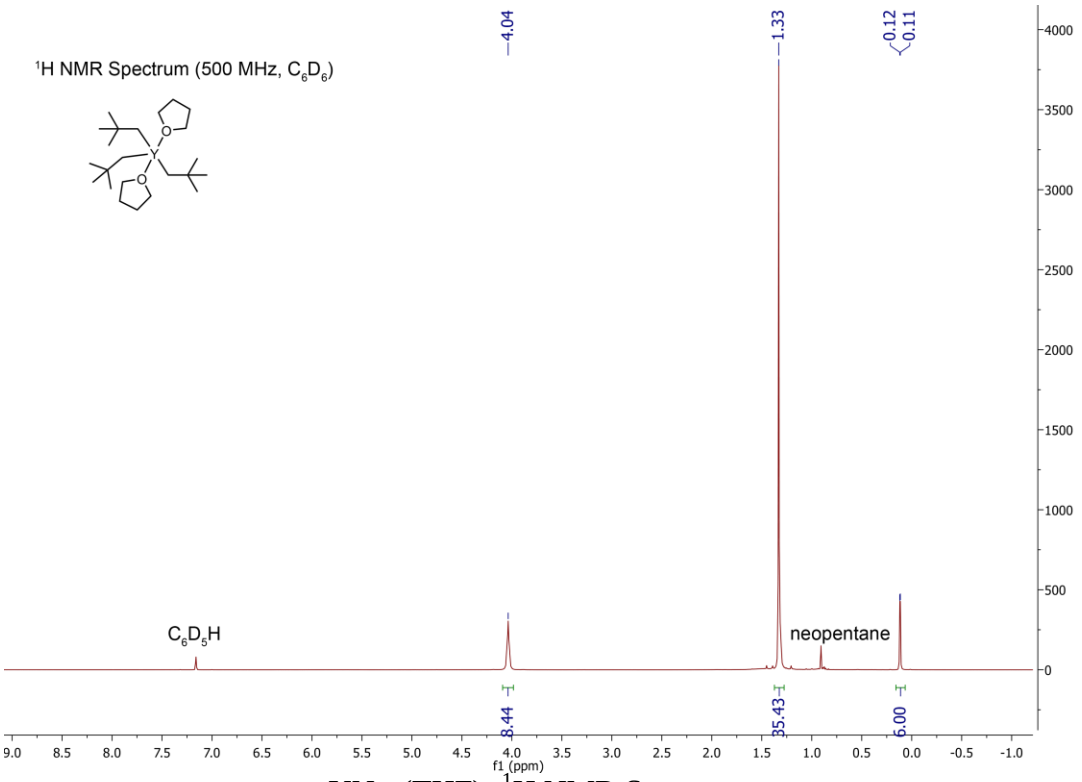

$YNp_3(THF)_2$ ^{1}H NMR Spectrum.

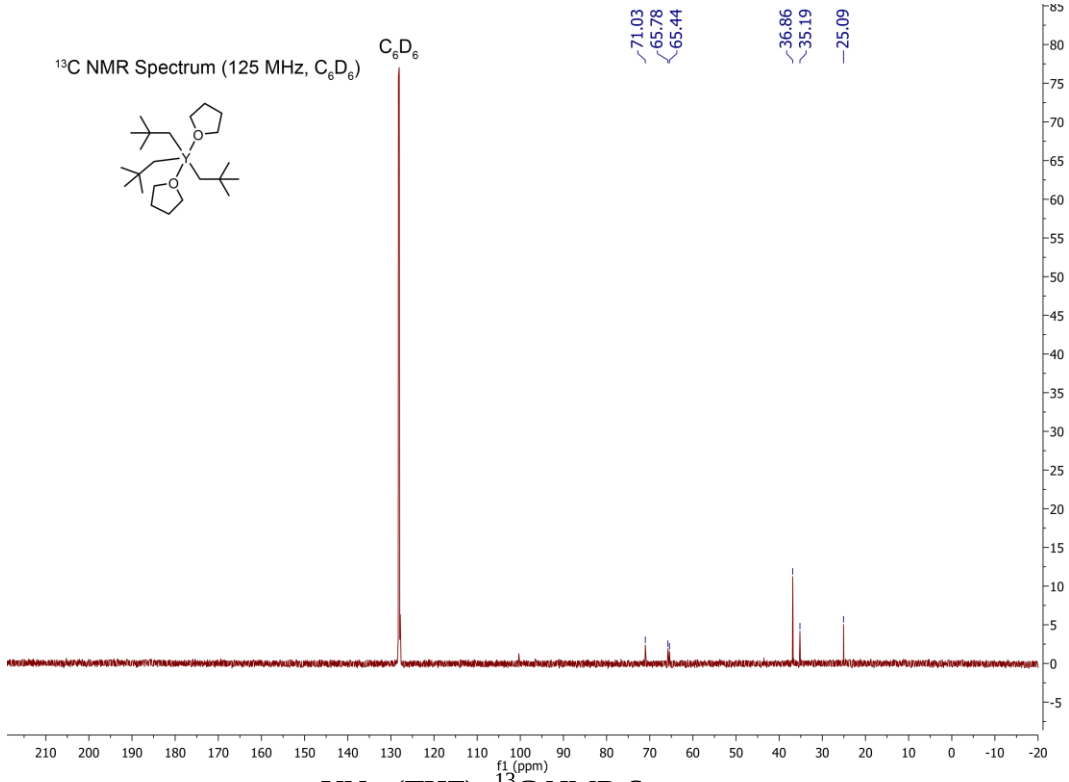

$YNp_3(THF)_2$ ^{13}C NMR Spectrum.

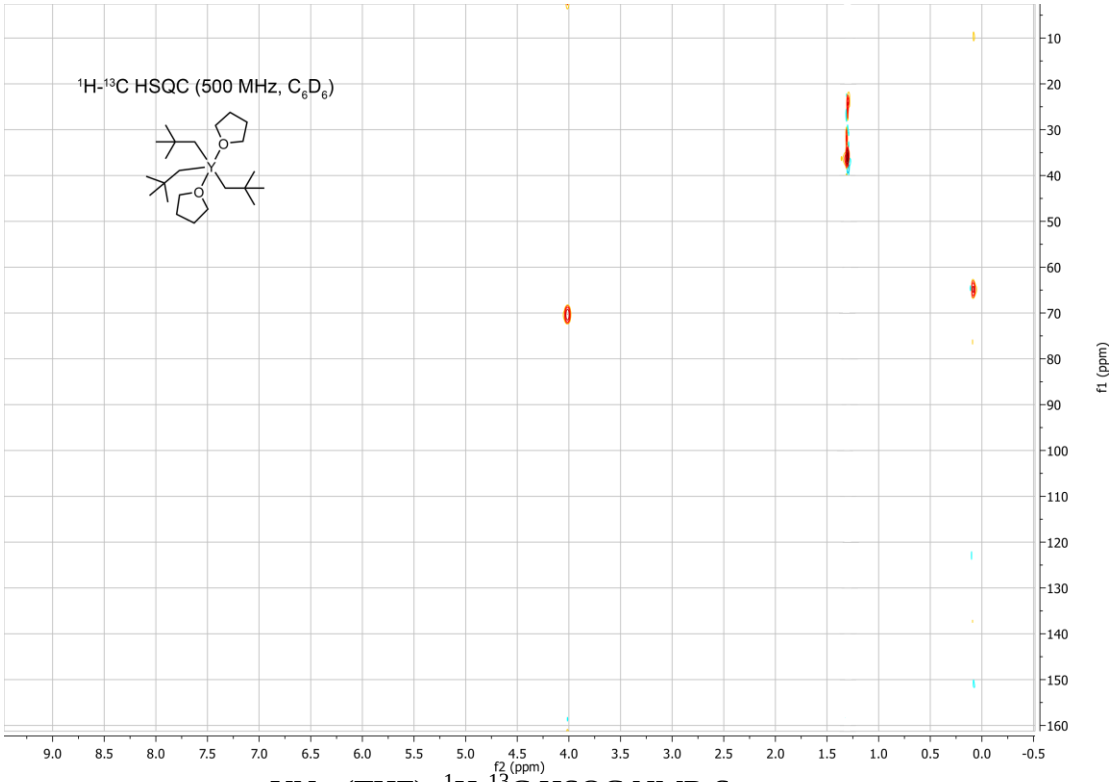

$YNp_3(THF)_2$ ^{1}H-^{13}C HSQC NMR Spectrum.

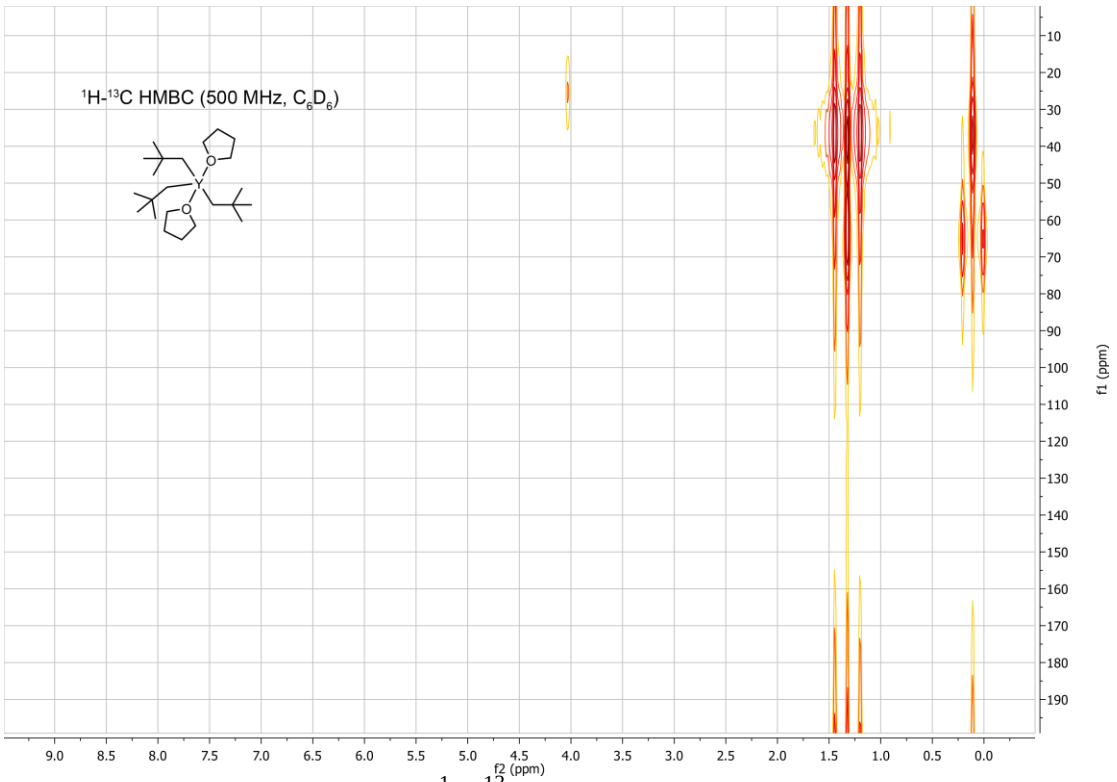

$YNp_3(THF)_2$ ^{1}H-^{13}C HMBC NMR Spectrum.

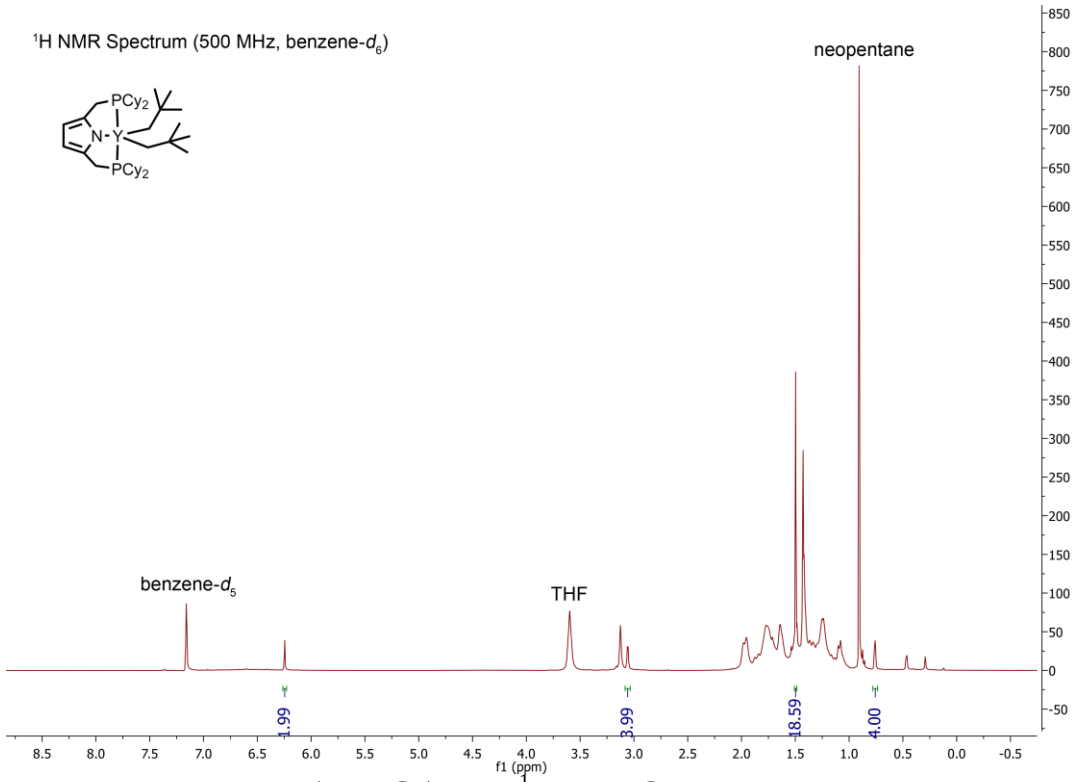

(PNP-Cy)YNp$_2$ ^{1}H NMR Spectrum.

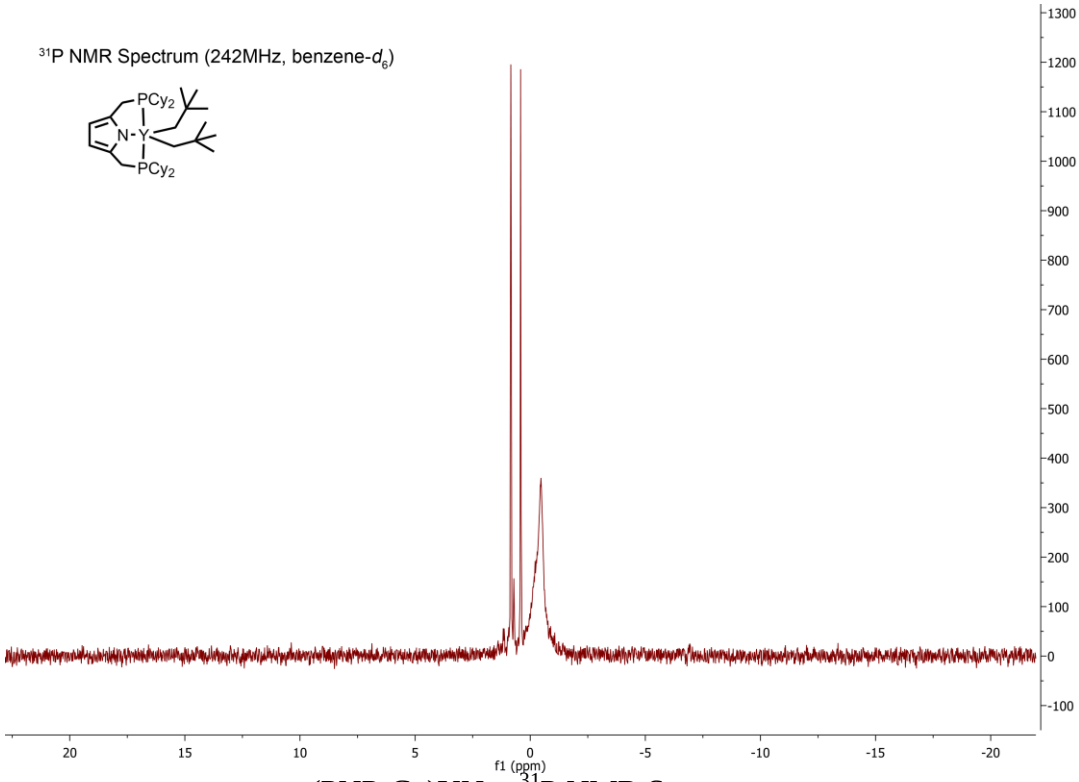

(PNP-Cy)YNp$_2$ ^{31}P NMR Spectrum.

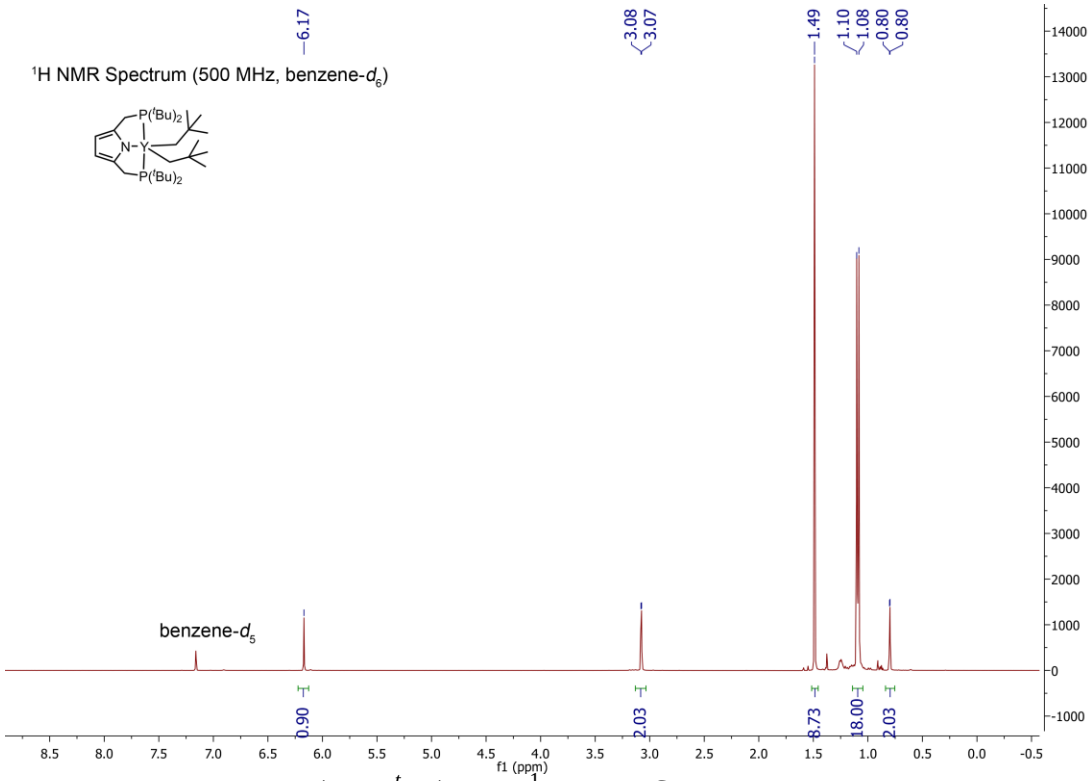

(PNP-^{t}Bu)YNp$_2$ ^{1}H NMR Spectrum.

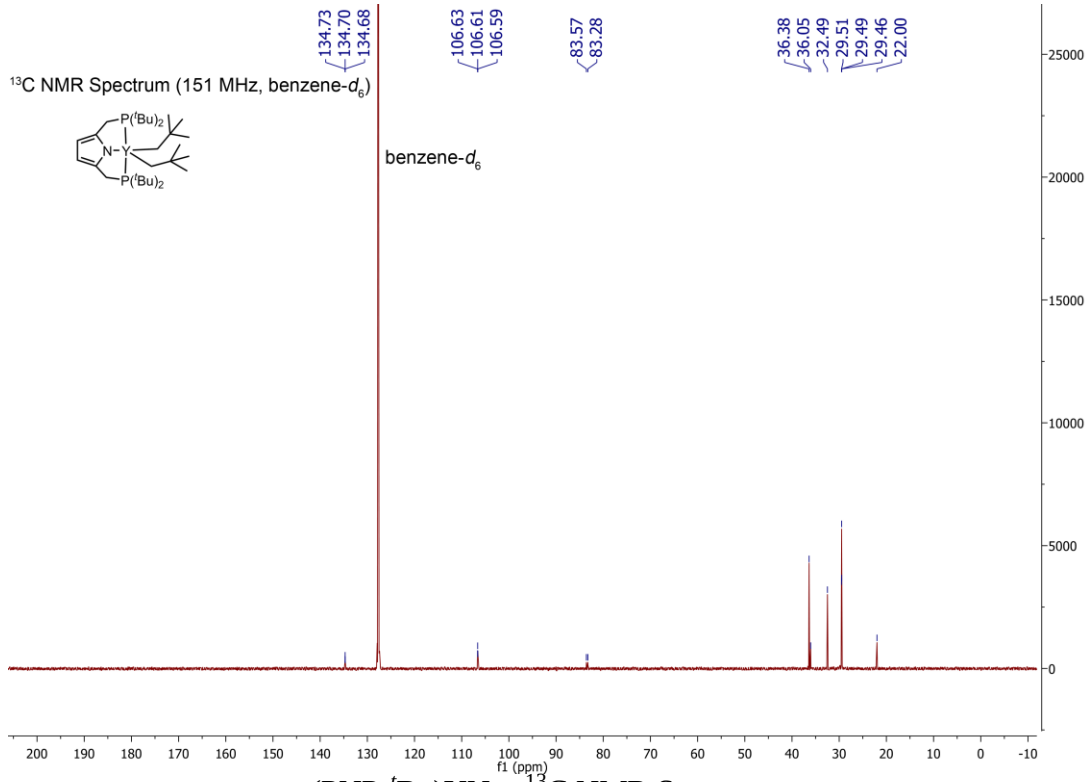

(PNP-^{t}Bu)YNp$_2$ ^{13}C NMR Spectrum.

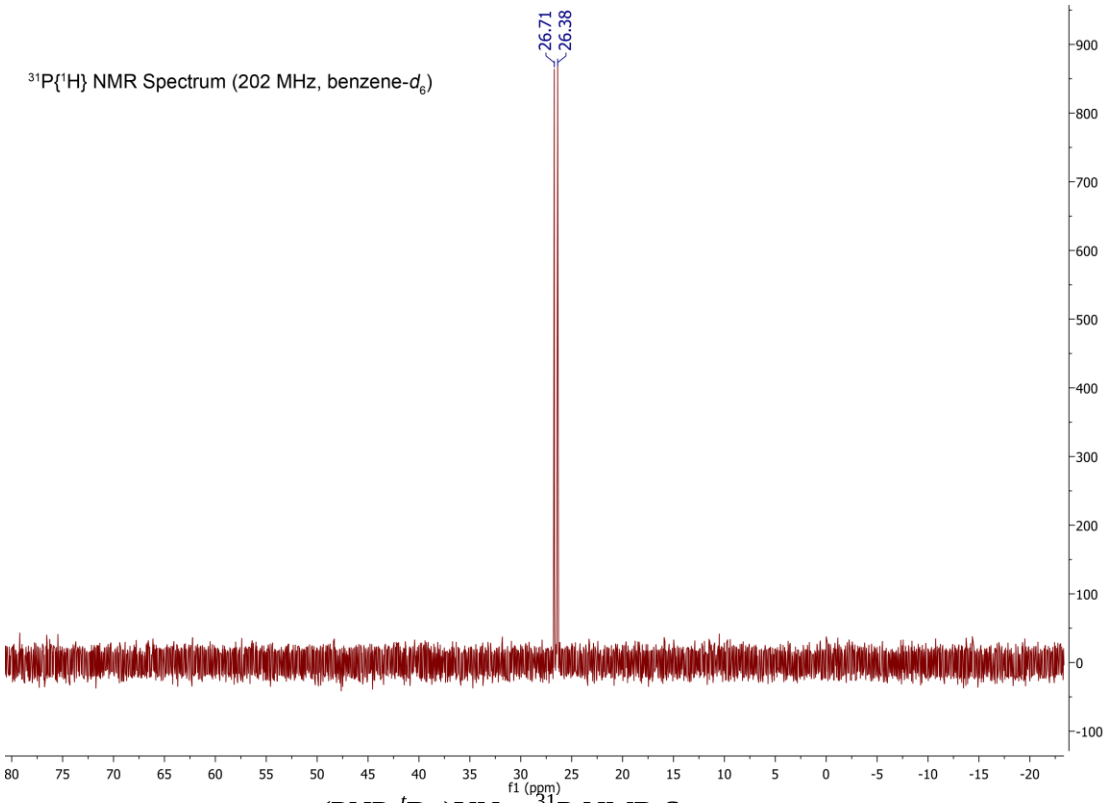

(PNP-^{t}Bu)YNp$_2$ ^{31}P NMR Spectrum.

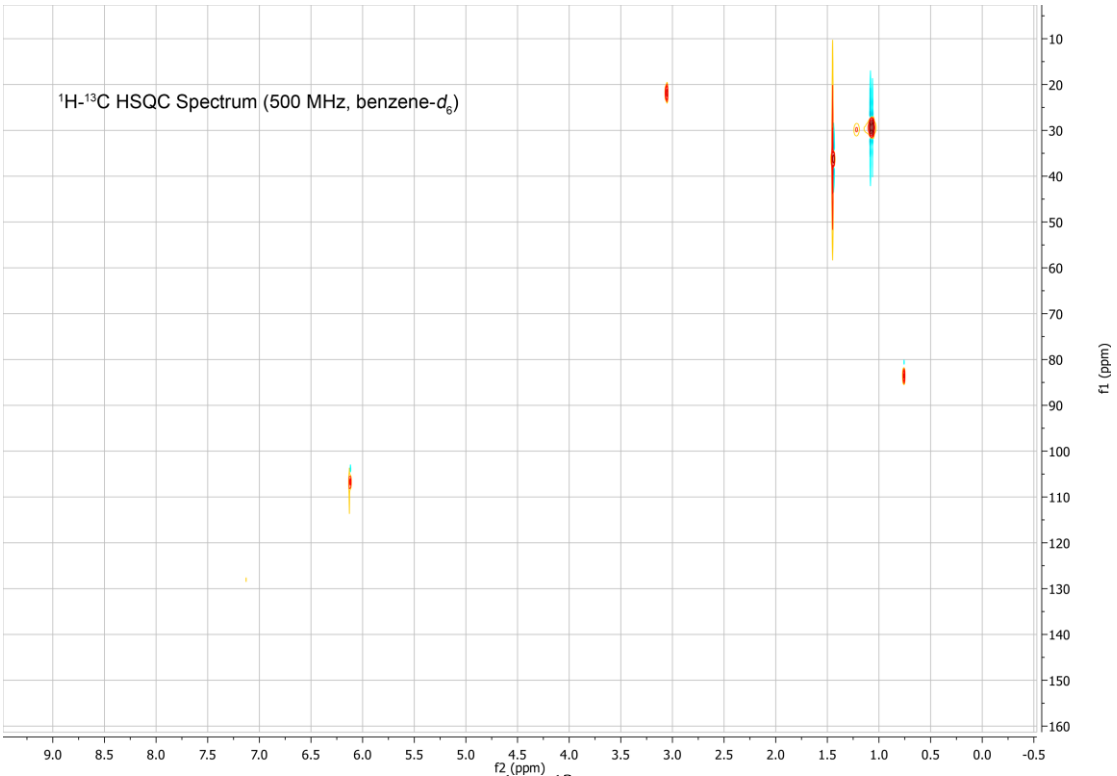

(PNP-^{t}Bu)YNp$_2$ ^{1}H- ^{13}C HSQC Spectrum.

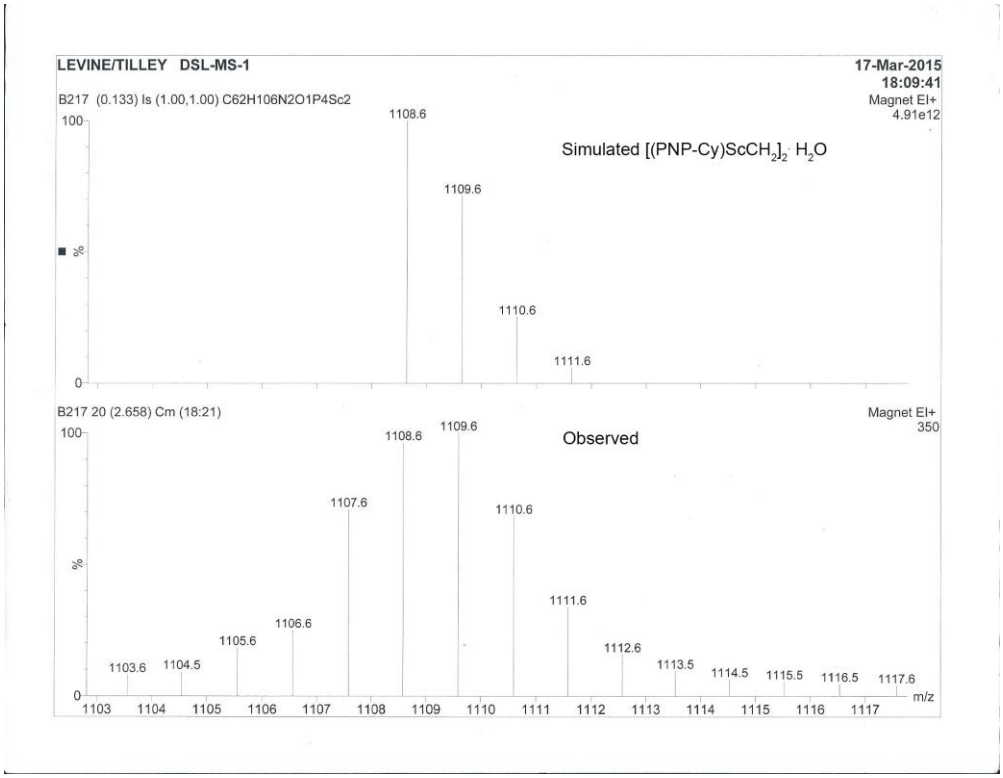

Mass-spectrum of **1**, showing mass peak + H_2O.

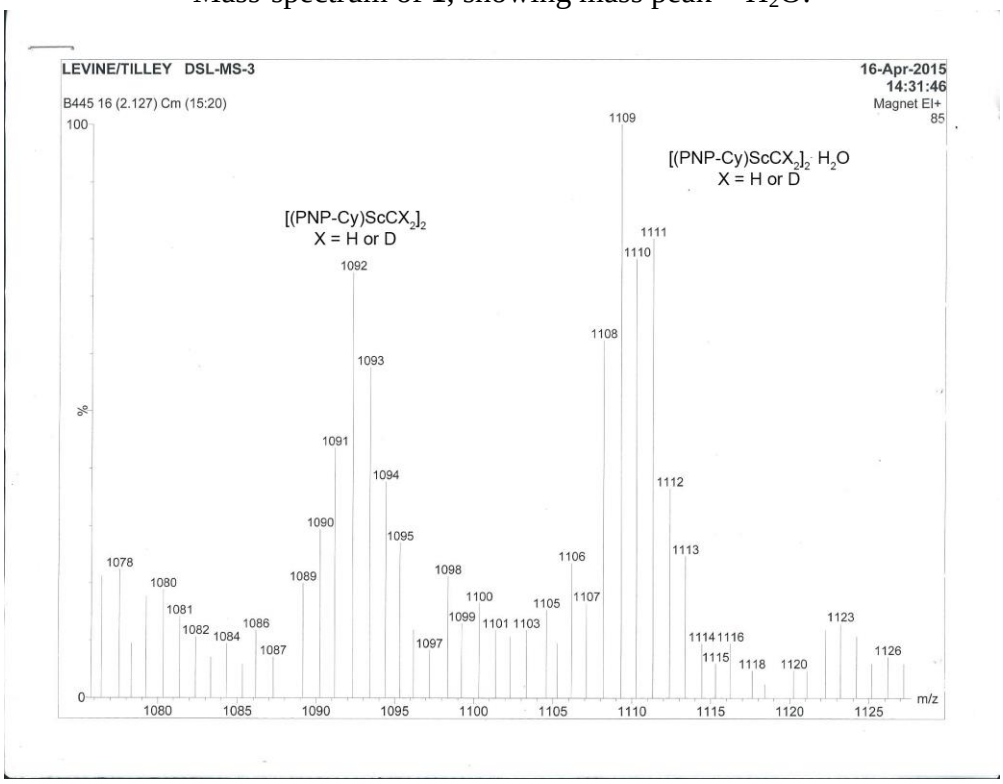

Mass-spectrum of **1-d_n**, showing mass peak and mass peak + H_2O. Note the shift to higher masses on deuteration.

X-ray Data Tables

Crystal data and structure refinement for YNp3(THF)2.

Identification code	YNp3(THF)2	
Empirical formula	C23 H49 O2 Y	
Formula weight	446.53	
Temperature	100(2) K	
Wavelength	0.71073 Å	
Crystal system	Monoclinic	
Space group	P 21/c	
Unit cell dimensions	a = 15.7139(6) Å	α= 90°.
	b = 10.2274(4) Å	β= 114.0110(10)°.
	c = 17.8300(6) Å	γ = 90°.
Volume	2617.54(17) $Å^3$	
Z	4	
Density (calculated)	1.133 Mg/m^3	
Absorption coefficient	2.240 mm^{-1}	
F(000)	968	
Crystal size	0.10 x 0.10 x 0.10 mm^3	
Theta range for data collection	1.419 to 25.398°.	
Index ranges	-18<=h<=18, -12<=k<=12, -20<=l<=21	
Reflections collected	27748	
Independent reflections	4800 [R(int) = 0.0537]	
Completeness to theta = 25.000°	99.9 %	
Absorption correction	Semi-empirical from equivalents	
Max. and min. transmission	0.7452 and 0.6739	
Refinement method	Full-matrix least-squares on F^2	
Data / restraints / parameters	4800 / 0 / 244	
Goodness-of-fit on F^2	1.320	
Final R indices [I>2sigma(I)]	R1 = 0.0611, wR2 = 0.1216	
R indices (all data)	R1 = 0.0734, wR2 = 0.1247	
Extinction coefficient	n/a	
Largest diff. peak and hole	0.851 and -1.251 $e.Å^{-3}$	

Crystal data and structure refinement for (PNP-tBu)YNp2.

Identification code	(PNP-tBu)YNp2	
Empirical formula	C32 H64 N P2 Y	
Formula weight	613.69	
Temperature	100(2) K	
Wavelength	0.71073 Å	
Crystal system	Triclinic	
Space group	P-1	
Unit cell dimensions	a = 11.2268(4) Å	α= 95.262(2)°.
	b = 18.2514(7) Å	β= 107.167(2)°.
	c = 18.4495(7) Å	γ = 96.588(2)°.

Volume	3556.6(2) $Å^3$
Z	4
Density (calculated)	1.146 Mg/m^3
Absorption coefficient	1.749 mm^{-1}
F(000)	1328
Crystal size	0.04 x 0.04 x 0.03 mm^3
Theta range for data collection	1.51 to 25.40°.
Index ranges	-13<=h<=13, -22<=k<=21, -22<=l<=22
Reflections collected	50816
Independent reflections	13051 [R(int) = 0.0667]
Completeness to theta = 25.00°	99.7 %
Absorption correction	Semi-empirical from equivalents
Max. and min. transmission	0.9823 and 0.9426
Refinement method	Full-matrix least-squares on F^2
Data / restraints / parameters	13051 / 0 / 685
Goodness-of-fit on F^2	1.018
Final R indices [I>2sigma(I)]	R1 = 0.0429, wR2 = 0.0757
R indices (all data)	R1 = 0.0744, wR2 = 0.0849
Largest diff. peak and hole	0.464 and -0.397 $e.Å^{-3}$

Chapter 3. Efficient and Selective Catalysis for Hydrofunctionalizations of Alkenes and Alkynes with PNP Complexes of Scandium and Yttrium

INTRODUCTION

Organometallic complexes of early transition metals in a d^0 electronic configuration are associated with two major types of reactions toward organic substrates, σ-bond metathesis and the insertion of multiple (*e.g.*, C=C) bonds.[1–5] However, these two reaction steps are rarely combined to form a catalytic cycle.[2,6–8] Improving this form of catalysis requires greater knowledge of the fundamental reaction steps. Early investigation into the less well-studied of these, σ-bond metathesis, revealed that there can be significant differences in rates between scandium and yttrium, spanning two orders of magnitude (Figure 1).[9] However, beyond these seminal reports, there have been relatively few studies that compare first and second row group III metal complexes with the same ligand set, and so the role of the metal center has not been extensively explored.[9,10]

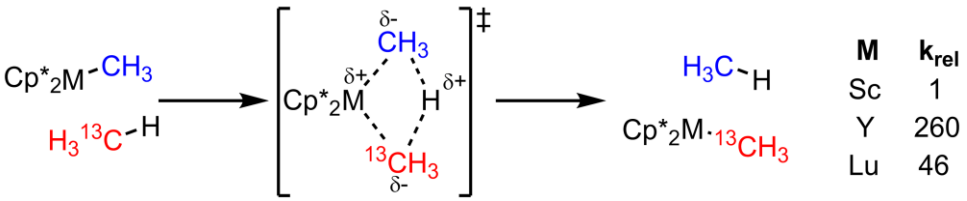

Figure 1. The σ-bond metathesis reaction, comparing the rates of Sc, Y, and Lu congeners in the methane activation reaction.[9]

The series of PNP-supported scandium alkyl complexes described in Chapter 1, such as (PNP-Cy)Sc(CH_2SiMe_3)$_2$ (**1-Sc**) (Figure 2), were found to react rapidly with hydrogen to form reactive hydride complexes that were trapped by olefins.[11,12] To gain more insight into differences in the catalytic activity of Sc and Y complexes, the yttrium congener was prepared and this hydrogenation reaction, as well as the related hydrosilation reaction, was elaborated into a catalytic cycle, which features both σ-bond metathesis and insertion events. Because insertion reactions are typically much faster than σ-bond metathesis in these complexes,[13] and the olefin insertion step occurs after the rate-determining metathesis, it was hoped that the rates of these hydrofunctionalization reactions would reflect the relative σ-bond metathesis rates for the Sc and Y complexes.

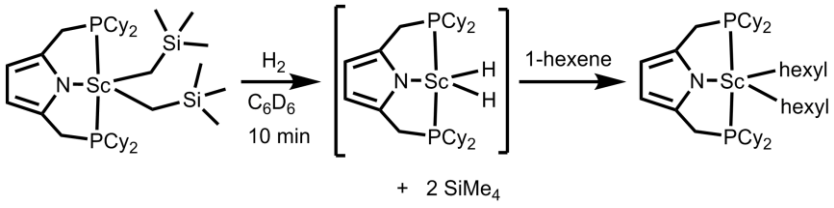

Figure 2. Previously described PNP-supported scandium complexes reacting with hydrogen.

RESULTS AND DISCUSSION

The second row congener of **1-Sc**, (PNP-Cy)Y(CH_2SiMe_3)$_2$ (**1-Y**) was prepared by addition of (PNP-Cy)H to a pentane solution of Y(CH_2SiMe_3)$_3$(THF)$_2$,[14] and displays a ^{1}H NMR

spectrum that is similar to that of the scandium analogue. However, it crystallizes as a dimer in the solid state (see Figure 3 and Appendix). As the ^{1}H NMR spectrum is inconsistent with the solid state structure, it is proposed that the molecule is monomeric in solution, or is involved in rapid equilibrium between dimer and monomer at room temperature.

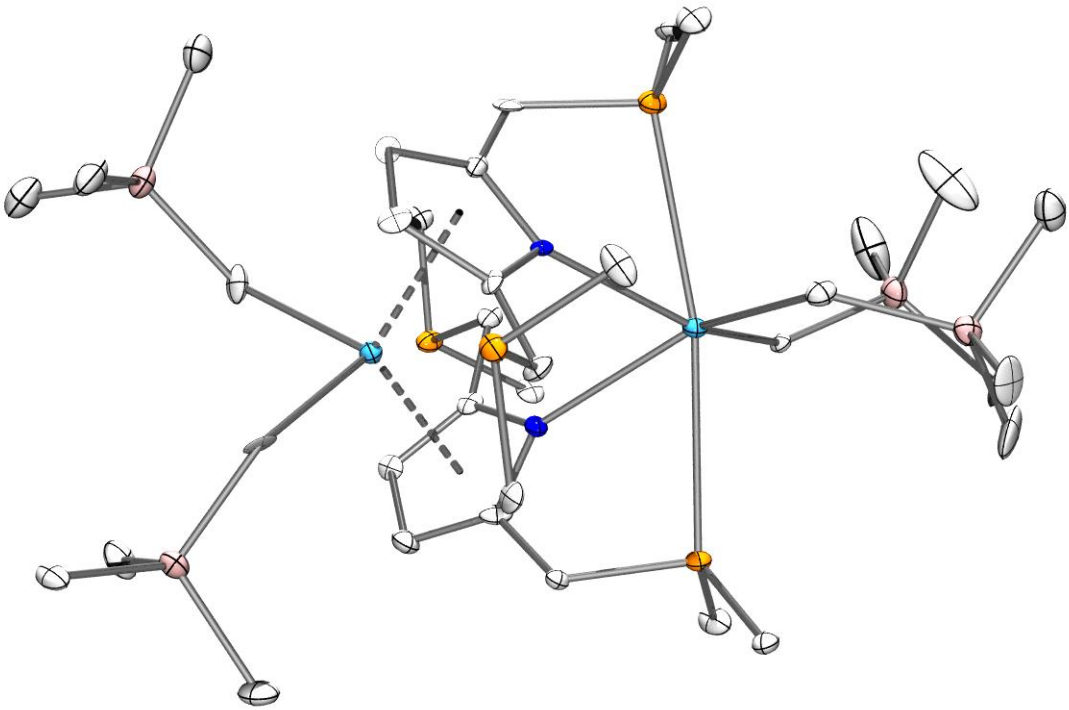

Figure 3. ORTEP diagram of dimeric **1-Y**. Hydrogen atoms omitted and cyclohexyl groups truncated to methyl groups for clarity. One phosphine arm of each ligand is coordinated to the right Y and one arm is uncoordinated. The right Y is a slightly distorted octahedron with *trans*-phosphines, *cis*-alkyl groups, and *cis*-η^1-pyrrolide groups. The left Y is a bent metallocene with two wedge alkyl groups and two η^5-pyrrolide groups.

Catalytic alkene hydrogenation served as the first comparison between **1-Sc** and **1-Y**. Primary olefins (e.g. 1-octene) were quantitatively hydrogenated to the corresponding alkane over the course of 7 h by 5 mol % **1-Sc** at 22 °C (Table 1, entry 1). The yttrium congener **1-Y**, while much faster to initiate the reaction (<10 min vs. 2 h for **1-Sc**, as monitored by formation of tetramethylsilane by ^{1}H NMR spectroscopy), requires 48 h to reach 90% yield of alkane (Table 1, entry 4). It may be that the yttrium dihydride complex, which is rapidly formed by reaction of the (PNP-Cy)Y(CH_2SiMe_3)$_2$ with hydrogen, is less stable than the scandium congener and therefore less effectively trapped by olefins before decomposing into an inactive mixture of products, leading to its lower apparent activity. Secondary olefins (cyclohexene) are also hydrogenated by these complexes, although the rates are somewhat slower (62% yield in 7 h for Sc, 10% yield in 48 h for Y, Table 1, entries 2, 5).

The selective semihydrogenation of alkynes to alkenes remains a significant synthetic challenge.[15,16] Owing to the fact that **1-Sc** and **1-Y** react more quickly with primary olefins than with secondary olefins, investigation to determine if these complexes would be competent

semihydrogenation catalysts, which to our knowledge has not been observed with d^0 metals, was pursued. Both catalysts proved to be highly selective for semihydrogenation of 3-hexyne to *cis*-3-hexene (>98% for Y, Table 1, entry 6, and 82% for Sc, Table 1, entry 3). The yttrium congener again suffered from rapid catalyst decomposition (observed as loss of ^{1}H NMR resonances for the catalyst resting state), yielding only 22% product; **1-Sc** attained >98% conversion before significant catalyst decomposition was observed (80% of Sc catalyst remained at the end of catalysis).

Table 1. Catalytic hydrogenation with **1-Sc** and **1-Y**.

Entry	M	Substrate	Time	Select.[a]	Yield[a]
1	Sc	1-octene	7 h	>98 %	>98 %
2	Sc	Cyclohexene	7 h	>98 %	62 %
3	Sc	3-hexyne	48 h	82%	82 %
4	Y	1-octene	48 h	>98 %	90 %
5	Y	Cyclohexene	48 h	>98 %	10 %
6	Y	3-hexyne	5 h	>98 %	22 %

Reaction conditions: 5 mol% catalyst, 23 °C. [a]Determined by ^{1}H NMR spectroscopy.

Hydrosilation, a related hydrofunctionalization reaction, introduces the possibility of regiochemical control as well as stereochemical control. The products of hydrosilation constitute a billion-dollar industry, making hydrosilation a lucrative industrial application of homogeneous catalysis. Selective semihydrosilation catalysts remain rare,[17,18] although the vinyl silane products they form are highly valuable materials in industry and in organic synthesis as masked ketone functionalities and as coupling partners in cross-coupling reactions.[19] While there are some examples of hydrosilations of alkenes and alkynes with yttrium[8,10,20–22] and thorium[23,24], there are no examples of semihydrosilation with scandium and, as such, no comparison of the first row and second row congeners (Sc and Y) with the same ligand set.

Alkene hydrosilation results are summarized in Table 2. These catalysts were found to be remarkably selective for a single hydrosilation product and in some cases extremely active, with **1-Y** again considerably faster than **1-Sc** to initiate (1 h for **1-Sc** vs. <5 min for **1-Y**). Under conditions in which the reaction proceeds, selectivities >98% are obtained in all cases. For substrates that could produce multiple regioisomers of hydrosilation products, the less hindered (that is, anti-Markovnikov) product is always exclusively formed; this may be attributed to the steric bulk near the metal centre, which favors 1,2-insertion over 2,1-insertion. Complex **1-Y** was found to be an extremely rapid catalyst, providing >98% yield in the hydrosilation of 1-hexene in <5 min at 23 °C with as little as 2 mol% catalyst, indicating a turnover frequency of >500 h^{-1}. For comparison, the lanthanocene catalysts of Marks catalyse this reaction with a turnover frequency of 120 h^{-1} to give 74% yield and 76% regioselectivty for one product.[6] Indeed, **1-Y** displays some of the highest turnover frequencies of any rare-earth or early transition metal catalyst for this reaction.[22] Secondary silanes require heating for the reaction to proceed at a reasonable rate. In accordance with the hypothesis that insertion to form secondary alkyl substituents is disfavored, cyclohexene also required heating to achieve reasonable turnovers. The combination of secondary silane and secondary olefin afforded no product with either catalyst. This reaction is proposed to proceed by reaction of **1-Sc** or **1-Y** with phenylsilane to

afford the silylated alkyl ligand and the respective reactive hydride complexes. These hydride complexes can then be trapped by olefins to regenerate alkyl complexes, allowing the catalyst to turn over (Figure 4).

Table 2. Catalytic hydrosilation with **1-Sc** and **1-Y**.

Entry	M	Silane	Alkene	Time	Select.[a]	Yield[a]
1	Sc	$PhSiH_3$	1-hexene	2 h	>98 %	>98 %
2[b]	Sc	$PhSiH_3$	cyclohexene	16 h	>98 %	59 %
3[b]	Sc	$PhSiH_3$	cyclohexene	68 h	>98 %	74 %
4[c]	Sc	$PhMeSiH_2$	1-hexene	130 h	>98 %	>98 %
5[c]	Sc	$PhMeSiH_2$	cyclohexene	84 h	N/A	0 %
6	Y	$PhSiH_3$	1-hexene	<10 min	>98 %	>98 %
7	Y	$PhSiH_3$	cyclohexene	16 h	>98 %	16 %
8[d]	Y	$PhMeSiH_2$	1-hexene	20 h	>98 %	68 %
9[d]	Y	$PhMeSiH_2$	cyclohexene	24 h	N/A	0 %

Reaction conditions: 5 mol% catalyst, 23 °C. [a]Determined by ^{1}H NMR spectroscopy. [b]Reaction carried out at 50 °C. [c]Reaction carried out at 80 °C. [d]Reaction carried out at 40 °C.

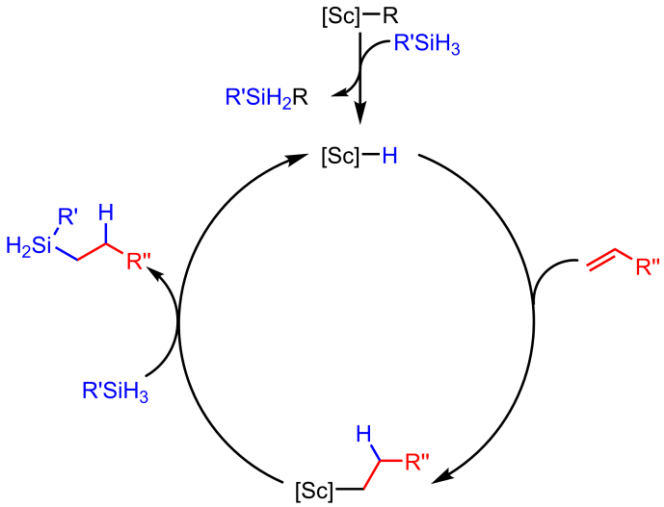

Figure 4. Proposed mechanism for catalytic hydrosilation. Hydrogenation is proposed to operate by an analogous mechanism.

In reactions with bulkier alkenes, **1-Y**, though faster to initiate and form product than **1-Sc**, does not afford as much product over time and reaches its maximum yield much earlier. This rapid production and rapid decline in activity suggests that **1-Y** suffers from decomposition, possibly owing to a more reactive yttrium hydride complex being ineffectively trapped by cyclohexene relative to decomposition pathways. The fact that more effective catalysis with **1-Y** is obtained when using a secondary silane (as opposed to a secondary olefin) suggests that the yttrium hydride alkyl complex is less susceptible to decomposition than the yttrium dihydride complex. In the case of **1-Y** and hydrogen or **1-Y** and a primary silane with less efficient hydride trap, the yttrium dihydride complex is rapidly formed and subsequently rapidly decomposes

before useful catalysis can be performed. In the regimes of efficient hydride trapping or slowly reacting (secondary) silanes, the yttrium alkyl hydride complex is intercepted before decomposition can occur. This explanation also qualitatively explains why **1-Sc** is a better catalyst in the cases where **1-Y** is poor; the Sc congener's slower reaction with silanes favors formation of the more persistent scandium alkyl hydride complexes, which react faster to continue catalysis than to form the more rapidly-decomposing scandium dihydride complexes.

Partial hydrosilation of alkynes was also found to be efficiently catalysed by **1-Sc** and **1-Y**. Using the symmetric, internal alkyne 3-hexyne, both complexes afford the (*E*)-vinyl silane product of *syn* addition of silane in high yield (>98%) and with >98% selectivity (Table 3, entries 1, 5). The unsymmetrical, internal alkyne methylphenylacetylene allows for an interesting regiochemical comparison, as the product where the silane is *trans* to the methyl group (**2**) is electronically preferred, while the product with the silane *trans* to the phenyl group (**3**) is sterically preferred.[25] Complex **1-Y** affords the electronically-preferred product in about 90% selectivity, similar to previously obtained catalysts.[25] In contrast, the **1-Sc** shows the opposite preference, producing the sterically-preferred product with about 66% selectivity. This difference may be attributed to the different ionic radii of the metal centres, with the smaller scandium centre less able to accommodate the more sterically demanding product insertion step than the larger yttrium centre, where the product formation is under greater electronic control.

Table 3. Catalytic partial hydrosilation with **1-Sc** and **1-Y**.

Entry	M	Silane	Alkyne	Time	Select.[a]	Yield[a]
1	Sc	$PhSiH_3$	EtCCEt	60 h	>98 %	>98 %
2[b]	Sc	$PhSiH_3$	MeCCPh	16 h	66%:33% **3**:**2**	55 %
3[b]	Sc	$PhSiH_3$	MeCCPh	87 h	66%:33% **3**:**2**	80 %
4	Sc	$PhSiH_3$	HCCiPr	20 min	95 %	>98 %
5	Y	$PhSiH_3$	EtCCEt	3.5 h	>98%	>98 %
6	Y	$PhSiH_3$	MeCCPh	10 h	10%:90% **3**:**2**	80 %
7	Y	$PhSiH_3$	MeCCPh	48 h	10%:90% **3**:**2**	89 %
8	Y	$PhSiH_3$	HCCiPr	24 h	N/A	0 %

Reaction conditions: 5 mol% catalyst, 23 °C. [a]Determined by ^{1}H NMR spectroscopy. [b]Reaction carried out at 40 °C.

Complex **1-Sc** also proved to be a very efficient catalyst for the anti-Markovnikov partial hydrosilation of terminal alkynes. This reaction is very difficult to accomplish owing to the highly acidic nature of the alkyne C–H bond. Examples of this reaction catalysed by thorium and uranium complexes require 24-48 h (sometimes with heating) and have low product selectivities (33-62%).[23,24] In contrast, **1-Sc** achieves quantitative conversion with 95% selectivity in 20 min at 23 °C; **1-Y** showed no catalytic activity.

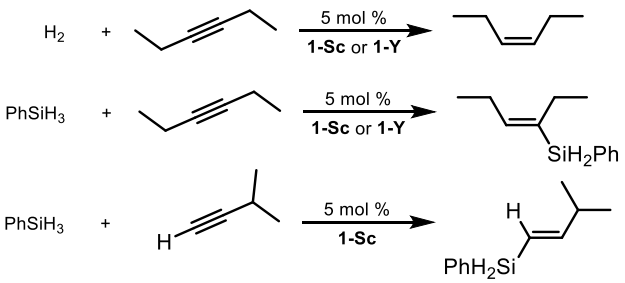

Figure 5. Summary of hydrofunctionalization catalysis with **1-Sc** and **1-Y**.

In order to further support the mechanism proposed above, DFT calculations were carried out on both the proposed catalytic cycle and on the initiation reaction. The calculated pathway is shown in Figure 6. As expected, the rate determining step was calculated to be the σ-bond metathesis step. The barrier was found to be 28.8 kcal/mol for scandium vs. 20.5 kcal/mol for yttrium. The initiation reaction was calculated to have a slightly higher barrier (29.9 kcal/mol for Sc, 27.7 kcal/mol for Y). Calculations indicate that the reaction proceeds through olefin insertion into a metal-hydride complex, as opposed to a metal-silyl complex, since the barrier to formation of the silyl complex is slightly higher than the hydride complex (by 1.1 kcal/mol for Sc, 7.3 kcal/mol for Y). The insertion of olefin (propylene in the calculation) into the methyl hydride complex was found to have a lower barrier for Sc (13.0 kcal/mol) than Y (17.5 kcal/mol). This suggests another possibility for scandium's superior performance relative to yttrium: the trapping reaction is more efficient with scandium than yttrium owing to this lower barrier, leading to less catalyst decomposition.

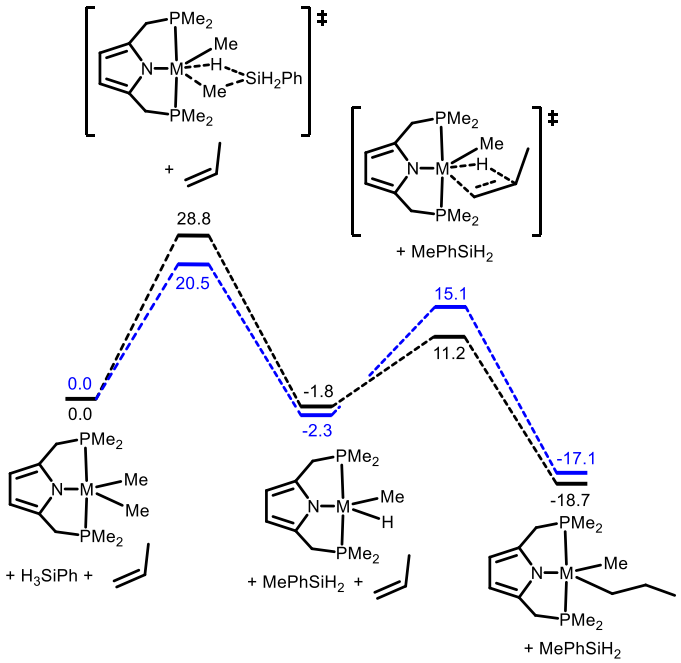

Figure 6. Calculated free energy reaction pathway for **1-Sc** (black) and **1-Y** (blue). All energies are given in kcal/mol

CONCLUSION

In summary, new efficient and selective hydrogenation, semihydrogenation, hydrosilation, and partial hydrosilation catalysts have been developed based on anionic PNP-supported scandium and yttrium complexes. It was found that Sc and Y complexes follow trends similar to that observed in methane activation, in which the σ-bond metathesis reaction is much more rapid with Y and Sc.[5,9] However, this greater reactivity does not necessarily result in a better catalyst, since in these cases catalyst decomposition and unwanted side-reactions also occur more rapidly. Calculations indicate that relatively less efficient trapping may be due to a lower barrier to olefin insertion into the scandium congener. Moreover, it was demonstrated that, possibly due to the different steric environments due to the different ionic radii of the two metals, the two congeners display regiochemical differences in the partial hydrosilation of alkynes. Future work will focus on strategies to stabilize the hydride intermediates in order to prevent catalyst decomposition and afford more active and general catalysts.

EXPERIMENTAL SECTION

General

Unless otherwise noted, all experiments were conducted in dry, oxygen-free solvents using standard Schlenk techniques or in a N_2 atmosphere glovebox. Deuterated solvents were purchased from Cambridge Isotope Laboratories, Inc. Benzene-d_6 was dried by vacuum distillation from Na/K alloy. Toluene-d_8 was dried by refluxing over molten sodium metal followed by vacuum distillation. Unless otherwise noted, reagents were obtained from commercial suppliers and used as received. 4-phenylpyridine was obtained from Aldrich and sublimed. (PNP-Cy)H, (PNP-Cy)Sc$(CH_2SiMe_3)_2$, Y$(CH_2SiMe_3)_3(THF)_2$ were prepared according to literature procedures.[11,14]

Analytical Methods

Solution NMR spectroscopy was performed using Bruker AV-300, AVB-400, AVQ-400, AV-500, or AV-600 MHz spectrometers at room temperature. ^{1}H, $^{13}C\{^{1}H\}$, and $^{31}P\{^{1}H\}$ NMR spectra were calibrated internally to either the resonance for the solvent or residual proteo solvent relative to tetramethylsilane. Elemental analyses were carried out by the College of Chemistry Microanalytical Laboratory at the University of California, Berkeley.

Computational Details

Calculations were carried out with Q-Chem 4.3,[26] employing the ωB97X-D range-separated hybrid functional and 6-31++G** basis set for non-metal atoms. Metal atoms were treated with the relativistic ECP and basis set of the Stuttgart group. Gibbs free energies were calculated at 298 K and 1 atm of pressure. The ligand cyclohexyl groups were truncated to methyl groups to save computational time.

X-ray Crystallography Details

X-ray diffraction data for crystals of (PNP-Cy)Y$(CH_2SiMe_3)_2$ were collected using a Bruker AXS modified four-circle diffractometer coupled CCD detector with Mo Kα (λ =

0.71073 Å) radiation monochromated by a system of QUAZAR multilayer mirrors. Crystals were kept at 100(2) K throughout collection. Data collection, refinement, and reduction were performed with Bruker APEX2 software (v. 2013.4). Structures were solved by direct methods using SHELXS-97. All structures were refined with SHELXL-97 with refinement of F^2 against all reflections by full-matrix least squares. In all models, non-hydrogen atoms were refined anisotropically, and hydrogen atoms were included at their geometrically-calculated positions and refined using a riding model. The 3D molecular structure figures were visualized with ORTEP 3.2, rendered with POV-Ray 3.6, and annotated with Adobe Photoshop CS6.

Synthesis of (PNP-Cy)Y(CH_2SiMe_3)$_2$. A solution of (PNP-Cy)H (341.7 mg, 0.70 mmol) in pentane (5 mL) was added to a solution of Y(CH_2SiMe_3)$_3$(THF)$_2$ (346.7 mg, 0.70 mmol) in pentane (5 mL) and the reaction mixture was then stirred for 1 h. The reaction mixture was concentrated to 3 mL and stored at -35 °C for 2 d to afford crystalline, colorless product (296.5 mg, 57% yield). ^{1}H NMR (500 MHz, C_6D_6) δ 6.22 (s, 2H, $^1J_{CH}$ = 163.5 Hz), 3.04 (d, $^2J_{HP}$ = 3.3 Hz, 4H), 2.03 – 1.44 (m, 24H), 1.38 – 1.17 (m, 12H), 1.12 – 0.99 (m, 8H), 0.44 (s, 18H, $^1J_{CH}$ = 116.2 Hz), 0.09 (d, $^2J_{YH}$ = 2.6 Hz, 4H, $^1J_{CH}$ = 100.6 Hz). ^{13}C{^{1}H} NMR (151 MHz, C_6D_6) δ 134.32, 107.09, 49.15 (d, $^1J_{YC}$ = 35.7 Hz), 33.22, 30.28 (d, J_{CP} = 3.3 Hz), 28.93 , 27.48 (t, J_{CP} = 5.9 Hz), 27.35 (t, J_{CP} = 4.4 Hz), 26.28, 21.87, 4.78. ^{31}P{^{1}H} NMR (202 MHz, C_6D_6) δ 2.46 (d, $^1J_{YP}$ = 70.5 Hz). The assignments and coupling constants were determined by ^{1}H-^{13}C HSQC and ^{1}H-^{13}C HMBC experiments (see Appendix). Anal. Calcd. for $C_{38}H_{72}YNP_2Si_2$: C, 60.85; H, 9.68; N, 1.87, Found: C, 61.18; H, 9.94; N, 1.50.

Typical procedure for catalytic hydrogenation. A sample of (PNP-Cy)Y(CH_2SiMe_3)$_2$ (7.5 mg, 0.01 mmol) was dissolved in 1 mL benzene-d_6, along with hexamethylbenzene (2.1 mg, 0.013 mmol) as an internal standard in a 5mm NMR tube with a Teflon screw cap. To this was added 1-octene (21.3 mg, 0.19 mmol). The tube was degassed to remove nitrogen, cooled to 77 K, and placed under vacuum. The tube was exposed to hydrogen at 1 atm for 2 min and then sealed. The sealed tube was allowed to warm to room temperature to attain a hydrogen pressure of approximately 3.9 atm due to gas expansion.The tube was sealed and monitored by ^{1}H NMR spectroscopy.

Typical procedure for catalytic hydrosilation. A sample of (PNP-Cy)Y(CH_2SiMe_3)$_2$ (7.5 mg, 0.01 mmol) was dissolved in 1 mL benzene-d_6, along with hexamethylbenzene (2.1 mg, 0.013 mmol) as an internal standard in a 5mm NMR tube with a Teflon screw cap. To this was added, subsequently, 1-octene (21.3 mg, 0.19 mmol) and $PhSiH_3$ (21.6 mg, 0.20 mmol). The tube was sealed and monitored by ^{1}H NMR spectroscopy.

REFERENCES

(1) Hartwig, J. *Organotransition Metal Chemistry: From Bonding to Catalysis*, 1 edition.; University Science books: Sausalito, Calif, 2009.
(2) Sadow, A. D.; Tilley, T. D. *J. Am. Chem. Soc.* **2003**, *125* (26), 7971.
(3) Sadow, A. D.; Tilley, T. D. *Organometallics* **2003**, *22* (17), 3577.
(4) Castillo, I.; Tilley, T. D. *J. Am. Chem. Soc.* **2001**, *123* (43), 10526.
(5) Thompson, M. E.; Baxter, S. M.; Bulls, A. R.; Burger, B. J.; Nolan, M. C.; Santarsiero, B. D.; Schaefer, W. P.; Bercaw, J. E. *J. Am. Chem. Soc.* **1987**, *109* (1), 203.
(6) Fu, P.-F.; Brard, L.; Li, Y.; Marks, T. J. *J. Am. Chem. Soc.* **1995**, *117* (27), 7157.
(7) Molander, G. A.; Dowdy, E. D. In *Lanthanides: Chemistry and Use in Organic Synthesis*; Kobayashi, P. S., Ed.; Topics in Organometallic Chemistry; Springer Berlin Heidelberg, 1999; pp 119–154.
(8) Molander, G. A.; Romero, J. A. C. *Chem. Rev.* **2002**, *102* (6), 2161.
(9) Watson, P. L.; Parshall, G. W. *Acc. Chem. Res.* **1985**, *18* (2), 51.
(10) Konkol, M.; Kondracka, M.; Voth, P.; Spaniol, T. P.; Okuda, J. *Organometallics* **2008**, *27* (15), 3774.
(11) Levine, D. S.; Tilley, T. D.; Andersen, R. A. *Organometallics* **2015**, *34* (19), 4647.
(12) Levine, D. S.; Tilley, T. D.; Andersen, R. A. *Organometallics* **2016**, *Just Accepted*, 10.1021/acs.organomet.6b00394.
(13) Barros, N.; Eisenstein, O.; Maron, L.; Tilley, T. D. *Organometallics* **2006**, *25* (24), 5699.
(14) Lappert, M. F.; Pearce, R. *J. Chem. Soc. Chem. Commun.* **1973**, No. 4, 126.
(15) Shen, R.; Chen, T.; Zhao, Y.; Qiu, R.; Zhou, Y.; Yin, S.; Wang, X.; Goto, M.; Han, L.-B. *J. Am. Chem. Soc.* **2011**, *133* (42), 17037.
(16) Yan, M.; Jin, T.; Ishikawa, Y.; Minato, T.; Fujita, T.; Chen, L.-Y.; Bao, M.; Asao, N.; Chen, M.-W.; Yamamoto, Y. *J. Am. Chem. Soc.* **2012**, *134* (42), 17536.
(17) Takahashi, T.; Bao, F.; Gao, G.; Ogasawara, M. *Org. Lett.* **2003**, *5* (19), 3479.
(18) Mo, Z.; Xiao, J.; Gao, Y.; Deng, L. *J. Am. Chem. Soc.* **2014**, *136* (50), 17414.
(19) Marciniec, B. In *Hydrosilylation*; Marciniec, B., Ed.; Advances In Silicon Science; Springer Netherlands, 2009; pp 87–123.
(20) Molander, G. A.; Retsch, W. H. *Organometallics* **1995**, *14* (10), 4570.
(21) Ge, S.; Meetsma, A.; Hessen, B. *Organometallics* **2008**, *27* (13), 3131.
(22) Trambitas, A. G.; Panda, T. K.; Jenter, J.; Roesky, P. W.; Daniliuc, C.; Hrib, C. G.; Jones, P. G.; Tamm, M. *Inorg. Chem.* **2010**, *49* (5), 2435.
(23) Dash, A. K.; Wang, J. Q.; Eisen, M. S. *Organometallics* **1999**, *18* (23), 4724.
(24) Dash, A. K.; Wang, J. X.; Berthet, J. C.; Ephritikhine, M.; Eisen, M. S. *J. Organomet. Chem.* **2000**, *604* (1), 83.
(25) Greenhalgh, M. D.; Frank, D. J.; Thomas, S. P. *Adv. Synth. Catal.* **2014**, *356* (2–3), 584.
(26) Shao, Y.; Gan, Z.; Epifanovsky, E.; Gilbert, A. T. B.; Wormit, M.; Kussmann, J.; Lange, A. W.; Behn, A.; Deng, J.; Feng, X.; Ghosh, D.; Goldey, M.; Horn, P. R.; Jacobson, L. D.; Kaliman, I.; Khaliullin, R. Z.; Kuś, T.; Landau, A.; Liu, J.; Proynov, E. I.; Rhee, Y. M.; Richard, R. M.; Rohrdanz, M. A.; Steele, R. P.; Sundstrom, E. J.; III, H. L. W.; Zimmerman, P. M.; Zuev, D.; Albrecht, B.; Alguire, E.; Austin, B.; Beran, G. J. O.; Bernard, Y. A.; Berquist, E.; Brandhorst, K.; Bravaya, K. B.; Brown, S. T.; Casanova, D.; Chang, C.-M.; Chen, Y.; Chien, S. H.; Closser, K. D.; Crittenden, D. L.; Diedenhofen, M.; Jr, R. A. D.; Do, H.; Dutoi, A. D.; Edgar, R. G.; Fatehi, S.; Fusti-Molnar, L.; Ghysels, A.;

Golubeva-Zadorozhnaya, A.; Gomes, J.; Hanson-Heine, M. W. D.; Harbach, P. H. P.; Hauser, A. W.; Hohenstein, E. G.; Holden, Z. C.; Jagau, T.-C.; Ji, H.; Kaduk, B.; Khistyaev, K.; Kim, J.; Kim, J.; King, R. A.; Klunzinger, P.; Kosenkov, D.; Kowalczyk, T.; Krauter, C. M.; Lao, K. U.; Laurent, A. D.; Lawler, K. V.; Levchenko, S. V.; Lin, C. Y.; Liu, F.; Livshits, E.; Lochan, R. C.; Luenser, A.; Manohar, P.; Manzer, S. F.; Mao, S.-P.; Mardirossian, N.; Marenich, A. V.; Maurer, S. A.; Mayhall, N. J.; Neuscamman, E.; Oana, C. M.; Olivares-Amaya, R.; O'Neill, D. P.; Parkhill, J. A.; Perrine, T. M.; Peverati, R.; Prociuk, A.; Rehn, D. R.; Rosta, E.; Russ, N. J.; Sharada, S. M.; Sharma, S.; Small, D. W.; Sodt, A.; Stein, T.; Stück, D.; Su, Y.-C.; Thom, A. J. W.; Tsuchimochi, T.; Vanovschi, V.; Vogt, L.; Vydrov, O.; Wang, T.; Watson, M. A.; Wenzel, J.; White, A.; Williams, C. F.; Yang, J.; Yeganeh, S.; Yost, S. R.; You, Z.-Q.; Zhang, I. Y.; Zhang, X.; Zhao, Y.; Brooks, B. R.; Chan, G. K. L.; Chipman, D. M.; Cramer, C. J.; III, W. A. G.; Gordon, M. S.; Hehre, W. J.; Klamt, A.; III, H. F. S.; Schmidt, M. W.; Sherrill, C. D.; Truhlar, D. G.; Warshel, A.; Xu, X.; Aspuru-Guzik, A.; Baer, R.; Bell, A. T.; Besley, N. A.; Chai, J.-D.; Dreuw, A.; Dunietz, B. D.; Furlani, T. R.; Gwaltney, S. R.; Hsu, C.-P.; Jung, Y.; Kong, J.; Lambrecht, D. S.; Liang, W.; Ochsenfeld, C.; Rassolov, V. A.; Slipchenko, L. V.; Subotnik, J. E.; Voorhis, T. V.; Herbert, J. M.; Krylov, A. I.; Gill, P. M. W.; Head-Gordon, M. *Mol. Phys.* **2015**, *113* (2), 184.

Chapter 3 Appendix

Spectroscopic Characterization

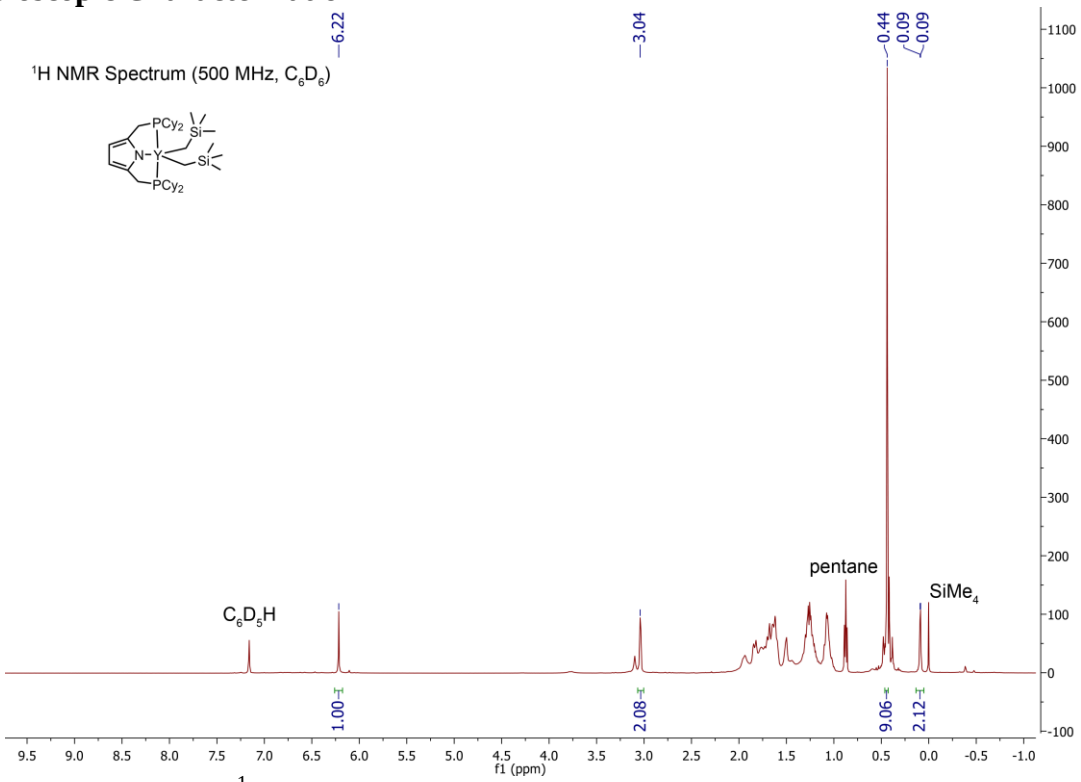

^{1}H NMR Spectrum of (PNP-Cy)Y(CH_2SiMe_3)$_2$.

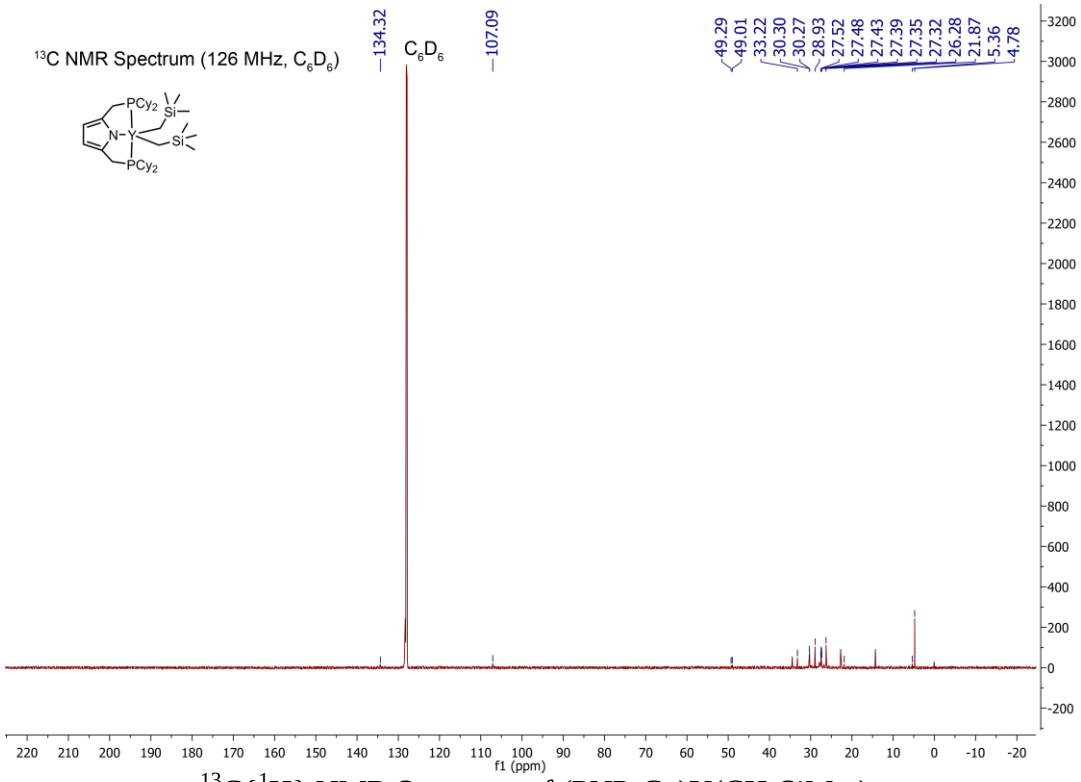

^{13}C{^{1}H} NMR Spectrum of (PNP-Cy)Y(CH_2SiMe_3)$_2$.

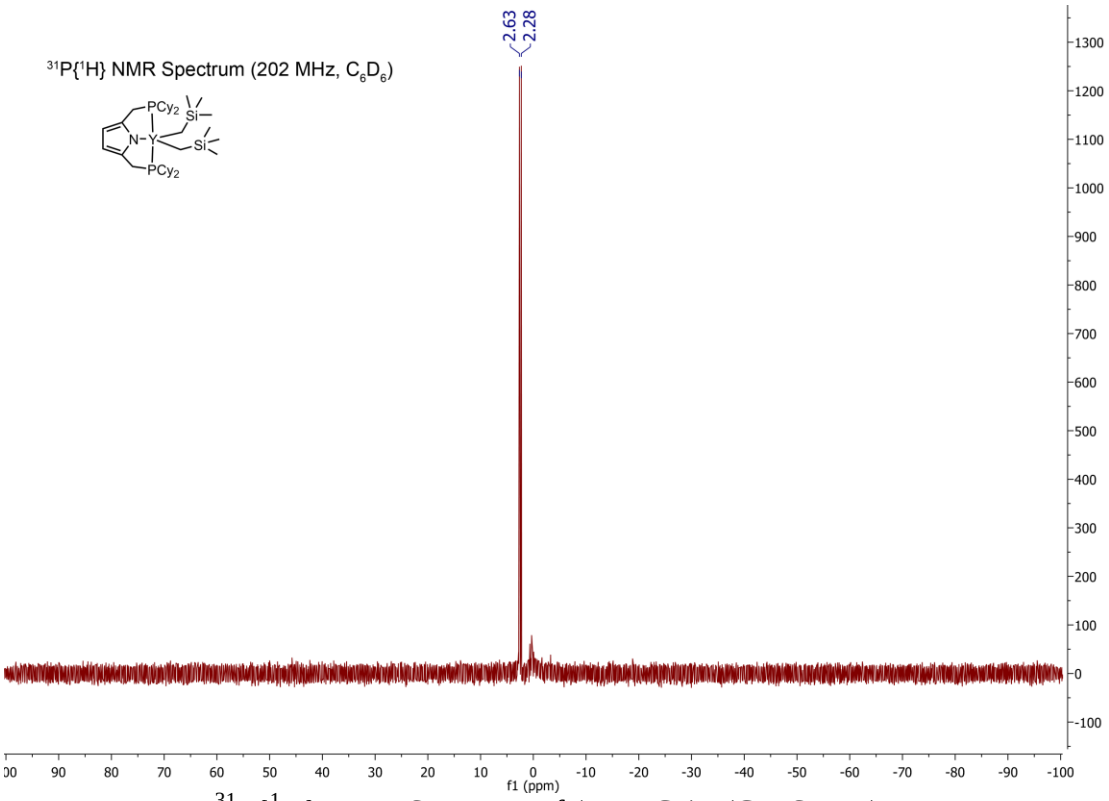

$^{31}P\{^{1}H\}$ NMR Spectrum of (PNP-Cy)Y(CH_2SiMe_3)$_2$.

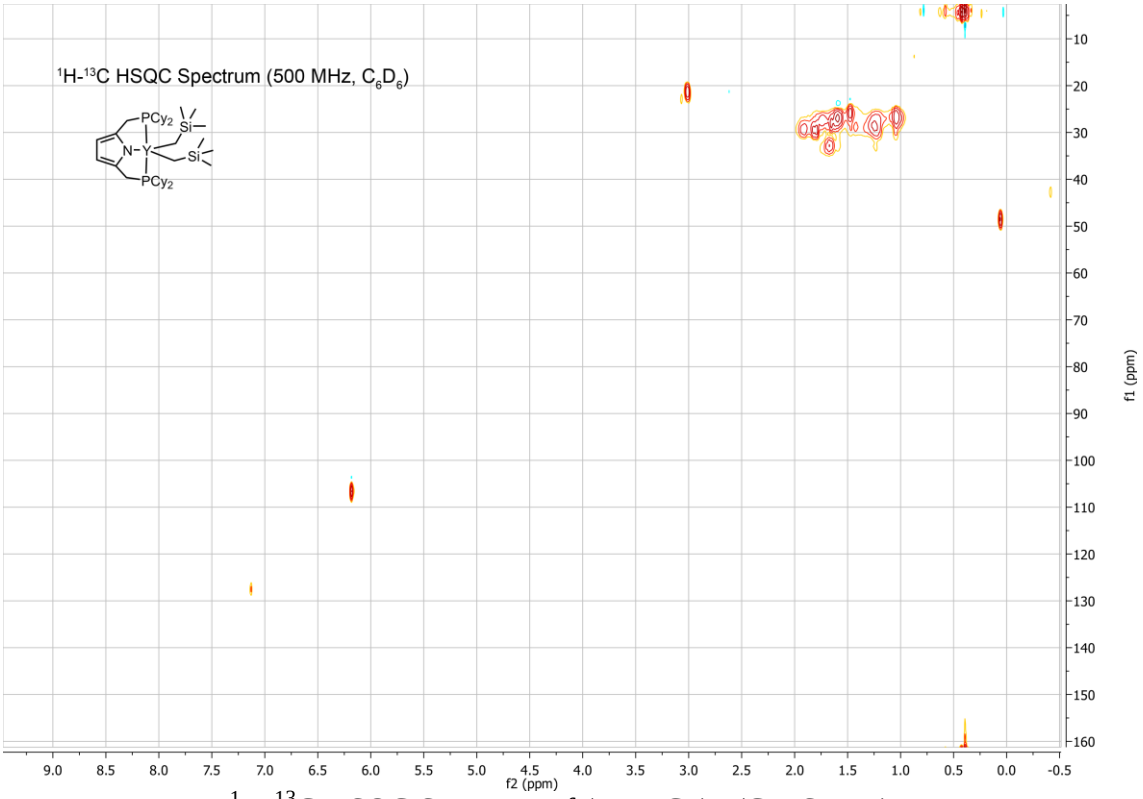

^{1}H-^{13}C HSQC Spectrum of (PNP-Cy)Y(CH_2SiMe_3)$_2$.

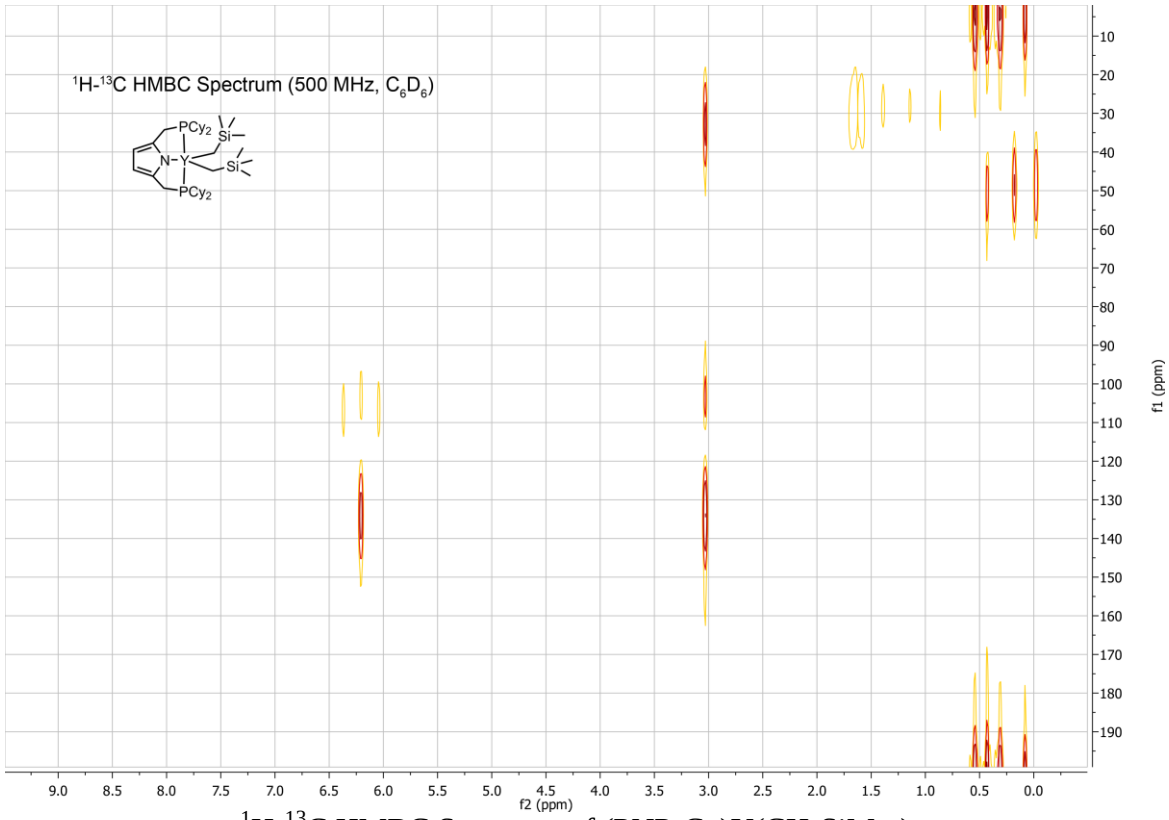

^{1}H-^{13}C HMBC Spectrum of (PNP-Cy)Y(CH_2SiMe_3)$_2$.

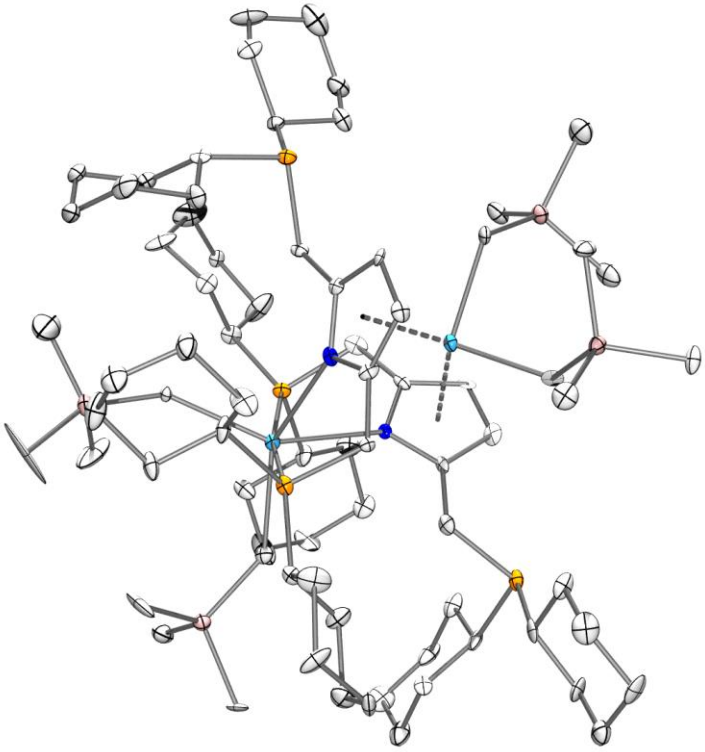

ORTEP diagram of (PNP-Cy)Y(CH_2SiMe_3)$_2$. Hydrogen atoms omitted for clarity.

X-ray Data Tables

Crystal data and structure refinement for (PNP-Cy)Y(CH2SiMe3)2.

Identification code	shelx	
Empirical formula	C76 H144 N2 P4 Si4 Y2	
Formula weight	1499.98	
Temperature	100(2) K	
Wavelength	0.71073 Å	
Crystal system	Triclinic	
Space group	P -1	
Unit cell dimensions	a = 14.5955(8) Å	α = 79.645(3)°.
	b = 16.2010(10) Å	β = 76.624(3)°.
	c = 20.8185(12) Å	γ = 80.373(3)°.
Volume	4670.5(5) $Å^3$	
Z	2	
Density (calculated)	1.067 Mg/m^3	
Absorption coefficient	1.391 mm^{-1}	
F(000)	1616	
Crystal size	0.08 x 0.08 x 0.02 mm^3	
Theta range for data collection	1.016 to 25.417°.	
Index ranges	-16<=h<=17, -19<=k<=19, 0<=l<=25	
Reflections collected	15860	
Independent reflections	15860 [R(int) = 0.087]	
Completeness to theta = 25.000°	95.9 %	
Absorption correction	Semi-empirical from equivalents	
Refinement method	Full-matrix least-squares on F^2	
Data / restraints / parameters	15860 / 42 / 806	
Goodness-of-fit on F^2	1.042	
Final R indices [I>2sigma(I)]	R1 = 0.0625, wR2 = 0.1416	
R indices (all data)	R1 = 0.1161, wR2 = 0.1692	
Extinction coefficient	n/a	
Largest diff. peak and hole	1.076 and -0.843 $e.Å^{-3}$	

Chapter 4. PNP-Supported Rare-Earth-Catalyzed Cross-Dehydrocoupling of Amines and Silanes

INTRODUCTION

Atom efficient methods are increasingly becoming an important strategy in chemical synthesis. The dehydrocoupling of main-group compounds, in which two coupling partners E–H and E'–H form a new E–E' bond with only H_2 as a byproduct, is a prime example of this idea.[1] Early metals and lanthanides have been employed as catalysts for these types of reactions, such as in N–B,[2–5] Si–Si,[6,7] P–P,[8] and B–B bond formation. The preparation of aminosilanes (Si–N) and silazanes (Si–N–Si) by a dehydrocoupling route has recently gained attention (Scheme 1).[9–16] Silicon-nitrogen bonds have important applications as protecting groups in organic chemistry,[17,18] bases,[19] ligands for metals,[20–23] silylating reagents,[24,25] and precursors for ceramic materials.[26] In addition to catalysts based on late metals (Pd,[27] Cr,[28] Cu,[29] Rh,[30] Ru,[31,32]), there are a number based on early d-block (Y,[14] Ti[33]) and f-block metals (Yb, Sm,[10,16] U[34]), and recently alkaline earth metals.[9,11,13,15,35] These catalyst have been proposed to proceed by an array of different mechanisms, including σ-bond metathesis, β-H elimination from 5-coodinate aminosilicates, as well as more exotic pathways involving multiple metal centers.[9,11,13,14,16] The different catalytic systems also have different selectivities, with some generating mixtures of silazanes, while, in others, careful control of the substrate stoichiometry can lead to relatively selective systems.[32] For example, Hill et al. generate mixtures of monoaminosilanes, bisaminosilanes, and silazanes when employing $M[N(SiMe_3)_2]_2$ (M = Mg, Ca, Sr) with primary silanes, while Nako et al. can obtain monoaminosilanes selectively with the similar substrates.[11,14]

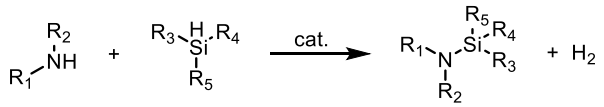

Scheme 1. Amine-silane dehydrocoupling reaction.

We recently reported the preparation of a class of monoanionic PNP-supported (2,5-bis(dicyclohexylphosphinomethyl)pyrrolide) group III complexes (Sc, Y) which are relatively active for σ-bond metathesis reactions.[36,37] These complexes were found to be competent hydrosilation catalysts, but the performance of these catalysts suffered with some substrates possibly due to the rate of trapping of an unstable hydride intermediate relative to its rate of decomposition.[38] If this postulate is correct, we hypothesized that increasing the trapping rate would result in increased catalytic efficiencies and performance. The reported PNP-supported alkyl complexes were shown to react rapidly with primary amines to form sTable 1mide complexes[36] and these compounds were investigated as amine-silane dehydrocoupling catalysts.

RESULTS

Stoichiometric preparation of aminosilanes from PNP-Supported amide complexes. Addition of ^{t}BuNH$_2$ (10.3 mg, 0.14 mmol) to a sample of (PNP-Cy)Sc(CH$_2$SiMe$_3$)$_2$ (50.0 mg, 0.07 mmol) in 5 mL of pentane resulted in the instantaneous formation of (PNP-Cy)Sc(NH^{t}Bu)$_2$, which was isolate and characterized as described in the Experimental Section, and 2 equiv. neopentane. Treatment of a sample of this amide complex (10.0 mg, 0.015 mmol) with 2 equiv of *p*-tolylsilane (4.0 mg, 0.03 mmol) in benzene-d_6 (1.0 mL) resulted in the immediate formation of 2 equiv of *p*-tolyl-(*t*-butylamino)silane and decomposition of the scandium complex,

presumed to be due to formation of an unstable metal hydride complex.[36,38] This confirmed that the amide complexes were capable of effecting the dehydrocoupling reaction. When excess $^{t}BuNH_2$ (0.20 mmol) and p-tolylsilane (0.20 mmol) were added to a sample of (PNP-Cy)Sc(CH_2SiMe_3)$_2$ (0.01 mmol) in benzene-d_6 (1.0 mL) in a sealed NMR tube, vigorous bubbling was observed. NMR spectroscopy revealed that, after 30 min at 22 °C, all (>99 %) *p*-tolylsilane and $^{t}BuNH_2$ was consumed and an equimolar amount of *p*-tolyl-(*tert*-butylamino)silane was observed, along with H_2 (0.01 mmol) (presumably more hydrogen is present in the headspace of the NMR tube). Hence, (PNP-Cy)ScR_2 is an effective and selective dehydrocoupling catalyst.

A comparison of the reactivity of the scandium complexes with heavier congeners was pursued to gain insight into the factors that control the rates of the dehydrocoupling reaction. The yttrium analog (PNP-Cy)Y(CH_2SiMe_3)$_2$ (**2**) has previously been reported.[38] As an additional comparison, the holmium congener was also prepared. Holmium has an covalent radius identical to yttrium, as well as several other similar properties, such as polarizability.[39–41] Differences in reactivity between Ho ($4f^{10}$) and Y ($4d^{0}$) could therefore be potentially enlightening. Preparation of Ho(CH_2SiMe_3)$_3$(THF)$_2$ has been reported, but the cited paper does not provide a synthesis.[42] We prepared this material by slow addition of a pentane solution (5 mL) of $LiCH_2SiMe_3$ (107.9 mg, 1.14 mmol) to a pentane suspension (5 mL) of $HoCl_3(THF)_{3.5}$ (200.0 mg, 0.38 mmol). After filtration to remove LiCl, storage at -35 °C afforded stable, pink, crystalline needles (69% yield). Addition of a (PNP-Cy)H (68.3 mg, 0.14 mmol) to Ho(CH_2SiMe_3)$_3$(THF)$_2$ (80.0 mg, 0.14 mmol) in pentane (10 mL) afforded (PNP-Cy)Ho(CH_2SiMe_3)$_2$ (**3**) in good yield (87%). The crystal structure of **3** was determined to be nearly identical to that of (PNP-Cy)Y(CH_2SiMe_3)$_2$ (see Appendix).

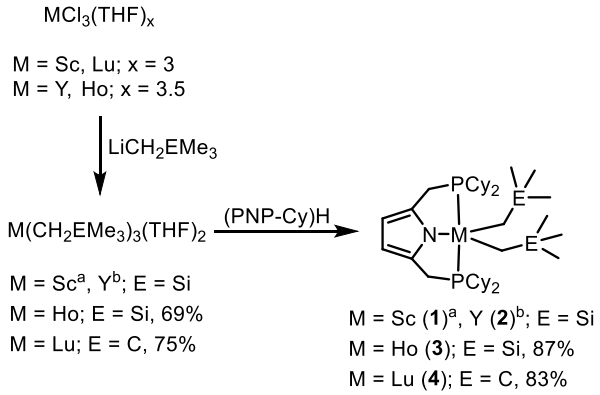

Scheme 2. Synthesis of PNP-supported metal complexes.

Table 1. Ionic properties of Sc^{3+}, Y^{3+}, Ho^{3+}, Lu^{3+}.[39,41,43]

	Sc	Y	Ho	Lu
Ionic radius (Å)	0.885	1.040	1.041	1.001
(Static) Polarizability (Å^3)	0.33	0.68	0.72	0.61

The complex Lu(CH_2CMe_3)$_3$(THF)$_2$ was prepared by addition of a pentane solution (5 mL) of Li(CH_2CMe_3) (141.2 mg, 1.81 mmol) to a pentane suspension of $LuCl_3(THF)_3$ (300 mg,

0.6 mmol, 5 mL). A sample of $Lu(CH_2CMe_3)_3(THF)_2$ (105 mg, 0.20 mmol) was treated with (PNP-Cy)H (96.1 mg, 0.20 mmol) to afford the complex (PNP-Cy)$Lu(CH_2CMe_3)_2$ (**4**) in good yield (83%). Since **1-4** are immediately converted into amide complexes on addition of amine, the different alkyl groups don't play a role in the reaction.

A study of the scope of the reaction with different amines, silanes, catalysts is summarized in Table 2. Addition of amine and silane (1 equiv) to catalyst **1-4** (5 mol%) in benzene-d_6 (1.0 mL) resulted in vigorous bubbling. Reactions were monitored by ^{1}H NMR spectroscopy and the reaction with all compounds are found to be first order in catalyst, first order in silane and zeroth order in amine (see Appendix).

Complex **1** is an efficient catalyst for the dehydrocoupling of relatively unhindered primary and secondary amines (H_2N^tBu and pyrrolidine) with $PhSiH_3$ (Table 2, entries 1 and 3), but are very sluggish with Ph_2SiH_2, requiring long reaction times (9-16 h) and/or heating (100 °C) (Table 2, entries 5-7). Hindered primary and secondary amines (H_2NDipp (Dipp = 2,6-diisoproylphenyl) and HN^iPr_2) with $PhSiH_3$ also require heating (60–100 °C) and very long reaction times (8-10 d) (Table 2, entries 2, 4). Tertiary silanes (Ph_3SiH) show no reactivity when **1** is used as a catalyst (Table 2, entries 8-10) even when heated to 100 °C for 12 days.

Interestingly, complexes **2** and **3** react with nearly identical kinetic profiles, requiring the same amount of time for all reactions studied. Extremely short reaction times (<10 min) for coupling H_2N^tBu or pyrrolidine and $PhSiH_3$ were observed for these complexes (Table 2, entries 11, 13, 21, 23), and these amines with Ph_2SiH_2 also proceeded efficiently and quickly (1-3 h) at ambient temperature (Table 2, entries 15, 17, 24, 26), as did HN^iPr_2 and $PhSiH_3$ (Table 2, entry 14). Dehydrocoupling of H_2NDipp required heating to 100 °C. With $PhSiH_3$ (Table 2, entry 12, 22), the reaction proceeds much more quickly than with **1** (3 h vs. 8 d), and with Ph_2SiH_2, though it requires long reaction times (12 d), in contrast with **1**, ultimately results in significant (80 %), selective product formation (Table 2, entries 16, 25). Using **2** or **3**, the least hindered amine studied, pyrrolidine, can be dehydrocoupled with tertiary silanes at 100 °C over 12 days.

Complex **4** is more similar to complexes **2** and **3** than **1**. Less than 10 minutes at 22 °C is required to couple H_2N^tBu or pyrrolidine and $PhSiH_3$ (Table 2, entries 30, 33). Dehydrocoupling of H_2NDipp and $PhSiH_3$ proceed similarly with **4** as with **2**/**3**, and considerably faster than **1** (30 h vs 8 d), under the same reaction conditions (Table 2, entries 31-32). With Ph_2SiH_2, slightly longer (20 min vs <10 min) is required for coupling with pyrrolidine with **4** compared with **2**/**3**. On the other hand, relatively unhindered primary amine H_2N^tBu required less time (1 h vs. 2 h) with **4** than with **2**/**3**. The more hindered H_2NDipp and Ph_2SiH_2 required heating to 100 °C and was considerably slower than **2**/**3** (22 d for 61 % yield vs. 12 d for 80 % yield). Pyrrolidine could be dehydrocoupled with Ph_3SiH at 100 °C much more slowly than with **2**/**3**, requiring over 22 d for 76 % yield vs. 12 d for 99 %.

Higher silazanes and bis- and tris-aminosilanes can be selectively prepared by increasing the reaction temperature to 100 °C, as well as the reaction time. An appropriate stoichiometry for amine and silane for the desired product was used, as summarized in Table 3, and added to a solution of 5 mol% of **1-4** in benzene-d_6 (1 mL), heated to 100 °C, and monitored by ^{1}H NMR spectroscopy.

Consistent with the behavior observed for the formation of simple aminosilanes, **1** is the least active catalyst. Extremely long reaction times (1-2 weeks) are required to obtain even miniscule yields. With the exception of bisaminosilanes of $PhSiH_3$ and $^tBuNH_2$ and pyrrolidine, which could be effectively synthesized in 10 d and 15 h, respectively (Table 3, entries 1,3), higher silazanes were not produced with **1** (yield <10%, Table 3, entries 2, 4-9).

Table 2. Summary of dehydrocoupling reactions of silanes and amines to form aminosilanes.

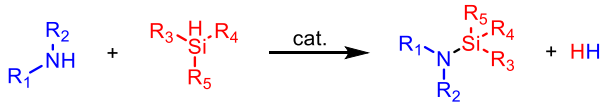

Entry	Catalyst	Silane	Amine	Time	Temp. (°C)	Yield (%)	Selectivity[c] (%)
1		$PhSiH_3$	$^tBuNH_2$	20 min	22	>99	>99
2			$DippNH_2$	8 d	100	>99	>99
3			$(CH2)_4NH$	<10 min	22	>99	>99
4			$(^iPr)_2NH$	10.5 d	60	99	>99
5	**1**	Ph_2SiH_2	$^tBuNH_2$	9 h	22	>99	>99
6	(Sc)		$DippNH_2$	13 d	100	trace	N/A
7			$(CH2)_4NH$	16 h	100	>99	>99
8		Ph_3SiH	$^tBuNH_2$	12 d	100	NR	N/A
9			$DippNH_2$	12 d	100	NR	N/A
10			$(CH_2)_4NH$	12 d	100	NR	N/A
11		$PhSiH_3$	$^tBuNH_2$	<10 min	22	>99	>99
12			$DippNH_2$	3 h	100	99	>99
13			$(CH_2)_4NH$	<10 min	22	>99[a]	>99
14			$(^iPr)_2NH$	3 h	22	>99	>99
15	**2**	Ph_2SiH_2	$^tBuNH_2$	2 h	22	98	>99
16	(Y)		$DippNH_2$	12 d	100	85	>99
17			$(CH_2)_4NH$	1 h	22	>99	>99
18		Ph_3SiH	$^tBuNH_2$	12 d	100	NR	N/A
19			$DippNH_2$	12 d	100	NR	N/A
20			$(CH_2)_4NH$	12 d	100	>99	>99
21		$PhSiH_3$	$^tBuNH_2$	<10 min	22	>99	>99
22			$DippNH_2$	3 h	100	98	>99
23			$(CH_2)_4NH$	<10 min	22	>99[a]	>99
24	**3**	Ph_2SiH_2	$^tBuNH_2$	2 h	22	97	>99
25	(Ho)		$DippNH_2$	12 d	100	80	>99
26			$(CH_2)_4NH$	1 h	22	>99	>99
27		Ph_3SiH	$^tBuNH_2$	12 d	100	NR	N/A
28			$DippNH_2$	12 d	100	NR	N/A
29			$(CH_2)_4NH$	12 d	100	>99	>99
30		$PhSiH_3$	$^tBuNH_2$	<10 min	22	>99	>99
31			$DippNH_2$	30 h	22	>99	>99
32			$DippNH_2$	3 h	100	>99	>99
33			$(CH_2)_4NH$	<10 min	22	>99[b]	>99
34	**4**	Ph_2SiH_2	$^tBuNH_2$	1 h	22	>99	>99
35	(Lu)		$DippNH_2$	22 d	100	61	>99
36			$(CH_2)_4NH$	20 min	22	>99	>99
37		Ph_3SiH	$^tBuNH_2$	12 d	100	NR	N/A
38			$DippNH_2$	12 d	100	NR	N/A
39			$(CH_2)_4NH$	22 d	100	76	>99

[a] Mixture of $PhSiH_2N(CH_2)_4$ and $PhSiH[N(CH_2)_4]_2$, 12%:88% [b] Mixture of $PhSiH_2N(CH_2)_4$ and $PhSiH[N(CH_2)_4]_2$, 20%:80% [c] Selectivity = moles product formed/moles starting material consumed

Table 3. Summary of dehydrocoupling reactions of silanes and amines to form silazanes and bis- and trisaminosilanes.

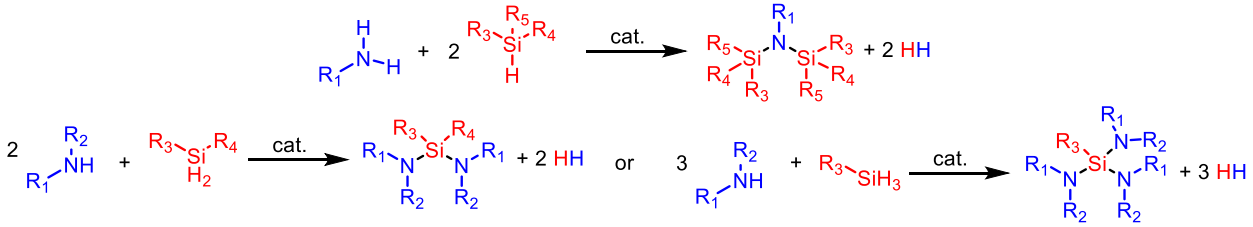

Entry	Catalyst	Silane	Amine	Time	Products	Yield (%)	Select. (%)
1	**1** (Sc)	$PhSiH_3$	2 $^tBuNH_2$	10 d	$PhSiH(NH^tBu)_2$	>99	>99
2			2 $DippNH_2$	12 d	$PhSiH(NHDipp)_2$	NR	N/A
3			2 $(CH_2)_4NH$	15 h	$PhSiH[N(CH_2)_4]_2$	>99	>99
4			3 $(CH_2)_4NH$	2.5 d	$PhSi[N(CH_2)_4]_3$	9	94
5		2 $PhSiH_3$	$^tBuNH_2$	16 d	$(PhSiH)_2N^tBu$	NR	N/A
6			$DippNH_2$	16 d	$(PhSiH)_2NDipp$	4	90
7		Ph_2SiH_2	2 $tBuNH_2$	13 d	$Ph_2Si(NH^tBu)_2$	NR	N/A
8			2 $(CH_2)_4NH$	5 d	$Ph_2Si[N(CH_2)_4]_2$	5	>99
9		2 Ph_2SiH_2	$DippNH_2$	13 d	$(Ph_2SiH)_2NDipp$	NR	N/A
10	**2** (Y)	$PhSiH_3$	2 $^tBuNH_2$	12 h	$PhSiH(NH^tBu)_2$	>99	98
11			2 $DippNH_2$	9 d	$PhSiH(NHDipp)_2$	99	>99
12			2 $(CH_2)_4NH$	<10 min	$PhSiH[N(CH_2)_4]_2$	>99	>99
13			3 $(CH_2)_4NH$	3.5 d	$PhSi[N(CH_2)_4]_3$	>99	98
14		2 $PhSiH_3$	$^tBuNH_2$	8 d	$(PhSiH)_2N^tBu$	49	98
15			$DippNH_2$	12 d	$(PhSiH)_2NDipp$	>99	>99
16		Ph_2SiH_2	2 $tBuNH_2$	22 d	$Ph_2Si(NH^tBu)_2$	20	>99
17			2 $(CH_2)_4NH$	6 d	$Ph_2Si[N(CH_2)_4]_2$	>99	>99
18		2 Ph_2SiH_2	$DippNH_2$	13 d	$(Ph_2SiH)_2NDipp$	NR	N/A
19	**3** (Ho)	$PhSiH_3$	2 $^tBuNH_2$	12 h	$PhSiH(NH^tBu)_2$	>99	98
20			2 $DippNH_2$	9 d	$PhSiH(NHDipp)_2$	99	>99
21			2 $(CH_2)_4NH$	<10 min	$PhSiH[N(CH_2)_4]_2$	>99	>99
22			3 $(CH_2)_4NH$	3.5 d	$PhSi[N(CH_2)_4]_3$	>99	98
23		2 $PhSiH_3$	$^tBuNH_2$	8 d	$(PhSiH)_2N^tBu$	48	92
24			$DippNH_2$	12 d	$(PhSiH)_2NDipp$	>99	>99
25		Ph_2SiH_2	2 $tBuNH_2$	22 d	$Ph_2Si(NH^tBu)_2$	21	>99
26			2 $(CH_2)_4NH$	6 d	$Ph_2Si[N(CH_2)_4]_2$	>99	>99
27		2 Ph_2SiH_2	$DippNH_2$	13 d	$(Ph_2SiH)_2NDipp$	NR	N/A
28	**4** (Lu)	$PhSiH_3$	2 $^tBuNH_2$	10 h	$PhSiH(NH^tBu)_2$	>99	>99
29			2 $DippNH_2$	22 d	$PhSiH(NHDipp)_2$	91	94
30			2 $(CH_2)_4NH$	<10 min	$PhSiH[N(CH_2)_4]_2$	>99	>99
31			3 $(CH_2)_4NH$	1.5 d	$PhSi[N(CH_2)_4]_3$	20	88
32		2 $PhSiH_3$	$^tBuNH_2$	4.5	$(PhSiH)_2N^tBu$	14	48
33			$DippNH_2$	22 d	$(PhSiH)_2NDipp$	11	41
34		Ph_2SiH_2	2 $^tBuNH_2$	22 d	$Ph_2Si(NH^tBu)_2$	8	>99
35			2 $(CH_2)_4NH$	5.5 d	$Ph_2Si[N(CH_2)_4]_2$	92	>99
36		2 Ph_2SiH_2	$DippNH_2$	22 d	$(Ph_2SiH)_2NDipp$	NR	N/A

Complexes **2** and **3** again behave identically and are much more active than **1**. Bisaminosilanes of $PhSiH_3$ and $^tBuNH_2$ and pyrrolidine can be prepared in 12 h to less than <10 minutes (Table 3, entries 10, 12, 19, 21). The trisaminosilane $PhSi[N(CH_2)_4]_3$ can be produced by the exhaustive dehydrocoupling of $PhSiH_3$ and pyrrolidine over the course of 3.5 days (Table 3, entries 13, 22). The extremely crowded bisaminosilane of H_2NDipp and $PhSiH_3$ can be prepared in 9 days from 2:1 mixture of amine and silane (Table 3, entries 11, 20). If the amine-silane ratio is reversed, the silazane $DippN(PhSiH_2)_2$ is exclusively produced instead in 12 d (Table 3, entries 15, 24). This stoichiometry effect can be understood to be due to the fact that **2**/**3** appears to react much more readily with less bulky silanes and amines. Hence, when primary amine is exhausted, the best coupling partners are the aminosilane's amine moiety and $PhSiH_3$. If instead the silane is exhausted, the best partners are the aminosilane's silane moiety and H_2NDipp. The bisaminosilane of Ph_2SiH_2 and pyrrolidine can be obtained after 6 d (Table 3, entries 17, 26). While, in most cases, H_2NDipp reacts more slowly than H_2N^tBu, that is not the case for the preparation of the silazane of H_2N^tBu and $PhSiH_3$ or the bisaminosilane of H_2N^tBu and Ph_2SiH_2, which require 8 d and 22 d, respectively to obtain any appreciable product (48% and 20% respectively, Table 3, entries 14, 16, 23, 25).

The reactivity of **4** is intermediate to **2**/**3** and **1,** though the selectivity was relatively low. The bisaminosilane of $PhSiH_3$ and H_2N^tBu and pyrrolidine is efficiently and selectively produced in 10 h or <10 min, respectively (Table 3, entries 28, 30). However, the trisaminosilane with pyrrolidine is formed in only low yield (20 %) and relatively low (88 %) selectivity (Table 3, entry 31). Silazanes prepared from $PhSiH_3$ and H_2N^tBu or H_2NDipp are formed in only low yields (14% and 11%, respectively) and very low selectivities (48% and 41%, respectively, Table 3, entries 32-33). This low selectivity suggests that coupling partners other than the parent silane are more readily dehydrocoupled with **4** than with **1**-**3**. $DippNH_2$ and $PhSiH_3$ require much longer times than **2**/**3** to form the bisaminosilane product (Table 3, entry 29). The bisaminosilane formed with Ph_2SiH_2 and $^tBuNH_2$ or pyrrolidine are also formed more slowly with **4** than with **2/3** (Table 3, entries 34-35).

Computational studies.

DFT calculations were employed to gain insight into the dehydrocoupling mechanism. A variety of mechanisms have been proposed for existing systems, including concerted, stepwise, and multimolecular mechanisms. Multimolecular mechanisms can be ruled out in this system since the reaction is first order in catalyst. The concerted and stepwise mechanisms are shown in Figure 1.

In the concerted mechanism, an incoming silane forms a kite-shaped transition state, in which the Si becomes pseudo-5-coordinate at the β-position of the kite, with the metal amide complex at an α-position, exchanging the metal's amide moiety with the silane's hydride moiety to form an aminosilane and a metal hydride complex (Figure 1, inside fork). In the stepwise mechanism, the incoming electrophilic silane is attacked by the nucleophilic metal amide, forming a stable 5-coordinate metal aminosilicate complex. This aminosilicate complex then undergoes β-H elimination to form the aminosilane product and a metal hydride complex. While the difference in the mechanisms is subtle, the two pathways differ principally in whether or not a stable 5-coordinate aminosilicate exists as an energy minimum. The metal hydride complex which is proposed to be formed is rapidly protonated by free amine to release H_2 and reform the starting amide. Because this last step has a low barrier, and has been investigated before, it was not investigated further here.[13,14]

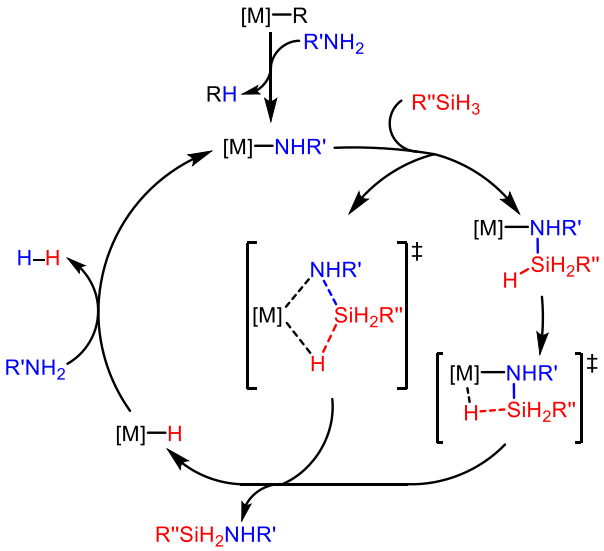

Figure 1. Possible catalytic cycles for dehydrocoupling: (inside fork) concerted σ-bond metathesis, (outside fork) stepwise *via* β-H elimination.

A stable 5-coodinate aminosilicate intermediate was found to exist for all metals investigated (Sc, Y, Lu, see Figure 2, Ho was not calculated since it behaves the same as Y and open-shell systems are more computationally demanding). Calculations also revealed a significant agostic interaction between the metal center and the Si–H bond, leading to aminosilicate complexes that are already significantly activated toward β-H elimination. The importance of Si–H agostic interaction to the structure and reactivity of early metal systems has only recently been recognized. The aminosilicate complex minima lie 12.8, 8.2, and 7.0 kcal/mol above the separated silane and metal amide complexes (M = Sc, Y, Lu), respectively, indicating that these complexes are only formed transiently. The β-H elimination transition state was found to lie just slightly above the aminosilicate intermediate for Sc (3.5 kcal/mol), and was found to be practically barrierless for Y and Lu (0.9 kcal/mol and 0.8 kcal/mol below the aminosilicate, respectively).

In order to gain insight into the interaction between the silane and the metal amide complex, the Si–N interaction was investigated by energy decomposition analysis (EDA).[44,45] The EDA decomposes the interaction energy into geometric distortion (GD, the energy cost of distorting the interacting fragments from their normal geometry to the interacting geometry), frozen interactions (which may be further separated into: Pauli repulsion, PAULI, principally what is described as steric interactions, and electrostatics, ELEC, corresponding to classical coulomb attraction/repulsion)[46], polarization stabilization (POL, the energy gained by electronic rearrangement within each fragment in response to the presence of the other fragment), and charge-transfer (CT, the energy gained by electrons being donated from one fragment to the other). Because the EDA method is best suited to systems without significant bond-breaking and since β-H elimination reaction has such a low barrier, the interaction interrogated is the silane-metal complex interaction in the intermediate aminosilicate complex.

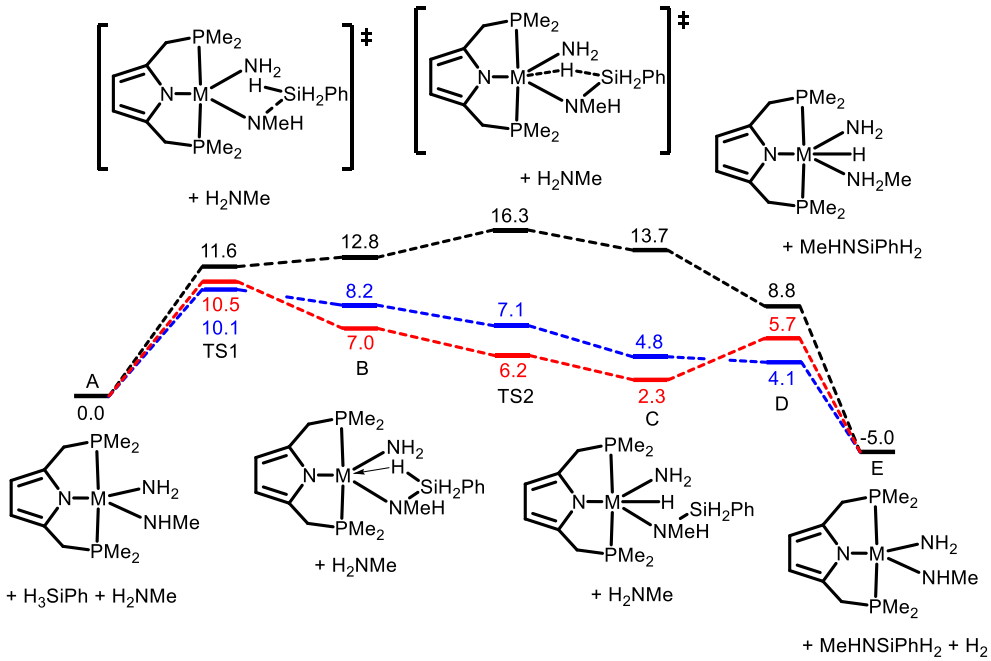

Figure 2. Calculated reaction pathway for amine-silane dehydrocoupling for Sc (black), Y (blue), and Lu (red). All energies are Gibbs free energies in kcal/mol. Because some barriers are so low (or barrierless), some of the transition state free energies appear below the surrounding intermediates in free energy. Since geometries are optimized for electronic energy, these discrepancies may be ascribable to entropic effect.

Table 4. Summary of EDA results for metal aminosilicate complexes. All energies in kcal/mol.

	Sc	Y	Lu
GD	19.4 (complex) 58.4 (silane)	20.9 (complex) 60.1 (silane)	21.1 (complex) 59.1 (silane)
ELEC	-222.0	-213.7	-213.6
PAULI	300.0	280.9	281.0
POL	-103.4	-107.7	-106.3
CT	-58.9	-50.7	-50.9

Between Sc and Y/Lu, the difference in the interaction energies of the silane and metal complex, and, hence, the difference in barrier heights, is attributable principally to differences in Pauli repulsion, that is, steric interactions between the incoming silane and metal complex. The less polarizable first row Sc induces a higher negative charge density on the amide N, which increases the electrostatic interaction and leads to high charge-transfer stabilization by donating charge from the N to the Si. The more polarizable amide complexes (Y is more polarizable than Lu[39–41]) show slightly higher polarization stabilization. The differences between the energy terms of Y and Lu are very slight and differences in the total interaction energy are principally due to the increased polarization stabilization of Y vs. Lu. Hence, the principal factors in determining interaction energies and, hence, barrier heights are determined by i) steric interactions (as indicated by the highly variable nature of the Pauli repulsion term) and ii) polarizability (as indicated by the more modest changes to the polarization term). The smaller first row metal center increases steric interactions between the complex and the silane and ultimately makes this

barrier the highest, while the more similarly sized Y and Lu are distinguished by their differing polarizabilities. This analysis would indicate that Y and Ho, since they have nearly identical ionic radii, metrical parameters by X-ray crystallography, and polarizability, should display identical reactivity, as was found. Indeed, these calculations concur with the observation that the reactivity of these complexes parallels the ionic radii and polarizability: Y~Ho > Lu >> Sc. These data may also indicate why the barium-based system of Bellini et. al.[13] is so effective; barium has a very large ionic radius (1.35 Å vs. 1.04 Å for Y/Ho) and is more polarizable than any of the metals studied here (~1.55 $Å^3$ vs. 0.72 $Å^3$ for Ho).

DISCUSSION

The high selectivities obtained with these catalysts are noteworthy as compared to other dehydrocoupling systems which often form oligomeric polysilazanes or mixtures of products. This selectivity may arise from the use of a bulky ligand which remains attached to the metal center throughout the catalytic cycle. Since the anchoring group of the ligand is a pyrrole, which is more acidic (pKa 17.5) than an amine (pKa 30-40), the amine ligand is preferentially deprotonated and attached to the metal. The ligand also appears to prevent product inhibition which is observed in some systems, by increasing the steric bulk around the metal center.

Generally speaking, as substrates become more bulky (especially in the cases of higher silazanes), the activity of **4** decreased faster than that of **2**/**3**. This effect may be due to fact that Y and Ho have larger ionic radii than Lu, allowing more space for the substrates to reach the metal center.

Complex **1** is both the smallest metal and has the least nucleophilic amide moiety, leading to its generally low, but highly selective, activity. The selectivity of **1** to produce only the monoaminosilane even with unhindered coupling partners opens the possibility of selectively preparing mixed aminosilanes and silazanes in a highly atom-efficient and controlled manner.

CONCLUSION

A range of PNP-supported rare earth metal complexes (Sc, Y, Ho, Lu) were synthesized and their reactivity for (1°, 2°) amine–(1°, 2°, 3°) silane dehydrocoupling assessed and compared. The equivalently-sized[43] and equally polarizable[39–41] yttrium and holmium complexes (**2**, **3**) performed identically to each other, indicating that the factors important to determining dehydrocoupling rates and efficiencies are among the shared properties of Y and Ho. These complexes performed superiorly to systems based on lutetium (**4**) which, though fairly active and selective for formation of aminosilanes, performs much more poorly for preparation of silazanes and bis- and trisaminosilanes. Scandium (**1**) was found to have the lowest activity but also some of the highest selectivity, forming almost exclusively monoaminosilane even for unhindered substrates, except under relatively forcing conditions. Computational studies indicate that the reaction proceeds by a stepwise formation of metal aminosilicate complexes, followed by β-H elimination to afford the aminosilane product and a metal amidohydride complex. This amidohydride complex is rapidly protonated by free amine to regenerate the metal bisamide complex. The differing nucleophilicities of the metal amide functionality was investigated to determine their origin via energy decomposition analysis and it was determined that steric interactions between the amide complex and the silane are the determining factors for controlling

the reaction barrier height, indicating why the observed reactivity trend parallels the ionic radii of the metal center.

EXPERIMENTAL SECTION

General

Unless otherwise noted, all experiments were conducted in dry, oxygen-free solvents using standard Schlenk techniques or in a N_2 atmosphere glovebox. Deuterated solvents were purchased from Cambridge Isotope Laboratories, Inc. Benzene-d_6 was dried by vacuum distillation from Na/K alloy. Toluene-d_8 was dried by refluxing over molten sodium metal followed by vacuum distillation. Unless otherwise noted, reagents were obtained from commercial suppliers and used as received. 4-phenylpyridine was obtained from Aldrich and sublimed. (PNP-Cy)H, (PNP-^{t}Bu)H, (PNP-Cy)Sc(CH_2SiMe_3)$_2$ were prepared according to literature procedures.[28]

Analytical Methods

Solution NMR spectroscopy was performed using Bruker AV-300, AVB-400, AVQ-400, AV-500, or AV-600 MHz spectrometers at room temperature. ^{1}H, ^{13}C{^{1}H}, and ^{31}P{^{1}H} NMR spectra were calibrated internally to either the resonance for the solvent or residual proteo solvent relative to tetramethylsilane. Elemental analyses were carried out by the College of Chemistry Microanalytical Laboratory at the University of California, Berkeley.

Computational Details

Calculations were carried out with the Gaussian09 rev D01 suite of programs, employing the ωB97X-D range-separated hybrid functional and 6-31++G** basis set for non-metal atoms. Metal atoms were treated with the relativistic ECP and basis set of the Stuttgart group. Gibbs free energies were calculated at 298 K and 1 atm of pressure. The ligand cyclohexyl groups were truncated to methyl groups to save computational time.

X-ray Crystallography Details

X-ray diffraction data for crystals of Ho(CH_2SiMe_3)$_3$(THF)$_2$ and (PNP-Cy)Ho(CH_2SiMe_3)$_2$ were collected using a Bruker AXS modified four-circle diffractometer coupled CCD detector with Mo Kα (λ = 0.71073 Å) radiation monochromated by a system of QUAZAR multilayer mirrors. Crystals were kept at 100(2) K throughout collection. Data collection, refinement, and reduction were performed with Bruker APEX2 software (v. 2013.4). Structures were solved by direct methods using SHELXS-97. All structures were refined with SHELXL-97 with refinement of F^2 against all reflections by full-matrix least squares. In all models, non-hydrogen atoms were refined anisotropically, and hydrogen atoms were included at their geometrically-calculated positions and refined using a riding model. The 3D molecular structure figures were visualized with ORTEP 3.2, rendered with POV-Ray 3.6, and annotated with Adobe Photoshop CS6.

Synthesis of (PNP-Cy)Sc(NH^{t}Bu)$_2$. A sample of (PNP-Cy)Sc(CH_2SiMe_3)$_2$ (50.0 mg, 0.07 mmol) in 5 mL of pentane was treated with ^{t}BuNH$_2$ (10.3 mg, 0.14 mmol). The volatile materials were removed to afford the desired, analytically-pure product (47 mg, 0.07 mmol).). ^{1}H NMR (500 MHz, C_6D_6) δ 6.26 (s, 2H), 3.96 (s, 2H), 3.02 (t, J = 2.3 Hz, 4H), 1.96 (d, J = 13.3

Hz, 4H), 1.86 – 1.62 (m, 14H), 1.62 – 1.54 (m, 6H), 1.47 (s, 18H), 1.42 – 1.33 (m, 8H), 1.14 (d, J = 7.8 Hz, 12H). ^{13}C NMR (126 MHz, C_6D_6) δ 134.80 (d, $^2J_{CP}$ = 5.4 Hz), 106.04, 54.17, 36.51, 35.57, 33.58 (t, J_{CP} = 2.6 Hz), 29.97 (t, J_{CP} = 2.3 Hz), 29.10, 27.59 (q, J_{CP} = 4.9, 4.2 Hz), 26.57 , 22.51. ^{31}P{^{1}H} NMR (202 MHz, C_6D_6) δ 2.43. Anal. Calcd. for $C_{38}H_{72}ScN_3P_2$: C, 67.53; H, 10.44; N 6.22, Found: C, 67.72; H, 10.17; N, 6.17.

Stoichiometric amine-silane dehydrocoupling. A sample of (PNP-Cy)Sc(NH^{t}Bu)$_2$ (10.0 mg, 0.015 mmol) in 1 mL of benzene-d_6 was treated with *p*-tolylsilane (4.0 mg, 0.03 mmol). ^{1}H NMR spectroscopy indicated formation of 2 equiv of *p*-tolyl-(*tert*-butylamino)silane.

Synthesis of Ho(CH$_2$SiMe$_3$)$_3$(THF)$_2$. Trimethylsilylmethyllithium (107.9 mg, 1.14 mmol) was dissolved in pentane (5 mL) and added dropwise to a stirred suspension of $HoCl_3(THF)_{3.5}$ (200 mg, 0.38 mmol) in pentane (5 mL). The pink reaction mixture became cloudy and produced a fine white precipitate. After stirring for 4 h, the reaction mixture was filtered through a fritted funnel and the filtrate was concentrated to 4 mL. The concentrated filtrate was cooled at -35 °C for 2 d to afford the product as large, pink needles (150 mg, 69 % yield). ^{1}H NMR (500 MHz, C_6D_6) δ 97.2 (br s, FWHM 720 Hz, ~18H), 59.0 (br hex, J = 132.6 Hz, ~0.5H), 56.3 (br hex, J = 132.6 Hz, ~0.5H), 54.0 (br hept, J = 132.6 Hz, ~3H), -77.0 (br s, FWHM 2104, ~1H). Anal. Calcd. for $C_{20}H_{49}HoO_2Si_3$: C, 42.09; H, 8.65, Found: C, 41.77; H, 8.43.

Synthesis of Lu(CH$_2$CMe$_3$)$_3$(THF)$_2$. Neopentyllithium (141.2 mg, 1.81 mmol) was dissolved in pentane (5 mL) and added dropwise to a stirred suspension of $LuCl_3(THF)_3$ (300 mg, 0.6 mmol) in pentane (5 mL). The reaction mixture became cloudy and produced a fine white precipitate. After stirring for 4 h, the reaction mixture was filtered through a fritted funnel and the filtrate was concentrated to 4 mL. The concentrated filtrate was cooled at -35 °C for 2 d to afford the product as large, colorless blocks (240 mg, 75 % yield). ^{1}H NMR (600 MHz, C_6D_6) δ 4.08 (t, 8H, J = 4.5 Hz, O(CH_2CH$_2$)$_2$), 1.38 (m, 8H, O(CH$_2$CH_2)$_2$), 1.32 (s, 27H, J_{CH} = 122.2 Hz, -CH$_2$C(CH_3)$_3$), -0.03 (s, 6H, $^1J_{CH}$ = 99.3 Hz, -CH_2C(CH$_3$)$_3$). ^{13}C NMR (151 MHz, C_6D_6) δ 76.62 (-*C*H$_2$C(CH$_3$)$_3$), 71.40 (O(*C*H$_2$CH$_2$)$_2$), 37.24 (-CH$_2$C(*C*H$_3$)$_3$), 35.84 (-CH$_2$*C*(CH$_3$)$_3$), 25.09 (O(CH$_2$*C*H$_2$)$_2$). The assignments and coupling constants were determined by ^{1}H-^{13}C HSQC and ^{1}H-^{13}C HMBC experiments (see Appendix). Anal. Calcd. for $C_{23}H_{49}LuO_2$: C, 51.87; H, 9.27, Found: C, 51.77; H, 9.22.

Synthesis of (PNP-Cy)Ho(CH$_2$SiMe$_3$)$_2$. A solution of (PNP-Cy)H (68.3 mg, 0.14 mmol) in pentane (5 mL) was added to a solution of Ho(CH$_2$SiMe$_3$)$_3$(THF)$_2$ (80.0 mg, 0.14 mmol) in pentane (5 mL) and the reaction mixture was stirred for 1 h. The volatile materials were removed to afford the desired pink product in high purity (100.6 mg, 87% yield). ^{1}H NMR (600 MHz, C_6D_6) δ139.89 (s, ~1H), 62.86 (s, ~12H), 1.21 (s, ~3H), 1.14 (s, ~1.5H), 0.82 (s, ~4H), -35.57 (s, ~3H), -45.02 (s, ~3H), -64.85 (s, ~3H), -70.14 (s, ~3H), -128.31 (s, ~2H), -152.70 (s, ~2H), -158.58 (s, ~2H), -198.96 (s, ~1H), -243.92 (s, ~2H). Anal. Calcd. for $C_{38}H_{72}HoNP_2Si_2$: C, 55.25; H, 8.79; N, 1.70, Found: C, 55.34; H, 8.97; N, 1.95.

Synthesis of (PNP-Cy)Lu(CH$_2$CMe$_3$)$_2$. A solution of (PNP-Cy)H (96.1 mg, 0.20 mmol) in pentane (5 mL) was added to a solution of Lu(CH$_2$CMe$_3$)$_3$(THF)$_2$ (105 mg, 0.20 mmol) in pentane (5 mL) and the reaction mixture was stirred for 1 h. The volatile materials were removed

to afford the desired colorless product in high purity (133.5 mg, 83% yield). ^{1}H NMR (600 MHz, C_6D_6) δ 6.24 (s, 2H, pyr-C*H*, $^{1}J_{CH}$ = 161.2 Hz), 3.04 (s, 4H, -C*H*$_2$PCy$_2$, $^{1}J_{CH}$ = 130.1 Hz), 1.87 (d, *J* = 13.2 Hz, 4H, -Cy), 1.82 – 1.70 (m, 8H, -Cy), 1.69 – 1.59 (m, 8H, -Cy), 1.57 – 1.50 (m, 4H, -Cy), 1.47 (s, 18H, -CH$_2$CC(C*H*$_3$)$_3$, $^{1}J_{CH}$ = 122.7 Hz), 1.34 (t, *J* = 12.7 Hz, 8H, -Cy), 1.15 – 1.02 (m, 12H, -Cy), 0.60 (s, 4H, -C*H*$_2$CMe$_3$, $^{1}J_{CH}$ = 98.6 Hz). ^{13}C NMR (151 MHz, C_6D_6) δ 134.62 (pyr-*C*), 106.66 (pyr-*C*H), 89.92 (-*C*H$_2$CMe$_3$), 36.92, 36.41, 33.43, 29.55, 28.60, 27.08 (q, *J* = 5.3, 4.6 Hz), 25.91, 21.76 (d, $^{1}J_{CP}$ = 4.3 Hz, -*C*H$_2$PCy$_2$). ^{31}P{^{1}H} NMR (202 MHz, C_6D_6) δ 10.91. The assignments and coupling constants were determined by ^{1}H-^{13}C HSQC and ^{1}H-^{13}C HMBC experiments (see Appendix). Anal. Calcd. for $C_{40}H_{72}LuNP_2$: C, 59.76; H, 9.03; N, 1.74, Found: C, 59.92; H, 8.98; N, 2.00.

Typical procedure for catalytic dehydrocoupling. A sample of (PNP-Cy)Y(CH$_2$SiMe$_3$)$_2$ (7.5 mg, 0.01 mmol) was dissolved in 1 mL benzene-d_6, along with hexamethylbenzene (2.1 mg, 0.013 mmol) as an internal standard in a 5mm NMR tube with a Teflon screw cap. To this was added, subsequently, ^{t}BuNH$_2$ (14.1 mg, 0.19 mmol) and PhSiH$_3$ (21.6 mg, 0.20 mmol). The tube was sealed and vigorous bubbling was immediately apparent. The sample was monitored by ^{1}H NMR spectroscopy.

REFERENCES

(1) Gauvin, F.; Harrod, J. F.; Woo, H. G. In *Advances in Organometallic Chemistry*; West, F. G. A. S. and R., Ed.; Academic Press, 1998; Vol. 42, pp 363–405.
(2) Stephens, F. H.; Pons, V.; Baker, R. T. *Dalton Trans.* **2007**, No. 25, 2613.
(3) Hamilton, C. W.; Baker, R. T.; Staubitz, A.; Manners, I. *Chem. Soc. Rev.* **2008**, *38* (1), 279.
(4) Staubitz, A.; Robertson, A. P. M.; Manners, I. *Chem. Rev.* **2010**, *110* (7), 4079.
(5) Rossin, A.; Peruzzini, M. *Chem. Rev.* **2016**.
(6) Tilley, T. D. *Acc. Chem. Res.* **1993**, *26* (1), 22.
(7) Corey, J. Y. Chemistry, B.-A. in O., Ed.; Advances in Organometallic Chemistry; Academic Press, 2004; Vol. 51, pp 1–52.
(8) Greenberg, S.; Stephan, D. W. *Chem. Soc. Rev.* **2008**, *37* (8), 1482.
(9) Dunne, J. F.; Neal, S. R.; Engelkemier, J.; Ellern, A.; Sadow, A. D. *J. Am. Chem. Soc.* **2011**, *133* (42), 16782.
(10) Xie, W.; Hu, H.; Cui, C. *Angew. Chem. Int. Ed.* **2012**, *51* (44), 11141.
(11) Hill, M. S.; Liptrot, D. J.; MacDougall, D. J.; Mahon, M. F.; Robinson, T. P. *Chem. Sci.* **2013**, *4* (11), 4212.
(12) Cosham, S. D.; Johnson, A. L.; Kociok-Köhn, G.; Molloy, K. C. *J. Organomet. Chem.* **2014**, *772–773*, 27.
(13) Bellini, C.; Carpentier, J.-F.; Tobisch, S.; Sarazin, Y. *Angew. Chem. Int. Ed.* **2015**, *54* (26), 7679.
(14) Nako, A. E.; Chen, W.; White, A. J. P.; Crimmin, M. R. *Organometallics* **2015**, *34* (17), 4369.
(15) Bellini, C.; Orione, C.; Carpentier, J.-F.; Sarazin, Y. *Angew. Chem. Int. Ed.* **2016**, *55* (11), 3744.
(16) Pindwal, A.; Ellern, A.; Sadow, A. D. *Organometallics* **2016**, *35* (11), 1674.

(17) Grellier, M.; Ayed, T.; Barthelat, J.-C.; Albinati, A.; Mason, S.; Vendier, L.; Coppel, Y.; Sabo-Etienne, S. *J. Am. Chem. Soc.* **2009**, *131* (22), 7633.
(18) Wuts, P. G. M.; Greene, T. W. *Greene's Protective Groups in Organic Synthesis*; John Wiley & Sons, Inc.: Hoboken, NJ, USA, 2006.
(19) Fieser, L. F.; Fieser, M.; Smith, J. G.; Ho, T.-L. *Reagents for organic synthesis*; Wiley: New York, 1967.
(20) Lipschutz, M. I.; Yang, X.; Chatterjee, R.; Tilley, T. D. *J. Am. Chem. Soc.* **2013**, *135* (41), 15298.
(21) Lipschutz, M. I.; Tilley, T. D. *Organometallics* **2014**, *33* (19), 5566.
(22) Cai, I. C.; Lipschutz, M. I.; Tilley, T. D. *Chem. Commun.* **2014**, *50* (86), 13062.
(23) Lipschutz, M. I.; Chantarojsiri, T.; Dong, Y.; Tilley, T. D. *J. Am. Chem. Soc.* **2015**, *137* (19), 6366.
(24) Roth, C. A. *Prod. RD* **1972**, *11* (2), 134.
(25) Tanabe, Y.; Misaki, T.; Kurihara, M.; Iida, A.; Nishii, Y. *Chem. Commun.* **2002**, No. 15, 1628.
(26) Blum, Y. D.; Schwartz, K. B.; Laine, R. M. *J. Mater. Sci. 24* (5), 1707.
(27) Sommer, L. H.; Citron, J. D. *J. Org. Chem.* **1967**, *32* (8), 2470.
(28) Matarasso-Tchiroukhine, E. *J. Chem. Soc. Chem. Commun.* **1990**, No. 9, 681.
(29) Liu, H. Q.; Harrod, J. F. *Can. J. Chem.* **1992**, *70* (1), 107.
(30) Wang, W. D.; Eisenberg, R. *Organometallics* **1991**, *10* (7), 2222.
(31) Biran, C.; Blum, Y. D.; Glaser, R.; Tse, D. S.; Youngdahl, K. A.; Laine, R. M. *J. Mol. Catal.* **1988**, *48* (2), 183.
(32) Königs, C. D. F.; Müller, M. F.; Aiguabella, N.; Klare, H. F. T.; Oestreich, M. *Chem. Commun.* **2013**, *49* (15), 1506.
(33) Liu, H. Q.; Harrod, J. F. *Organometallics* **1992**, *11* (2), 822.
(34) Wang, J. X.; Dash, A. K.; Berthet, J. C.; Ephritikhine, M.; Eisen, M. S. *J. Organomet. Chem.* **2000**, *610* (1–2), 49.
(35) Buch, F.; Harder, S. *Organometallics* **2007**, *26* (21), 5132.
(36) Levine, D. S.; Tilley, T. D.; Andersen, R. A. *Organometallics* **2015**, *34* (19), 4647.
(37) Levine, D. S.; Tilley, T. D.; Andersen, R. A. *Organometallics*, 10.1021/acs.organomet.6b00394.
(38) Chapter 3
(39) Fraga, S.; Saxena, K. M. S.; Karwowski, J. *Handbook of Atomic Data*; Elsevier Science Ltd: Amsterdam ; New York, 1977.
(40) *CRC Handbook of Chemistry and Physics, 96th Edition*, 96 edition.; Haynes, W. M., Ed.; CRC Press, 2015.
(41) Clavaguéra, C.; Dognon, J.-P. *Chem. Phys.* **2005**, *311*, 176.
(42) Schumann, H.; Freckmann, D. M. M.; Dechert, S. *Z. Für Anorg. Allg. Chem.* **2002**, *628* (11), 2422.
(43) Shannon, R. D. *Acta Cryst* **1976**, *A32*, 751.
(44) Khaliullin, R. Z.; Cobar, E. A.; Lochan, R. C.; Bell, A. T.; Head-Gordon, M. *J. Phys. Chem. A* **2007**, *111* (36), 8753.
(45) Horn, P. R.; Head-Gordon, M. *J. Chem. Phys.* **2015**, *143* (11), 114111.
(46) Horn, P. R.; Mao, Y.; Head-Gordon, M. *J. Chem. Phys.* **2016**, *144* (11), 114107.

Chapter 4 Appendix

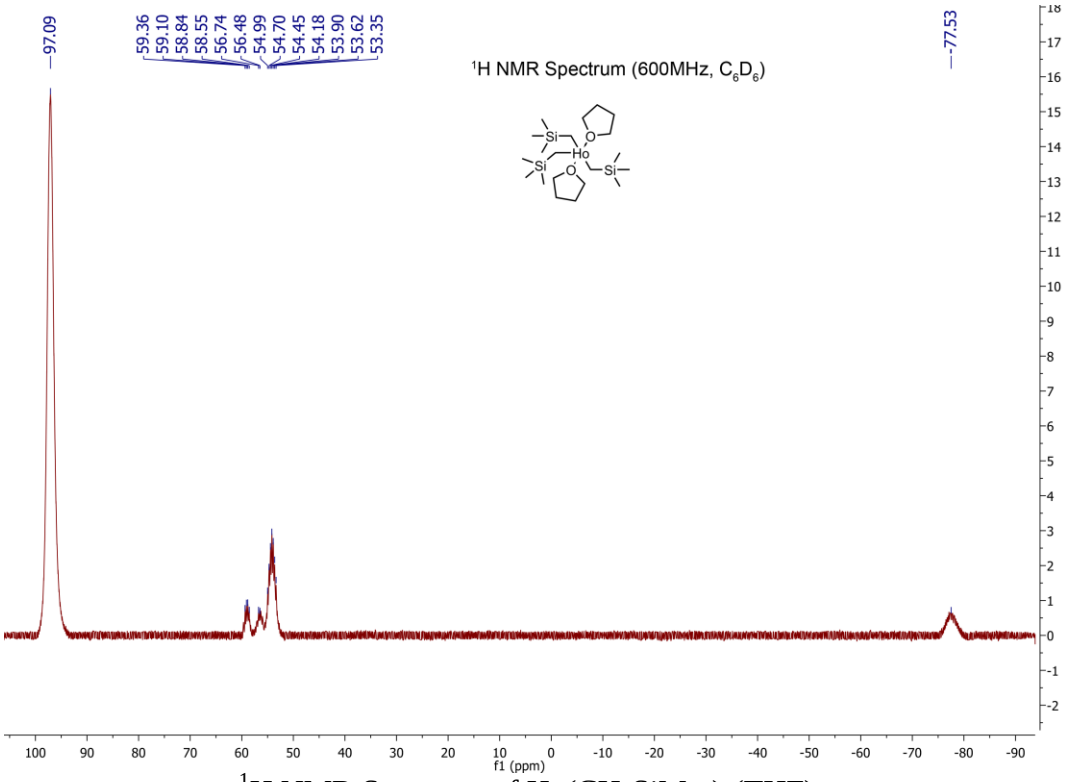

^{1}H NMR Spectrum of $Ho(CH_2SiMe_3)_3(THF)_2$.

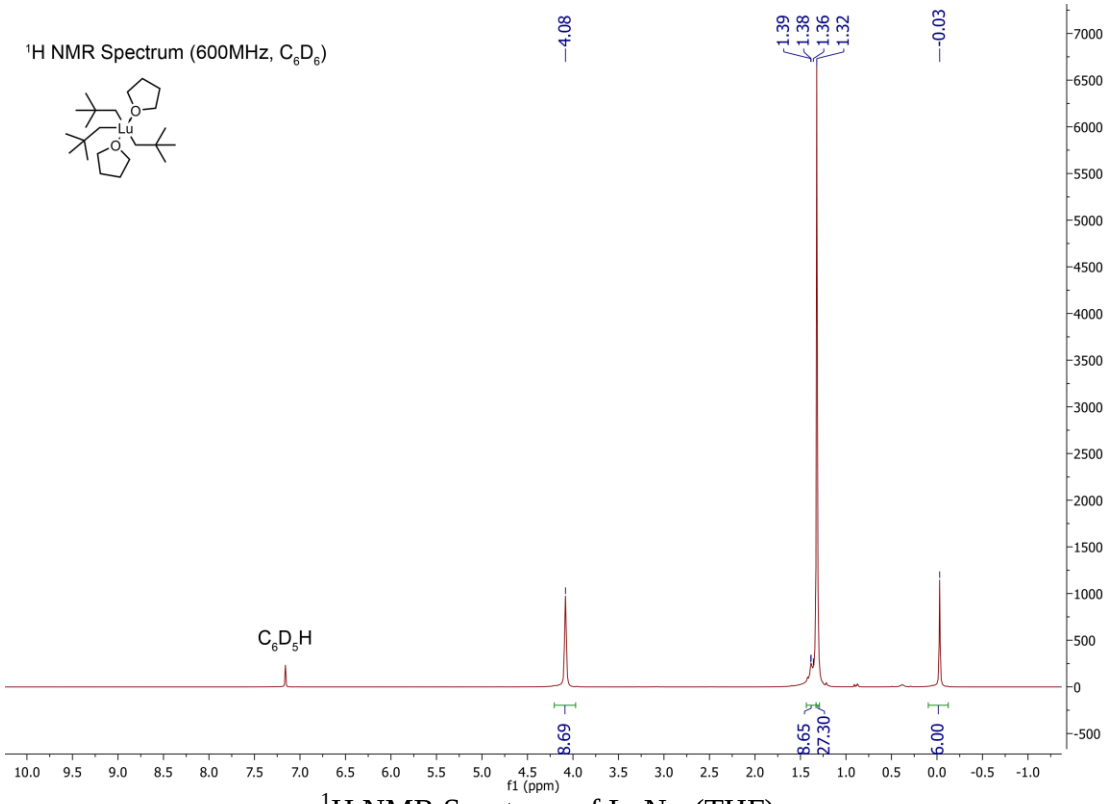

^{1}H NMR Spectrum of $LuNp_3(THF)_2$.

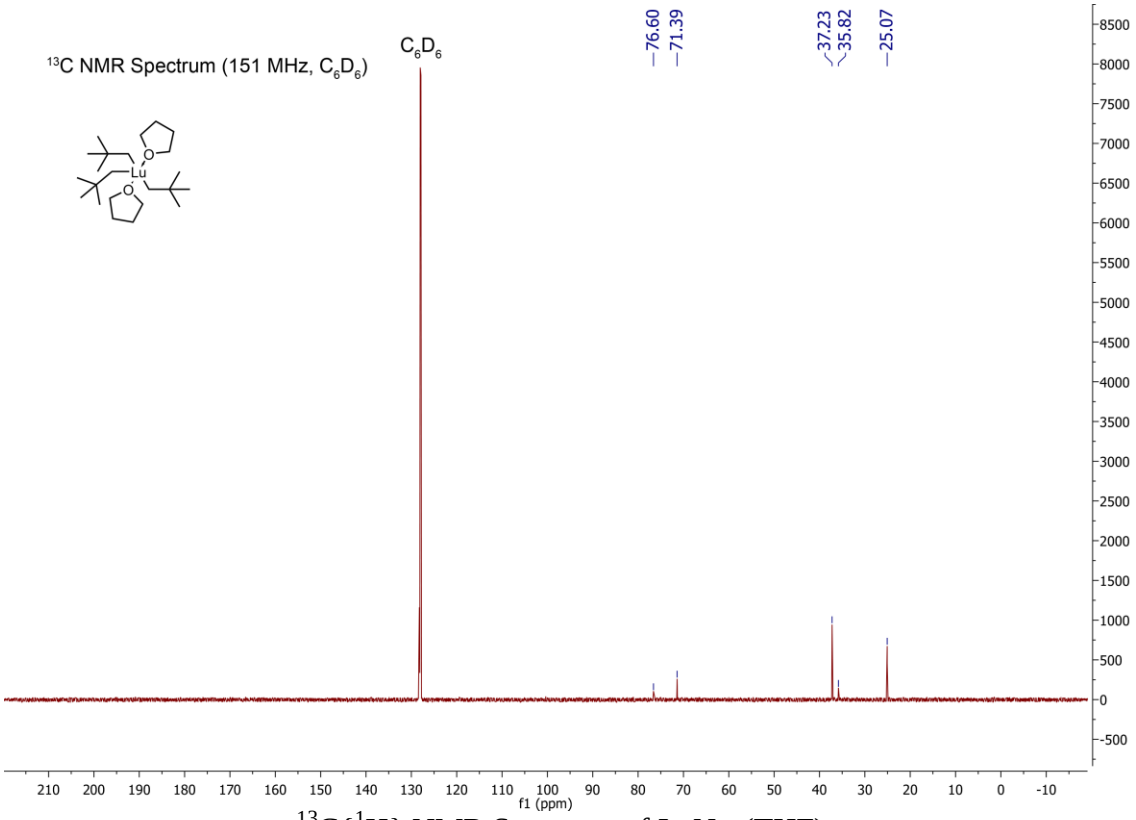

$^{13}C\{^{1}H\}$ NMR Spectrum of $LuNp_3(THF)_2$.

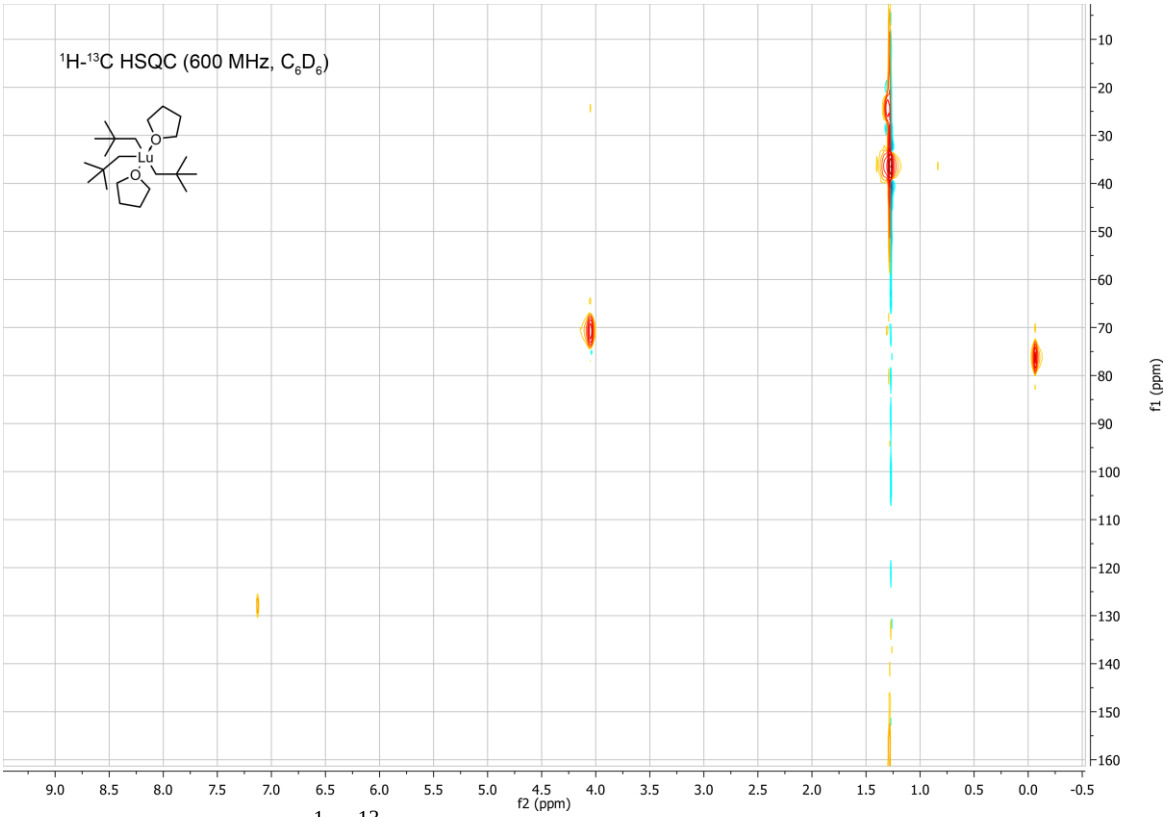

^{1}H-^{13}C HSQC Spectrum of $LuNp_3(THF)_2$.

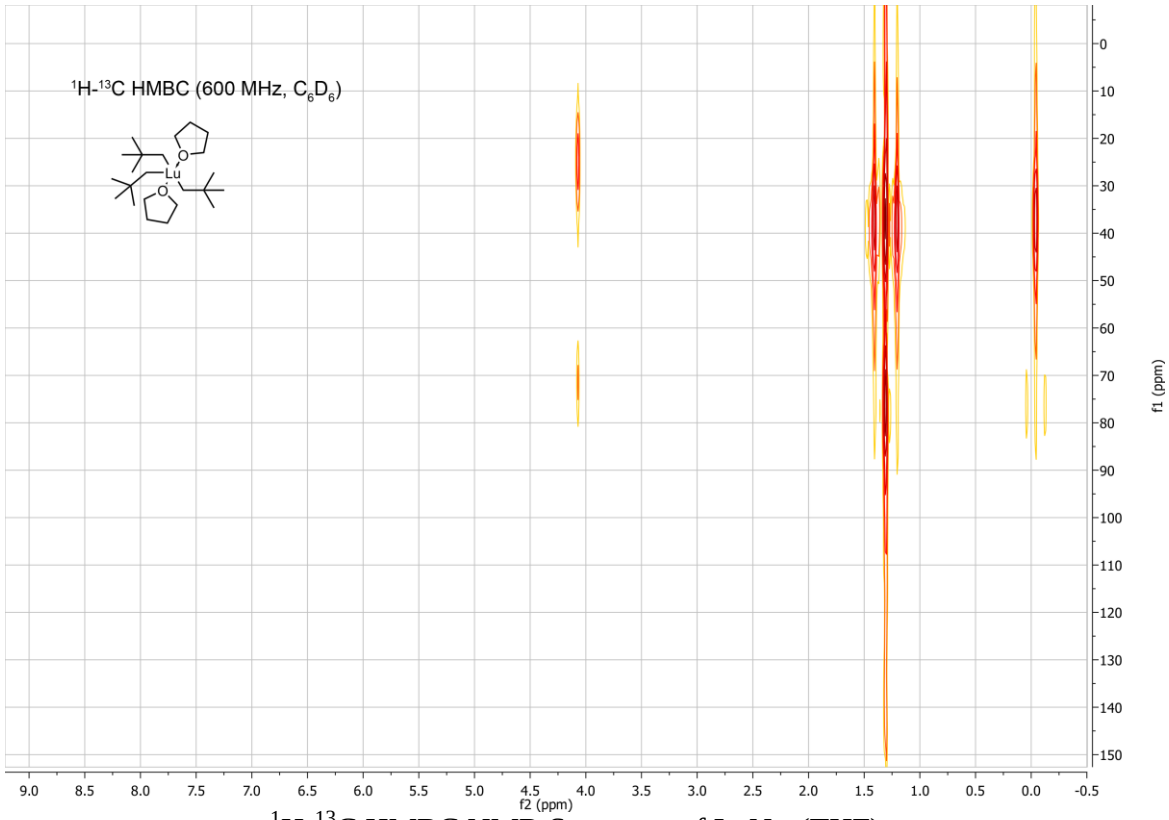

^{1}H-^{13}C HMBC NMR Spectrum of $LuNp_3(THF)_2$.

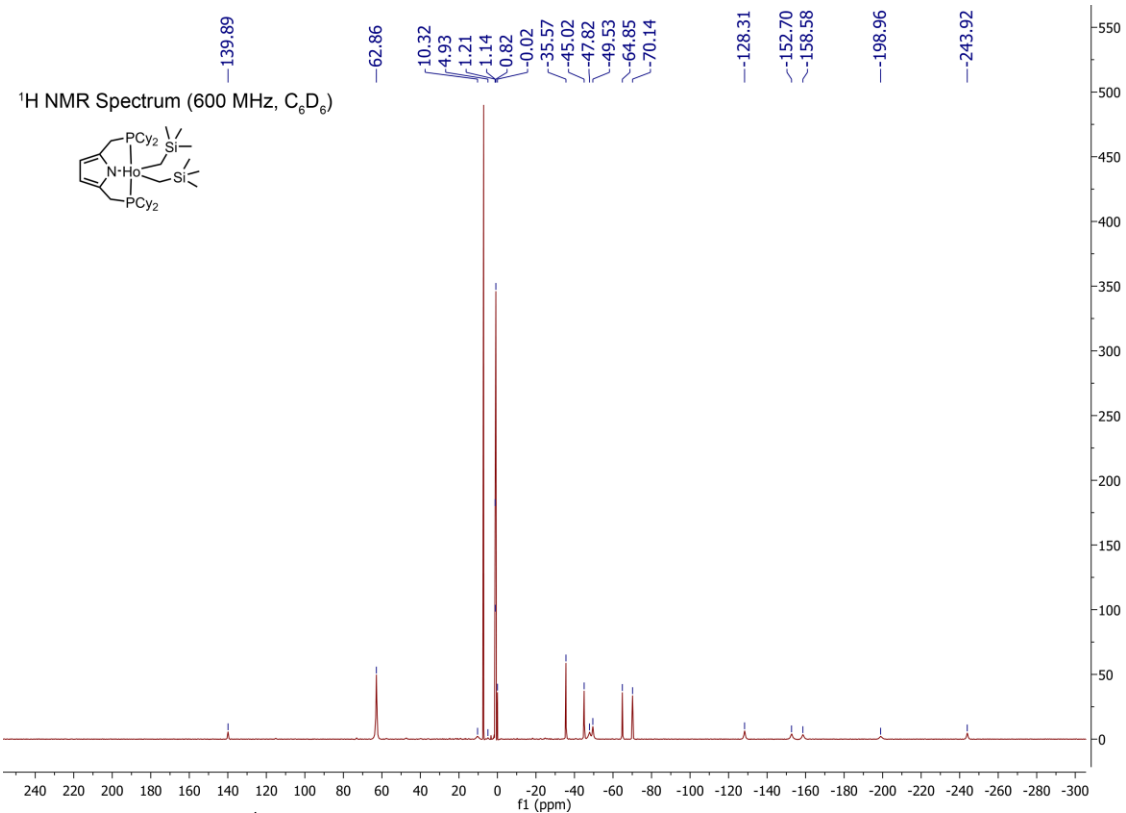

^{1}H NMR Spectrum of (PNP-Cy)Ho$(CH_2SiMe_3)_2$.

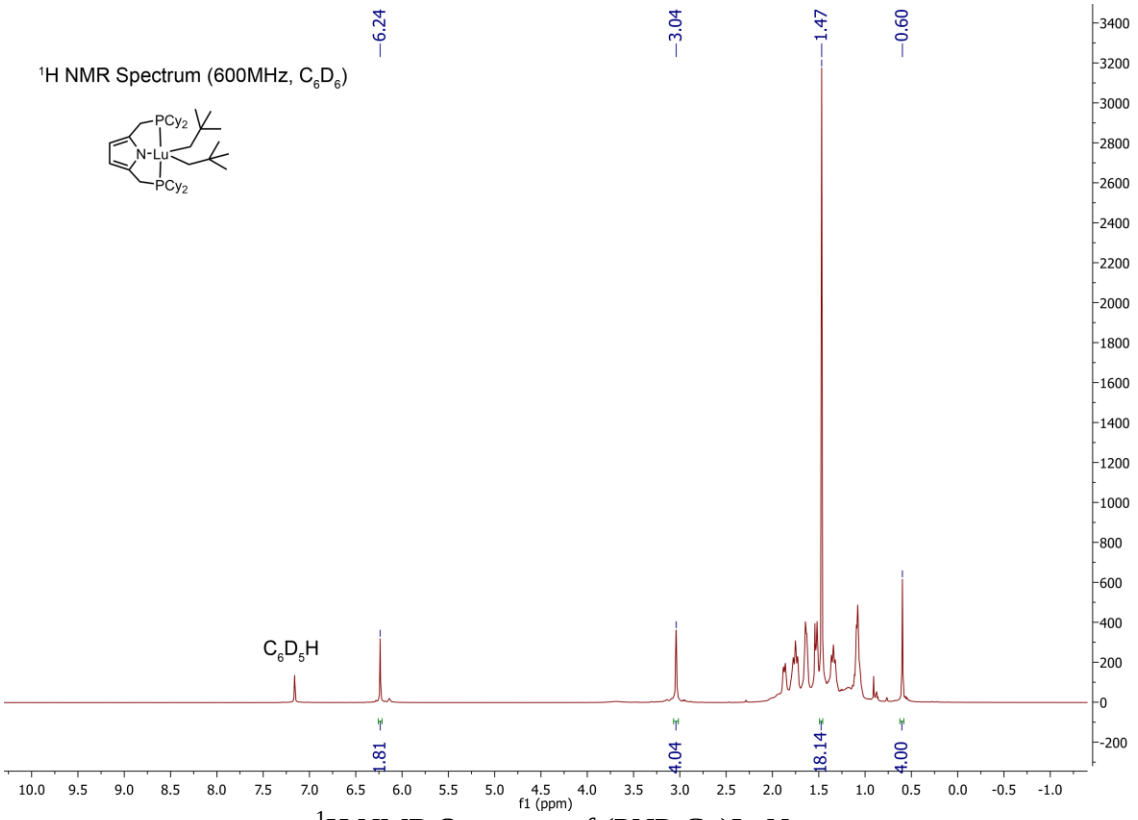

^{1}H NMR Spectrum of (PNP-Cy)LuNp$_2$.

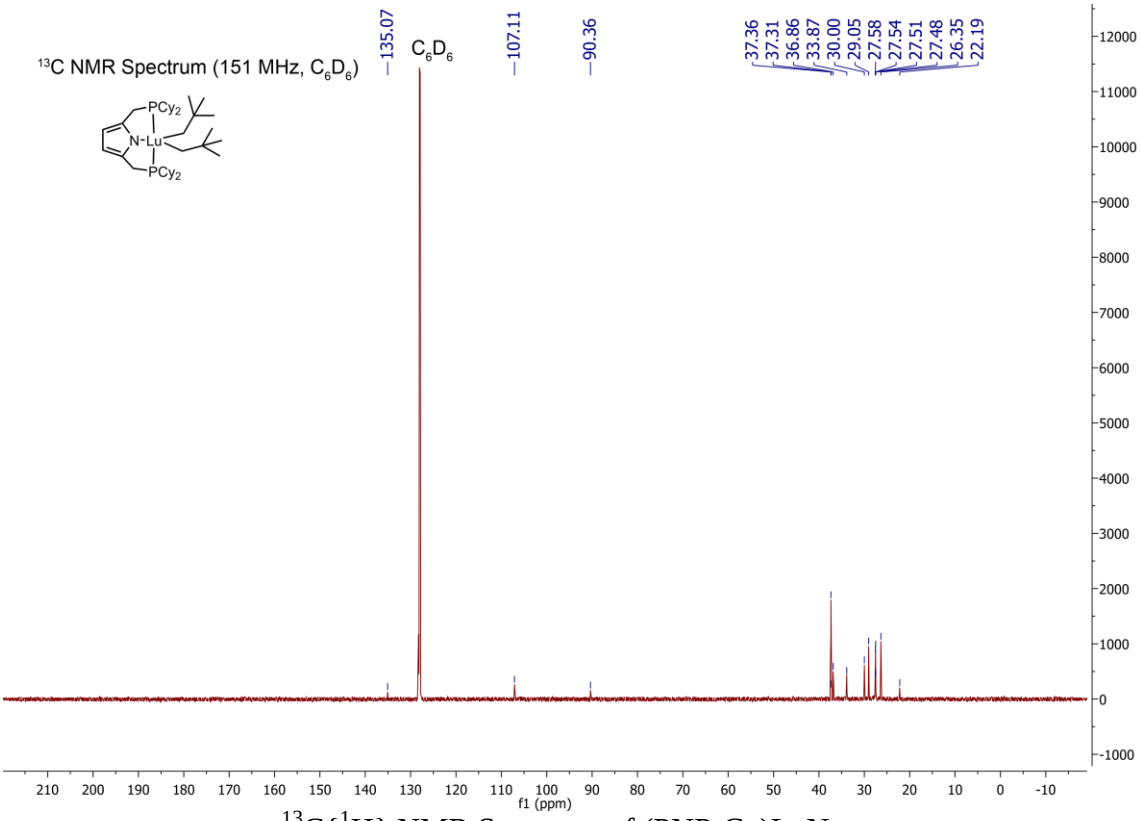

^{13}C{^{1}H} NMR Spectrum of (PNP-Cy)LuNp$_2$.

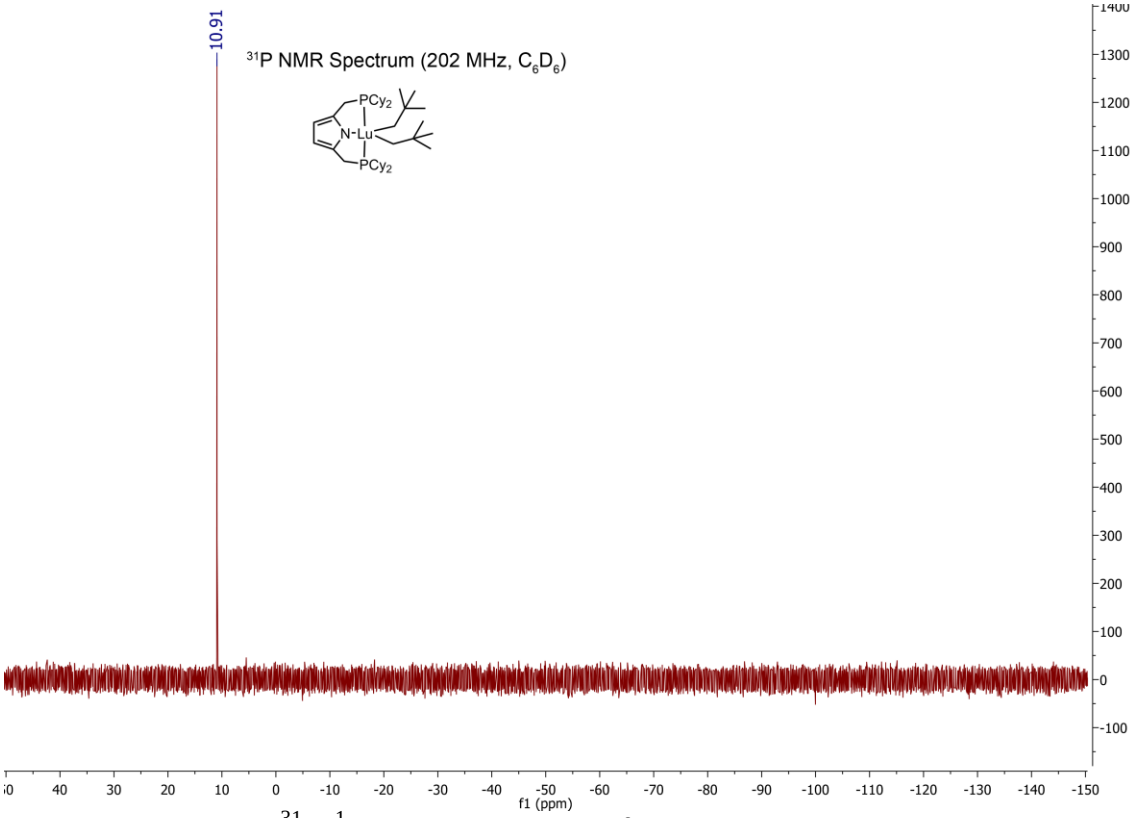

$^{31}P\{^{1}H\}$ NMR Spectrum of (PNP-Cy)LuNp$_2$.

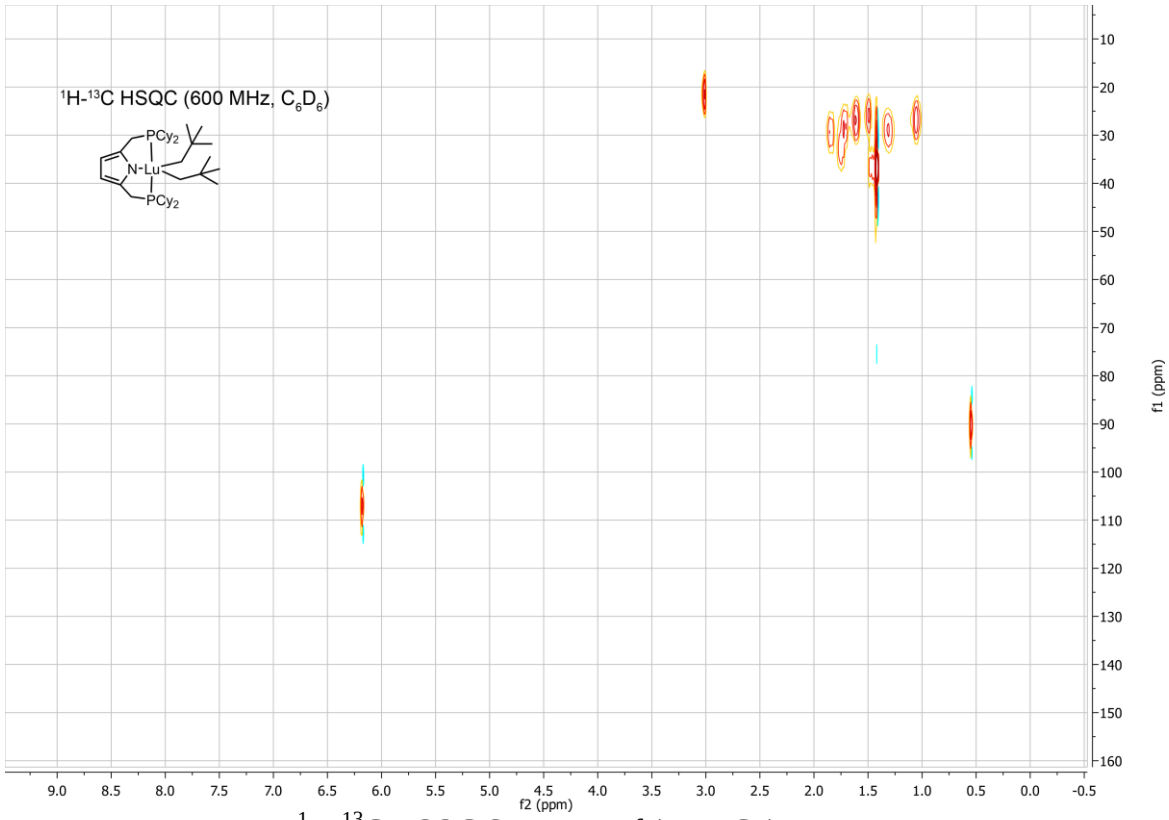

^{1}H-^{13}C HSQC Spectrum of (PNP-Cy)LuNp$_2$.

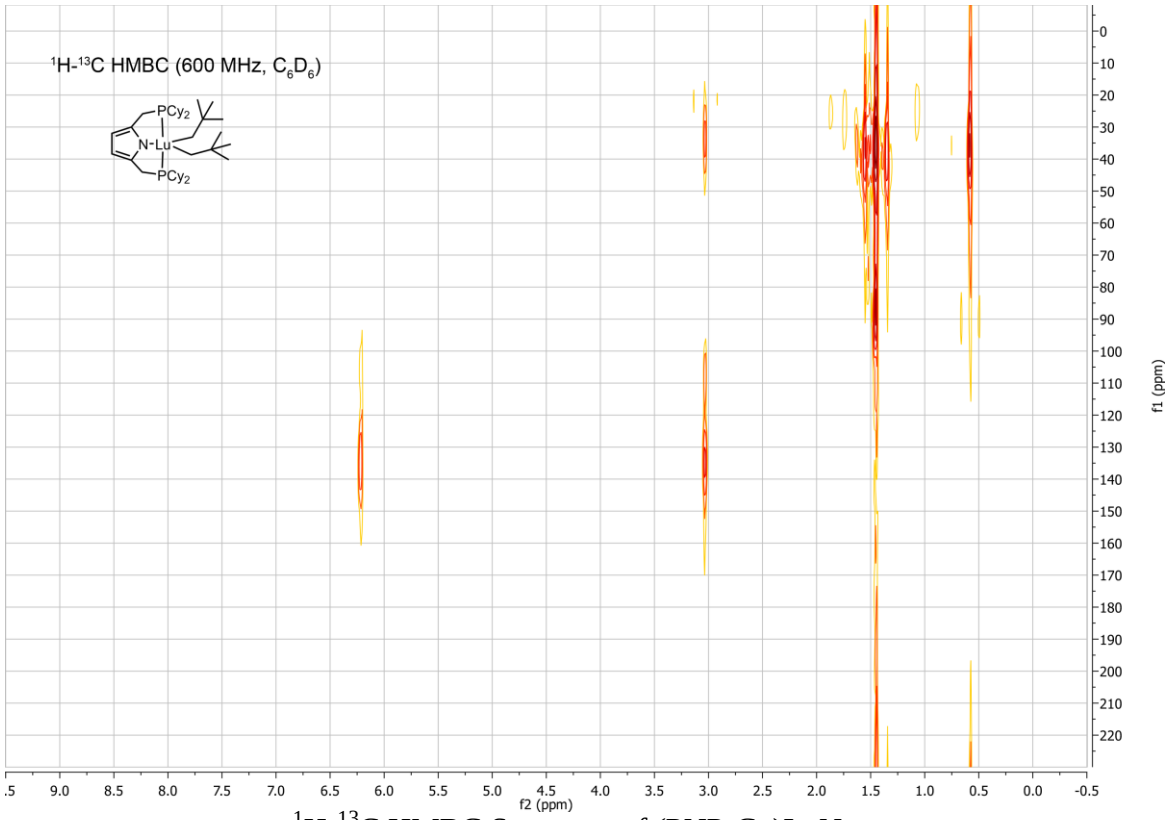

^{1}H-^{13}C HMBC Spectrum of (PNP-Cy)LuNp$_2$.

2. Reaction Order

First Order Dependence on Silane:

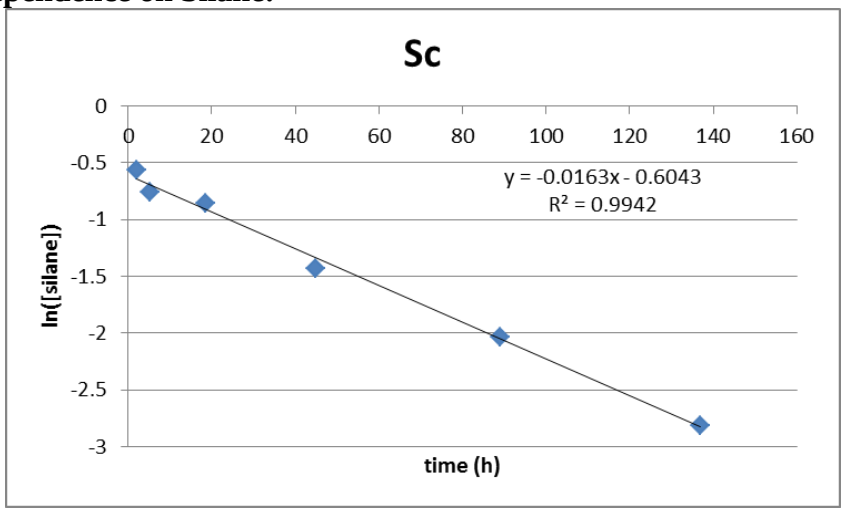

ln([PhSiH$_3$]) vs. time for the Sc-catalyzed dehydrocoupling.

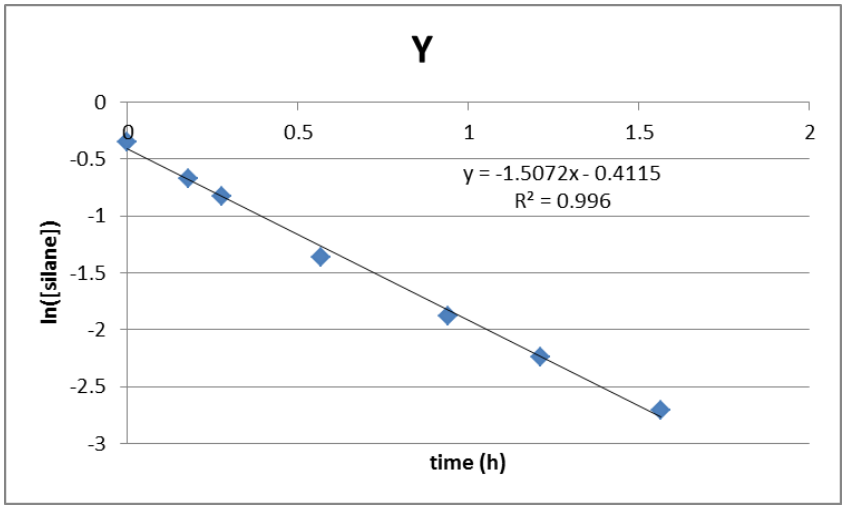

ln([$PhSiH_3$]) vs. time for the Y-catalyzed dehydrocoupling.

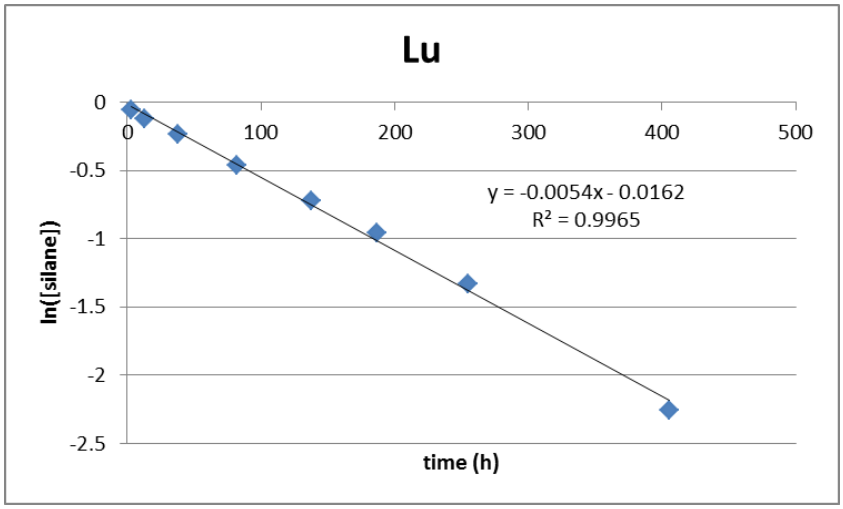

ln([$PhSiH_3$]) vs. time for the Lu-catalyzed dehydrocoupling.

Zeroth Order Dependence on Amine

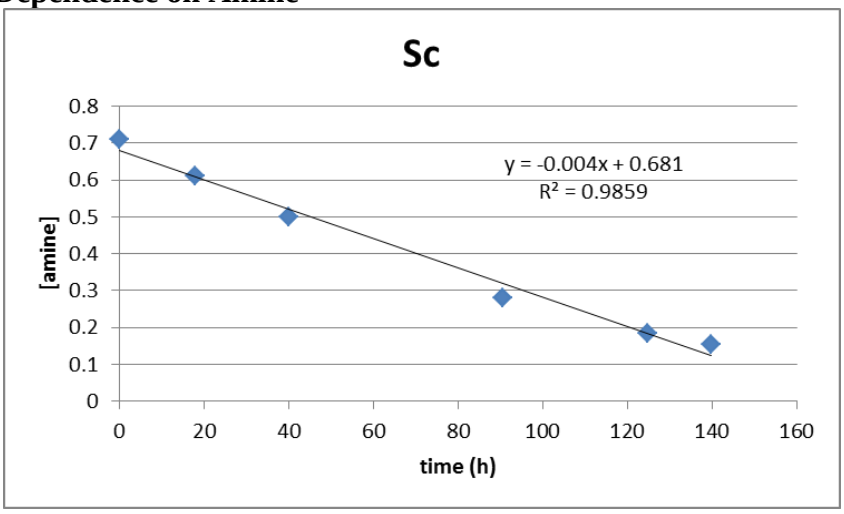

[amine] vs. time for the Sc-catalyzed dehydrocoupling.

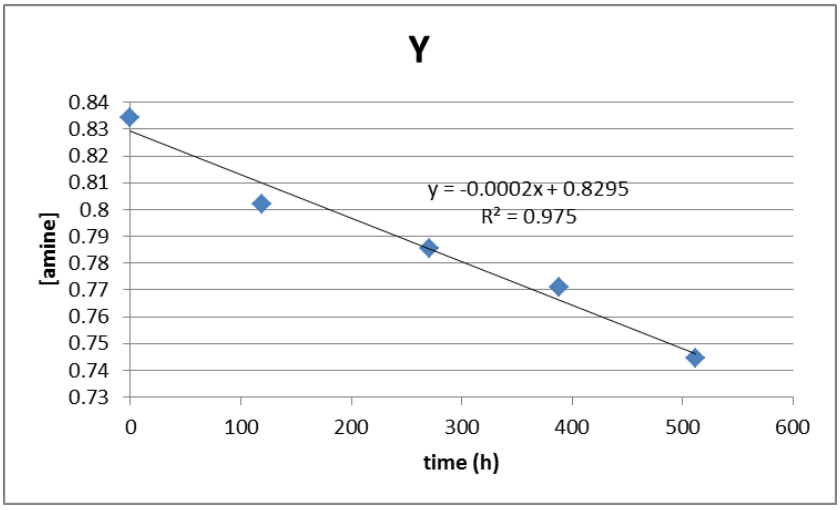

[amine] vs. time for the Y-catalyzed dehydrocoupling.

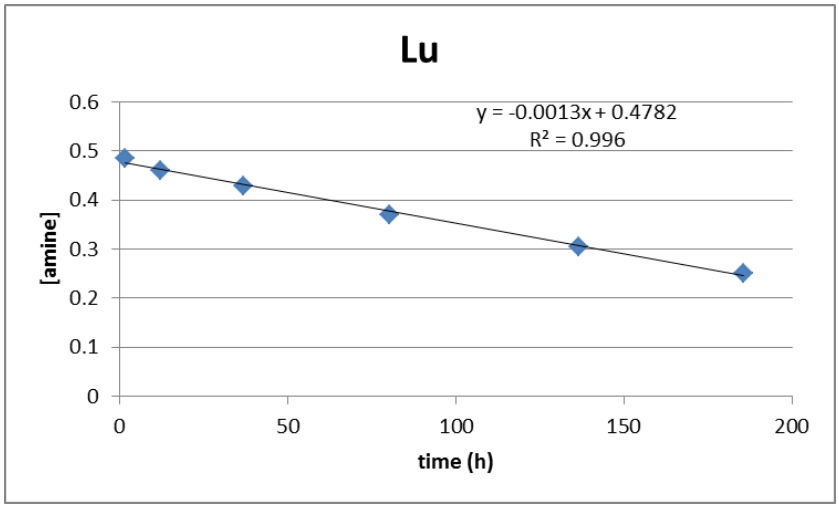

[amine] vs. time for the Lu-catalyzed dehydrocoupling.

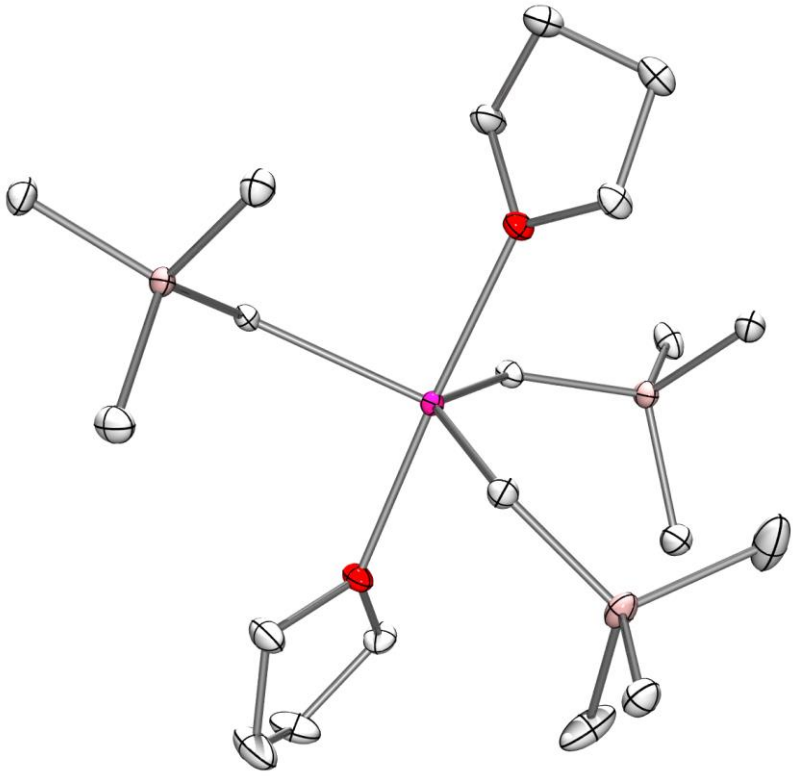

ORTEP diagram of $Ho(CH_2SiMe_3)_3(THF)_2$.

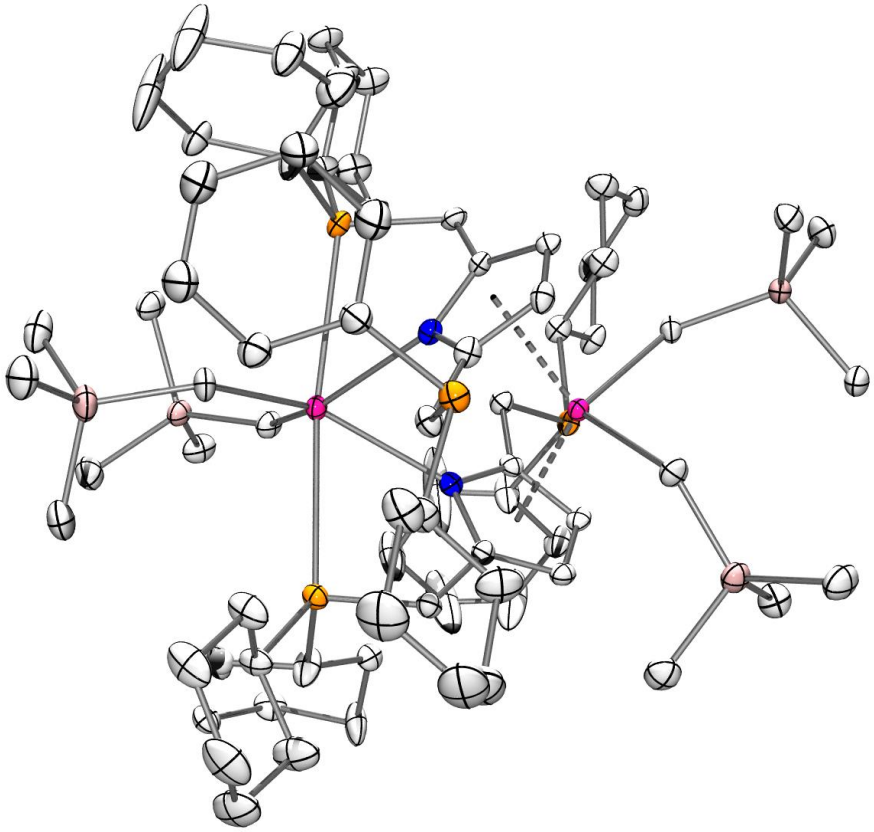

ORTEP diagram of $(PNP\text{-}Cy)Ho(CH_2SiMe_3)_2$.

X-ray Data Tables

Crystal data and structure refinement for Ho(CH2SiMe3)3(THF)2.

Identification code	shelx	
Empirical formula	C20 H49 Ho O2 Si3	
Formula weight	570.79	
Temperature	100(2) K	
Wavelength	0.71073 Å	
Crystal system	Monoclinic	
Space group	$P2_1/n$	
Unit cell dimensions	a = 10.6124(6) Å	α= 90°.
	b = 18.5537(13) Å	β= 95.028(2)°.
	c = 14.6365(9) Å	γ = 90°.
Volume	2870.8(3) $Å^3$	
Z	4	
Density (calculated)	1.321 Mg/m^3	
Absorption coefficient	2.892 mm^{-1}	
F(000)	1176	
Crystal size	0.10 x 0.10 x 0.05 mm^3	
Theta range for data collection	1.776 to 25.405°.	
Index ranges	-12<=h<=12, -20<=k<=22, -17<=l<=17	
Reflections collected	39943	
Independent reflections	5250 [R(int) = 0.0493]	
Completeness to theta = 25.000°	99.7 %	
Absorption correction	Semi-empirical from equivalents	
Max. and min. transmission	0.4707 and 0.4072	
Refinement method	Full-matrix least-squares on F^2	
Data / restraints / parameters	5250 / 0 / 244	
Goodness-of-fit on F^2	1.061	
Final R indices [I>2sigma(I)]	R1 = 0.0250, wR2 = 0.0508	
R indices (all data)	R1 = 0.0323, wR2 = 0.0540	
Extinction coefficient	n/a	
Largest diff. peak and hole	1.443 and -1.147 $e.Å^{-3}$	

Crystal data and structure refinement for (PNP-Cy)Ho(CH2SiMe3)2.

Identification code	shelx	
Empirical formula	C81 H156 Ho2 N2 P4 Si4	
Formula weight	1724.17	
Temperature	100(2) K	
Wavelength	0.71073 Å	
Crystal system	Monoclinic	
Space group	$P2_1/c$	
Unit cell dimensions	a = 19.8494(6) Å	α= 90°.
	b = 22.5853(7) Å	β= 102.6080(10)°.
	c = 19.9167(6) Å	γ = 90°.
Volume	8713.4(5) $Å^3$	

Z	4
Density (calculated)	1.314 Mg/m^3
Absorption coefficient	1.972 mm^{-1}
F(000)	3624
Crystal size	0.200 x 0.080 x 0.020 mm^3
Theta range for data collection	1.051 to 25.422°.
Index ranges	-23<=h<=23, -27<=k<=27, -24<=l<=24
Reflections collected	125948
Independent reflections	16030 [R(int) = 0.0654]
Completeness to theta = 25.000°	99.9 %
Absorption correction	Semi-empirical from equivalents
Max. and min. transmission	0.5777 and 0.4883
Refinement method	Full-matrix least-squares on F^2
Data / restraints / parameters	16030 / 0 / 1019
Goodness-of-fit on F^2	1.079
Final R indices [I>2sigma(I)]	R1 = 0.0459, wR2 = 0.1093
R indices (all data)	R1 = 0.0647, wR2 = 0.1211
Extinction coefficient	n/a
Largest diff. peak and hole	2.864 and -0.712 $e.Å^{-3}$

Chapter 5. Understanding the σ-Bond Metathesis Reaction through Energy Decomposition Analysis

INTRODUCTION

For the past 30 years, there has been a concerted effort on the part of synthetic chemists to activate the C--H bonds of alkanes in a selective, catalytic manner.[1,2] The direct functionalization of C--H bonds could lead to new ways to produce materials, pharmaceuticals, and fuels.[3,4] One mechanism for C--H activation that does not involve oxidation of a metal center is a σ-bond metathesis process (see Figure 1).[5] Indeed, the first organometallic complex to activate methane did so by this mechanism.[6] Sigma-bond metathesis is mainly encountered with d^0 metals and lanthanides, which are unable to undergo oxidative addition due to their lack of d-electrons.[7] Despite the early successes in C--H activation by early transition metals, relatively few systems are known that carry out this chemistry catalytically.[8–12]

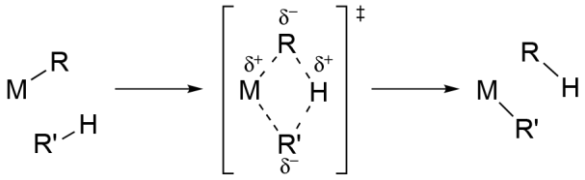

Figure 1. Mechanism for σ-bond metathesis.

Previous results by the groups of Bercaw[13] and Watson[6,14] have demonstrated the ability of permethylscandocene and permethyllutocene alkyl complexes to activate aliphatic C--H bonds, while Tilley and coworkers have employed such complexes catalytically to effect the hydromethylation of alkenes,[9] dehydrocoupling of silanes,[10] and dehydrogenative silation of methane.[11] Unfortunately, these catalysts suffer from long reaction times and low turnover numbers. It is noteworthy that all of these systems employ the same bis(Cp*) (Cp*= $[C_5Me_5]^-$) ligand set or modifications thereof. As such, considerable work has been carried out to produce a range of non-Cp based ligand sets that might perform the same chemistry with greater activity.[15]

We originally hypothesized that the key feature of the Cp* ligand that allows it to support σ-bond metathesis is its high polarizability and strong donating ability. Previous computational studies have focused on the σ-bond metathesis transition state as a proton transfer (or transfer of any group that occupies the β position of the 4-center transition state in Figure 1) between the R^- groups, which are stabilized by the electropositive metal.[16] We proposed that more polarizable ligands lead to a more polarizable metal center, and a more polarizable metal increases the extent of the metal's orbital and hence it's effective positive field. This allows the R^- groups to feel the effect of the electropositive metal more strongly and better stabilizes the transition state, lowering the activation energy for the proton transfer reaction. Hence, we believed polarizable ligands were key to producing active complexes for σ-bond metathesis. Although, as discussed below, the characterization of the transition state being principally stabilized by polarization may be misleading and that greater polarizability of the metal center is rather associated with a greater ability to form covalent bonds in the transition state.

Understanding the relevant factors in σ-bond metathesis has been previously explored in the literature, although no success has been had at accounting for the relative activation barriers, when, for example, changing the identity of the metal center while fixing the ligand set.[17] While factors such as ionic radius and steric effects (in a general, non-quantitative sense) have been considered, these do a poor job accounting for the observed trends. However, even a gross examination of the data, using the calculated free-atom polarizabilities of the metal centers, indicates a decent correlation between increasing polarizability and decreasing (methane self-

exchange; Scheme 2) the activation barrier. Moreover, tunneling through the barrier may play an important role in lowering the effective activation energy of this reaction by as much as 40%.[18,19]

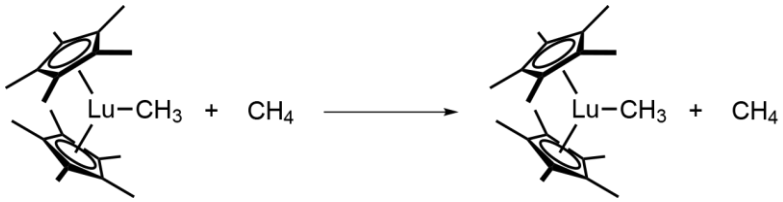

Scheme 2. Methane self-exchange reaction depicted with $(Cp^*)_2LuMe$.

METHODS

In order to obtain greater support for the connection between polarizability and activation energy of σ-bond metathesis, the ligand set was fixed the identity of the metal center varied while the activation barrier for the methane self-exchange reaction of $(Cp^*)_2MMe$ (see Scheme 2) for M = Sc, Y, La, Ce, Pr, Nd, Sm, Ho, Yb, Lu was calculated. Ground and transition state structure optimizations were accomplished using DFT (B3LYP-D3) with the SBKJC basis set and SBKJC effective core potential (3-21G for H) in the gas phase.[20]

In order to investigate the nature of the stabilization of the transition state, the optimized transition state of $(Cp^*)_2MMe$ (M = Sc, Y, La) was subjected to absolutely localized molecular orbital energy decomposition analysis (ALMO EDA), declaring $[(Cp^*)_2M]^+$ as one fragment and $[CH_3\text{-}H\text{-}CH_3]^-$ as the other (see Figure 2).[21] This technique breaks up the stabilization into physically relevant contributions, namely "frozen density" (stabilization from bringing the two fragments together without allowing the density to relax; in this case dominated by Coulombic stabilization of bringing a cation and anion together), polarization (stabilization within each fragment due to intrafragment relaxation), and charge transfer (stabilization between fragments due to interfragment relaxation). Due to the heavy atom nature of the metal center, a small-core effective core potential was used. Basis set superposition error correction calculations are incompatible with ECP's and so BSSE could not be corrected.

EDA of ground state geometries was employed to quantify the polarizability of the metal center in the ground state. Since the methyl group is constant and retains the same polarizability across the different metal complexes, differences in polarization stabilization in the various complexes are attributable to the ability of the metal-containing fragment to be polarized. Hence, we may use the polarization stabilization of the ground state as a quantitative measure of the polarizability of the metal center, probed by a reference charge (the methyl anion).

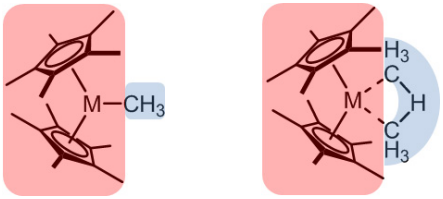

Figure 2. Fragments used for EDA calculations. Positive charges were assigned to red fragents, while negative charges were assigned to blue fragments.

EDA calculations were carried out with the CRENBL basis set/ECP for the metal and 6-311++G* for the other atoms, using B3LYP-D3. A single Roothaan step perturbative correction was used for the charge transfer calculations. Higher order relaxation effects were found to be small (<1 kcal/mol) in almost all cases.

RESULTS AND DISCUSSION

A plot of the calculated electronic barrier heights vs. the static polarizability of the 3+ ions reveals the relation between these two parameters. The data is summarized in Table 2. There does appear to be a correlation between polarizability and barrier height, but this analysis does not provide an explanation as to why this would be the case.

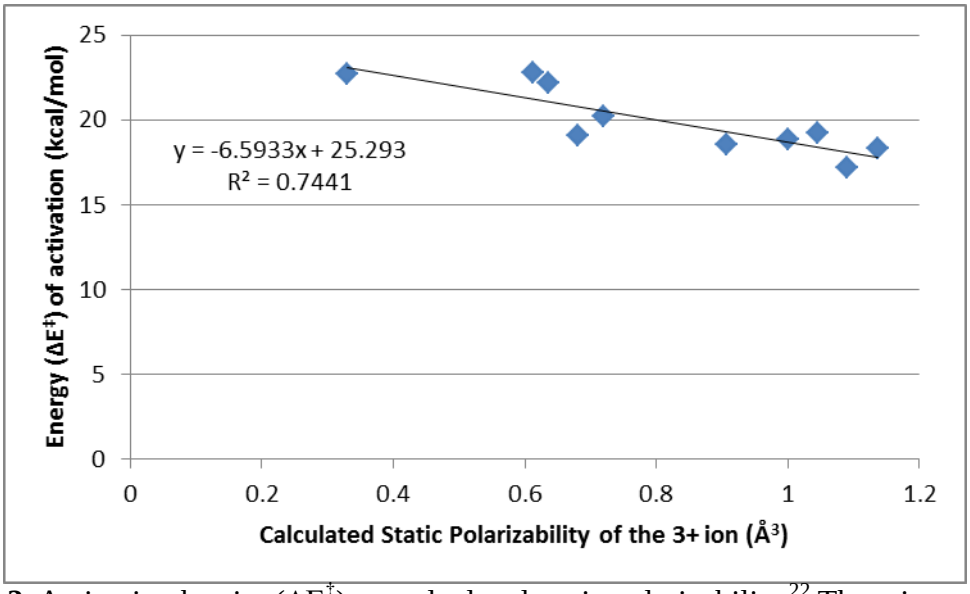

Figure 3. Activation barrier ($\Delta E^{\ddagger}$) vs. calculated static polarizability.[22] There is a negative correlation between increasing polarizability and the barrier height for self-exchange.

M	Static Polarizability (Å^3)	Barrier height (kcal/mol)
Sc	0.33	22.7
Y	0.68	19.1
La	1.136	18.3
Ce	1.09	17.1
Pr	1.045	19.2
Nd	1.001	18.9
Sm	0.906	18.6
Ho	0.72	20.2
Yb	0.636	22.2
Lu	0.612	22.8

Table 1. Polarizability[22,23] and barrier height data.

Energy decomposition analysis revealed several informative effects. The largest stabilizing term in an absolute sense in both the ground and transition states is, unsurprisingly, the Coulombic stabilization of bringing an anion and cation together. Polarization of the methyl-methane fragment, the classic explanation for stabilization of the σ-bond metathesis transition state, while certainly an important stabilizing factor, was similar or slightly weaker than the charge-transfer contribution. Comparison of polarization stabilization of methyl anion in the ground state, to methyl-methane in the transition state revealed that polarization stabilization goes down in the transition state relative to the ground state. On the other hand, charge-transfer stabilization (generally) increases in the transition state, lowering the barrier by an average of 3 kcal/mol. Similar results were obtained with B3PW91-D3 and ωB97X-D.

The increase in C-T stabilization can be rationalized by considering the energy gap between the metal orbitals and the ligand fragment orbitals. The methyl-methane fragment is destabilized relative to its ground state considerably by its geometric distortion (absent largely from the ground state methyl and free methane). This raises the energy of its orbitals and leads to a decrease in the energy gap (see Figure 4, left). Additionally, there is greater orbital overlap due to the fact that the ground-state structure is stabilized only by an a_1 interaction, while the transition state additionally has interactions with the b_2 metal *d*-orbitals (see Figure 4, right). Since the strength of covalent interactions varies inversely with energy gap and proportionally to overlap, we would expect the covalency in the transition state to increase.

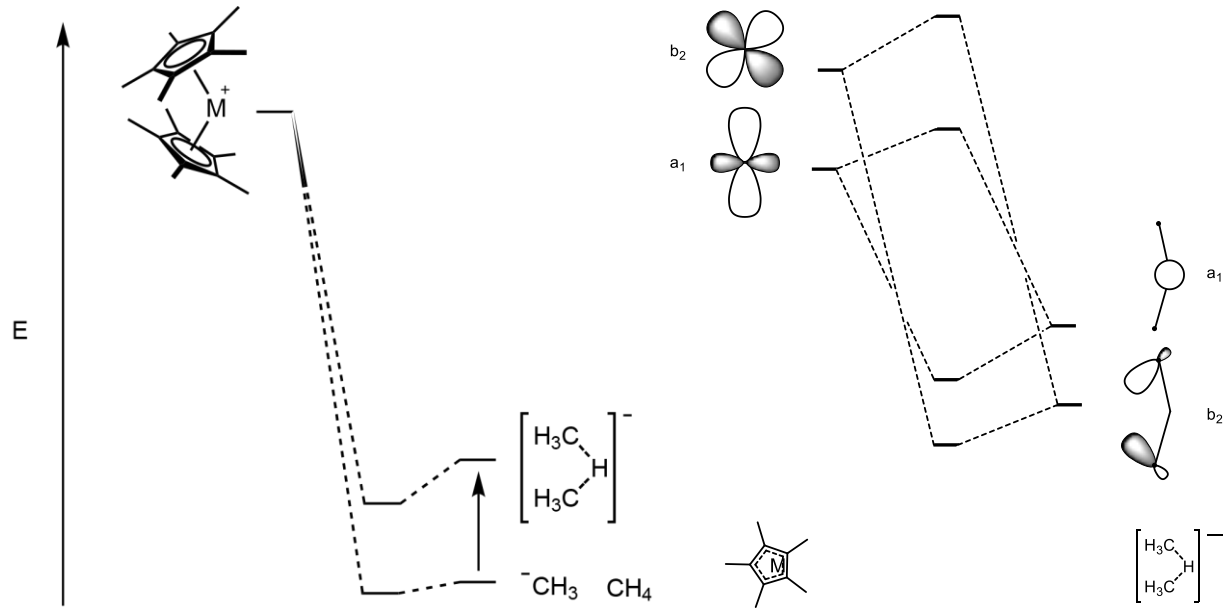

Figure 4. Increased charge-transfer stabilization is expected on going from the ground state to transition state, because the energy gap is decreased (left) and there are greater orbital overlap (right, the b_2 orbital is non-bonding in the ground state).

The effect of covalency in the transition state has been largely ignored in the theoretical and practical literature concerning σ-bond metathesis. Very recently, a report presented evidence that the more facile σ-bond metathesis which occurs with a uranium complex faster than its analogous thorium complex was due to participation of 5f orbitals of uranium, leading to more covalency in the transition state for uranium than for thorium.[24] This result also supports our

analysis. Since increased covalency in the complexes preferentially stabilizes the transition state, the barriers are lowered for more polarizable complexes.

A quantitative measure for polarizability in the complexes of interest might produce a better fit for the data in Figure 3 and Table 1. Using the absolute ground state polarization stabilizations from EDA calculations and comparing them to our calculated barriers, a strong linear relation is observed (see Figure 5). Unfortunately, only three points were available due to problems with EDA on open shell systems. However, these limited data seem to indicate that polarizability in the ground state has significant predictive power for the facility of σ-bond metathesis.

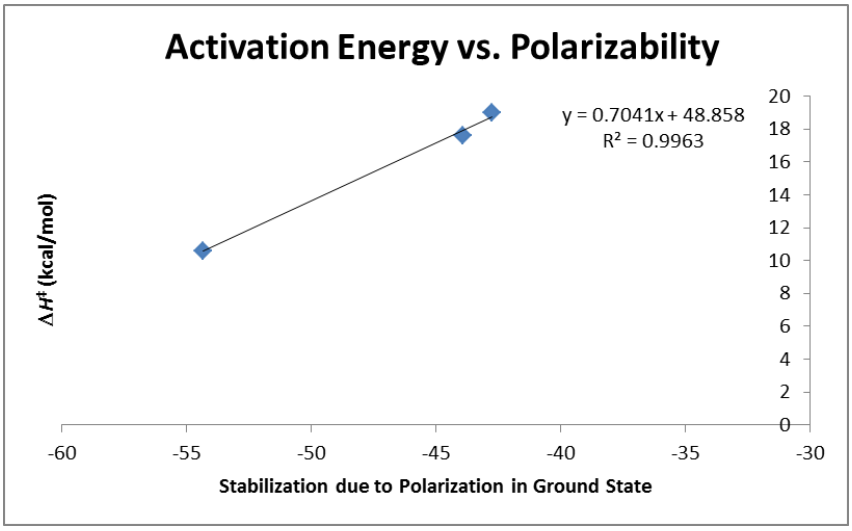

Figure 5. Activation energy vs. the polarization stabilization of the ground state Cp^*_2MMe from the EDA.

Instead of the polarization stabilization from the EDA, one can also compute the polariability of the complexes directly by the definiton of polarizability:

$$P = -\frac{\partial^2 U}{\partial E^2}$$

That is, the polarizability is the (negative of) the second derivative of the electronic energy with respect to an applied field, with the static polarizability being the value at zero applied field.

Figure 6. Applying an E field to the complex along the M-CH_3 axis.

We thus calculated polarizability in this way (see Figure 6) and again obtain a linear relation (see Figure 7).

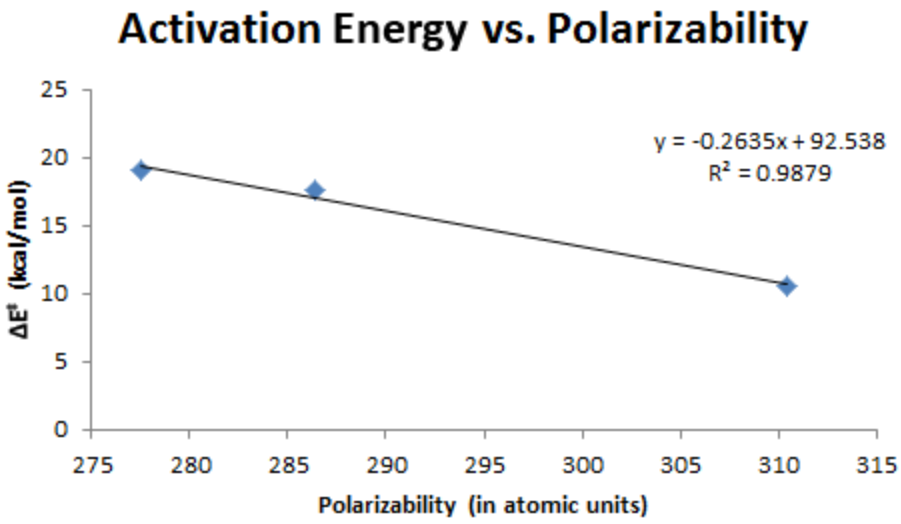

Figure 7. Activation energy vs. static polarizability computed as the second derivative of the electronic energy with respect to applied electric field strength.

During the course of locating transition states, some unexpected behavior was observed. In the case of europium (7th lanthanide, 6 unpaired spin for Eu(III)), the transition state calculation initially optimized to the expected transition state and then fell apart into a Eu(II) σ-methane complex and a methyl radical (verified by Mulliken net atomic spins). The expected transition state before breakup also shows non-trivial unpaired spin density on the α-position carbons (~3 and ~2 a.u.). The redox-activity in this transition state prompted an investigation of unpaired spin density in the various transition states (see Table 2).

Metal	Total spin	Spin densities on α carbons	Spin density on the metal
Sc[a]	0	0; 0	0
Y[a]	0	0; 0	0
La[a]	0	0; 0	0
Ce	1	-0.0118; -0.0104	1.0604
Pr	2	-0.0036; -0.0043	2.0658
Nd	3	-0.0109; -0.0123	3.0968
Sm	5	-0.5265; -0.4713	5.8842
Eu	6	0.2020; 0.3438	5.6646
Ho	4	-0.0038; -0.0064	4.0682
Yb	1	0.3820; 0.3797	0.3555
Lu[a]	0	0; 0	0

[a] Calculated with restricted orbitals

Table 2. Unpaired spin density on α-carbons in the σ-bond metathesis transition states.

It has previously been observed that Yb is notable for its inability to activate even the relatively weak and acidic C--H bonds of tetramethylsilane and this has been non-quantitatively ascribed to the relatively low-lying Yb(II) oxidation state.[17] We hypothesize that Cp^*_2YbMe,

while mostly $Cp^*_2Yb(III)$ with CH_3^- ligand, bears a non-trivial contribution from $Cp^*_2Yb(II)$ and methyl radical. This leads to a transition state with less covalency (rather than share the electron density, the Yb has oxidized the metal-carbon bond by one electron, populating its *f* shell to bring it to an f^{14} state, hence less stabilization, and a higher activation barrier. There has not been a satisfactory theoretical explanation for why accesibility of the Yb(II) state would prevent σ-bond metathesis until now.[17]

CONCLUSIONS

We have shown strong evidence that polarizability of the metal complex plays a determining role in the ability of a given complex to effectively carrying out C–H activation *via* σ-bond metathesis. The electronic barrier can, with some accuracy, be determined by measures of the polarizability of the ground state complex. These measures may be the polarization stabilization of ground state fragment responding to the field of an anionic alkyl ligand (determined by ALMO EDA) or the second derivative of the metal complex's electronic energy with respect to an applied electric field (along the $M–CH_3$ axis). The ALMO EDA also suggested the reason why polarization is important for σ-bond metathesis: while the ground state metal–methyl interaction is largely ionic, the metal–(methyl-methane) is stabilized by covalency. Since more polarizable metals are more able to engage in covalent interactions and this preferentially stabilizes the transition state, the barrier is lowered for polarizable complexes. The importance of charge-transfer in the transition state may suggest why Yb complexes do not readily undergo σ-bond metathesis; the low lying Yb(II) state (in which the metal-carbon bond has been oxidized) mixes with the Yb(III) state and makes the charge-transfer stabilization less (since there is less charge to be transferred from the oxidized bond).

REFERENCES

(1) Arndtsen, B. A.; Bergman, R. G.; Mobley, T. A.; Peterson, T. H. *Acc. Chem. Res.* **1995**, *28* (3), 154.
(2) Bergman, R. G. *Nature* **2007**, *446* (7134), 391.
(3) Labinger, J. A.; Bercaw, J. E. *Nature* **2002**, *417* (6888), 507.
(4) Crabtree, R. H. *J. Chem. Soc. Dalton Trans.* **2001**, No. 17, 2437.
(5) Ziegler, T.; Folga, E.; Berces, A. *J. Am. Chem. Soc.* **1993**, *115* (2), 636.
(6) Watson, P. L. *J. Am. Chem. Soc.* **1983**, *105* (21), 6491.
(7) Balcells, D.; Clot, E.; Eisenstein, O. *Chem. Rev.* **2010**, *110* (2), 749.
(8) Castillo, I.; Tilley, T. D. *Organometallics* **2001**, *20* (26), 5598.
(9) Sadow, A. D.; Tilley, T. D. *J. Am. Chem. Soc.* **2003**, *125* (26), 7971.
(10) Sadow, A. D.; Tilley, T. D. *Organometallics* **2003**, *22* (17), 3577.
(11) Sadow, A. D.; Tilley, T. D. *Angew. Chem. Int. Ed.* **2003**, *42* (7), 803.
(12) Sadow, A. D.; Tilley, T. D. *J. Am. Chem. Soc.* **2005**, *127* (2), 643.
(13) Thompson, M. E.; Baxter, S. M.; Bulls, A. R.; Burger, B. J.; Nolan, M. C.; Santarsiero, B. D.; Schaefer, W. P.; Bercaw, J. E. *J. Am. Chem. Soc.* **1987**, *109* (1), 203.
(14) Watson, P. L. *J. Chem. Soc. Chem. Commun.* **1983**, No. 6, 276.
(15) Piers, W. E.; Emslie, D. J. H. *Coord. Chem. Rev.* **2002**, *233–234*, 131.
(16) Barros, N.; Eisenstein, O.; Maron, L.; Tilley, T. D. *Organometallics* **2006**, *25* (24), 5699.
(17) Barros, N.; Eisenstein, O.; Maron, L. *Dalton Trans.* **2006**, No. 25, 3052.
(18) Sherer, E. C.; Cramer, C. J. *Organometallics* **2003**, *22* (8), 1682.
(19) Woodrum, N. L.; Cramer, C. J. *Organometallics* **2006**, *25* (1), 68.
(20) Cundari, T. R.; Stevens, W. J. *J. Chem. Phys.* **1993**, *98* (7), 5555.
(21) Khaliullin, R. Z.; Cobar, E. A.; Lochan, R. C.; Bell, A. T.; Head-Gordon, M. *J. Phys. Chem. A* **2007**, *111* (36), 8753.
(22) Clavaguéra, C.; Dognon, J.-P. *Chem. Phys.* **2005**, *311*, 176.
(23) *CRC Handbook of Chemistry and Physics, 96th Edition*, 96 edition.; Haynes, W. M., Ed.; CRC Press, 2015.
(24) Gardner, B. M.; Cleaves, P. A.; Kefalidis, C. E.; Fang, J.; Maron, L.; Lewis, W.; Blake, A. J.; Liddle, S. T. *Chem. Sci.* **2014**, *5* (6), 2489.

Chapter 6. A New Energy Decomposition Analysis Designed for Bonded Interactions

INTRODUCTION

In the previous chapter, ALMO EDA was employed to develop a model for determining barrier heights in the σ-bond metathesis reaction. While this was possible by defining the interaction of the alkyl group as an anion interaction with a cationic metal complex, this is a biased representation which presupposes the character of the bond. An improvement to the EDA must be made to treat these single covalent bonds in a spin-pure (i.e. non-symmetry broken), unbiased way.

Practical chemistry relies on the qualitative application of physical and chemical principles (e.g. electrostatics, polarizability, electronegativity, etc.) to understand the interaction of molecules when investigating the synthesis and reactivity of molecular systems. Theoretical chemistry, on the other hand, does away with these principles in favor of a quantitative quantum mechanical treatment with no specific appeal to any of these ideas. The success of the former approach suggests that there is value in thinking about chemistry in the context of these heuristics. At the heart of the matter is the question: What is the nature of the chemical bond?[1–3]

Since the advent of quantum mechanics, there has been over eighty years of work on this problem, which shall be briefly summarized here. At the level of the role of different terms in the Hamiltonian, there were originally two possibilities that could explain the origin of the stability of the covalent bond. Since chemical bonding in elementary systems such as the one-electron bond in H_2^+ is associated with an increase in electron density in the bonding region led to the suggestion[4] that this was electrostatically favored (i.e. lowered the potential energy). However, detailed analysis has supported the competing possibility that delocalization of previously localized electrons in the molecule in fact lowers the kinetic energy. This result has been established for simple systems by Ruedenberg and co-workers,[2,5] Kutzelnigg,[6] and others.[7–9] Ruedenberg et al.,[10] as well as others[11–13] have also reported progress towards extracting similar information from more complex molecules.

Numerous other methods have also been developed to analyze chemical bonds, from a variety of complementary perspectives. One of the most widely used is Weinhold et al.'s Natural Bond Orbital (NBO) analysis,[14] which yields localized orbitals, information on hybridization, chemical bonds, atomic charges, and predominant Lewis structures. Topological analysis of the electron density, as developed in the quantum theory of atoms-in-molecules (QTAIM)[15] is another well-developed method for diagnosing the presence of chemical bonds (via so-called bond critical points), as well as partitioning an energy into intra-atomic and inter-atomic terms. Other topological methods involve increasingly complicated functions of the density and the kinetic energy density, of which the electron localization function (ELF) is a prominent example. A variety of other methods exist for partitioning a bond energy into sums of terms that are physically interpretable.[16,17]

At the same time, much progress has been made in analyzing non-bonded interactions into contributions that include dispersion, permanent and induced electrostatics which are well-defined in the non-overlapping regime, as well as Pauli repulsion and charge transfer. These schemes include perturbative methods such as Symmetry Adapted Perturbation Theory (SAPT)[18–25] method and Natural Energy Decomposition Analysis (NEDA),[26–28] and methods based on variationally optimized, constrained, intermediate wavefunctions, such as Kitaura and Morokuma (KM) EDA,[29] the Ziegler-Rauk approach for the Xα method[30–32] and the equivalent Block-Localized Wavefunction (BLW-EDA)[33,34] of Mo and Gao and Absolutely Localized Molecular Orbital (ALMO-EDA) of Head-Gordon et al.[35–39] Such energy decomposition analysis

(EDA) schemes have had considerable success at describing the interactions of closed-shell fragments as well as open-shell--closed-shell interactions.[40–42]

A number of the general EDA schemes mentioned for non-bonded interactions above have been applied to bonded interactions,[30–32,43,44] these schemes usually group all of the terms assignable to the bond (polarization, charge-transfer, etc.) into a single orbital interactions term, possibly separable into different wavefunction symmetries (e.g. σ, π bonding).[45] We are interested to develop methods specifically for the variational energy decomposition analysis of chemical bonds relative to radical fragments. Motivated by earlier work in our group on the ALMO-EDA for non-bonded interactions, the objective is to define a sequence of constraints which can be ascribed to deletion of specific physical effects, such as charge transfer, polarization, and spin coupling. Our perspective of a sequence of progressively weaker variational constraints contrasts with energy partitioning methods that do not define optimized intermediate states.

This chapter describes the design and implementation of an EDA for single bonds, the simplest case. The homolytic separation of a single bond into two doublet radical fragments cannot be accomplished in a spin-pure way using single determinant theory. The simplest spin-pure wavefunction involves recoupling two electrons in two orbitals, which is variously known as CAS(2,2),[46] one-pair perfect pairing,[47] and two-configuration SCF.[48] The EDA reported here defines a sequence of constraints that yield three intermediate variational energies in addition to the final CAS(2,2) energy. A descriptive and non-mathematical discussion of the design principles is given in the following section on Design Principles, followed by the mathematical framework that enables the constraints to be exactly satisfied. After mentioning some computational details, we present results and discussion for a variety of single bonds, whose character varies considerably, including some consideration of the effect of solvation.

DESIGN PRINCIPLES

Our objective is to construct a bonded energy decomposition analysis that adheres to the following criteria (these are the essential parts of a longer list suggested for a non-bonded EDA[37]): 1) all energies should be calculated using valid fermionic wavefunctions, 2) all such wavefunctions should be spin-pure, 3) the method should qualitatively correctly describe the interaction over the entire potential energy surface, 4) the method should be variational with respect to a well-defined total interaction energy.

In this work, the absolutely localized molecular orbital (ALMO) EDA is extended to accomplish these goals by decomposing the one-pair perfect pairing (PP1) energy (or, equivalently, the CAS(2,2) energy). Two (non-orthogonal) fragments are defined as the two halves of the bond of interest and the orbitals are optimized in isolation as restricted open-shell fragments. These fragments are then brought together with frozen orbitals to form a high-spin supersystem (giving rise to a frozen orbital term, FRZ). The unpaired electrons in this supersystem are then used to generate the singlet configuration state function, in which the ALMO constraint prevents charge-transfer between the fragments (giving a term due to spin-coupling of the bond electrons, SC). This CSF is allowed to relax subject to the CT-preventing ALMO constraint (giving a polarization term, POL). Finally, the ALMO constraint is relaxed to give the one-pair perfect pairing solution (giving a term assignable to charge-transfer, CT).

We therefore partition the single bonded interaction of interest into five terms:

$$\Delta E_{\text{interaction}} = \Delta E_{\text{GEOM}} + \Delta E_{\text{FRZ}} + \Delta E_{\text{SC}} + \Delta E_{\text{POL}} + \Delta E_{\text{CT}} \quad (1)$$

The first term, $\mathbf{\Delta E_{GEOM}}$, is the energy penalty associated with distorting each radical fragment to the geometry it adopts in the interacting complex. Each radical fragment is described by a spin-pure $\left(\boldsymbol{S = \frac{1}{2}; M_s = +\frac{1}{2}}\right)$ single determinant (i.e. restricted open shell Hartree-Fock).

The second term, $\mathbf{\Delta E_{FRZ}}$, is the energy change associated with bringing the two radical fragments together from infinite separation to form a spin-pure triplet single determinant wavefunction ($\boldsymbol{S = 1; M_s = +1}$). The triplet wavefunction is constructed without allowing the orbitals to relax. By design, $\mathbf{\Delta E_{FRZ}}$ is entirely a non-bonded interaction, and for this reason will typically be repulsive for a chemical bond. It includes contributions from inter-fragment electrostatics, Pauli repulsion, exchange-correlation, and dispersion (although dispersion is not present in the current implementation since it is based on Hartree-Fock theory). Since this term is analogous to the existing ALMO frozen term, it may be decomposed into those contributions if desired using the ALMO frozen decomposition scheme.[38,39]

The third term, $\mathbf{\Delta E_{SC}}$, is the only term that has no analog in the ALMO-EDA for non-bonded interactions, and is the energy difference due to changing the coupling of the two radical electrons from high-spin triplet to low-spin singlet. It accounts for the delocalization effects associated with singlet coupling of two electrons forming the single bond, while continuing to use the frozen orbitals. $\mathbf{\Delta E_{SC}}$ is expected to be often a dominant term in covalent bond formation.

The fourth term, $\mathbf{\Delta E_{POL}}$, is the energy change associated with the orbitals of each fragment relaxing in the presence of the field of the other fragment, without any charge transfer, subject to singlet spin coupling. $\mathbf{\Delta E_{POL}}$ is the term that includes the effect of atomic orbital contraction that has been discussed for simple homonuclear diatomics.[10] It also includes contributions from polarization in the bond. The original atomic-orbital based ALMO-EDA polarization term does not have a well-defined basis set limit;[49] as the basis set gets larger, there is sufficient flexibility that orbitals can contort to approximate the final wavefunction, including charge-transfer. The use of fragment electric response functions (FERFs) as an alternative ALMO basis resolves this issue.[37] In this scheme, the virtual orbitals available for polarization are only those which are necessary for describing the response of each fragment to an applied electric field. We will use the dipole and quadrupole (DQ) FERFs to define the fragment virtual spaces within which the polarization energy is minimized. This guarantees a well-defined basis set limit: the polarization term describes how much the fragments relax due to the dipole-quadrupole field generated by the other fragments.

The final term, $\mathbf{\Delta E_{CT}}$, contains charge-transfer contributions relating to electrons from one fragment being transferred to the other fragment. It is clearly the dominant term in ionic bonds, and is also expected to be important in bonds of the so-called charge-shift type.[50–52]

THEORY

We employ the tensor formulation for working with non-orthogonal orbitals[53] and use the following notation in this work: total wavefunction: Ψ; Slater determinant: φ; determinant indices: Hebrew letters ב,א,…; fragment indices: capital Roman *X*, *Y*,…; AO indices: lower case Greek μ, ν,…; occupied MO indices: *i*, *j*,…; generic MO indices *r*, *s*,…. Large dots are used as placeholders to clarify index ordering. Covariant indices are given as subscripts and contravariant indices as superscripts.

Frozen Energy

For readers unfamiliar with the ALMO scheme,[35,36] we outline the method below. The system of interest is partitioned into some number of interacting fragments (in this case, the two sides of the bond of interest). Separate restricted open-shell single-point calculations are performed on each of the fragments in isolation (at the geometry of interacting system). The resulting fragment MO coefficients are assembled into a high-spin (triplet for a single-bond), unrestricted supersystem MO coefficient matrix by block-diagonal concatenation. The orbitals are thus said to be absolutely localized on a given fragment. Note that, while orbitals within a fragment are orthogonal, between fragments, this is generally not the case. The supersystem wavefunction is still spin-pure because the fragment blocks are restricted open-shell and are high-spin coupled.

The concatenated MO coefficients of the supersystem give rise to a supersystem "frozen" density matrix, $\mathbf{P_{FRZ}}$ for both alpha and beta spins, defined by the subspace spanned by the frozen occupied orbitals:

$$P_{\alpha,\mathrm{FRZ}}^{X\mu Y\nu} = (T_{\alpha,\mathrm{FRZ}})_{\bullet\, Xi}^{X\mu\,\bullet} (\sigma_\alpha)^{XiYj} (T_{\alpha,\mathrm{FRZ}})_{\bullet\, Yj}^{Y\nu\,\bullet} \tag{2}$$

where $\boldsymbol{\sigma_\alpha^{XiYj}}$ is the contravariant alpha occupied MO metric and is needed to form a valid projector. This matrix is identity only when the fragments are orthogonal and there is no overlap between them. Hence, in general, the frozen density is not the sum of the non-interacting densities. The contravariant alpha occupied MO metric is the inverse of the occupied, occupied block of the covariant alpha MO overlap matrix, $\boldsymbol{(\sigma_\alpha)_{XiYj}}$:

$$(\sigma_\alpha)_{XiYj} = (T_\alpha)_{\bullet\, Xi}^{X\mu\,\bullet} S_{X\mu Y\nu} (T_\alpha)_{\bullet\, Yj}^{Y\nu\,\bullet} \tag{3}$$

Where $\boldsymbol{S_{X\mu Y\nu}}$ is the covariant atomic orbital overlap matrix. We then calculate the frozen contribution by the difference between the sum of single point energies for the separated fragments and the energy of the supersystem, that is, the trace of the frozen density with the supersystem core Hamiltonian and Fock matrices, formed from the frozen density:

$$E_{\mathrm{FRZ}} = \frac{1}{2} \mathrm{tr}\left[(\boldsymbol{H}_{\mathrm{core}} + \boldsymbol{F}_{\alpha,\mathrm{FRZ}})\boldsymbol{P}_{\alpha,\mathrm{FRZ}} + (\boldsymbol{H}_{\mathrm{core}} + \boldsymbol{F}_{\beta,\mathrm{FRZ}})\boldsymbol{P}_{\beta,\mathrm{FRZ}}\right] \tag{4}$$

$$\Delta E_{\mathrm{FRZ}} = E_{\mathrm{FRZ}} - \sum_{Z}^{\mathrm{Frgm}} E_Z \tag{5}$$

In highly symmetric systems, the unpaired spin-orbital on each fragment resides in a degenerate energy eigenspace, and so there are many degenerate solutions for the fragments (see Figure 1). While these different solutions are degenerate for the fragments, the supersystem assembled from these different fragments solutions are not degenerate. To resolve this ambiguity, the initially formed high-spin supersystem energy is spin-flipped to a spin-coupled wavefunction (see following sections), which is optimized with respect to orbital rotations subject to the ALMO constraint. These polarized fragments are then used as the initial guess for a new fragment calculation which is minimized, subsequently, with respect to doubly occupied-virtual orbital rotations, singly occupied-virtual rotations, and finally all orbital rotations. This stepwise

relaxation procedure is to ensure that the polarized fragments unpolarize with the singly-occupied orbital in the correct orientation. These unpolarized fragments are then used to construct the true frozen supersystem wavefunction.

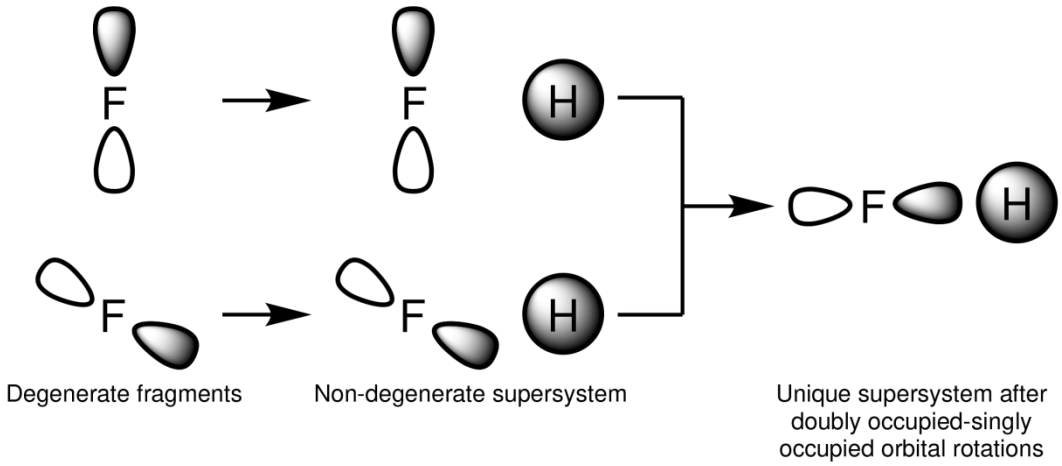

Figure 1. An example of a case where there are many degenerate solutions for the fragments (the F atom), but the assembled supersystem (HF) is not necessarily degenerate. The unpaired spin-orbital is shown. To form a unique supersystem, the supersystem energy is optimized with respect to doubly occupied-singly occupied rotations. These rotations allow the unpaired spin to rotate to the optimal orientation without allowing the fragments to polarize.

In principal, this reorientation and unpolarization procedure could result in fragments in a low-lying electronic excited state. We therefore define and electronic distortion energy analogous to the geometric distortion energy, as the energy difference between the fragments in the lowest electronic state and the fragments in the electronic state of the interacting complex. Generally, this term is zero, but it can be positive. The energy change from not resolving this ambiguity can be substantial. For example, for an F atom in an HF molecule, the frozen terms due to different singly-occupied orientations can be >50 kcal/mol.

Since this method is an extension of the ALMO EDA scheme, it inherits the ALMO scheme's ability to further separate the frozen term into terms corresponding to permanent electrostatic interactions, Pauli repulsion, and dispersion.[39]

Spin-coupling

In order to generate the singlet CSF from the triplet frozen supersystem wavefunction, a spin flip is applied to each of the unpaired electrons in each fragment space to form a 2-configurational wavefunction, which is relaxed with respect to doubly occupied-singly occupied rotations as was done for the frozen wavefunction for the same reason. Since the two determinants that make up the CSF are spin complements, the CI coefficients are equal.

$$|\Psi_{\mathrm{SC}}\rangle = N\left(|\phi_{\aleph}\rangle + |\phi_{\beth}\rangle\right) \tag{6}$$

where $\boldsymbol{N}$ is a normalization factor. The spin-coupling energy is then calculated as the energy difference between the frozen supersystem energy and the energy of the 2-configurational wavefunction:

$$E_{\mathrm{SC}} = N^2(E_{\text{א}} + E_{\text{ב}} + 2E_{\text{בא}}) \tag{7}$$

$$\Delta E_{\mathrm{SC}} = E_{\mathrm{SC}} - E_{\mathrm{FRZ}} \tag{8}$$

This energy change may be positive or negative depending on which of the triplet or the singlet is lower in energy. Generally, if a bond is forming, the singlet will be lower in energy and the energy change is negative.

Polarization

In order to calculate the variational polarization energy subject to the ALMO constraint while ensuring spin-purity, we require each fragment to continue to be described by a set of restricted open-shell orbitals. The spin-coupled determinants are already ALMO wavefunctions due to the block-diagonal nature of the MO coefficients matrix; the ALMO constraint is maintained by only allowing rotations within a fragment. In this section, we derive expressions for the gradient of the energy with respect to non-orthogonal orbital rotations within each determinant and also for the interdeterminantal Hamiltonian matrix element.

Recall that the energy of the 2-configurational wavefunction is given by $\boldsymbol{E = N^2(E_{\text{א}} + E_{\text{ב}} + 2E_{\text{בא}})}$. Ignoring normalization and differentiating with respect to an orbital rotation in arbitrary determinant ג:

$$\frac{\partial E}{\partial \Delta_{\text{ג}Zp\text{ג}Zq}} = \frac{\partial E_{\text{א}}}{\partial \Delta_{\text{ג}Zp\text{ג}Zq}} + \frac{\partial E_{\text{ב}}}{\partial \Delta_{\text{ג}Zp\text{ג}Zq}} + 2\frac{\partial E_{\text{בא}}}{\partial \Delta_{\text{ג}Zp\text{ג}Zq}} \tag{9}$$

We first calculate the gradient within each determinant, that is, the first two terms (the determinant indices will be temporarily elided since they are all the same in this case). The energy of each determinant is given by

$$\frac{1}{2}\,\mathrm{tr}\left[(\boldsymbol{H}_{\mathrm{core}} + \boldsymbol{F}_{\alpha})\boldsymbol{P}_{\alpha} + (\boldsymbol{H}_{\mathrm{core}} + \boldsymbol{F}_{\beta})\boldsymbol{P}_{\beta}\right] \tag{10}$$

We denote an orbital rotation between orbital $\boldsymbol{p}$ and $\boldsymbol{q}$ in fragment $\boldsymbol{Z}$ by $\boldsymbol{\Delta_{Zp,Zq}}$. Then,

$$\frac{\partial E_{\text{א}}}{\partial \Delta_{Zp,Zq}} = (F_{\alpha})_{B\nu A\mu}\frac{\partial (P_{\alpha})^{A\mu B\nu}}{\partial \Delta_{Zp,Zq}} + (F_{\beta})_{B\nu A\mu}\frac{\partial (P_{\beta})^{A\mu B\nu}}{\partial \Delta_{Zp,Zq}} \tag{11}$$

The required partial derivatives are:

$$\begin{aligned}\frac{\partial P^{A\mu B_{\nu}}}{\partial \Delta_{Zp,Zq}} &= T^{A\mu\,\bullet}_{\bullet\,Ai}(\sigma)^{AiBj}\frac{\partial T^{B\nu\,\bullet}_{\bullet\,Bj}}{\partial \Delta_{Zp,Zq}} + T^{A\mu\,\bullet}_{\bullet\,Ai}\frac{\partial (\sigma)^{AiBj}}{\partial \Delta_{Zp,Zq}}T^{B\nu\,\bullet}_{\bullet\,Bj} \\ &\quad + \frac{\partial T^{A\mu\,\bullet}_{\bullet\,Ai}}{\partial \Delta_{Zp,Zq}}(\sigma)^{AiBj}T^{B\nu\,\bullet}_{\bullet\,Bj} \qquad (12) \\ &= T^{A\mu\,\bullet}_{\bullet\,Ai}(\sigma)^{AiBj}C^{B\nu\,\bullet}_{\bullet\,Br}(\delta^{Br}_{Zp}\delta^{Bj}_{Zq} - \delta^{Br}_{Zq}\delta^{Bj}_{Zp}) - T^{A\mu\,\bullet}_{\bullet\,Ai}\frac{\partial (\sigma)^{AiBj}}{\partial \Delta_{Zp,Zq}}T^{B\nu\,\bullet}_{\bullet\,Bj} \\ &\quad + C^{A\mu\,\bullet}_{\bullet\,Aw}(\delta^{Aw}_{Zp}\delta^{Ai}_{Zq} - \delta^{Aw}_{Zq}\delta^{Ai}_{Zp})(\sigma)^{AiBj}T^{B\nu\,\bullet}_{\bullet\,Bj} \qquad (13)\end{aligned}$$

$$\frac{\partial(\sigma)^{Ai\gamma Bj\epsilon}}{\partial\Delta_{Zp,Zq}} = -\sum_{X,Y}^{\text{Frgm}}(\sigma)^{Ai\gamma Xl}\left(\frac{\partial(\sigma)_{Xl,Ym}}{\partial\Delta_{Zp,Zq}}\right)(\sigma)^{Ym,Bj\epsilon} \tag{14}$$

$$\begin{aligned} &= -\sum_{X,Y}\Big[(\sigma)^{Ai\gamma,Xl}C^{X\lambda}_{\bullet\,Xs}(\delta^{Xs}_{Zp}\delta^{Xl}_{Zq}-\delta^{Xs}_{Zq}\delta^{Xl}_{Zp})S_{X\lambda,Y\xi}T^{Y\xi}_{\bullet\,Ym}(\sigma)^{Ym,Bj\epsilon} \\ &\quad +(\sigma)^{Ai\gamma,Xl}T^{X\lambda}_{\bullet\,Xl}S_{X\lambda,Y\xi}C^{Y\xi}_{\bullet\,Yt}(\delta^{Yt}_{Zp}\delta^{Yl}_{Zq}-\delta^{Yt}_{Zq}\delta^{Yl}_{Zp})(\sigma)^{Ym,Bj\epsilon}\Big] \end{aligned} \tag{15}$$

Combining terms and contracting with $\boldsymbol{F_{B\nu,A\mu}}$

$$\begin{aligned} F_{B\nu,A\mu}\frac{\partial P^{A\mu B_\nu}}{\partial\Delta_{Zp,Zq}} &= C^{X\lambda}_{\bullet\,Xs}(1-S_{X\lambda,Y\xi}P^{Y\xi B\nu})F_{B\nu,A\mu}T^{A\mu}_{\bullet\,Ai\gamma}(\sigma)^{Ai\gamma Xl}(\delta^{Xs}_{Zp}\delta^{Xl}_{Zq}-\delta^{Xs}_{Zq}\delta^{Xl}_{Zp}) \\ &\quad +(\sigma)^{Ym,Bj\epsilon}T^{B\nu}_{\bullet\,Bj\epsilon}F_{B\nu,A\mu}(1-P^{A\mu X\lambda}S_{X\lambda Y\xi})C^{Y\xi}_{\bullet\,Yt}(\delta^{Yt}_{Zp}\delta^{Ym}_{Zq}-\delta^{Yt}_{Zq}\delta^{Ym}_{Zp}) \end{aligned} \tag{16}$$

Which gives the matrix equation

$$\frac{\partial E_{\boldsymbol{\aleph}}}{\partial\Delta_{pq}} = 2\left\{\left[(\boldsymbol{\sigma}^{-1}_{\boldsymbol{\alpha}})^m\boldsymbol{T}^{\boldsymbol{T}}_{\boldsymbol{\alpha}}\boldsymbol{F}_{\boldsymbol{\alpha}}(\boldsymbol{1}-\boldsymbol{P}_{\boldsymbol{\alpha}}\boldsymbol{S})\boldsymbol{C}_t+(\boldsymbol{\sigma}^{-1}_{\boldsymbol{\beta}})^m\boldsymbol{T}^{\boldsymbol{T}}_{\boldsymbol{\beta}}\boldsymbol{F}_{\boldsymbol{\beta}}(\boldsymbol{1}-\boldsymbol{P}_{\boldsymbol{\beta}}\boldsymbol{S})\boldsymbol{C}_t\right](\delta^t_p\delta^m_q-\delta^t_q\delta^m_p)\right\}_{ZZ} \tag{17}$$

where the superscript $\boldsymbol{m}$ denotes rows of the occupied metric and the subscript $\boldsymbol{t}$ denotes columns of the MO coefficient matrix.

The gradient for the interdeterminantal matrix element follows a similar derivation. We define $\boldsymbol{D_{\beth\aleph}}$, the determinant of the overlap matrix between the two determinants, $\boldsymbol{D_{\aleph\aleph}}$ and $\boldsymbol{D_{\beth\beth}}$, the determinants of each determinant's overlap matrix, $\boldsymbol{F_{\aleph\mu\beth\nu}}$, the transition Fock matrix, $\boldsymbol{P^{\beth\nu\aleph\mu}}$, the transition density matrix, and $\boldsymbol{g^{\beth Bj,\aleph Ai}}$ is the inverse of the non-symmetric interdeterminantal occupied MO metric (the interdeterminantal analog of $\boldsymbol{\sigma}$ above). Let $\boldsymbol{U=\frac{1}{2}\left(h_{\aleph\mu\beth\nu}+F_{\aleph\mu\beth\nu}\right)P^{\beth\nu\aleph\mu}}$.

$$\frac{\partial E_{\boldsymbol{\beth\aleph}}}{\partial\Delta_{\boldsymbol{\gimel}Zp\boldsymbol{\gimel}Zq}} = \frac{\partial D_{\boldsymbol{\beth\aleph}}/(D_{\boldsymbol{\aleph\aleph}}D_{\boldsymbol{\beth\beth}})^{1/2}U}{\partial\Delta_{\boldsymbol{\gimel}Zp\boldsymbol{\gimel}Zq}} \tag{18}$$

$$\begin{aligned} &= \frac{D_{\boldsymbol{\beth\aleph}}}{(D_{\boldsymbol{\aleph\aleph}}D_{\boldsymbol{\beth\beth}})^{1/2}}F_{\boldsymbol{\aleph}\mu\boldsymbol{\beth}\nu}\frac{\partial P^{\boldsymbol{\beth}\nu\boldsymbol{\aleph}\mu}}{\partial\Delta_{\boldsymbol{\gimel}Zp\boldsymbol{\gimel}Zq}}+E_{\boldsymbol{\beth\aleph}}g^{\boldsymbol{\beth}Bj,\boldsymbol{\aleph}Ai}\frac{\partial g_{\boldsymbol{\beth}Bj,\boldsymbol{\aleph}Ai}}{\partial\Delta_{\boldsymbol{\gimel}Zp\boldsymbol{\gimel}Zq}} \\ &\quad -\frac{1}{2}E_{\boldsymbol{\beth\aleph}}\left(\sigma^{\boldsymbol{\beth}Cn,\boldsymbol{\beth}Do}\frac{\partial\sigma_{\boldsymbol{\beth}Cn,\boldsymbol{\beth}Do}}{\partial\Delta_{\boldsymbol{\gimel}Zp\boldsymbol{\gimel}Zq}}+\sigma^{\boldsymbol{\aleph}Ev,\boldsymbol{\aleph}Fw}\frac{\partial\sigma_{\boldsymbol{\aleph}Ev,\boldsymbol{\aleph}Fw}}{\partial\Delta_{\boldsymbol{\gimel}Zp\boldsymbol{\gimel}Zq}}\right) \end{aligned} \tag{19}$$

$$P^{\boldsymbol{\beth}B\nu,\boldsymbol{\aleph}A\mu} = T^{\boldsymbol{\beth}B\nu}_{\bullet\,\boldsymbol{\beth}Bj}(g^{\boldsymbol{\beth}Bj,\boldsymbol{\aleph}Ai})T^{\boldsymbol{\aleph}A\mu}_{\bullet\,\boldsymbol{\aleph}Ai} \tag{20}$$

$$g^{\boldsymbol{\beth}Bj,\boldsymbol{\aleph}Ai} = \left[T^{\boldsymbol{\aleph}A\lambda}_{\bullet\,\boldsymbol{\aleph}Ai}S_{\boldsymbol{\aleph}A\lambda\boldsymbol{\beth}B\sigma}T^{\boldsymbol{\beth}B\sigma}_{\bullet\,\boldsymbol{\beth}Bj}\right]^{-1} \tag{21}$$

Note that when $\text{א} = \text{ב}$, this expression reduces to the on-determinantal result derived above. Without loss of generality, we assume that orbital rotations are in the א determinant. The first term's derivation is nearly identical to the on-determinantal case and gives the matrix expression

$$\frac{D_{\text{בא}}}{(D_{\text{אא}}D_{\text{בב}})^{1/2}}\left\{\left(\left[\left(\boldsymbol{g}_{\alpha}^{-1}\right)^{T}\right]^{l}\boldsymbol{T}_{\text{ב}\alpha}^{T}\boldsymbol{F}_{\alpha}^{T}(\boldsymbol{1}-\boldsymbol{P}_{\alpha}^{T}\boldsymbol{S})\boldsymbol{C}_{\text{א}s}\right.\right.$$
$$\left.\left.+\left[\left(\boldsymbol{g}_{\beta}^{-1}\right)^{T}\right]^{l}\boldsymbol{T}_{\text{ב}\beta}^{T}\boldsymbol{F}_{\beta}^{T}(\boldsymbol{1}-\boldsymbol{P}_{\beta}^{T}\boldsymbol{S})\boldsymbol{C}_{\text{א}s}\right)(\delta_{p}^{s}\delta_{q}^{l}-\delta_{q}^{s}\delta_{p}^{l})\right\}_{ZZ} \tag{22}$$

where the superscript $\boldsymbol{l}$ denotes rows of the occupied metric and the subscript $\boldsymbol{s}$ denotes columns of the MO coefficient matrix. The second and third terms together give the matrix expression

$$E_{\text{בא}}\left\{\left(\left[\left(\boldsymbol{g}_{\alpha}^{-1}\right)^{T}\right]^{i}\boldsymbol{T}_{\text{ב}\alpha}^{T}+\left[\left(\boldsymbol{g}_{\beta}^{-1}\right)^{T}\right]^{i}\boldsymbol{T}_{\text{ב}\beta}^{T}-\left[\boldsymbol{\sigma}_{\text{א}\alpha}^{-1}\right]^{i}\boldsymbol{T}_{\text{א}\alpha}^{T}-\left[\boldsymbol{\sigma}_{\text{א}\beta}^{-1}\right]^{i}\boldsymbol{T}_{\text{א}\beta}^{T}\right)\boldsymbol{S}\boldsymbol{C}_{\text{א}r}(\delta_{p}^{r}\delta_{q}^{i}-\delta_{q}^{r}\delta_{p}^{i})\right\}_{ZZ} \tag{23}$$

where the superscript $\boldsymbol{i}$ denotes rows of the occupied metric and the subscript $\boldsymbol{r}$ denotes columns of the MO coefficient matrix. When $\text{א} = \text{ב}$, this expression is zero.

This gradient expression is used to generate a RO gradient expression, that is, doubly occupied-singly occupied rotations, doubly occupied-virtual rotations, and singly occupied-virtual rotation are all carried out independently. This maintains the RO nature of each fragment and, hence, spin-purity of the total wavefunction. The energy change (which must be negative) due to this orbital relaxation is defined as the polarization energy term.

It should also be observed that some of this polarization is "constant-density" polarization,[38] which relieves some Pauli-repulsion and may be thought of as a deficiency in the initially defined spin-coupled wavefunction. However, based on previous results, we neglect this relatively minor component of the polarization energy.

Charge-transfer

The relaxation of the ALMO constraint on the above 2-configurational wavefunction is the one-pair perfect pairing energy or, equivalently, CAS(2,2). The energy difference between the unconstrained PP energy and the polarized wavefunction energy is always negative and attributed to charge-transfer, a process that is formally forbidden before due to the ALMO constraint. As a result, the EDA described in this paper is therefore equivalently described as a PP-EDA or a CAS(2,2)-EDA.

Computational Details

A development version of Q-Chem 4.3 was used for all calculations.[54] Geometries and EDA for each system were calculated at the HF/aug-cc-pvtz level.

RESULTS AND DISCUSSION

The EDA scheme introduced here is designed to follow the formation of a bond via a sequence of constrained variational calculations that bring together the two sides of the bond from infinite separation of the fragments. The initial supersystem wavefunction (from which the

frozen energy term derives) corresponds to bringing together fragments with doublet-optimized orbitals in the most energetically favorable way. The spin-coupled wavefunction then represents the jump to the singlet surface and so reports on the singlet-triplet gap of the doublet-optimized orbitals. We argue that this energy difference then indicates how "covalent" a bond is, as covalency loosely corresponds to the idea that electrons would rather be coupled than not coupled. The polarization term allows the orbitals to relax in the field of the other fragment and hence large numbers correspond to how polar a bond is, or rather, how much energy is released by the density distorting to respond to the field of the other fragment. The final charge-transfer term corresponds to the energy stabilization due to charge flow between fragments. As one would expect, this term is dominant for ionic molecules, but still plays an important, if smaller, role for classical covalent molecules.

Though this method is a MO-based method, it has clear connections to valence-bond descriptions of molecules. The ALMO-constrained, spin-coupled and polarized wavefunctions, with their non-orthogonal interacting valence doublet fragments, are analogous to the valence-bond covalent picture (see Figure 2). The unconstrained, final wavefunction then corresponds to the 4-configurational extension of this VB wavefunction to include ionic terms in which both electrons of the bond lie on one fragment. Hence, the charge-transfer term in this method also includes what has been described as "charge-shift bonding".[50–52]

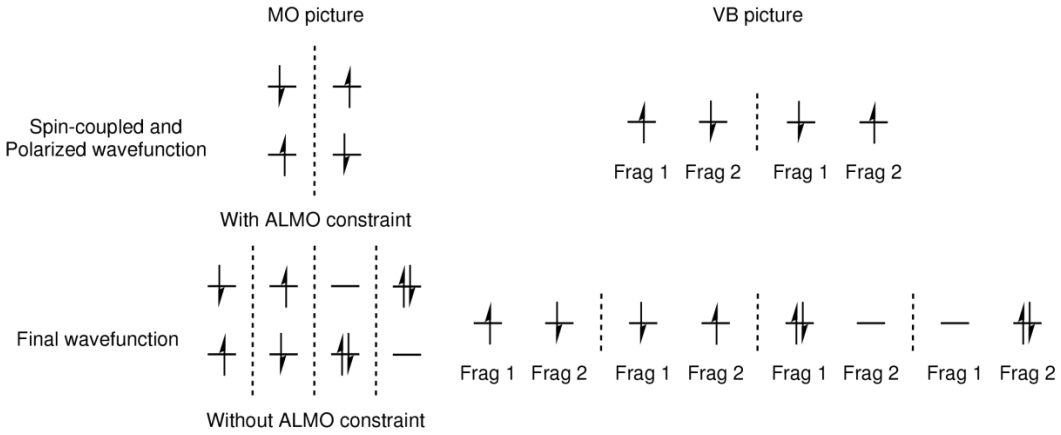

Figure 2. MO vs. VB picture of EDA intermediate wavefunctions.

To verify that the EDA behaves as expected, we investigated a few representative and pathological bonds (Figure 3 and Table 1). Classic, non-polar covalent bonds such as H_2 and ethane are indeed dominated by spin-coupling. Polarization and charge transfer make up only a small portion of the interaction energy (bond energy). As we move to more polar bonds, as in HCl, polarization becomes highly important to the interaction in addition to spin-coupling, giving what we would call a typical polar covalent bond. Molecules which feature charge-transfer contributions that are similar in magnitude to the spin-coupling term are considered "charge-shift bonds", as exemplified by F_2, a canonical "charge-shift" bond. One of the strongest single bonds, the Si–F bond of SiF_4, which has high spin-coupling, polarization, and charge-transfer could be equivalently thought of as a polar covalent bond with ionic character or a polar charge-shift bond. When the bond is truly ionic, as in LiF, neither spin-coupling nor polarization are significant and the bond energy is dominated by the charge transfer term. Hence, the consideration of the terms of this EDA gives a "fingerprint" for classical chemical concepts of

bonding. This fingerprint was obtained without any explicit reference to these concepts and the method gives a quantitative description of these qualitative chemical heuristics.

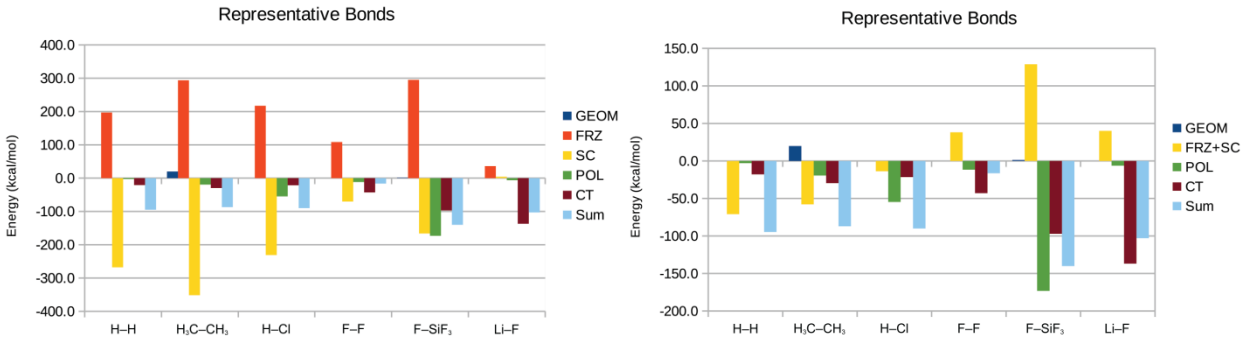

Figure 3. a) EDA of some representative bonds. b) EDA of some representative bonds with the frozen term summed into the spin-coupling term.

Table 1. EDA of representative bonds. All energies in kcal/mol. Numbers in parenthesis are the percentage of the total stabilization each term represents. Exact is CCSD(T)/aug-cc-pvtz.

	GEOM	FRZ	SC	POL	CT	Sum	Exact
H–H	0.0	196.9	-267.9 (91.9)	-2.9 (1.0)	-20.8 (7.1)	-94.7	-107.4
$H_3C–CH_3$	19.9	293.7	-351.6 (87.8)	-19.5 (4.9)	-29.6 (7.4)	-87.1	-91.4
H–Cl	0.0	217.2	-231.0 (75.2)	-54.7 (17.8)	-21.5 (7.0)	-90.0	-106.4
F–F	0.0	108.5	-70.3 (56.3)	-11.7 (9.4)	-42.9 (34.4)	-16.4	-30.4
$F–SiF_3$	1.3	295.1	-166.3 (38.1)	-173.2 (39.7)	-97.1 (22.2)	-140.1	-166.0
Li–F	0.0	35.9	4.2	-6.3 (4.4)	-136.8 (95.6)	-103.0	-137.4

One feature of this methods is that, unlike some methods,[44] each relevant energy term is relatively similar in magnitude to the total interaction energy. By avoiding large changes in large numbers, trends can be more easily seen, as evidenced by the gradual decrease in the importance of simple spin-coupling and concomitant increase in the importance of charge-transfer in first row element–H bonds (Figure 4 and Table 2). First-row atoms are highly electronegative and not very polarizable and so the move rightward along the first row leads principally to charge-shift bonds rather than polar covalent bonds except in the case of ammonia. One way to see this trend more clearly is to sum the frozen term and the spin-coupling term. When spin-coupling dominates the bonding (i.e. when the bond is simply covalent), the spin-coupling stabilization makes up for all of the frozen term's destabilization and much of the bond strength. Moving to the right, spin-coupling is insufficient to solely account for both the frozen term and the bond strength. Polarization and charge-transfer effects are required, culminating in the charge-shift bonds in H_2O and HF where the spin-coupling can't even account for all of the frozen destabilization. Of course, this is not to say that spin-coupling is unimportant in these molecules; this FRZ+SC way of the looking at the bond is biased against spin-coupling by forcing that term

alone to account for all of the frozen destabilization, but it is a convenient way to investigate trends amongst the three main bonding contributors.

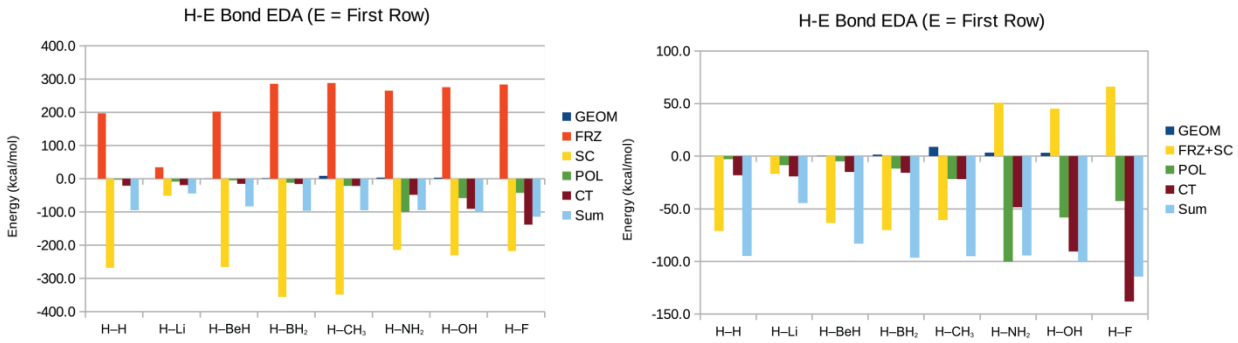

Figure 4. a) EDA of first row element–H bonds. Note the gradual increase in importance of charge-transfer as the element becomes more electronegative. b) EDA of first row element–H bonds with the frozen term summed into the spin-coupling to give a clearer view of the importance of different effects on a more bond-energy relevant scale.

Table 2. EDA of first row element–H bonds. All energies in kcal/mol. Numbers in parenthesis are the percentage of the stabilization each term represents. Exact is CCSD(T)/aug-cc-pvtz.

	GEOM	FRZ	SC	POL	CT	Sum	Exact
H–H	0.0	196.9	-267.9 (91.9)	-2.9 (1.0)	-20.8 (7.1)	-94.7	-107.4
H–Li	0.0	34.3	-51.1 (65.0)	-8.6 (10.9)	-19.0 (24.1)	-44.4	-58.3
H–BeH	0.2	202.3	-265.6 (93.0)	-4.9 (1.7)	-15.0 (5.3)	-83.0	-97.4
H–BH_2	1.4	285.7	-355.8 (92.8)	-11.8 (3.1)	-15.8 (4.1)	-96.1	-111.2
H–CH_3	8.8	288.0	-348.6 (89.0)	-21.5 (5.5)	-21.6 (5.5)	-94.9	-112.2
H–NH_2	3.3	265.1	-214.2 (59.1)	-100.1 (27.6)	-48.4 (13.3)	-94.3	-114.6
H–OH	3.2	275.6	-230.4 (60.8)	-58.1 (15.3)	-90.4 (23.9)	-100.2	-124.4
H–F	0.0	283.6	-217.5 (54.7)	-42.5 (10.7)	-138.0 (34.7)	-114.3	-140.1

The EDA as bonds are broken also lends insight into the nature of the bonded interaction. By inspection of the H_2 EDA of dissociation (Figure 5a), one can see that the bonding in H_2 is dominated by spin-coupling everywhere on the potential curve. In contrast, the bond in HF (Figure 5b) at shorter bond lengths (near equilibrium) has higher spin-coupling than charge-transfer but as the bond is stretched charge-transfer becomes relatively more important and spin-coupling and charge-transfer are about equal in magnitude. In other words, while the spin-coupling decays as the bond is stretched, the slower to decay ionic stabilization due to charge-transfer keeps the bond from weakening as much. This observation is reflective of the oft-cited

fact that ionic contributions are important to understanding the strong bond in HF and that the dipole moment for HF increases as the bond is stretched.

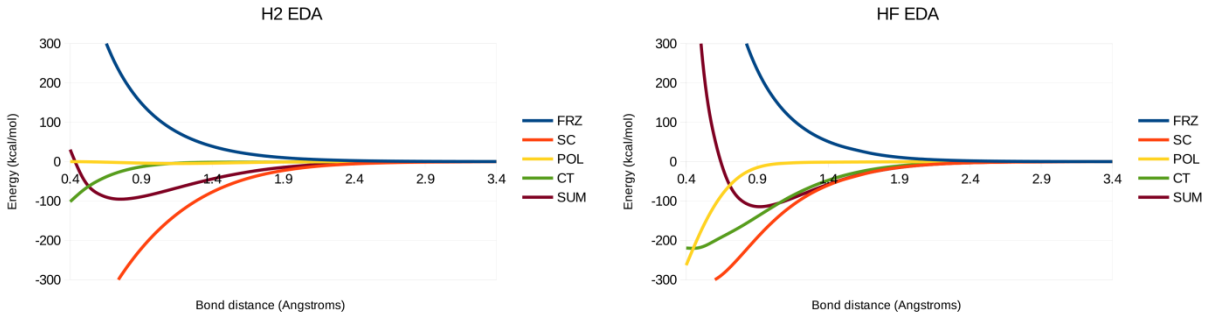

Figure 5. a) EDA of H_2 along its dissociation curve. Note that spin-coupling is dominant along the entire surface. b) EDA of HF along its dissociation curve. Note that spin-coupling and polarization are small and the bond is dominated by charge-transfer.

The EDA can be used to study environmental effects on bonded interactions as well. Solvation can play a huge role in the nature of bonds particularly by stabilizing charge-separated states.[55] We investigated the effect of solvent on the HCl molecule. Experimentally, in the gas phase, HCl is a polar covalent molecule, while it dissociates into ions when dissolved in water.[56] Adding two explicit water molecules to HCl, one near the H and the other near the Cl (see Figure 6a), dramatically changes the results of the EDA of the H–Cl bond (see Figure 6b). The bond energy increases in the partially solvated case, so we normalize the charge transfer and polarization terms by the total stabilizing interactions and consider the size of each term as a percentage of the total stabilization. Charge-transfer, a small component of the gas-phase bond (8.3%), more than doubles in importance (16.9%) in the partially solvated case. Simultaneously, the spin-coupling term drops from 75.1% in the gas phase to 60.4% in the partially solvated case. The increasing importance of the CT term and decreasing importance of the SC term indicate that the bond is becoming more ionic as water molecules are added. These results quantitatively describe the transformation of HCl from a polar covalent molecule to a polar covalent molecule with ionic character, to what is ultimately an ionic bond in solution as water molecules are added to the first solvation shell.

Table 3. EDA of gas phase and partially solvated HCl. All energies in kcal/mol. Numbers in parenthesis are the percentage of the total stabilization each term represents.

	GEOM	FRZ	SC	POL	CT	Sum
H–Cl	0.0	148.1	-176.1 (75.1)	-39.1 (16.7)	-19.4 (8.3)	-86.5
$H_2O{\cdot}H{-}Cl{\cdot}H_2O$	0.0	172.9	-171.5 (60.4)	-64.3 (22.6)	-48.1 (16.9)	-111.0

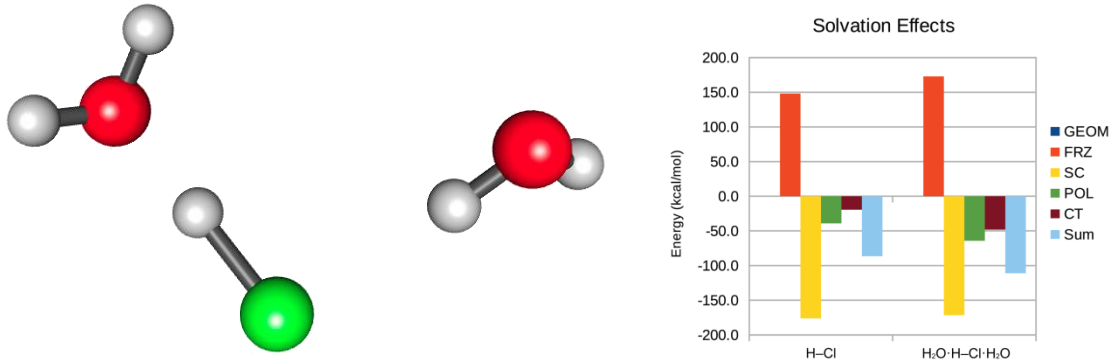

Figure 6. a) Solvated HCl model with two explicit water molecules. b) Effects of solvation on H--Cl bond EDA. Increase in CT and decreased in polarization indicate that the molecule becomes more ionic when solvated partially by water.

CONCLUSIONS

We have developed an extension of ALMO-EDA to single bonds in a spin-pure way, which allows the qualitatively correct bond energy to be decomposed. This method includes a new EDA term, spin-coupling, to describe the "covalency" of the bond in an energetic way. This scheme recovers chemical concepts of bonding and furthermore parametrizes these concepts quantitatively. Encouragingly, the method nicely capture differences in the character of different single bonds, and in addition the method is sensitive to even subtle environmental changes, such as solvation.

Currently, this method is only implemented for single-bonds corresponding to the CAS(2,2) wavefunction; the extension to multiple-bonds may be accomplished in several ways depending on which method, such as larger CAS($\boldsymbol{n,n}$) expansions or the CCVB method,[57] is employed to give the final interaction energy. Currently, there is also a lack of dynamical correlation in these energy terms, a problem which remains to be addressed and is currently being investigated. The promising results obtained here suggest that these extensions are worthwhile.

REFERENCES

(1) Pauling, L. *The Nature of the Chemical Bond and the Structure of Molecules and Crystals: An Introduction to Modern Structural Chemistry*, 3 edition.; Cornell University Press: Ithaca, N.Y., 1960.
(2) Ruedenberg, K. *Rev. Mod. Phys.* **1962**, *34* (2), 326.
(3) Nascimento, M. A. C. *J. Braz. Chem. Soc.* **2008**, *19* (2), 245.
(4) Kołos, W.; Wolniewicz, L. *J. Chem. Phys.* **1965**, *43* (7), 2429.
(5) Feinberg, M. J.; Ruedenberg, K. *J. Chem. Phys.* **1971**, *54* (4), 1495.
(6) Driessler, F.; Kutzelnigg, W. *Theor. Chim. Acta* **1976**, *43* (1), 1.
(7) Goddard III, W. A.; Wilson Jr., C. W. *Theor. Chim. Acta* **1972**, *26* (3), 211.
(8) Bacskay, G. B.; Reimers, J. R.; Nordholm, S. *J. Chem. Educ.* **1997**, *74* (12), 1494.
(9) Bacskay, G. B.; Nordholm, S. *J. Phys. Chem. A* **2013**, *117* (33), 7946.
(10) Schmidt, M. W.; Ivanic, J.; Ruedenberg, K. *J. Chem. Phys.* **2014**, *140* (20), 204104.
(11) Cardozo, T. M.; Nascimento, M. A. C. *J. Chem. Phys.* **2009**, *130* (10), 104102.

(12) Fantuzzi, F.; Nascimento, M. A. C. *J. Chem. Theory Comput.* **2014**, *10* (6), 2322.
(13) Fantuzzi, F.; Cardozo, T. M.; Nascimento, M. A. C. *J. Phys. Chem. A* **2015**, *119* (21), 5335.
(14) Reed, A. E.; Curtiss, L. A.; Weinhold, F. *Chem. Rev.* **1988**, *88* (6), 899.
(15) Bader, R. F. W. *Acc. Chem. Res.* **1985**, *18* (1), 9.
(16) Blanco, M. A.; Martín Pendás, A.; Francisco, E. *J. Chem. Theory Comput.* **2005**, *1* (6), 1096.
(17) Rahm, M.; Hoffmann, R. *J. Am. Chem. Soc.* **2015**, *137* (32), 10282.
(18) Rybak, S.; Jeziorski, B.; Szalewicz, K. *J. Chem. Phys.* **1991**, *95* (9), 6576.
(19) Jeziorski, B.; Moszynski, R.; Szalewicz, K. *Chem. Rev.* **1994**, *94* (7), 1887.
(20) Adams, W. H. *Theor. Chem. Acc.* **2002**, *108* (4), 225.
(21) Misquitta, A. J.; Jeziorski, B.; Szalewicz, K. *Phys. Rev. Lett.* **2003**, *91* (3), 33201.
(22) Misquitta, A. J.; Podeszwa, R.; Jeziorski, B.; Szalewicz, K. *J. Chem. Phys.* **2005**, *123* (21), 214103.
(23) Stone, A. J.; Misquitta, A. J. *Chem. Phys. Lett.* **2009**, *473* (1–3), 201.
(24) Hohenstein, E. G.; Sherrill, C. D. *Wiley Interdiscip. Rev. Comput. Mol. Sci.* **2012**, *2* (2), 304.
(25) Lao, K. U.; Herbert, J. M. *J. Phys. Chem. Lett.* **2012**, *3* (22), 3241.
(26) Glendening, E. D.; Streitwieser, A. *J. Chem. Phys.* **1994**, *100* (4), 2900.
(27) Schenter, G. K.; Glendening, E. D. *J. Phys. Chem.* **1996**, *100* (43), 17152.
(28) Glendening, E. D. *J. Phys. Chem. A* **2005**, *109* (51), 11936.
(29) Kitaura, K.; Morokuma, K. *Int. J. Quantum Chem.* **1976**, *10* (2), 325.
(30) Ziegler, T.; Rauk, A. *Inorg. Chem.* **1979**, *18* (7), 1755.
(31) Ziegler, T.; Rauk, A. *Inorg. Chem.* **1979**, *18* (6), 1558.
(32) Mitoraj, M. P.; Michalak, A.; Ziegler, T. *J. Chem. Theory Comput.* **2009**, *5* (4), 962.
(33) Mo, Y.; Gao, J.; Peyerimhoff, S. D. *J. Chem. Phys.* **2000**, *112* (13), 5530.
(34) Mo, Y.; Bao, P.; Gao, J. *Phys. Chem. Chem. Phys.* **2011**, *13* (15), 6760.
(35) Khaliullin, R. Z.; Head-Gordon, M.; Bell, A. T. *J. Chem. Phys.* **2006**, *124* (20), 204105.
(36) Khaliullin, R. Z.; Cobar, E. A.; Lochan, R. C.; Bell, A. T.; Head-Gordon, M. *J. Phys. Chem. A* **2007**, *111* (36), 8753.
(37) Horn, P. R.; Head-Gordon, M. *J. Chem. Phys.* **2015**, *143* (11), 114111.
(38) Horn, P. R.; Head-Gordon, M. *J. Chem. Phys.* **2016**, *144* (8), 84118.
(39) Horn, P. R.; Mao, Y.; Head-Gordon, M. *J. Chem. Phys.* **2016**, *144* (11), 114107.
(40) Żuchowski, P. S.; Podeszwa, R.; Moszyński, R.; Jeziorski, B.; Szalewicz, K. *J. Chem. Phys.* **2008**, *129* (8), 84101.
(41) Hapka, M.; Żuchowski, P. S.; Szczęśniak, M. M.; Chałasiński, G. *J. Chem. Phys.* **2012**, *137* (16), 164104.
(42) Horn, P. R.; Sundstrom, E. J.; Baker, T. A.; Head-Gordon, M. *J. Chem. Phys.* **2013**, *138* (13), 134119.
(43) Bickelhaupt, F. M.; Baerends, E. J. In *Reviews in Computational Chemistry*; Lipkowitz, K. B., Boyd, D. B., Eds.; John Wiley & Sons, Inc., 2000; pp 1–86.
(44) Hopffgarten, M. von; Frenking, G. *Wiley Interdiscip. Rev. Comput. Mol. Sci.* **2012**, *2* (1), 43.
(45) Hendrickx, K.; Braida, B.; Bultinck, P.; Hiberty, P. C. *Comput. Theor. Chem.* **2015**, *1053*, 180.

(46) Roos, B. O. In *Advances in Chemical Physics*; Lawley, K. P., Ed.; John Wiley & Sons, Inc., 1987; pp 399–445.
(47) Hay, P. J.; Hunt, W. J.; Goddard, W. A. *J. Am. Chem. Soc.* **1972**, *94* (24), 8293.
(48) Jensen, F. *Introduction to Computational Chemistry*, 2 edition.; Wiley: Chichester, England ; Hoboken, NJ, 2007.
(49) Azar, R. J.; Horn, P. R.; Sundstrom, E. J.; Head-Gordon, M. *J. Chem. Phys.* **2013**, *138* (8), 84102.
(50) Shaik, S.; Danovich, D.; Wu, W.; Hiberty, P. C. *Nat. Chem.* **2009**, *1* (6), 443.
(51) Anderson, P.; Petit, A.; Ho, J.; Mitoraj, M. P.; Coote, M. L.; Danovich, D.; Shaik, S.; Braïda, B.; Ess, D. H. *J. Org. Chem.* **2014**, *79* (21), 9998.
(52) Zhang, H.; Danovich, D.; Wu, W.; Braïda, B.; Hiberty, P. C.; Shaik, S. *J. Chem. Theory Comput.* **2014**, *10* (6), 2410.
(53) Head-Gordon, M.; Maslen, P. E.; White, C. A. *J. Chem. Phys.* **1998**, *108* (2), 616.
(54) Shao, Y.; Gan, Z.; Epifanovsky, E.; Gilbert, A. T. B.; Wormit, M.; Kussmann, J.; Lange, A. W.; Behn, A.; Deng, J.; Feng, X.; Ghosh, D.; Goldey, M.; Horn, P. R.; Jacobson, L. D.; Kaliman, I.; Khaliullin, R. Z.; Kuś, T.; Landau, A.; Liu, J.; Proynov, E. I.; Rhee, Y. M.; Richard, R. M.; Rohrdanz, M. A.; Steele, R. P.; Sundstrom, E. J.; III, H. L. W.; Zimmerman, P. M.; Zuev, D.; Albrecht, B.; Alguire, E.; Austin, B.; Beran, G. J. O.; Bernard, Y. A.; Berquist, E.; Brandhorst, K.; Bravaya, K. B.; Brown, S. T.; Casanova, D.; Chang, C.-M.; Chen, Y.; Chien, S. H.; Closser, K. D.; Crittenden, D. L.; Diedenhofen, M.; Jr, R. A. D.; Do, H.; Dutoi, A. D.; Edgar, R. G.; Fatehi, S.; Fusti-Molnar, L.; Ghysels, A.; Golubeva-Zadorozhnaya, A.; Gomes, J.; Hanson-Heine, M. W. D.; Harbach, P. H. P.; Hauser, A. W.; Hohenstein, E. G.; Holden, Z. C.; Jagau, T.-C.; Ji, H.; Kaduk, B.; Khistyaev, K.; Kim, J.; Kim, J.; King, R. A.; Klunzinger, P.; Kosenkov, D.; Kowalczyk, T.; Krauter, C. M.; Lao, K. U.; Laurent, A. D.; Lawler, K. V.; Levchenko, S. V.; Lin, C. Y.; Liu, F.; Livshits, E.; Lochan, R. C.; Luenser, A.; Manohar, P.; Manzer, S. F.; Mao, S.-P.; Mardirossian, N.; Marenich, A. V.; Maurer, S. A.; Mayhall, N. J.; Neuscamman, E.; Oana, C. M.; Olivares-Amaya, R.; O'Neill, D. P.; Parkhill, J. A.; Perrine, T. M.; Peverati, R.; Prociuk, A.; Rehn, D. R.; Rosta, E.; Russ, N. J.; Sharada, S. M.; Sharma, S.; Small, D. W.; Sodt, A.; Stein, T.; Stück, D.; Su, Y.-C.; Thom, A. J. W.; Tsuchimochi, T.; Vanovschi, V.; Vogt, L.; Vydrov, O.; Wang, T.; Watson, M. A.; Wenzel, J.; White, A.; Williams, C. F.; Yang, J.; Yeganeh, S.; Yost, S. R.; You, Z.-Q.; Zhang, I. Y.; Zhang, X.; Zhao, Y.; Brooks, B. R.; Chan, G. K. L.; Chipman, D. M.; Cramer, C. J.; III, W. A. G.; Gordon, M. S.; Hehre, W. J.; Klamt, A.; III, H. F. S.; Schmidt, M. W.; Sherrill, C. D.; Truhlar, D. G.; Warshel, A.; Xu, X.; Aspuru-Guzik, A.; Baer, R.; Bell, A. T.; Besley, N. A.; Chai, J.-D.; Dreuw, A.; Dunietz, B. D.; Furlani, T. R.; Gwaltney, S. R.; Hsu, C.-P.; Jung, Y.; Kong, J.; Lambrecht, D. S.; Liang, W.; Ochsenfeld, C.; Rassolov, V. A.; Slipchenko, L. V.; Subotnik, J. E.; Voorhis, T. V.; Herbert, J. M.; Krylov, A. I.; Gill, P. M. W.; Head-Gordon, M. *Mol. Phys.* **2015**, *113* (2), 184.
(55) Anslyn, E. V.; Dougherty, D. A. *Modern Physical Organic Chemistry*, 1st ed.; University Science: Sausalito, CA, 2005.
(56) Masia, M.; Forbert, H.; Marx, D. *J. Phys. Chem. A* **2007**, *111* (49), 12181.
(57) Small, D. W.; Lawler, K. V.; Head-Gordon, M. *J. Chem. Theory Comput.* **2014**, *10* (5), 2027.

Chapter 7. Efforts Towards the Synthesis of 1,3-Dilithiopropanes

INTRODUCTION

In Chapter 2, we described a method for preparing early metal alkylidene complexes by first accessing a metalacyclobutane. This was achieved by rate-limiting γ-H abstraction from a neopentyl group. An alternative, direct route to metalacyclobutanes and thence alkylidene complexes would permit further exploration of the chemistry of these highly reactive species.

In the 1980s, 1, 3-dibromomagnesiopropanes were reported by Seetz and Bickelhaupt,[1] and used to prepare metalacyclobutanes of Ti,[2] Zr,[2] Hf,[2] V,[3] Mo,[4] W,[4] Re,[5] Ge,[6] and Sn.[7] Many aspects of this chemistry have been reviewed by these authors.[8,9] Dilithiopropanes were also prepared from these di-Grignard reagents.[10,11] Seetz et al. showed that only the *gem*-dimethyl propanes were stable, but that these were quite stable. However, these molecules have to my knowledge, never been used by any other researcher despite their obvious utility. This was likely due to the low yields reported in these papers (14-18%) and the limited details. The full details were published in book form only, and required a complex, one-use only, custom glass apparatus (see Figure 1), careful, sub-3°C temperature control over days to obtain these small yields.[12]

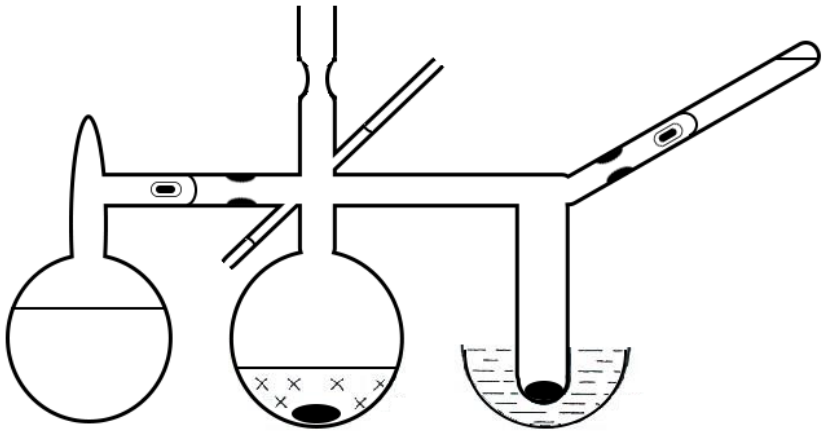

Figure 1. The custom glass apparatus for preparing 1,3-di-Grignard reagents. The left most flask contains solvent. The central flask contains twice-sublimed magnesium and is the reaction flask. The right flask is warmed by a bath 3°C above room temperature. The right break seal is used to add the dibromopropane. The entire apparatus is sealed under 10^{-6} mBar vacuum.

It was therefore clear that an alternative synthetic method was required.

RESULTS AND DISCUSSION

Direct Metalation

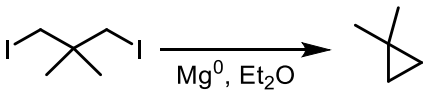

Scheme 1. Direct metalation of alkyl iodides with Mg results in cyclization.

The standard method of preparing Grignard reagents, and the one employed by Seetz and Bickelhaupt, involves the direct treatment of alkyl halides with magnesium metal. When

diiodopropane (100 mg, 0.31 mmol) in 10 mL of Et_2O was slowly added to magnesium metal, only 1,1-dimethylcyclopropane was detected by ^1H NMR spectroscopy. This suggested that the cyclization, probably accelerated by the Thorpe-Ingold Effect in which germinal methyl groups accelerate cyclization,[13] was faster than the second metalation step.
Rieke metals[14] have been used to prepare Grignard reagents of readily cyclizable molecules (see Scheme 2), by allow the metalation reaction to occur at very low temperatures when cyclization is less facile.

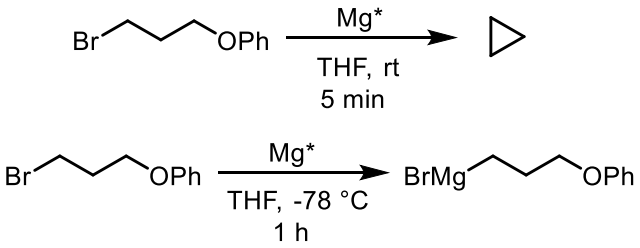

Scheme 2. Rieke metal allow Grignard reagents to be prepared at low temperature to prevent their cyclization.

Unfortunately, the Thorpe-Ingold effect seems to render cyclization so facile that it occurs even at low temperatures. Rieke zinc produces alkylzinc halides which are poorer nucleophiles and so might also be kinetically slower to cyclize. Again, only cyclized product was observed (see Scheme 3).

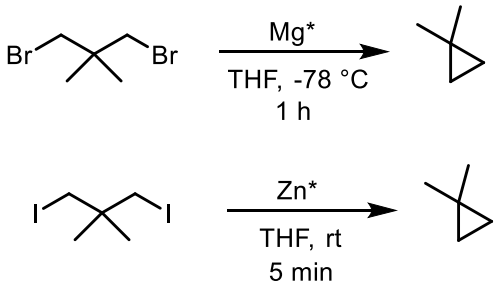

Scheme 3. Rieke metals also produce only cyclized products.

Li/E Exchange

Since it seemed that the rates of the cyclization reactions of these metals were too uncontrolled to obtain the materials desired, an alternate route was sought taking advantage of the ability of elements to undergo Li/element exchange.

Li/I Exchange

The most commonly employed Li/E exchange, originally developed by Negishi, is rapid, high-yielding and used to prepare α,ω-Li$(CH_2)_n$Li (n = 4, 5, 6) in excellent yield. The reaction proceeds by two addition of two equivalents of ^{t}BuLi per I. The first equivalent undergoes Li/I exchange generating an alkyllithium and ^{t}BuI. The second equivalent carries out an E2 elimination on the resulting ^{t}BuI to give LiI, isobutylene, and isobutene (see Scheme 4).

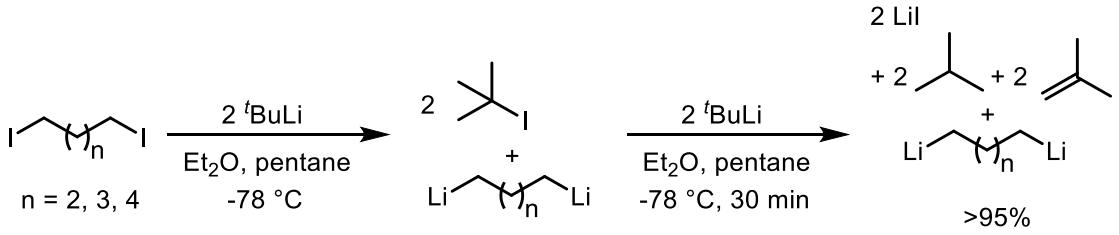

Scheme 4. Li/I Exchange

In the case of diiodopropanes though, even the extremely fast Li/I exchange could not compete with the rates of cyclization and only dimethylcyclopropane were produced even in thawing diethyl ether.

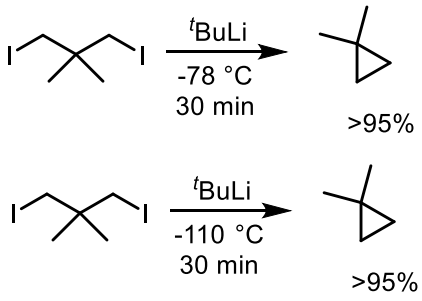

Scheme 5. Li/I exchange results in cyclized products.

Grignard/I exchange is also possible. Addition of a solution of ^{i}PrMgCl to diiodopropane did result in formation of ^{i}PrI and an unknown white product, insoluble in diethyl ether that did not react as a di-Grignard reagent.

Li/Sn Exchange

Another common Li/E exchange is Li/Sn exchange. This reaction sets up an equilibrium between the Sn reagent and the lithium reagent and so it is most commonly employed for the preparation of vinyllithium reagents, since the equilibrium lies toward vinyllithium and alkyltin and away from alkyllithium and vinyltin.[15] In order to prepare a bis(alkyltin)propane reagent, the ability of tin(II) compounds to formally oxidatively add alkyliodides was employed (see Scheme 6).

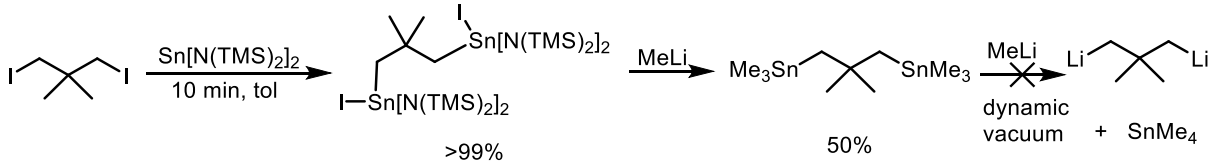

Scheme 6. Bis(trialkyltin)propanes can be prepared but the dilithiopropane was not formed.

The isolatable Sn(II) compound $Sn[N(TMS)_2]_2$ was treated with diiodopropane to afford the tin (IV) compound bis($[N(TMS)_2]_2ISn$)propane in excellent yield (>99%). This material was treated with 6 equiv MeLi in diethyl ether to afford the reported bis(Me_3Sn)propane in 50 % yield. Treatment of this material with MeLi should set up an equilibrium between the

dilithiopropane and the low boiling $SnMe_4$ which could be removed under dynamic vacuum, driving the reaction to completion. The equilibrium, however lies too far toward MeLi and bis(Me_3Sn)propane, according to the McEwan-Streitweiser-Applequist-Dessy pKa scale[16] (see Table 1) for any observable transformation to occur.

Compound	**pKa**
toluene (α-position)	35
ethylene	36.5
benzene	37
cyclopropane	39
methane	40
ethane	42
neopentane	44
propane (*s*-position)	44
cyclohexane	45

Table 1. Selected acidities on the McEwan-Streitweiser-Applequist-Dessy pKa scale. Note that only cyclohexane is measure to be more basic than neopentane.

Treatment of bis([$N(TMS)_2$]$_2$ISn)propane at low temperatures with 6 equiv ^{n}BuLi affords the bis(Bu_3Sn)propane in 50% yield. Further treatment with excess ^{n}BuLi results in a mixture of tin containing products as determined by ^{1}H NMR spectroscopy. Treatment of bis([$N(TMS)_2$]$_2$ISn)propane with 8 equiv cyclohexyllithium at low temperature also affords only a mixture of tin containing products. It is possible that various tin oligomers and polymers are formed from initially-formed $(R_3Sn)CH_2CMe_3CH_2Li$ preventing clean formation of the desired dilithiopropane product.

Li/Te Exchange

Li/Te exchange is considered one of the most robust methods of preparing lithium reagents by Li/element exchange. It is fast (almost as fast as Li/I), works for secondary alkyllithium reagents.[17] Moreover, $^-$TeR is a poor leaving group which could shut down cyclization pathways. Bis(RTe)propanes have been prepared before and can be easily accomplished by addition of an alkyllithium reagent to elemental Te in frozen THF to generate RTeLi which nuclephilically attacks even hindered positions such as in a neopentyl group.[18,19] In this way, bis(PhTe)propane was prepared in good yield (80%).

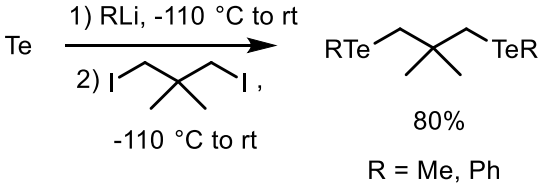

Scheme 7. Preparation of bis(RTe)propanes.

The bis(PhTe)propane, when treated with ^{t}BuLi over 1 week slowly formed dimethylcyclopropane as determined by ^{1}H NMR spectroscopy. To attempt to accelerate the reaction, ^{s}BuLi was used instead of ^{t}BuLi. The reaction still afforded only dimethylcyclopropane,

but after 20 minutes. Treatment of the bis(PhTe)propane with CyLi at -78 °C afforded dimethylcyclopropane over 1 hour. To obtain a less nucleophilic exchanged group, ^{i}PrMgCl was employed instead of a lithium reagent,[20] no conversion was observed after 3 days. From this data, we surmise that if any group is present which can be extruded as a leaving group, even a poor one, after the first exchange, cyclization will occur. Seetz was able to synthesize the lithium reagent from the Grignard by first preparing the bis(BrHg)propane. Since the $^{-}$HgBr is not a stable group, no cyclization occurred in this case. Therefore, in order to prepare dilithiopropanes without cyclization, one must proceed via a pathway that never produces a strongly nucleophilic carbon which can react to cyclize.

Oxidative addition of alkyliodide to Hg

It was reported Hg formally oxidatively adds alkyliodides under photolytic conditions, catalyzed by Hg_2I_2.[21] Hence, this was attempted with diiodopropane. Unfortunately, only unreacted starting material was recovered, in addition to dimethylcyclopropane.

Hg/B Exchange

Mercury/boron exchange is a usually reliable although not environmentally-friendly route to prepare alkylmercury compounds from alkylboranes.[22] The bis(borane)propane was prepared by a copper-catalyzed borylation[23] to give bis(Bpin)propane in good yield.

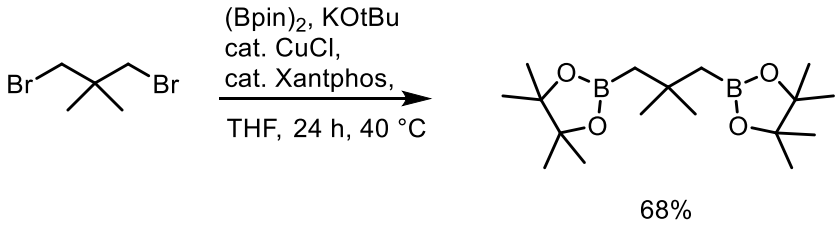

Scheme 8. Copper-catalyzed borylation of the dibromopropane.

Since mercuration proceeds most readily with trialkylboranes, the bis(Bpin)propane was converted into bis(B^{i}Pr$_2$)propane by treatment with 4 equiv ^{i}PrMgCl in diethyl ether. The use of isopropyl groups was an attempt to minimize unwanted mercury products; secondary alkyl groups do not undergo Hg/B exchange.[22] Unfortunately, bis(B^{i}Pr$_2$)propane did not react with mercuric acetate in 48 hours. Mercury-boron exchange is reported to be extremely fast and reaction of primary alkylboranes and $Hg(OAc)_2$ only does not occur when the borane is too sterically congested. We suggest that if bis(BMe$_2$)propane were used instead of the isopropyl analogue, the Hg/B exchange would occur readily and hence allow convenient, high-yielding access to bis(BrHg)propane, which can easily be converted to the dilithiopropane by addition of alkyllithium reagents (based on the kinetics of the Li/Te reaction with ^{t}BuLi vs, ^{s}BuLi, we also suggest that the week-long reaction time required by Seetz[10] was due to use of the highly bulky ^{t}BuLi and that the reaction would proceed much more readily with ^{s}BuLi). However, this pathway would also generate 4 equiv MeHgBr per molecule of bis(BrHg)propane. This toxic compound would have to be separated from the desired product and disposed. Owing to these considerations, this approach was not attempted.

CONCLUSIONS

Despite several reports that dilithio- and di(bromomagnesio)propanes can be prepared, for all intents and purposes, this is not the case. Direct metalation (Rieke Mg, Rieke Zn) and many Li/element (element = I, Sn, Te) exchange reactions have been pursued but ultimately lead to cyclization due to the presence, after the monolithium reagent is formed, of a nucleophile and an electrophile in the same molecule, whose cyclization is accelerated by the Thorpe-Ingold Effect. Mercury-boron exchange can almost certainly be used to avoid this and access this class of molecules. However, considerable alkylmercury byproducts would be produced by such a method, which should be avoided for safety and waste disposal reasons.

EXPERIMENTAL SECTION

General

Unless otherwise noted, all experiments were conducted in dry, oxygen-free solvents using standard Schlenk techniques or in a N_2 atmosphere glovebox. Deuterated solvents were purchased from Cambridge Isotope Laboratories, Inc. Benzene-d_6 was dried by vacuum distillation from Na/K alloy. Unless otherwise noted, reagents were obtained from commercial suppliers. Rieke magnesium and zinc and 1,3-dihalopropanes were prepared according to published procedures.[14,24,25]

Analytical Methods

Solution NMR spectroscopy was performed using Bruker AV-300, AVB-400, AVQ-400, AV-500, or AV-600 MHz spectrometers at room temperature. ^{1}H, $^{13}C\{^{1}H\}$, and $^{11}B\{^{1}H\}$ NMR spectra were calibrated internally to either the resonance for the solvent or residual proteo solvent relative to tetramethylsilane. Elemental analyses were carried out by the College of Chemistry Microanalytical Laboratory at the University of California, Berkeley.

Direct metalation with magnesium

Magnesium (175 mg, 7.2 mmol) was suspended in diethyl ether (10 mL) and an iodine crystal was added. Once the solution decolorized, 1,3-diiodo-2,2-dimethylpropane (100 mg, 0.31 mmol) in 10 mL diethyl ether was added dropwise over 30 min and stirred for 1 h. Analysis of an aliquot of the reaction mixture by ^{1}H NMR spectroscopy revealed only starting material and 1,1-dimethylcyclopropane.

Direct metalation with Rieke magnesium

To a THF or diethyl ether (10 mL) suspension of Rieke magnesium (138 mg, 5.7 mmol) at -78 °C was added a THF or diethyl ether solution (10 ml) of 1,3-dibromo-2,2-dimethylpropane (172.5 mg, 0.75 mmol). After 1 hour, the reaction mixture was filtered and analyzed by ^{1}H NMR spectroscopy, which showed only formation of dimethylcyclopropane.

Direct metalation with Rieke zinc

A sample of Rieke zinc (16.2 mg, 0.25 mmol) was suspended in THF-d_8 and 1,3-diiodo-2,2-dimethylpropane (20.0 mg, 0.06 mmol). ^{1}H NMR spectroscopy indicated the formation of dimethylcyclopropane as the only product. No reaction was observed when 1,3-dibromo-2,2-dimethylpropane is used instead.

Lithium/iodide exchange

-78 °C:

1,3-diiodopropane (324 mg, 1.0 mmol) in diethyl ether (2 mL) was cooled to -78 °C. A solution of ^{t}BuLi (2.47 mL, 1.7 M in pentane, 4.2 mmol) was added dropwise. After stirring for 30 min, an aliquot was quenched with water and analyzed for neopentane by ^{1}H NMR spectroscopy. No neopentane was found.

-110 °C:

Diethyl ether (2 mL) was cooled to -110 °C in a diethyl ether slush bath. To this was added tBuLi (2.5 mL, 1.7 M in pentane, 4.25 mmol). A diethyl ether (10 mL) solution of 1,3-diiodopropane (328 mg, 1.01 mmol) was added dropwise down the side of the flask to allow it to cool before contact with the reaction mixture over 20 min. The reaction mixture was slowly warmed to room temperature and trimethylsilylchloride (500 μL, 2.1 mmol) was added to quench the reaction. No evidence of bis-1,3-trimethylsilyl-2,2-dimethylpropane was found by ^{1}H NMR spectroscopy.

Lithium/tin exchange

1,3-bis(iodobis(HMDS)Sn)-2,2-dimethylpropane. 1,3-diiodo-2,2-dimethylpropane (250 mg, 0.77 mmol) was added to a toluene solution (10 mL) of $Sn[N(TMS)_2]_2$ (678.8 mg, 1.55 mmol). The orange-red reaction mixture immediately became colorless and was stirred for 10 min and the toluene was removed under reduced pressure to afford the off-white product. ^{1}H NMR (500 MHz, benzene-d_6) δ 2.40 (s, $^{2}J_{SnH}$ = 13.4 Hz, $^{2}J_{SnH}$ = 63.0 Hz, 4H), 0.44 (s, 72H), 0.30 (s, 6H).

1,3-bis(trimethylstannyl)-2,2-dimethylpropane. 1,3-bis(iodobis(HMDS)Sn)-2,2-dimethylpropane (481.2 mg, 0.4 mmol) was dissolved in diethyl ether (8 mL) and methylithium (1.5 mL, 1.6M in diethyl ether, 2.4 mmol) was added at room temperature. After stirring for 30 min, 0.2 M HCl (10 mL) was added to the reaction mixture and the mixture was washed with 0.2 M HCl (3x10 mL). The organic layers were collected, dried over $MgSO_4$ and the volatile materials were removed by vacuum to afford the product as a colorless oil (80 mg, 50 % yield). ^{1}H NMR (500 MHz, $CDCl_3$) δ 1.08 (s, $^{2}J_{SnH}$ = 53.8 Hz, 4H), 1.02 (s, 6H), 0.08 (s, $^{2}J_{SnH}$ = 49.6 Hz, $^{2}J_{SnH}$ = 52.0 Hz, 18H). ^{119}Sn NMR (^{1}H-^{119}Sn HMBC, $CDCl_3$) δ 6.27. This is consistent with the published spectroscopy.[10]

Treatment with MeLi. 1,3-bis(trimethylstannyl)-2,2-dimethylpropane (70 mg, 0.18 mmol) was dissolved in dibutyl ether. Methyllithium (220 μL, 1.6M in diethyl ether) was added and the reaction was placed under dynamic vacuum for 28 hours until all solvent was removed. The resulting residue was analyzed by ^{1}H NMR spectroscopy; no reaction had occurred.

1,3-bis(tributylstannyl)-2,2-dimethylpropane. 1,3-bis(iodobis(HMDS)Sn)-2,2-dimethylpropane (1.07 g, 0.89 mmol) was dissolved in diethyl ether (30 mL) and cooled to -78 °C. Butyllithium (3.27 mL, 1.6M in hexane, 5.24 mmol) was added slowly at -78 °C. The reaction mixture was allowed to slowly warm to 22°C. After stirring for 10 min at 22 °C, 0.2 M HCl (10 mL) was added to the reaction mixture and the mixture was washed with 0.2 M HCl (3x10 mL). The organic layers were collected, dried over $MgSO_4$ and the volatile materials were

removed by vacuum to afford the product as a colorless oil (90 mg, 54 % yield). ^{1}H NMR (500 MHz, benzene-d_6) δ 1.72 – 1.51 (m, 12H), 1.51 – 1.31 (m, 12H), 1.08 – 0.93 (m, 18H), 0.93 – 0.81 (m, 10H), 0.11 (s, $^{2}J_{SnH}$ = 55.1 Hz, 12H). ^{119}Sn NMR (^{1}H-^{119}Sn HMBC, $CDCl_3$) δ -3.30.

Treatment with ^{n}BuLi. 1,3-bis(tributylstannyl)-2,2-dimethylpropane (200 mg, 0.31 mmol) was dissolved in pentane and nBuLi (1.9 mL, 1.6M in hexanes) was added. 1H NMR spectroscopy of an aliquot revealed only a mixture of tin-containing products.

Preparation of cyclohexyllithium. Lithium wire (1.6% Na, high sodium lithium is required, 2.50 g, 36.02 mmol) was washed with pentane under N_2, cut into small bits, and suspended in pentane (250 mL). Cyclohexylchloride was added dropwise. The reaction was heated to reflux and then heating was stopped. Purple-black precipitate formed. The reaction mixture was stirred for 15 h, at which point it was filtered through Celite and crystallized from cold pentane to give 1.75g of pure, white cyclohexyllithium (16.4 % yield).

Treatment with CyLi. 1,3-bis(iodobis(HMDS)Sn)-2,2-dimethylpropane (10 mg, 0.008 mmol) was dissolved in C_6D_6 (1.0 mL). Cyclohexyllithium (6.0 mg, 0.066 mmol) was added and the reaction was monitored by ^{1}H NMR spectroscopy. Only a mixture of tin-containing products were observed, not including $SnCy_4$.

Lithium/tellurium exchange

1,3-bis(methyltelluro)-2,2-dimethylpropane. Tellurium metal (492.4 mg, 3.86 mmol) was ground into a powder and suspended in THF (5 mL), which was frozen in an N_2 bath. Methyllithium (2.4 mL, 1.6M in diethylether) was added to the top of the frozen reaction mixture, which was allowed to thaw, forming a yellow, clear solution. The solution was refrozen and 1,3-diiodo-2,2-dimethylpropane (500 mg, 1.54 mmol) was added to the top. The reaction mixture was allowed to thaw again and stirred for 1.5 h. The reaction mixture was then quenched with 10 mL brine solution and extracted (3x10mL) with diethyl ether and dried over $MgSO_4$. The solvent was removed by rotary evaporation to afford 1,3-bis(methyltelluro)-2,2-dimethylpropane (80% yield). ^{1}H NMR (400 MHz, $CDCl_3$) δ 2.82 (s, $^{2}J_{TeH}$ = 22.3 Hz, 4H), 1.89 (s, $^{2}J_{TeH}$ = 21.1 Hz, 6H), 1.12 (s, 6H).

1,3-bis(phenyltelluro)-2,2-dimethylpropane. Tellurium metal (892 mg, 6.99 mmol) was ground into a powder and suspended in THF (5 mL), which was frozen in an N_2 bath. Phenyllithium (588 mg, 6.99 mmol) in THF (5 mL) was added to the top of the frozen reaction mixture, which was allowed to thaw, forming a yellow, clear solution. The solution was refrozen and 1,3-diiodo-2,2-dimethylpropane (905.8 mg, 2.80 mmol) was added to the top. The reaction mixture was allowed to thaw again and stirred for 1.5 h. The reaction mixture was then quenched with 10 mL brine solution and extracted (3x10mL) with diethyl ether and dried over $MgSO_4$. The solvent was removed by rotary evaporation to afford 1,3-bis(phenyltelluro)-2,2-dimethylpropane (80% yield). ^{1}H NMR (500 MHz, C_6D_6) δ 7.69 (ddd, J = 8.1, 5.6, 1.4 Hz, 4H), 7.06 – 6.73 (m, 6H), 2.95 (s, $^{2}J_{TeH}$ = 22.3 Hz, 4H), 0.98 (s, 6H). ^{13}C NMR (126 MHz, C_6D_6) δ 138.92, 137.83, 129.48, 129.41, 36.01, 29.30, 27.31.

Treatment with ^{t}BuLi. 1,3-bis(phenyltelluro)-2,2-dimethylpropane (23 mg, 0.05 mmol) was dissolved in C_6D_6 (1 mL). ^{t}BuLi (180 μL, 1.6 M in pentane) was evaporated to dryness and added to the reaction mixture. Monitoring by ^{1}H NMR spectroscopy reveals the initial formation

of 1,3-bis(*tert*-butyltelluro)-2,2-dimethylpropane (^{1}H NMR (600 MHz, C_6D_6) δ 2.89 (s, $^2J_{TeH}$ = 13.6 Hz, 4H), 1.51 (s, 18H), 1.16 (s, 6H).) and 1,1-dimethylcyclopropane, which grows in over the course of 1 week.

Treatment with ^{s}BuLi. 1,3-bis(phenyltelluro)-2,2-dimethylpropane (23 mg, 0.05 mmol) was dissolved in C_6D_6 (1 mL). ^{s}BuLi (180 μL, 1.4 M in cyclohexane) was evaporated to dryness and added to the reaction mixture. Monitoring by ^{1}H NMR spectroscopy reveals the rapid formation of 1,1-dimethylcyclopropane.

Treatment with CyLi. CyLi (29.8 mg, 0.3 mmol) was dissolved in THF-d_8 (1 mL) at -78 °C. 1,3-bis(phenyltelluro)-2,2-dimethylpropane (23.8 mg, 0.05 mmol) was added to the reaction mixture. After an hour, ^{1}H NMR spectroscopy reveals the formation of 1,1-dimethylcyclopropane.

Treatment with ^{i}PrMgCl. ^{i}PrMgCl (29.8 mg, 0.3 mmol) was dissolved in THF-d_8 (1 mL). 1,3-bis(phenyltelluro)-2,2-dimethylpropane (23.8 mg, 0.05 mmol) was added to the reaction mixture. No reaction was observed by ^{1}H NMR spectroscopy after 3 days.

Oxidative addition of alkyliodide to Hg. Iodine (1.71 g, 6.7 mmol) in ethanol (5 mL) was added to mercury (10.1 g, 50.3 mmol) and shaken. This mixture became hot, turned red and then the solvent became green. The mixture was filtered on a Buchner funnel. The solid was added to a 20 mL Teflon-stoppered Schlenk flask with 1,3-diiodo-2,2-dimethylpropane (3.76 g, 11.6 mmol) and photolyzed under a mercury arc lamp at 50 °C for 4 h. No significant reaction occurred; the only non-starting material product was 1,1-dimethylcyclopropane.

Hg/B exchange

1,3-bis(pinacolatoboryl)-2,2-dimethylpropane. 1,3-dibromo-2,2-dimethylpropane (1.00 g, 4.3 mmol), CuCl (65 mg, 0.65 mmol), KO^{t}Bu (976 mg, 8.7 mmol), XantPhos (378 mg, 0.65 mmol), and $(Bpin)_2$ (2.43 g, 9.57 mmol) were combined in THF (100 mL) and stirred at 40 °C for 2 days. The reaction mixture was filtered through a short silica plug. The resulting material was purified by column chromatography eluting with ethyl acetate:hexanes (5:95). Removing the volatile materials affords the desired product (704 mg, 58 % yield). ^{1}H NMR (500 MHz, $CDCl_3$) δ 1.23 (s, 24H), 1.06 (s, 6H), 0.91 (s, 4H). ^{13}C{^{1}H} NMR (126 MHz, $CDCl_3$) δ 82.79, 31.97, 31.60, 25.09. ^{11}B{^{1}H} NMR (193 MHz, $CDCl_3$) δ 32.79.

1,3-bis(di-*iso*-propylboryl)-2,2-dimethylpropane. 1,3-bis(pinacolatoboryl)-2,2-dimethylpropane (599.2 mg, 1.85 mmol) was dissolved in diethylether (12.0 mL). A solution of ^{i}PrMgCl (3.7 mL, 2.0M in diethyl ether) was added dropwise. White precipitate formed after about 1 minute and the reaction was stirred for 1 h. The reaction mixture was filtered to remove the salts. The volatile materials were removed under vacuum and resulting residue was extracted with pentane and filtered. The pentane was removed under vacuum to afford the product as a colorless oil (300 mg, 61% yield). ^{1}H NMR (600 MHz, C_6D_6) δ 1.90 (hept, J = 7.1 Hz, 4H), 1.50 (s, 4H), 1.20 (s, 6H), 0.95 (d, J = 7.2 Hz, 24H). ^{13}C{^{1}H} NMR (151 MHz, C_6D_6) δ 34.72, 33.90, 33.46, 22.77, 17.78. ^{11}B{^{1}H} NMR (193 MHz, C_6D_6) δ 85.47.

Treatment with $Hg(OAc)_2$.1,3-bis(di-*iso*-propylboryl)-2,2-dimethylpropane (293.6 mg, 1.11 mol) was dissolved in THF (10 mL). Mercuric acetate (708.5 mg, 2.22 mmol) was added

and the reaction mixture was stirred for 48 hours. The reaction mixture was then poured into a fast stirring aqueous solution of NaBr. The resulting material contained only $HgBr_2$ and starting material.

REFERENCES

(1) Seetz, J. W. F. L.; Hartog, F. A.; Böhm, H. P.; Blomberg, C.; Akkerman, O. S.; Bickelhaupt, F. *Tetrahedron Lett.* **1982**, *23* (14), 1497.
(2) Seetz, J. W. F. L.; Schat, G.; Akkerman, O. S.; Bickelhaupt, F. *Angew. Chem. Int. Ed. Engl.* **1983**, *22* (3), 248.
(3) Seetz, J. W. F. L.; Van de Heisteeg, B. J. J.; Schat, G.; Akkerman, O. S.; Bickelhaupt, F. *J. Organomet. Chem.* **1984**, *275* (2), 173.
(4) Van de Heisteeg, B. J. J. Vrije Universiteit Amsterdam 1987,.
(5) de Boer, H. J. R.; van de Heisteeg, B. J. J.; Flöel, M.; Herrmann, W. A.; Akkerman, O. S.; Bickelhaupt, F. *Angew. Chem. Int. Ed. Engl.* **1987**, *26* (1), 73.
(6) Seetz, J. W. F. L.; Van De Heisteeg, B. J. J.; Schat, G.; Akkerman, O. S.; Bickelhaupt, F. *J. Organomet. Chem.* **1984**, *277* (3), 319.
(7) Seetz, J. W. F. L.; Schat, G.; Akkerman, O. S.; Bickelhaupt, F. *J. Am. Chem. Soc.* **1983**, *105* (10), 3336.
(8) Bickelhaupt, F. *Angew. Chem. Int. Ed. Engl.* **1987**, *26* (10), 990.
(9) Seetz, J. W. F. L.; Ent, H.; Rookhuizen, R. B.; Akkerman, O. S.; Bickelhaupt, F. *Recl. Trav. Chim. Pays-Bas* **1988**, *107* (3), 160.
(10) Seetz, J. W. F. L.; Schat, G.; Akkerman, O. S.; Bickelhaupt, F. *J. Am. Chem. Soc.* **1982**, *104* (24), 6848.
(11) Akkerman, O. S.; Bickelhaupt, F. *J. Organomet. Chem.* **1988**, *338* (2), 159.
(12) Seetz, J. W. F. L.; Van De Heisteeg, B. J. J.; de Boer, H. J. R.; Schat, G.; Akkerman, O. S.; Bickelhaupt, F. In *Organometallic Syntheses*; Eisch, J. J., Ed.; Elsevier: Amsterdam, 1988; pp 392–395.
(13) Anslyn, E. V.; Dougherty, D. A. *Modern Physical Organic Chemistry*, 1st ed.; University Science: Sausalito, CA, 2005.
(14) Reuben D. Rieke; Timothy P. Burns; Richard M. Wehmeyer; Bruce E. Kahn. In *High-Energy Processes in Organometallic Chemistry*; ACS Symposium Series; American Chemical Society, 1987; Vol. 333, pp 223–245.
(15) Davies, A. G. In *Organotin Chemistry*; Wiley-VCH Verlag GmbH & Co. KGaA, 2004; pp 373–382.
(16) Wakefield, B. J. In *The Chemistry of Organolithium Compounds*; Pergamon, 1974; pp 26–50.
(17) Reich, H. J.; Medina, M. A.; Bowe, M. D. *J. Am. Chem. Soc.* **1992**, *114* (27), 11003.
(18) Hope, E. G.; Kemmitt, T.; Levason, W. *Organometallics* **1987**, *6* (1), 206.
(19) Hope, E. G.; Kemmitt, T.; Levason, W. *Organometallics* **1988**, *7* (1), 78.
(20) Aso, Y.; Yamashita, H.; Otsubo, T.; Ogura, F. *J. Org. Chem.* **1989**, *54* (23), 5627.
(21) Maynard, J. L. *J. Am. Chem. Soc.* **1932**, *54* (5), 2108.
(22) Larock, R. C.; Brown, H. C. *J. Am. Chem. Soc.* **1970**, *92* (8), 2467.
(23) Ito, H.; Kubota, K. *Org. Lett.* **2012**, *14* (3), 890.
(24) Rydon, H. N. *Org. Synth.* **1971**, *51*, 44.
(25) Landauer, S. R.; Rydon, H. N. *J. Chem. Soc. Resumed* **1953**, No. 0, 2224.